GEOTECHNICAL SPECIAL PUBLICATION NO. 202

EXPERIMENTAL AND APPLIED MODELING OF UNSATURATED SOILS

PROCEEDINGS OF SESSIONS OF GEOSHANGHAI 2010

June 3–5, 2010
Shanghai, China

HOSTED BY
Tongji University
Shanghai Society of Civil Engineering, China
Chinese Institution of Soil Mechanics and Geotechnical Engineering, China

IN COOPERATION WITH
Alaska University Transportation Center, USA
ASCE Geo-Institute, USA
Deep Foundation Institute, USA
East China Architectural Design & Research Institute Company, China
Georgia Institute of Technology, USA
Nagoya Institute of Technology, Japan
Transportation Research Board (TRB), USA
The University of Newcastle, Australia
The University of Illinois at Urbana-Champaign, USA
The University of Kansas, USA
The University of Tennessee, USA
Vienna University of Natural Resources and Applied Life Sciences, Austria

EDITED BY
Laureano R. Hoyos
Xiong Zhang
Anand J. Puppala

Published by the American Society of Civil Engineers

Library of Congress Cataloging-in-Publication Data

GeoShanghai International Conference (2010)
Experimental and applied modeling of unsaturated soils : proceedings of the GeoShanghai 2010 International Conference, June 3-5, 2010, Shanghai, China / edited by Laureano R. Hoyos, Xiong Zhang, Anand J. Puppala.
p. cm. -- (Geotechnical special publication ; 202)
Includes bibliographical references and index.
ISBN 978-0-7844-1103-2
1. Soil mechanics--Simulation methods--Congresses. 2. Zone of aeration--Simulation methods--Congresses. 3. Soil moisture--Measurement--Congresses. I. Hoyos, Laureano R., 1972- II. Zhang, Xiong, 1971- III. Puppala, Anand J. IV. Title.

TA710.A1G368 2010b
624.1'5136011--dc22 2010012086

American Society of Civil Engineers
1801 Alexander Bell Drive
Reston, Virginia, 20191-4400

www.pubs.asce.org

ISBN 978-0-7844-1103-2
Manufactured in the United States of America.

Preface

Geotechnical and civil engineers all over the world continue to face problems with a wide range of geosystems involving materials that remain under partially saturated conditions throughout the year. The lack of education and training among engineering graduates and practitioners to properly deal with unsaturated soil conditions has resulted in faulty or excessively conservative designs, frequent construction delays, and deficient long-term performance of built infrastructure. Over the last few decades, however, the discipline of unsaturated soil mechanics has begun to receive increasing attention worldwide, providing better explanations for soil behavioral patterns than conventional saturated soil mechanics.

This Geotechnical Special Publication on *Experimental and Applied Modeling of Unsaturated Soils* comprises a total of 28 peer-reviewed papers selected for presentation at the Unsaturated Soils sessions of the *GeoShanghai 2010* conference held in Shanghai, China, June 3-5, 2010, and hosted by Tongji University. The sessions were organized and sponsored by the Committee on Unsaturated Soils of the Geo-Institute of the ASCE, with co-sponsorship of the Technical Committee No. 6 (TC6) on Unsaturated Soils of the International Society for Soil Mechanics and Geotechnical Engineering (ISSMGE).

The current GSP is the latest in a successful series of special publications published by the Geo-Institute documenting the most recent advances in the unsaturated soil mechanics discipline, starting with GSP No. 68 on *Unsaturated Soil Engineering Practice* from the first Geo-Institute Conference in Logan, Utah, July 15-19, 1997. The papers included in this GSP have been divided into two broad categories. Part I on *General Characterization and Constitutive Behavior* is devoted to some of the most recent advances in characterization and prediction of engineering properties, mechanical response and constitutive behavior of unsaturated soil materials, included compacted, collapsible and expansive soils. Part II on *Applied Modeling and Analysis* is devoted to the most recent advances in the state of the art concerning both laboratory and field measurements of unsaturated soil properties and phenomena for particular practical applications, including centrifuge testing and ground-penetrating radar (GPR). Papers dealing with unsaturated slope stability analyses and foundation heave predictions as affected by environmental variables such as rainfall, freeze-thaw, vegetation and water migration in the vadose zone are also included in this second part.

Each of the papers included in this publication received at least two positive peer reviews. The Editors would like to express their most sincere appreciation to all of the anonymous reviewers for their diligent work, with special thanks to Ms. Claudia Velosa, doctoral candidate at the University of Texas at Arlington, for her valuable

assistance in the final editing of the papers, and to Mrs. Donna Dickert of the ASCE for patiently coordinating the logistics of the publication process.

Laureano R. Hoyos
Associate Professor, University of Texas at Arlington, Arlington, Texas, USA

Xiong Zhang
Assistant Professor, University of Alaska at Fairbanks, Fairbanks, Alaska, USA

Anand J. Puppala
Professor, University of Texas at Arlington, Arlington, Texas, USA

Contents

Part II: Applied Modeling and Analyses

Indexes

Retention Properties and Compressibility of a Compacted Soil

C. Kai[1], and Z. Qing[2]

[1] Southwest Jiaotong University, School of Civil Engineering, Chengdu, Sichuan, 610031, P.R. China, e-mail:cuikai80@hotmail.com
[2] Southwest Jiaotong University, School of Civil Engineering, Chengdu, Sichuan, 610031, P.R. China, e-mail:zq253401327@163.com

ABSTRACT: Soil-water retention properties and compressibility are closely related to the stability of geotechnical engineering structures made of compacted soils. In the present study, the water retention curve of a compacted soil from Northern France was characterized using either suction control method or suction measurement. The results obtained showed a good correspondence between the two methods. Then, these two experimental methods were used in oedometer compression test to highlight the factors influencing the compression properties, especially in terms of changes in compression index as a function of initial suction and initial structure (i.e. density). In the case of low density (1.1 Mg/m^3), the results evidenced different zones for the variations of compression index, separated by a stress threshold. Compression index did not change significantly when suction values were relatively high and the applied vertical stresses were lower than the identified threshold stress.

INTRODUCTION

The soil compressibility is highly variable both in time and space because it depends on soil type (texture), soil structure (porosity) and soil moisture (suction). To ensure the stability of structures involving compacted soils, it is essential to understand the water retention property and volume change behaviour of the soils under the combined mechanical and hydraulic effects. Most of results have been obtained for soils with very high dry bulk densities, and showed that compression index decreases with increasing suction. But for some loose soils such as compacted soils, some authors have found that it decreases with suction (Zhang et al. 1997, Défossez et al. 2003) while others have observed that soil suction has an insignificant effect (Larson et al. 1980, Smith et al. 1997, Arvidsson and Keller 2004, Imhoff et al. 2004, Mosaddeghi et

al. 2006). In the present work, the water retention properties of a compacted soil taken from Northern France were characterized using either suction control method or suction measurement. Osmotic suction control method was used for the desiccation path and suction measurement using high capacity tensiometer was applied for the humidification path. Then, these two experimental methods were used in oedometer compression test to investigate the suction effect on the compression properties.

MATERIALS

For this study, a compacted loamy soil (17.3% clay, 77.7% silt, 5% sand) from a site at Mons in Northern France was used. The soil has a liquid limit of 29%, a plasticity index of 6 and a solid density of 2.7 Mg/m^3. Air-dried soil was passed through 2 mm sieve. The water content of the soil powder is 2%.

TESTING EQUIPMENT AND PROCEDURE

Suction Control Method

The osmotic technique for suction control testing is based on the use of a cellulose semi-permeable membrane and an aqueous solution of organic polyethylene glycol (PEG) molecules. When the soil is separated from the PEG solution by the membrane, water can cross the membrane whereas the PEG molecules in solution cannot due to their large size. The water stops flowing once equilibrium state is reached; there is thus the same suction in the PEG solution and the soil. This suction is known from the PEG calibration curve. According to Delage et al. (1998) and Delage and Cui (2000), there is a unique relationship between PEG concentration, C (g PEG/g water) and suction, s (MPa), independent of the molecular weight of the PEG.

Oedometer compression tests were conducted with suction state controlled using the osmotic technique to study the compression index. A standard oedometer was adapted to the osmotic technique, allowing compression tests at controlled suction. Figure 1 shows the osmotic-based oedometer employed. The cell base was grooved to homogenize the distribution of the PEG solution; a fine sieve was placed over the grooves to protect the semi-permeable membrane placed between the sieve and the soil sample. A closed circuit activated by a peristaltic pump was designed to circulate the PEG solution. A one-litre bottle was used to ensure a quasi-constant concentration in spite of water exchanges with the soil sample. A capillary tube placed on the sealed bottle allowed monitoring water exchanges between the PEG solution and the soil sample. The bottle was placed in a thermostatic water bath at 20±0.5°C to avoid any temperature effects on the water exchange measurements.

In addition, the entire system was installed in an air-conditioned room (20±1°C). In order to quantify the change of water volume due to temperature and evaporation, a second bottle full of PEG solution with a capillary tube was placed in the water bath.

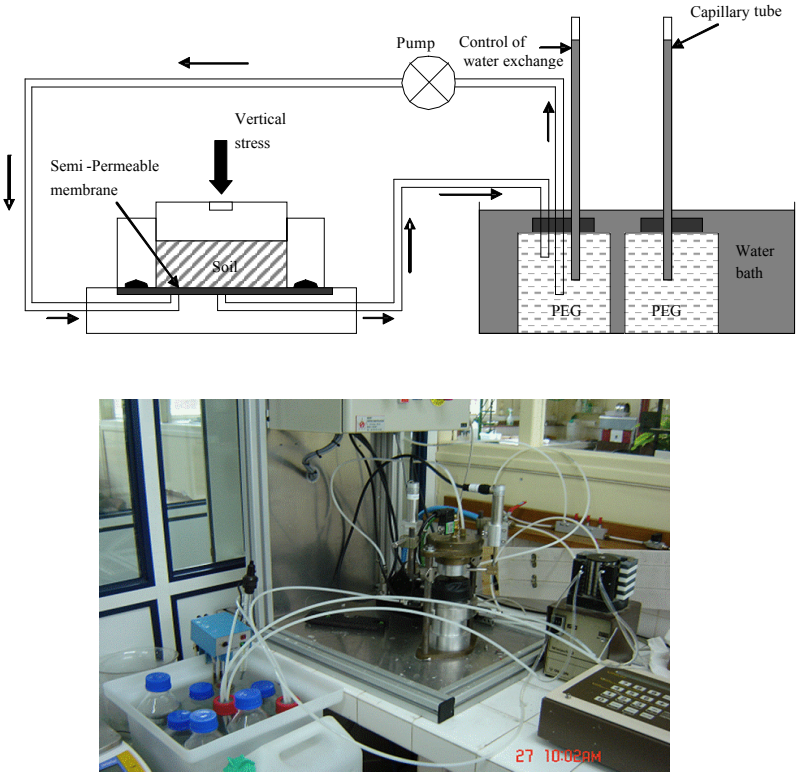

Figure 1. Schematic of osmotic oedometer and actual picture

Series I: For each sample preparation, 103.62 ± 0.05 g dry powder was used. The soil powder was humidified by pulverization to reach 12.5% water content; the sample was prepared by compaction in the oedometer cell to reach dimensions of 70 mm in diameter and 24 mm high, with a dry bulk density of 1.1 Mg m^{-3}. The initial suction of the compacted sample before compression test was about 200 kPa, estimated by the tensiometer considered in the other experimental method: suction measurement. Series II: Test samples were prepared at different initial water content w_i = 12.5, 13, 16 and 25% which supply the initial suctions near to 200, 100, 50 and 10 kPa separately.

For the series I, the six compression tests were performed at different suctions: 0, 10, 50, 100, 180 and 200 kPa, each test having been started with a suction application process under zero vertical stress. The suction was applied either by circulating PEG solution of the desired concentration or pure water (for zero suction). Equilibrium was indicated by stabilization of the solution level in the capillary tube,

when there was no change in variation of water volume in the capillary tube or in the soil. It was observed that equilibrium time depended on the amplitude of suction changes: three days for 200 kPa and 18 days for zero suction. For the series II, PEG solutions provided separately suctions of 10, 50,100 or 200 kPa for the four samples with different initial water content. The equilibrium time was 1 day for these samples.

Compression was performed under constant suction condition by step-loading using a pneumatic system: 10-20-50-100-200-400-800 kPa. Loading time of each stress was function of time needed to reach suction equilibrium again (about 40 min for each step). The displacement stabilization was controlled by two sensors (accuracy of 0.01 mm) symmetrically installed on both sides of the oedometer cell. Loading time took Unloading was carried out following the same stress steps until 50 kPa. The final water content was determined by oven-drying at 105°C for 24 hours.

Suction Measurements

The suction of soil specimens was measured using a tensiometer inserted through an opening in the base pedestal in a standard 70 mm diameter oedometer, as shown in Figure 2. The sample was placed inside the oedometer in contact with the tensiometer, then covered by a load cap to enable vertical loading by the piston. A neoprene membrane was used to cover the soil and cap in order to avoid any evaporation that could cause increase of soil suction. The pore-water pressure u_w measured with the tensiometer corresponds to the soil suctions.

The tensiometer used (Figure 3) is of Imperial College type, which has been successfully used in performing suction measurements under laboratory conditions (Dineen and Burland 1995, Ridley and Burland 1996, Tarantino et al. 2000, Tarantino and Mongiovì 2001, 2002, Ridley et al. 2003). It has provided excellent performance in terms of accuracy, measurement duration and operating tension range (0-1.5 MPa: Tarantino and Mongiovì 2001). It was used by Cui et al. (2007) to monitor field suction changes. The tensiometer consists of a porous ceramic stone with a 1.5 MPa air entry value, a water reservoir 0.1 mm thick and a strain gauge attached to the diaphragm plate.

Soil samples were prepared by compacting soil fragments < 2mm which were re-wetted at different initial water contents, w_i = 12.5, 14.3, 16, 19.8 and 25%, by water spraying. The same mass of dry soil was used for all samples (103.62 ± 0.05 g). Initial compaction was carried out directly in an oedometer to prepare soil samples. The final dimensions of the soil samples were: diameter 70 mm; height 24 mm; corresponding to a bulk dry density of 1.1 Mg m^{-3}.

After producing the soil sample, vertical stresses of 10, 20, 50, 100, 200, 400 and 800 kPa were applied step by step using a controlled pneumatic system. Unloading was carried out following the same stress steps until 50 kPa. Tests were performed under undrained conditions for water phase. The vertical displacement was recorded using two transducers (accuracy of 0.01 mm) installed symmetrically (Figure 2). The final water content was determined by oven-drying at 105°C for 24 h. During loading and unloading, suction changes were continuously monitored by the tensiometer installed on the oedometer. Three compression tests were performed for each initial water content conditions.

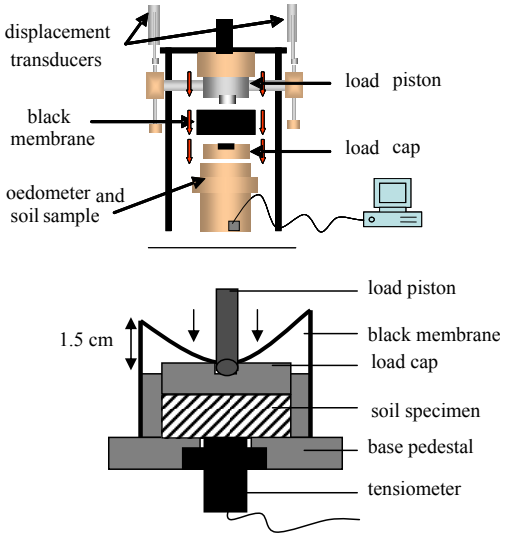

Figure 2. Oedometer equipped with tensiometer for suction monitoring. (Schematic layout of the neoprene membrane covering the oedometer cell: an air pocket of 15 mm high is provided between the membrane and the cell.)

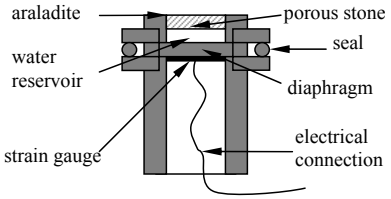

Figure 3. Schematic of Imperial College type tensiometer

RESULTS AND DISCUSSION

Figure 4 presents the water retention curve obtained using the osmotique technique (Series I) and tensiometer in the low suction range of 0-200 kPa. Continuous suctions decrease is observed with increasing water content. The results obtained showed a good correspondence between the two methods.

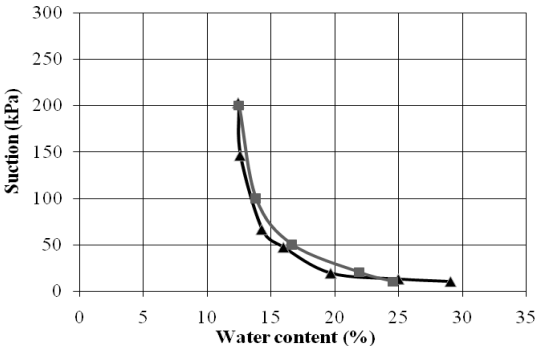

Figure 4. Water retention curve of compacted loamy soil at 1.1 Mg/m^3 dry bulk density measured via osmotic technique (squares) and tensiometer (triangles)

Figure 5 shows suction variation with vertical stress for a soil sample with an initial water content of 16% and an initial dry bulk density of 1.1 Mg m^{-3}. There is a stress threshold σ_t of about 400 kPa after which soil suction decreased. The stress threshold (σ_t) after which soil suction decreased and the corresponding initial suction (s_i) are presented on TABLE 1 for all the samples in the tests with suction measurement. Suction remained constant for soil samples at a water content of 12.5 and 14.3%. For soil samples with a water content higher than 16%, suction initially remained constant up to a stress threshold value (σ_t) after which it decreased. This domain is delimited by a threshold stress (σ_t) which depends on the initial soil suction. The higher the initial suction, the higher the stress threshold: w = 16, 19.8 and 25%, threshold stress σ_t was respectively 400, 200 and 50 kPa, much higher than the corresponding precompression stress (34, 21, 16 kPa). This shows that the threshold stress σ_t would be lower with low precompression stress, but the domain of constant soil suction was larger than that delimited by the precompression stress.

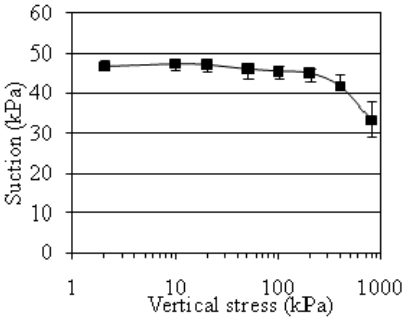

Figure 5. Suction variation with vertical stress for a soil sample with an initial water content of 16% and an initial dry bulk density of 1.1 Mg/m^3. (The points indicate the average values from three tests, while the vertical bars indicate the standard errors.)

Table 1. Results of tests with measurements of soil suction

Initial water content	w_i (%)	12.5	14.3	16	19.8	25
Initial soil suction	s_i (kPa)	146	66	47	19	13
Threshold stress value	σ_t (kPa)	—	—	400	200	50
Precompression stress	σ_p (kPa)	33±2	24±1	34±6	21±2	16±3

Figure 6 presents the variations of compression index C_c with suction obtained with two experimental tests: tests with suction measurement and tests with suction control (Series I). C_c does not vary significantly with suction until 10 kPa for the two tests. Figure 7 shows void ratio (e) versus vertical stress ($\log\sigma_v$) for soil samples of suction measurement test with initial water contents of 16% or 25% and an initial dry bulk density of 1.1 Mg m^{-3}. C_c was calculated from the maximum values of $\Delta e/\Delta\log\sigma_v$ with two σ_v values (50 and 100 kPa for 16%; 20 and 50 kPa for 25%) which were lower than their stress threshold σ_t (400 kPa for 16%; 50 kPa for 25%) (Table 1). The used σ_v values for C_c were always lower than its stress threshold for different initial water contents (Figure 6). The precompression stress, σ_p, was determined by the intersection of two straight lines. Figure 7 shows also that the compression index C_c would be different with changing suction when the applied vertical stress exceeded the stress threshold σ_t.

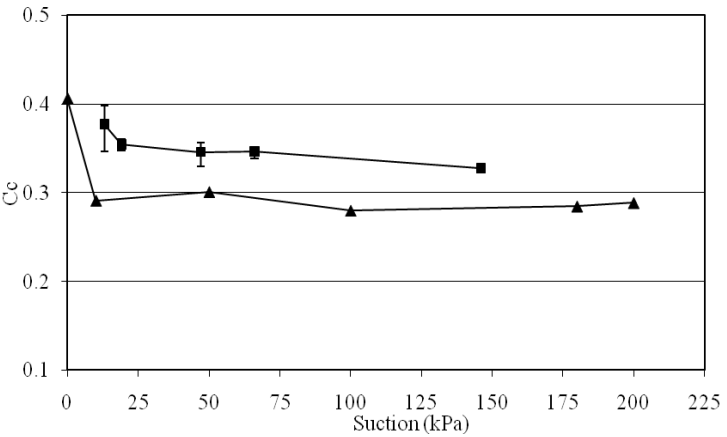

Figure 6. Variations of compression index C_c versus suction obtained from suction measurement tests (squares) and oedometric tests with suction control (Series I) (triangles). (The compression index was estimated from the maximum values of $\Delta e/\Delta\log\sigma_v$ of the compression curve. The points indicate the average values from three tests, while the vertical bars indicate the standard errors.)

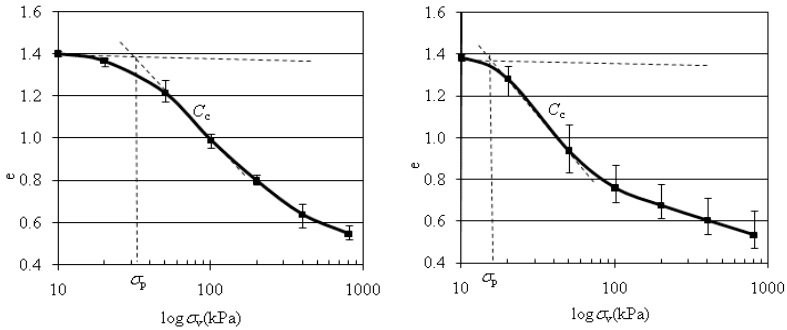

Figure 7. Void ratio versus vertical stress of suction measurement test for soil samples with initial water contents of 16% (left) or 25% (right)

It can be observed that the compression index C_c depends on both the range of suctions (Figure 6 and 7) and the range of applied vertical stress (TABLE 1). Two zones can be identified, as follows:

- Zone 1: applied vertical stress is lower than the stress threshold ($\sigma < \sigma_t$) and soil suction is high ($s >> 0$ kPa). In this zone, the compression index does not vary significantly with suction.
- Zone 2: applied vertical stress is higher than the stress threshold ($\sigma > \sigma_t$) and soil suction is close to zero ($s \approx 0$). In this zone, the compression index was estimated from the maximum values of $\Delta e/\Delta \log \sigma_v$. It can be observed that the results are in agreement with the well known observations on fine-grained unsaturated soils in geotechnical engineering: the compression index decreases when suction increases (e.g. Alonso et al. 1990).

While the preparation at different moisture contents (Series II) produced samples having different initial soil structure, the compression index is also almost constant (0.29) in the suction range between 10 and 200 kPa (the results were not shown in this paper), according to Series I with the same initial soil structure for a bulk dry density of 1.1 Mg m^{-3}.

CONCLUSIONS

The compacted loamy soil studied in this work shows a weak water retention capacity. In terms of compressibility properties, different zones were identified for the variations of compression index; theses zones are separated by a distinct stress threshold. The compression index did not show significant changes when suctions are relatively high and when applied vertical stresses were lower than the threshold stress. Furthermore, the results obtained are in good agreement with most results obtained on fine-grained unsaturated soils: the compression index decreases with increasing suction.

REFERENCES

Alonso, E.E., Gens, A. and Josa, A. (1990). A constitutive model for partially saturated soils. Géotechnique, 40, 405-430.

Arvidsson, J. and Keller, T. (2004). Soil precompression stress. I. A survey of Swedish arable soils. Soil Tillage Res., 77: 85-95.

Cui, Y.J., Tang, A.M., Mantho, A. and De Laure, E. (2007). Monitoring field soil suction using miniature tensiometer. Journal of Geotechnical Testing, 31 (1), 95-100.

Défossez, P., Richard, G., Boizard, H. and O'Sullivan, M. (2003). Modelling change in soil compaction due to traffic as function of soil water content. Geoderma, 116, 89-105.

Delage, P., Howat, M. and Cui, Y.J. (1998). The relationship between suction and swelling properties in a heavily compacted unsaturated clay. Engineering Geology, 50, 31-48.

Delage, P. and Cui, Y.J. (2000). L'eau dans les sols non saturés. Extrait de la collection, Techniques de l'ingénieur, C301, 1-20.

Dineen, K. and Burland, J.B.(1995). A new approach to osmotically controlled oedometer testing. In: Unsaturated Soils, Proceeding 1st International Conference on Unsaturated Soils (ed. E.E. Alonso and P. Delage), 459-465. Balkema, Rotterdam.

Imhoff, S., Da Silva, A.P. and Fallow, D. (2004). Susceptibility to compaction, load support capacity, and soil compressibility of Hapludox. Soil Science Society of America Journal, 68, 17-24.

Larson, W.E., Gupta, S.C. and Useche, R.A. (1980). Compression of agricultural soils from eight soil orders. Soil Sci. Soc. Am. J., 44, 450-457.

Mosaddeghi, M.R., Hemmat, A., Hajabbasi, M.A., Vafaeian, M. and Alexandrou, A. (2006). Plate sinkage versus confined compression tests fir In Situ soil compressibility studies. Biosystems Engineering, 93, 325-334.

Ridley, A.M., and Burland, J.B. (1996). A pore pressure probe for the in situ measurement of a wide range soil suctions. In: Advances in Site Investigation Practice (ed. C. Craig), 510-520. Thomas Telford, London.

Ridley, A.M., Dineen, K., Burland, J.B. and Vaughan, P.R. (2003). Soil matrix suction: some examples of its measurement and application in geotechnical engineering. Géotechnique, 53, 241-253.

Smith, C.W., Johnston, M.A. and Lorentz, S. (1997). Assessing the compaction susceptibility of South African forestry soils. II, Soil properties affecting compactibility and compressibility. Soil Tillage Res., 43, 335-354.

Tarantino, A., Mongiovì, L. and Bosco, G. (2000). An experimental investigation on the independent isotropic stress variables for unsaturated soils. Géotechnique, 50, 275-282.

Tarantino, A. and Mongiovì, L. (2001). Experimental procedures and cavitation mechanisms in tensiometer measurements. Geotechnical and Geological Engineering, 19, 189-210.

Tarantino, A. and Mongiovì, L. (2002). Design and construction of a tensiometer for direct measurement of matric suction. In: Unsaturated Soils, Proc. of 3rd Int. Conf. on Unsaturated Soils (ed. J.F.T. Jucá, T.M.P. de Campos and F.A.M. Marinho). 319-324. Recife, Brasil.

Zhang, H., Hartge, K.H. and Ringe, H.(1997). Effectiveness of organic matter incorporation in reducing soil compactibility. Soil Sci. Soc. Am. J., 61, 239-245.

Model for Prediction of Shear Strength with Respect to Degree of Saturation

Sh. Ma[1], M. Huang[2], Q. Fan[3], X. Zhang[4], and P. Hu[5]

[1] Associate Professor, Guangxi University, Guangxi Nanning 530004, P.R. China; e-mail: mashaokun@sina.com
[2] Professor and Dean, Department of Geotechnical Engineering, Tongji University, Shanghai 200092 , P.R.China, mshuang@tongji.edu.cn
[3] Professor, Guangxi University, Guangxi Nanning 530004, P.R. China; qiuyan@gxu.edu.cn
[4] Professor, Guangxi University, Guangxi Nanning 530004, P.R. China; zhxingui@gxu.edu.cn
[5] Lecturer, School of Civil Engineering and Architecture, University of Jinan, Shandong Jinan 250022, P.R.China; pinghu2002@163.com

ABSTRACT: A new prediction model for unsaturated soil shear strength parameters with respect to degree of saturation is presented in this paper. Details of the model formulation and the determination of model parameters are described and reported. Introducing shear strength parameters of saturated soil, the model can be used in practice engineering involving both unsaturated soils and saturated soils. Moreover, more soil engineering characteristics can be captured in the new model compared with previous analogous models. The validity of this model is verified through a number of shear strength data available in the published literature. To verify the model against Yunnan red clay from China, a series of constant-water content triaxial tests have been carried out on both saturated and unsaturated specimens. Details of the experimental program and results are presented in this paper.

INTRODUCTION

The contribution of matric suction to soil's shear strength needs to be evaluated and its stability further examined (Terzaghi et al. 1996). Relationships between water content and shear strength are often useful for geotechnical designs. Several semi-empirical functions have been proposed in recent years to predict shear strength of unsaturated soils using the soil-water characteristic curve (Fredlund et al. 1996, Vanapalli et al. 1996, Khalili et al. 1998). However, in-situ stress states and drying-wetting induced hysteresis are ignored in these equations.

Meanwhile, some empirical shear strength functions with respect to matric suction have also been presented (Escario et al. 1989, Tekinsoy et al. 2004, Shen 1996). Although these shear strength functions have been found to be consistent with observed experimental behavior in some range of degree of saturation, experimental measurements of matric suction are difficult, time-consuming and require costly laboratory facilities. This has, to some degree, limited the application of the shear strength theories mentioned above in the research and academic arenas. It is therefore important to develop a simpler approach for predicting the shear strength of an unsaturated soil for various engineering applications. The degree of saturation is relatively easy to be measured, so a shear strength formula based on saturation degree instead of suction has valuable significance in practical engineering. The contribution of matric suction to shear strength can be taken into account via total stress analyses under undrained condition. In this paper, a model based on parameters of saturated soil has been developed to predict the shear strength of an unsaturated soil.

CONSTANT-WATER CONTENT TRIAXIAL TEST PROGRAM

Triaxial tests were conducted using a GDS Unsaturated Triaxial Testing System for soils (UNSAT). The initial consolidation process was carried out in the same manner for both the constant-water content (CW) test and the consolidated drain (CD) test. Once equilibrium conditions were achieved under the applied pressures (i.e., isotropic confining pressure σ_3, pore-air pressure u_a, and pore-water pressure u_w), the specimen was sheared under drained conditions for the pore-air phase and undrained conditions for the pore-water phase. The pore-air pressure is maintained at the value to which the specimen was subjected during consolidation stage. On the other hand, the pore-water pressure is measured by the pressure transducer mounted on the base plate (Fredlund and Rahardjo 1993).

Test Specimens

Triaxial specimens in this study consisted of red clay obtained from Kunming~Anning highway KO+592 segment, Yunnan province, in south-west China. Yunnan red clay is usually homogeneous, soft and highly adhesive. The proportion of clay with particles diameter less than 0.005mm can reach 55%~70%, and particles are quite uniform and highly dispersive. The predominant minerals include kaolinite, illite, montmorillonite, chlorite, and quartz. Triaxial specimens were 38 mm in diameter, 76mm high, and all prepared by static compaction. The physical properties and state indices of triaxial test specimens are summarized in Table 1.

Stress Paths

In order to obtain total stress parameters c and ϕ with different degree of saturation, three series of constant-water content triaxial tests were carried out. The consolidation

stage of every series is undertaken under constant suction, so that the water content of the specimens is identified before shearing. Degrees of saturation are 60%, 75% and 100%, respectively, and the corresponding suctions are 210 kPa, 50 kPa and 0 kPa, according to the soil-water characteristic curve.

Table 1. Physical/mechanical properties and state indices of red clay specimens

Specific gravity G_S	**Liquid limit** ω_L	**Plastic limit** ω_P	**Plasticity index** I_P	**Free swell index** δ_{ef}	**Wet density** ρ (kg/m^3)	**Void ratio** e	**Water content** ω
2.87	43%	24%	19	30	1.832×10^3	0.95	25.1%

Figure1 shows a schematic diagram illustrating the stress paths adopted in the tests. A typical stress path induced on an isotropically compressed and saturated soil specimen is denoted as $O-C-D-E-F$, where $O-C-D$ is the wetting path during saturation of the initially unsaturated specimen and $D-E$ and $E-F$ are the stress paths for isotropic compression and undrained shearing, respectively. For tests on unsaturated soil, specimens were tested at required initial suctions by following either path $O-C-D-G$ at suction = 50 kPa, or path $O-C-D-G'$ at suction = 210 kPa. The specimens were isotropically compressed to net mean stress values of 100 kPa, 200 kPa, and 400 kPa (e.g. $G-X$ or $G'-X'$), respectively, and then sheared under a constant-water content condition (e.g. $X-Y$ or $X'-Y'$).

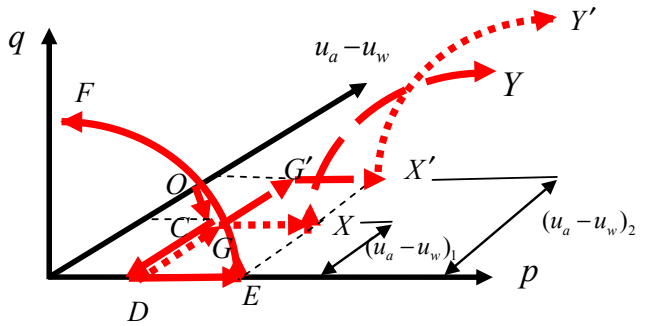

Figure 1. Typical stress paths performed during constant-water content triaxial tests

As shown in Figure1, a three-dimension stress space *p:q:s* is defined in terms of three state variables as follows: net mean stress, p = (1/3) (σ_1+ 2σ_3) - u_a); deviator stress, ($q=\sigma_1-\sigma_3$); and, matric suction, s = (u_a-u_w); where σ_1 is the major principle stress, and σ_3 is the minor principle stress.

Shear Strength Envelopes

Figure 2 shows the strength envelopes obtained for different degrees of saturation. Shear strength parameters such as total cohesion c and friction angle ϕincrease with the reduction of degree of saturation. Moreover, the effect on total cohesion is more pronounced than that on friction angle. These results are consistent with previous experiment data reported by Escario et al. (1990), Yang et al. (2003), and Ling and Yin (2007).

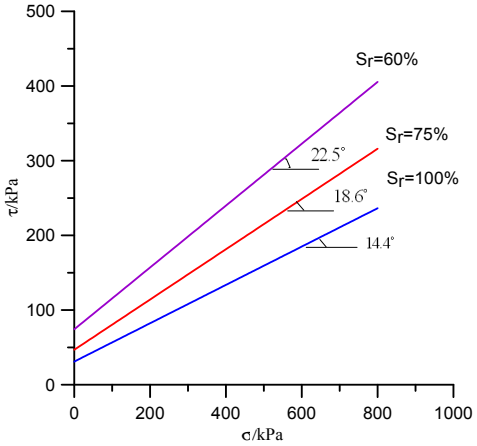

Figure 2. Total stress strength envelopes from triaxial tests

UNSATURATED SOIL SHEAR STRENGTH FUNCTION

The contribution of matric suction on shear strength is often taken into account in terms of total strength parameters under undrained condition. In the past few decades, numerous researchers (Yang et al. 2003, Ling and Yin 2007) have proposed different semi-empirical shear strength models with respect to water content. However, their models can be best-fitted to experimental data only in a certain narrow range of high degrees of saturation, and may become unfeasible for lower degrees of saturation or higher suctions. The reason may be that their tests were mainly carried out under low suction or high saturation.

Escario et al. (1990) investigated shear strength of unsaturated soil by direct shear tests under controlled suction (up to 15 MPa). Three soil types such as Madrid grey clay, Guadalix red clay, and Madrid clayey sand, which cover a wide range of soil materials, were used. It was found that the shear strength increases up to a certain maximum for considerably high suctions. The relations between suction and shear strength in terms of total strength parameters c and $\phi$for Guadalix red clay and Madrid clayey sand were plotted as shown in Figure3. Naturally, the total strength parameters c and ϕincrease up to a maximum for greater suctions, and the effect of suction on apparent cohesion is more apparent than that on friction angle.

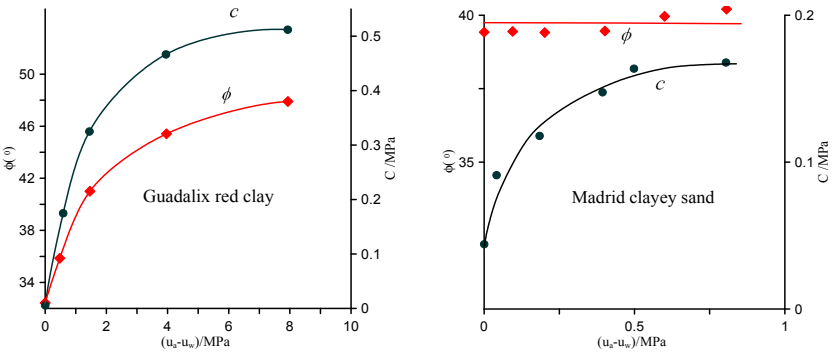

Figure 3. Variation of c and ϕ with suction (modified after Escario et al. 1990)

Based on previous experimental results (Escario et al. 1990, Yang et al. 2003, Ling and Yin 2007), a new semi-empirical shear strength model with respect to degree of saturation is proposed herein as follows:

$$c = c_0 \mathrm{e}^{a(1-S_r^b)} \tag{1}$$

$$\varphi = \varphi_0 + d \ln\left(\frac{S_r^2 + 1}{2}\right) \tag{2}$$

where S_r is the degree of saturation; a, b, and d are soil parameters expressed as functions of the degree of saturation; c_0 and ϕ are cohesion and friction angle of saturated soil, respectively. It can be concluded from Eqs. (1) and (2) that c and ϕ will be constant when S_r infinitely tends to zero (i.e., higher suctions), which is consistent with previous experimental results reported by Escario et al. (1990).

COMPARISION WITH EXPERIMENTAL RESULTS

The validation of the new model proposed in this paper should be verified against laboratory test results. Figure 4 shows the model predictions and experimental data reported by Ling and Yin (2007). It can be seen that the new model can predict reasonably well the shear strength parameters. According to the model proposed by Ling and Yin (2007), c and ϕ will be very large for low S_r, and zero or negative for higher S_r since the model proposed by Ling and Yin.(2007) is a linear function. Thus it can be used in very limited range. The model proposed in this paper overcomes these disadvantages. Furthermore, it can be inferred that the effect of the saturation degree on total cohesion is more obvious than that on friction angle, as shown by both the model predictions and the experiment data.

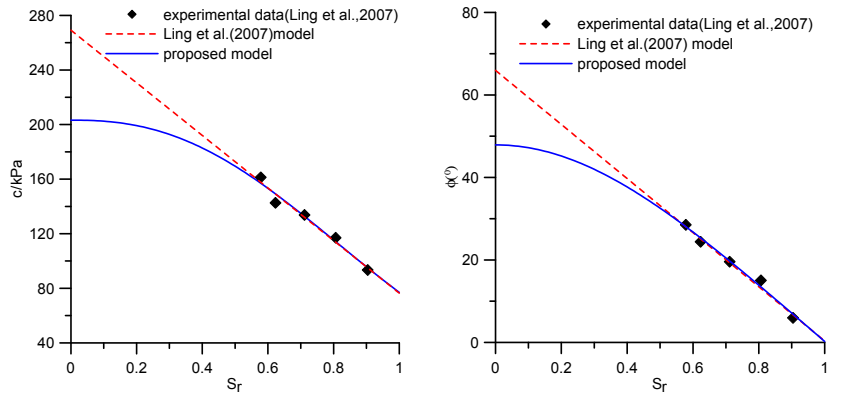

Figure 4. Comparison of predicted and experimental total strength parameters

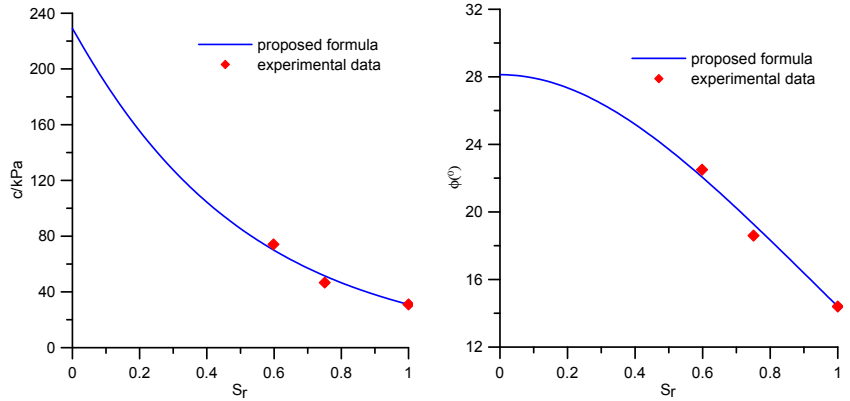

Figure 5. Predicted and experimental total strength parameters for Yunnan red clay

Figure 5 shows the model predictions and experimental data for Yunnan red clay used in this study. It can be seen that the models can predict reasonably well the shear strength parameters. An empirical model based on results for Yunnan red clay can be proposed as follows:

$$c = c_0 \mathrm{e}^{a(1-S_\mathrm{r}^b)} = 31\mathrm{e}^{2(1-S_\mathrm{r}^{1.02})} \tag{3}$$

$$\varphi = \varphi_0 + d\ln\left(\frac{S_\mathrm{r}^2+1}{2}\right) = 14.4 - 19.8\ln\left(\frac{S_\mathrm{r}^2+1}{2}\right) \tag{4}$$

CONCLUSIONS

An empirical model based on parameters of saturated soil was developed to predict the shear strength of an unsaturated soil. Given the introduction of saturated shear strength parameters, the proposed model could be used in engineering applications involving both unsaturated and saturated soils, with only a few soil parameters needed in its use. Moreover, the model is capable of capturing some key observed features, such as the shear strength increasing up to a maximum with suction, and a more pronounced effect of suction on apparent cohesion than on apparent friction angle.

ACKNOWLEDGMENTS

This research project was financially supported by research grant No.2004 318 223 11 provided by the National West Communication Construction Technology Project. The authors also wish to thank Associate Professor Chen bao at the Tongji University in China and Liu yi-lin at Highway Research Institute of Ministry of Communications in China for their invaluable discussion with the project.

REFERENCES

Escario, V. and Juca, J. (1989). Strength and deformation of partly saturate soils. Proceedings of the 12th International Conference on Soil Mechanics and Foundation Engineering. 11. Rio De Janeiro, Brazil.p.43–46.

Fredlund, D. G. and Rahardjo, H. (1993). Soil Mechanics for Unsaturated Soils John Wiley and Sons, New York.

Fredlund, D.G., Xing, A., Fredlund, M.D., and Barbour, S.L.(1996). The relationship of the unsaturated soil shear strength to the soil-water characteristic curve." Canadian Geotechnical Journal, 33(3):440-448.

Khalili, N. and Khabbaz, M.H. (1998). A unique relationship for $\chi$for the determination of the shear strength of unsaturated soils. Geotechnique. 48(5):681–687.

Ling, H., Yin, Z.Z. (2007). Variation of unsaturated soil strength with water contents. Chinese Journal of Rock Mechanics and Engineering.26(7):1499-1503 (in Chinese).

Shen, Z.J. (1996). The problems in the present studies on mechanics for unsaturated soils. Proceedings of the Symposium on Geotechnical Aspects of Regional Soils. Nanjing, China: Atomic Energy Press, 1–9. (In Chinese).

Terzaghi, K., Peck, R.B. and Mesri, G. (1996). Soil mechanics in engineering practice. Third ed., John Wiley and Sons Inc., New York.

Tekinsoy, M A., Kayadelen, C., Keskin, M.S., et al. (2004). An equation for predicting shear strength envelope with respect to matric suction. Computers and Geotechnics. 31(7):589–593.

Vanapalli, S.K., Fredlund, D.G., Pufahl, D.E. et al. (1996). Model for the prediction of shear strength with respect to soil suction. Canadian Geotechnical Journal, 33(3):379–392.

Yang, Q., He, J. and Luan, M.T. (2003). Comparative study on shear strength of unsaturated red clay and expansive soils. Rock and Soil Mechanics. 24(1):13–16 (in Chinese).

Simple Modeling of Stress-strain Relation for Unsaturated Soil

H. Kyokawa[1], M. Kikumoto[2], T. Nakai[3], and H. Shahin[4]

[1] Graduate student, Department of Civil Engineering, Nagoya Institute of Technology, Goikso-cho,
Showa-ku, Nagoya, 466-8555, Japan; kyo5810@tuti1.ace.nitech.ac.jp
[2] Assistant professor, ditto
[3] Professor, ditto
[4] Associate professor, ditto

ABSTRACT: Though stress-strain characteristics of unsaturated soils are complicated and rather different from those of saturated soils, it should be described properly by a constitutive model for soils because soil usually stays under an unsaturated condition in actual field. In the current study, a simple elastoplastic model for saturated soil is extended to one applicable to unsaturated soils. The proposed model is formulated using the Bishop's effective stress and the residual strength is, therefore, assumed to be constant. In the proposed model, the decrease (or increase) in the degree of saturation is linked with upward (or downward) movement of normally consolidated line in the compression plane of mean effective stress and void ratio, by which the typical volumetric and distortional behaviors of unsaturated soils are properly described. In addition, a simple method to extend classical water retention curves such as van Genuchten's equation to be able to incorporate the influences of suction histories and density is proposed and applied to the proposed model. In the present paper, the outline of the proposed model is explained and applicability of the model is discussed through typical results of simulations.

INTRODUCTION

It is usually known that suction, which is surface tension of the void water remaining around the soil particles, increases the stiffness and strength of unsaturated soils. Compression behavior of an unsaturated soil is compared with that of saturated sample in Figure 1 (Honda 2000).

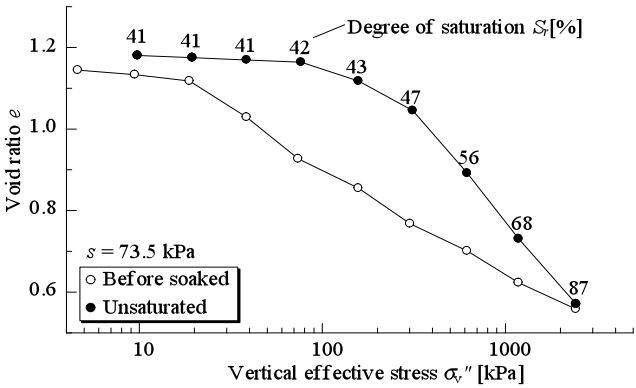

Figure 1. Results of consolidation tests under constant suction (after Honda 2000)

Closed plots in this figure indicate the result of drained water and exhausted air one-dimensional consolidation test under constant suction, s = 73.5 kPa on Catalpo clay, besides several values of the degree of saturation are indicated. Opened plots show the corresponding result of the saturated sample. In this figure, the proposed vertical effective stress defined as eq. (1) by Bishop (1959) is plotted against void ratio.

$$\sigma_{ij}'' = \sigma_{ij} - u_a\delta_{ij} + \chi(u_a - u_w)\delta_{ij} = \sigma_{ij}^{net} + S_r s\delta_{ij} \tag{1}$$

In equation (1), a parameter χ is given as a function of the degree of saturation S_r and is assumed to be equal to S_r for simplicity. It can be seen from Figure. 1 that the unsaturated sample initially shows relatively high stiffness and stays in a looser state under a same confining pressure compared with saturated sample. The unsaturated soil sample then undergoes significant compression from a stress level of around 200 to 300 kPa due to subsequent consolidation, the degree of saturation increases due to the volumetric compression and the compression line of the unsaturated sample finally approaches to the asymptotes similar to that of normally consolidated, saturated sample.

In the current study, an elastoplastic model for saturated soils (Nakai et al. 2009) is extended in order to describe the typical behaviors of unsaturated soils. The behavior of unsaturated soil is modelled relatively simply through the following two phases, i.e., (a) soil having a lower degree of saturation is able to stay in a looser state in the plane of confining pressure and void ratio compared with that having a higher degree of saturation; (b) the degree of saturation varies not only for the suction but also for the variation of the void ratio (density).

It is shown that collapse behavior of unsaturated soil during soaking process, which is volumetric compression due to the degradation of the surface tension due to the reduction of suction, can be also explained by the proposed model.

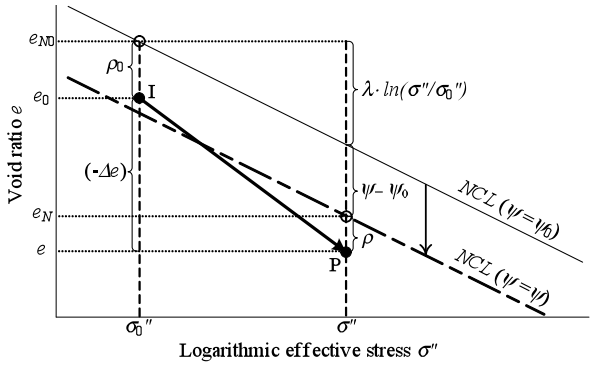

Figure 2. Volumetric mechanism of unsaturated soils in the proposed model

ONE DIMENSIONAL CONSTITUTIVE MODEL FOR UNSATURATED SOIL

A simple one-dimensional model for unsaturated soil, which is formulated based on the unified method to describe the influences of the various characteristics of soil (Nakai et al. 2009) using Bishop's effective stress, is presented in this section. In order to describe the behavior of unsaturated soils explained in the previous section, normally consolidated line (*NCL*) is shifted downward / upward in the plane of void ratio e and effective confining stress σ depending on the increase / decrease of the degree of saturation without changing its shape. Figure 2 shows the outline of the model for unsaturated soils considering the influence of the variation of the degree of saturation. In the proposed model, the position of the *NCL* in the compression plane is always changing with the variation in the degree of saturation. Vertical distance of the current *NCL* from that of the saturated sample is, hence, defined as a state variable ψ to represent the new position of the *NCL*. e_N is the reference void ratio on the *NCL* under the same confining pressure. $\rho (= e_{NC} - e)$ is a state variable representing the influences of density and confining pressure, which is defined as the difference of void ratio from the current state to the *NCL*. Points I ($\sigma'' = \sigma''_0$, $e = e_0$, $\rho = \rho_0$) and P ($\sigma'' = \sigma''$, $e = e$, $\rho = \rho$) represent the initial state and the current state, respectively. The change in void ratio ($-\Delta e$) of an overconsolidated, unsaturated soil is, then, divided into three components as Eq. (2):

$$(-\Delta e) = \{(e_{N0} - e_N) - (\rho_0 - \rho)\} = \lambda \ln \frac{\sigma''}{\sigma_0''} - (\rho_0 - \rho) - (\psi_0 - \psi) \quad (2)$$

where the first term $\lambda \ln(\sigma''/\sigma''_0)$ is equivalent to the volume change of the normally consolidated soil (λ is compression index), the second term $\rho - \rho_0$ ($= d\rho$) represents

the effect of overconsolidation, and ψ - ψ_0 represents the influence of "unsaturated state" through the vertical shift of the *NCL*. The vertical shift of the *NCL* of unsaturated soils is assumed to be proportional to the variation in the degree of saturation as follow:

$$\psi(S_r) = -l(1 - S_r) \tag{3}$$

where l is a material parameter. Assuming a usual nonlinear elastic relation as Cam clay model, the plastic component of the change of void ratio ($-\Delta e$)^p is obtained as follow.

$$(-\Delta e)^p = (-\Delta e) - (-\Delta e)^e = (\lambda - \kappa)\ln\frac{\sigma''}{\sigma_0''} - (\rho_0 - \rho) - (\psi_0 - \psi) \tag{4}$$

This equation can be rewritten and a yield function f of the general elasto-plastic theory is introduced as equation (5).

$$f = F - \{H + (\rho_0 - \rho) + (\psi_0 - \psi)\} \quad where \quad F = (\lambda - \kappa)\ln\frac{\sigma''}{\sigma_0''}, H = (-\Delta e)^p \tag{5}$$

The state variable ρ, which represents the influence of density and confining pressure, is assumed to decrease with the development of the plastic deformation. An evolution law for the state variable ρ is, hence, given as equation (6).

$$d\rho = -G(\rho)(-\Delta e^p) = -a\rho(-\Delta e^p) \tag{6}$$

where a is a material parameter. From the consistency condition (df = 0), a one-dimensional constitutive relationship of unsaturated soils is obtained.

$$d(-e) = d(-e)^p + d(-e)^e = \left\{\frac{\lambda - \kappa}{1 + G(\rho)} + \kappa\right\}\frac{d\sigma''}{\sigma''} + \frac{1}{1 + G(\rho)}\frac{d\psi}{dS_r}dS_r \tag{7}$$

Loading condition is given simply by assuming that the plastic component of the variation of void ratio is always compressive as follow:

$$\begin{cases} d(-e) = d(-e)^e + d(-e)^p & if \quad d(-e)^p > 0 \\ d(-e) = d(-e)^e & if \quad d(-e)^p \le 0 \end{cases} \tag{8}$$

MODELING OF WATER RETENTION CURVE CONSIDERING THE INFLUENCE OF HYSTERESIS AND DENSITY

A model for water retention curve is necessary in order to formulate a constitutive model for unsaturated soils using the degree of saturation as a key parameter. It is well-known that suction has a dominant effect on the water retention of unsaturated soils and soil water retention curves usually trace different paths according to drying and wetting. It is also indicated through some experimental studies (e.g. Tarantino and

Tombolato 2005) that volumetric behaviour also influences the water retention characteristic and the degree of saturation, thus, rises due to volumetric compression even if suction is kept constant (Figure 1). Therefore, in the present study, a simple model for the water retention curve of unsaturated soils, which can consider not only the influence of suction but also the influences of hydraulic hysteresis and density, is proposed.

In order to keep the formulation of the model as simple as possible, a well-known, classical equation for water retention curves proposed by van Genuchten (1980) is extended. Firstly, the hydraulic hysteresis effect due to the suction history is described. Figure 3 shows the schematic diagram of the modelling. Two curves representing the highest and the lowest boundaries of the degrees of saturation, which are usually called the main drying curve and the main wetting curve respectively, are described by the non-hysteretic van Genuchten's equation as follows.

$$f_d(S_r, s) = S_{\min} + (S_{\max} - S_{\min})\left[1 + (\alpha_d s)^n\right]^{-m} - S_r = F_d(s) - S_r = 0 \tag{9}$$

$$f_w(S_r, s) = S_{\min} + (S_{\max} - S_{\min})\left[1 + (\alpha_w s)^n\right]^{-m} - S_r = F_w(s) - S_r = 0 \tag{10}$$

where S_{min}, S_{max}, n, m and α are material parameters for van Genuchten's equation and the subscripts d and w of the parameter α denote that for the main drying and wetting curves, respectively. As any state of water retention lies between two main curves, a variable I_w defined as the ratio of interior division of the current state between two reference states on the main curves is introduced as an intermediary in the proposed model as follows:

$$I_w = \frac{S_r - S_r^w}{S_r^d - S_r^w} \tag{11}$$

where S_r^d and S_r^w are degrees of saturation of the reference states on the main drying and wetting curves under current suction, respectively. This variable I_w bound by 0 for the main wetting curve and 1 for the main drying curve provides a simplified, scalar representation of the current state of hydraulic hysteresis. It increases monotonically from 0 to 1 as the degree of saturation decreases, and vice versa. An evolution law for this state variable I_w is, therefore, given as equation (12).

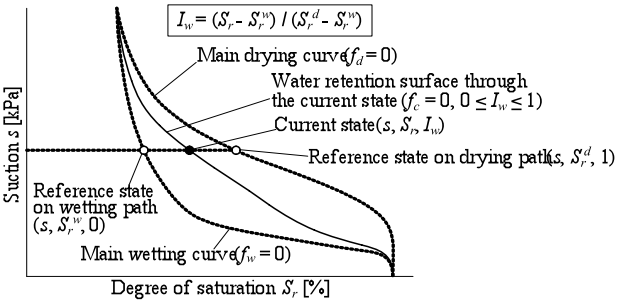

Figure 3. Modelling of the hydraulic hysteresis effect

$$dI_w = h(I_w)dS_r = \begin{cases} -\xi(1-I_w)^3 dS_r & when \;\; dS_r \le 0 \\ -\xi I_w{}^3 dS_r & when \;\; dS_r > 0 \end{cases} \tag{12}$$

From equations (9), (10) and (11), a function f_c representing the water retention surface through the current state (s, S_r, I_w) is given as follow.

$$f_c(s, S_r, I_w) = I_w F_d(s) + (1-I_w)F_w(s) - S_r = 0 \tag{13}$$

As any hydraulic state of unsaturated soil always locates on the water retention surface, the incremental form of the water retention curve is given by applying the consistency condition $df_c = 0$ to equation (13).

$$dS_r = \frac{\partial f_c}{\partial s} ds \left[1 + \frac{\partial f_c}{\partial I_w} h(I_w) \right]^{-1} \tag{14}$$

Secondly, the influence of volume change on the water retention is considered by applying a modified suction s^* defined by equation (15) in stead of the ordinary suction s.

$$s^* = s \left(\frac{e}{N_{sat}} \right)^{\xi_e} \tag{15}$$

ξ_e is a material parameter controlling the influence of density and N_{sat} represents the reference void ratio of saturated, normally consolidated soil under atmospheric pressure. The modified suction s^* varies due to the variation of void ratio, and the increase in the degree of saturation induced by the volumetric compression as indicated in Figure 1 can be taken into account in the proposed model. In addition, as the influence of the volume change is considered in the modified suction s^*, any model for water retention curve can easily be extended by replacing the ordinary suction with the modified suction s^*.

VERIFICATION OF PROPOSED MODEL BY PARAMETRIC STUDY

In order to verify the proposed model, a series of simulations of consolidation tests under constant suction and subsequent soaking tests are carried out. Tables 1 and 2 show the material parameters for Fujinomori clay. Figure 4 shows the calculated results of consolidation tests under constant suction (s = 49, 98, 196, 294 kPa) on over consolidated Fujinomori clay. In the calculation, suction is firstly increased to a prescribed value from saturated initial state, and consolidation tests are, then, carried out. Figures (a) and (b) show the variations of void ratio and degree of saturation with net stress σ_{net} (= σ - u_a), respectively. It is indicated from Figure 4 that the proposed model can describe the typical unsaturated soil behaviours such as: unsaturated soil

initially shows relatively high stiffness and it can stay in a region looser than the *NCL* for saturated one; unsaturated soil undergoes a significant compression from a certain stress level, the degree of saturation increases in response to the volumetric compression and compression line of unsaturated soil finally converges to the *NCL* similar to the saturated one. It is also known that the sample having larger suction and lower degree of saturation shows stiffer behaviour.

Table 1. Material parameters for stress-strain relationship

λ	0.104	Compression Index	a	100	Effect of over consolidated
κ	0.01	Swelling Index	l	5.0	Effect of unsaturated
N	0.83	Void ratio under 98kPa			

Table 2. Material parameters for water retention relationship

$S_{r\min}$	10.0	Minimum S_r	m	0.1	Shape of main drying / wetting curve
$S_{r\max}$	100.0	Maximumu S_r	n	2.0	
α	0.03	Position of main drying curve	ξ	100	Influence of suction histories
β	0.10	Position of main wetting curve	ξ_e	5.0	Influence of void ratio

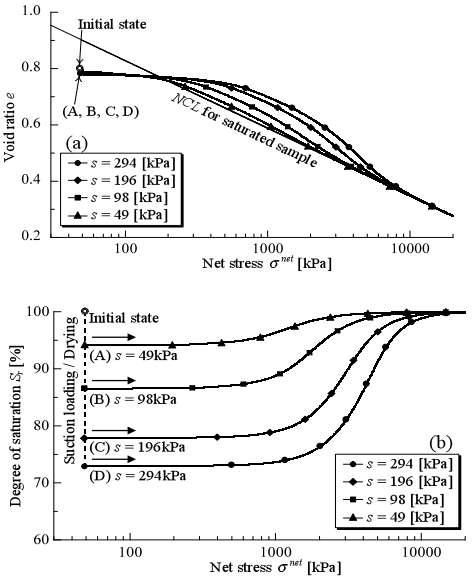

Figure 4. Simulations of consolidation tests under constant suction

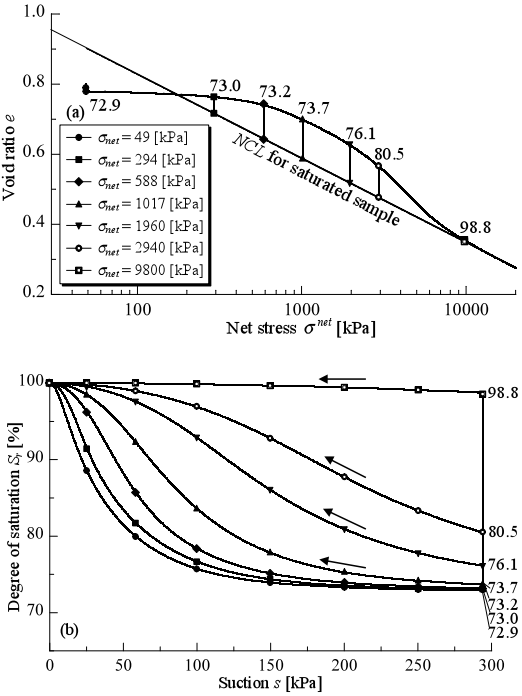

Figure 5. Simulations of soaking tests under constant net stress

Figure 5 shows the calculated results of soaking test. The samples are, firstly compressed to a prescribed net stress (σ_{net} = 49, 294, 588, 1017, 1960, 2940, 9800 kPa) under constant suction of 294kPa and they are, then, saturated by decreasing suction to zero. Figure (a) shows the relationship between net stress and void ratio, while (b) shows the relationship between suction and degree of saturation during soaking. It is seen from Figure 5 that the proposed model suitably reproduces typical soaking collapse behaviours of unsaturated soils, which are usually reported by the past experimental studies (e.g. Jennings and Burland 1962). It is also known that the proposed model suitably predicts the difference of the amount of volume change due to the stress level. Moreover, the proposed model can describe the soaking-induced expansive behaviour of unsaturated, over consolidated sample, which are qualitatively similar to the experimental results by Sun et al. (2007).

CONCLUSIONS

A simple method, by which ordinary elasto-plastic model for saturated soils can be extended to one incorporating necessary descriptions of different aspects of constitutive behaviour of unsaturated soils, has been developed. The main issues in modelling the unsaturated soil behaviour are: (a) volumetric behaviour related with the variation in the degree of saturation; (b) hydraulic behaviour associated with saturation, suction, hydraulic hysteresis or void ratio changes. The proposed constitutive model is formulated using the Bishop's effective stress and normally consolidated line which is shifted downward or upward in the void ratio e and logarithm of confining pressure σ plane depending the increase or decrease in the degree of saturation. A simple method for extending ordinary classical models for water retention curves, by which the effects of hydraulic hysteresis and void ratio can be simply incorporated, has also been proposed. Validity of the proposed model for unsaturated soils is checked through a series of simulations of consolidation and collapse tests on unsaturated soils and typical behaviours of unsaturated soils such as soaking collapse phenomena are suitably described by the proposed model.

REFERENCES

Bishop, A. W. (1959). The principle of effective stress, Teknisk Ukeblad, 39, 859-863.

Honda, M. (2000). PhD Thesis, Kobe University, Japan.

Jennings, J. E. B. and Burland, J. B. (1962) Limitations to the use of effective stresses in partly saturated soils, Géotechnique, 12(2), 125-144.

Nakai, T. et al. (2009) Simple and unified method for describing various characteristics of geo materials - Influences of density, bonding, time effects and others, Applied Mechanics, JSCE, 12, 371-382 (in Japanese).

Sun, D., Sheng, D. and Xu, Y. (2007) Collapse behavior of unsaturated compacted soil with different initial densities, Can. Geotech. J., 44, 673-686.

Tarantino, A. and Tombolato, S. (2005) Coupling of hydraulic and mechanical behavior in unsaturated compacted clay, Géotechnique, 55(4), 307-317.

Vvan Genuchten, M. Th. (1980) A closed-form equation for predicting the hydraulic conductivity of unsaturated soils, Soil Sci. Soc. Am. J., 44, 892-898.

Effect of Stress Paths on Shear Strength Response of Unsaturated Gassy Sand from Hangzhou Metro Project

Y. Wang[1], H. Tian[1], and Y. Fan[1]

[1] Institute of Rock and Soil Mechanics, Chinese Academy of Sciences, State Key Laboratory and Geotechnical Engineering, Wuhan, Hubei 430070, China; email: wang831yong@163.com; thn2006@163.com; fanyoujie1985@163.com.

ABSTRACT: To study the effects of stress paths on shear strength characteristics of unsaturated sand, a series of conventional triaxial compression (CTC), reduced triaxial compression (RTC), and reduced triaxial extension (RTE) tests were conducted on shallow gassy sand from the Hangzhou Metro project, China. Tests were carried out by using a stress path unsaturated triaxial test system, capable of reproducing stress paths that are normally induced on soils in subway construction projects. Results show that the stress-strain relationship of unsaturated sand under various stress paths has different characteristics and the strength parameters are closely related to the particular stress path followed. Effective cohesion and apparent cohesion are affected significantly by the stress path, but effects on the internal friction angle are not important. Relationships between apparent cohesion and matric suction from various stress paths induced on unsaturated sand can be described via power functions. A unified shear strength model was then devised for gassy sand along different triaxial stress paths.

INTRODUCTION

Stress path refers to the stress trajectory that a point within a soil mass has been subject to under external forces, which defines the pattern stress variation (Feng 2007). The mechanical response of the soil is not only related to the distribution and magnitude of these forces, but also to the experienced stress path. A soil sample tested under different stress paths will lead to varying characteristics in terms of strength and deformation. Stress paths can simulate the true process of stress variations in the soil mass in actual geotechnical projects, revealing the effects of the process on soil mechanical properties. Research on this topic is essential to assessing feasible design parameters in practice and to establish the constitutive laws governing soil behavior considering its stress path

dependency. The majority of previous findings on stress path effects are related to soils under saturated state, while studies focusing on stress path effects on unsaturated soil response have been scarcely reported (Lade et al. 1976 and Jeda 1994).

The Hangzhou Metro project in China, currently under construction, involves sandy soils with a considerable presence of gases, mainly composed of methane, which were subjected to high pressure during the course of this investigation. The presence of this gas in the soil poses a threat to the entire construction project. The shallow gas mainly buries in sand lenses or sand pockets with larger porosity. The sand is called shallow gassy sand, belonging to a special unsaturated soil. The gas is closed, isolated from the atmosphere and its gaseous phrase is interconnected. A common phenomenon in gassy soil is the unloading or sudden drop in the gas pressure. Recently, engineering disasters and accidents induced by shallow gas have been increasingly reported (Tang et al. 1996, Xu et al. 2003).

Using a GDS type unsaturated triaxial test system, capable of simulating typical stress paths experienced by soils in subway construction projects, a series of triaxial tests at different matric suction and net stress states were conducted on several triaxial specimens of unsaturated gassy sand, sampled from the Hangzhou Metro project, in order to study the effects of stress paths on the shear strength parameters of unsaturated soil materials.

SOIL SAMPLES AND TESTING METHOD

Soil samples were taken from critical sections in Hangzhou Metro. Gassy sand is green-grayish, containing humic organic matters and a small amount of shell debris. Average dry density of the gassy sand is 1.54g/cm^3, void ratio 0.733, porosity 42%, and relative density of 0.67 (medium dense sand). Test results from grain size analysis are shown in Table 1. The soil classifies as well-graded silty sand with only a small fraction of clay, uniformity coefficient 19.7 and coefficient of curvature 7.5. Soil water characteristic curve (SWCC) of gassy sand was measured in a 5 bar ceramic plate extractor and the results are shown in Figure 1**.** Air-entry value of gassy sand is about 5 kPa, with residual volumetric water content about 15%, corresponding to a matric suction of 18-20 kPa. Therefore, the triaxial tests focused on shear strength characteristics of gassy sand under matric suction states within 100 kPa.

Table 1. Grain size distribution of gassy sand from Hangzhou MTR project

Soil Type	Percentage of the Particle Composition (%)				
	>0.5mm	**0.5-0.25mm**	**0.25-0.075mm**	**0.075-0.005mm**	**<0.005mm**
Silty Sand	0.8	3.0	73.5	14.6	8.1

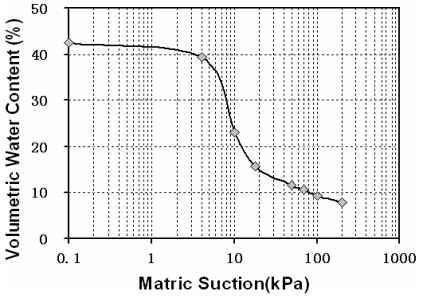

Figure 1. SWCC of gassy sand from Hangzhou MTR project

There are mainly three types of stress paths that are usually experienced by most soils involved in subway construction projects. Conventional triaxial compression (σ_3 unchanged, while σ_1 increased, CTC) is a loading stress path representing the stress state of soil when the surface of semi-infinite body is under a uniform load. Reduced triaxial compression (σ_1 unchanged, while σ_3 decreased, RTC) and reduced triaxial extension (σ_3 unchanged, while σ_1 decreased, RTE) are both unloading stress paths describing the stress states of a soil when a tunnel or foundation pit are excavated, respectively.

A series of CTC, RCT and RTE triaxial tests were performed in a GDS type unsaturated triaxial test system to study the effects of various stress paths on shear strength properties of gassy sand. Matric suction, $s = (u_a - u_w)$, of the samples were controlled at 0 kPa, 10 kPa, 30 kPa and 100 kPa, under corresponding net confining pressures, $(\sigma - u_a)$, of 100 kPa, 200 kPa and 300kPa, respectively. Samples have a 50 mm diameter and 100 mm height. Samples were prepared into a controlled dry density of 1.54g/cm^3. In all cases, shearing stage was carried out after isotropic consolidation and pore-fluid equalization. CTC stress paths were carried out via strain-controlled with a strain rate of 0.075 mm/min. Both RTC and RTE stress paths were carried out via stress-controlled with a stress rate of 0.1 kPa/min.

TEST RESULTS AND ANALYSIS

Deviatoric stress versus strain response of gassy sand for various stress paths is shown in Figure 2. It can be readily noted that the stress-strain response is highly stress-path dependent. Under CTC stress paths, in most cases the stress-strain curves do not show a peak stress before failure, while showing strain-hardening phenomenon. Only at lower net confining pressures and higher suction states, a slight strain-softening phenomenon is observed. Under RTC stress paths, the stress-strain curves of gassy sand show a rigid-plastic response, with the soil reaching a peak strength under small strains, while the stress remains around the peak value with for further increases in strain until failure. For higher suction states, the sand shows traces of strain-softening, too.

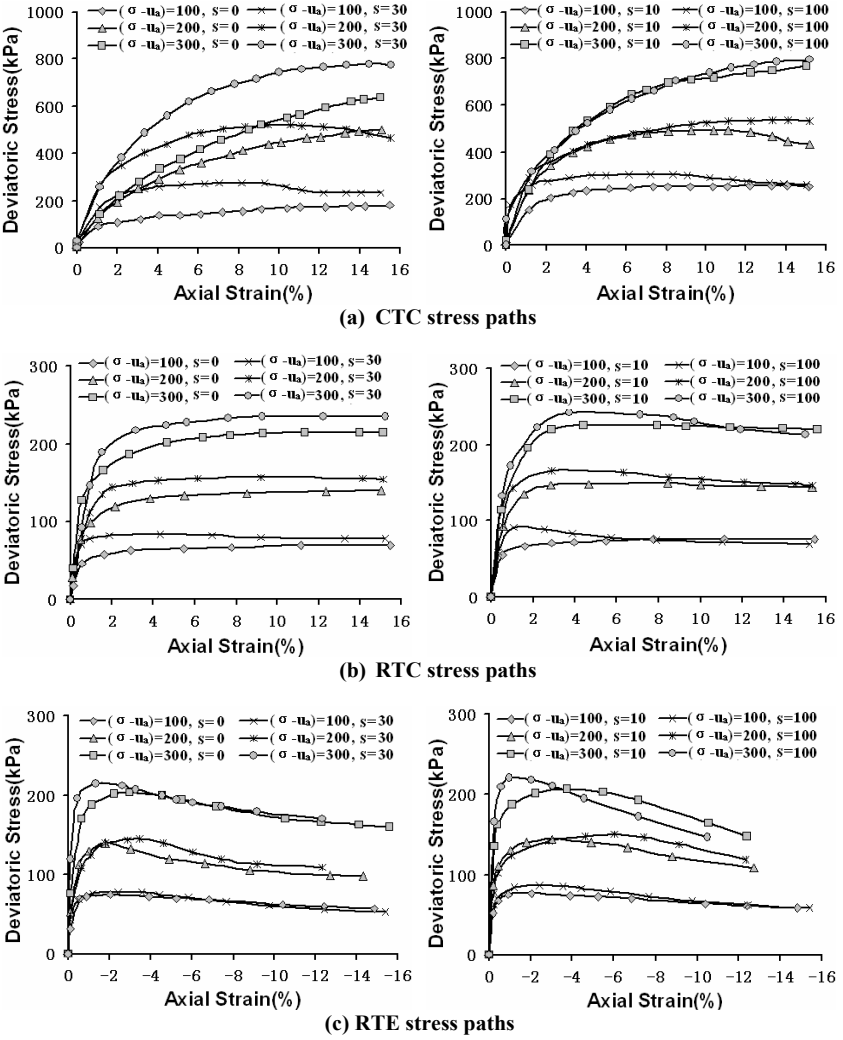

Figure 2. Deviatoric stress vs. strain response of gassy sand for various stress paths

Under RTE stress paths, strain-softening of with a clear peak strength appears obvious, with the strength quickly dropping until failure. As both the net confining pressure and matric suction increase, the strain-softening behavior becomes more apparent. In general, soil strength for all stress paths tends to increase with matric suction. Matric

suction exacerbates the dilatancy experienced by sand, however, the extent to which the soil dilates is a function of the level of net stresses and the stress path followed. Using the two-factor shear strength theory for unsaturated soils, that is, using total cohesion c_T to combine effective cohesion c' and apparent cohesion τ_{us}, $c_T = c' + \tau_{us}$, shear strength parameters of gassy sand for various stress paths can be assessed, as shown in Table 2.

Table 2. Shear strength parameters of gassy sand from various stress paths

Stress Path	Matric Suction (kPa)	Total Cohesion c_T (kPa)	$\tau_{us} = c_T - c'$ (kPa)	φ' (°)	φ^b (°)
Conventional Triaxial Compression	0	8.0	0.0	32.7	33.7
	10	20.1	12.1	34.2	31.2
	30	26.8	18.8	33.8	20.6
	100	32.4	24.4	34.0	13.7
Reduced Triaxial Compression	0	1.0	0.0	32.5	32.5
	10	6.4	5.4	32.6	28.4
	30	7.9	6.9	35.1	13.0
	100	14.6	13.6	35.2	7.7
Reduced Triaxial Extension	0	1.6	0.0	30.7	30.7
	10	4.3	2.7	30.9	15.1
	30	7.9	6.3	31.9	11.9
	100	9.5	7.9	32.2	4.5

It can be noticed from Table 2 that the shear strength parameters of gassy sand are different under various stress paths, even when the sand has been subject to the same net confining pressure and suction state, which substantiates the significant stress path dependency of unsaturated shear strength parameters. An increase in suction leads to an increase in total cohesion c_T, but the contribution of soil suction towards this strength parameter depends on the particular stress path induced on the soil. Effective cohesion c' is significantly affected by the stress path, while effective friction angle φ' is not considerably affected, changing only $1^\circ \sim 2^\circ$. Parameter φ^b represents the contribution of suction to shear strength, which generally decreases at higher suctions, regardless of the stress path followed; however, the extent of the reduction varies with the stress path.

An existing study (Kong et al. 2005) shows that the relationship between apparent cohesion τ_{us} and matric suction, $s = (u_a - u_w)$, may not follow a linear function in shallow gassy sand, as postulated in the two-factor theory, and it may actually be best represented through the following: $\tau_{us} = as^b$. Results from nonlinear regression analyses using this expression are summarized in Figure 3. Values of fitting parameters *a* and *b* are stress path dependent, and can be summarized as follows: CTC stress paths, $a = 3.44$ and $b = 0.43$; RTC stress paths, $a = 0.56$, $b = 0.68$; RTE stress paths, $a = 1.50$, $b = 0.37$.

Therefore, the shear strength of unsaturated sand under different stress paths can be expressed by a unified formula as follows:

$$\tau_f = c' + (\sigma_n - u_a)\tan\varphi' + as^b \quad (1)$$

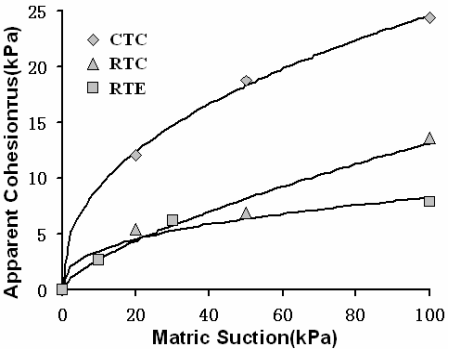

Figure 3. Variation of apparent cohesion with suction for various stress paths

CONCLUSIONS

Stress paths have significant effects on the strength of unsaturated sand. The stress-strain relationship shows different characteristics in various stress paths. Matric suction aggravates the dilatancy effect of the sand, and its degree is subject to the net stress and stress path. Parameters of the shear strength are closely related to the stress path. It has the dramatic influence to effective cohesion c' and apparent cohesion τ_{us}, but a little effect on effective friction angle φ'. The relationships between apparent cohesion and matric suction of sand are all in accord with the power function, and then the strength of gassy sand in various stress paths can be described by a unified formula..

REFERENCES

Feng, S.J. and Wang, Y.X. (2007). Research on influence of stress path on mechanical properties of saturated Sand. Journal of University of science and Technology Beijing, 19(3), 85-89.

Jeda, J. (1994). Stress-path dependent shear strength of sand. Journal of Geotechnical Engineering, 120(6), 958-974.

Kong, L.W., Guo, A.G., Chen, J.B., and Liu, G.S. (2005). On strength property of gassy fine sand and model tests of pile foundation. Proceedings of the 16th International Conference on Soil Mechanics and Geotechnical Engineering, Osaka, Japan, 4, 2009-2012.

Lade, P.V. and Duncan, J.M. (1976). Stress-path dependent behavior of cohesionless soil. Proc, ASCE, 102(GT1), 42-48.

Tang, Y.Q., Ye, W.M. and Zhang, Q.H. (1996). Marsh gas in soft stratum at the estuary of the Yangtse River and safety measures of construction of the tunnel. Journal of Tongji University, 24(4), 465-470.

Xu, Z.G. and Meng, J.B. (2003). "Influence and disposal of methane on sluice foundation." Zhejiang Hydrotechnics, (2): 70-71.

A Novel Suction-Controlled Ring Shear Testing Apparatus for Unsaturated Soils

L.R. Hoyos[1], C.L. Velosa[2], and A.J. Puppala[3]

[1] Associate Professor, University of Texas at Arlington, Texas 76019, e-mail: lhoyos@uta.edu
[2] Ph.D. Candidate, University of Texas at Arlington, Texas 76019, e-mail: clilianav@hotmail.com
[3] Professor, University of Texas at Arlington, Texas 76019, e-mail: anand@uta.edu

ABSTRACT: Today, it is well known that most geotechnical infrastructure resting on or made of unsaturated soils experience a wide range of deformations. Calculation of foundation settlement, for instance, requires a good estimation of soil stiffness at relatively small strains. Analyses of slopes, embankments, and soil bearing capacity, on the other hand, require adequate estimation of shear strength, from peak to residual. To date, there is limited experimental evidence of unsaturated soil response at mid-to-large strain levels corresponding to residual shear strength, and virtually no research work is available that spans the whole range of deformations in unsaturated soils using ring shear testing technique under controlled-suction states. This paper introduces a novel ring shear apparatus suitable for testing unsaturated soil samples over a whole range of deformations via axis-translation technique. The lower annular platen features a full set of 5-bar ceramics for control of pore-water pressure during constant-suction RS testing. The paper outlines the full development of the apparatus, including details of its main components and the test procedures. Results from a preliminary series of suction-controlled ring shear tests on compacted silty sand are presented.

INTRODUCTION

In recent years, the basic hypotheses of most elasto-plastic constitutive frameworks postulated for unsaturated soils have been validated via suction-controlled oedometer, triaxial and direct shear testing (e.g. Alonso et al. 1990, Wheeler and Sivakumar 1995, Burland and Ridley 1996, Cui and Delage 1996, Hoyos and Macari 2001, Fredlund 2006). These devices, however, allow for the application of loads along limited modes and levels of strain and/or deformation. Today, it is well known that most geotechnical infrastructure resting on or made of unsaturated soil materials experience a wide range of deformations. Calculation of shallow foundation settlement, for instance, requires a

good estimation of the soil stiffness at relatively small strains. Analyses of slopes, embankments and soil bearing capacity, on the other hand, require adequate estimation of shear strength, from peak to residual state. To date, however, experimental evidence of unsaturated soil response at mid-to-large strain levels corresponding to residual shear strength is very limited, and virtually no research work is available that spans the whole range of deformations in unsaturated soils via ring shear testing technique under controlled-suction states.

This paper introduces a novel, servo-controlled ring shear apparatus suitable for testing unsaturated soil samples over a full range of deformations via the axis-translation technique. The lower annular platen features a full set of 5-bar ceramics for control of pore-water pressure during constant-suction RS testing. The following sections outline the full development of the apparatus, including details of its main components and the test procedures. Results from a preliminary series of suction-controlled ring shear tests on compacted silty sand are then presented.

PREVIOUS WORK

Recently, Infante et al. (2007) reported a first attempt at modifying a conventional, Bromhead type, ring shear device for soil testing under controlled low-suction states via axis-translation technique. Around the same time, Vaunat et al. (2006) reported a modified Bromhead type ring shear apparatus for soil testing under controlled high-suction states via vapor transfer technique. In both cases, low and medium plasticity clayey soils were tested. They reported an increase in the residual friction angle with an increase in the applied suction. This was associated to partial aggregation of the clayey particles, which caused the soil to behave more like a granular material. The authors also observed that the unsaturated residual strength is independent of the applied vertical stress and the suction stress history. The results, however, are far from conclusive, and the modified devices offered plenty of room for further refinement and development.

A NOVEL SUCTION-CONTROLLED RING SHEAR APPARATUS

The general design of the novel apparatus introduced herein is based upon the original RS apparatus developed by Bromhead (1979), in which the specimen is placed inside the annular space formed between the two concentric rings of a lower rotational cell. The RS apparatus developed in this work features two servo-controlled actuators: one pneumatic actuator for normal loads and one electrical actuator for shear loads. The apparatus allows for the application of vertical stress up to750 kPa, monotonic torque up to 113 ton-m, constant suction up to 1,500 kPa (via axis translation), and more than 360-degree-range of continuum angular deformation. The device features three main modules: (1) Main cell with rotational shear system, including normal load and torque actuators; (2) Data acquisition/process control system with performance/data reduction software for real-time calculations of shear stress and average linear displacements; and (3) Suction control panel. Further details are summarized in the following.

Main Cell

The main cell of the RS device, including the rotational shear system, consists of all of the following: (a) Pneumatic servo-controlled actuator for application of vertical loads up to 8000 N; (b) Electrical servo-motor actuator for application of torsional loads up to 5000 ton-m; (c) Linear variable differential transducer (LVDT) to measure vertical deformations; (d) Electrical sensors for real-time measurements of shear torque, shear angular deformation, and vertical load; (f) Adjustable top and bottom stainless-steel loading platens; and, (h) Reinforced-acrylic confining cell with 1000-kPa air pressure capacity. Figure 1 shows a panoramic view of the entire suction-controlled ring shear test layout, including the data acquisition and process control system, GCTS suction control panel, and fully assembled cell.

The upper annular platen of the main cell houses a full set of six coarse porous stones, which are evenly distributed along the central perimeter of its bottom surface, for application and control of pore-air pressure u_a. Likewise, the lower annular platen houses a series of six, high-air-entry, 15-bar ceramics for application and control of pore-water pressure u_w. The ceramics are sealed with adjacent sintered stainless-steel rings in order to prevent pore-air leakage into the water system, as shown in Figure 2. Soil samples conform to the annular space between the two concentric rings of the lower rotating platen, having a 3.8-in (9.65-cm) inner diameter, 6-in (15,24-cm) outer diameter, and a range of adjustable heights between 0.6-1.25 in (0.5-3.0 cm).

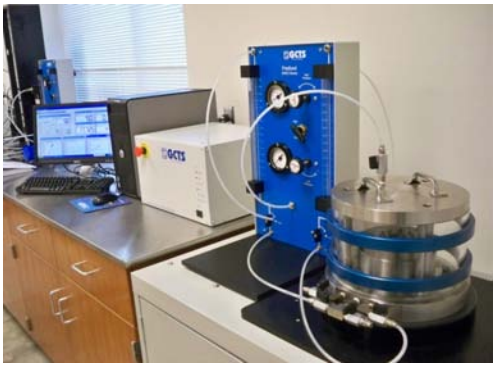

Figure 1. Panoramic view of entire suction-controlled ring shear test layout

Figure 2. Upper platen (shown upside down), lower platen, and bottom torsional gear

Vertical pressure, prior to shearing, is applied to the soil specimen through the upper platen. During controlled-suction shearing, the lower assembly containing the specimen is rotated by a hydro-electrical drive unit while the upper part is restrained. Ring shear (torsional shearing) and axis translation (controlled-suction) processes are then independently controlled by two separate systems: the load/shearing actuators and the suction control panel. The core system of the RS apparatus was manufactured by Geotechnical Consulting and Testing System (GCTS), Tempe, Arizona.

DA/PC System

The data acquisition and process control system, as shown in Figure 1, consists of the following: (1) A SCON-1500 digital servo controller and acquisition system; (2) A DSB-11 universal signal conditioning board (for load cells and LVDTs); (3) GCTS ring shear software for real-time measurement, processing and control of test variables such as shear stress, normal stress and angular deformation; and (4) IBM-PC unit.

Suction Control Panel

A GCTS suction control panel is used for the independent control of pore-air pressure u_a and pore-water pressure u_w during suction-controlled RS testing, as shown in Figure 1. The panel features a flushing mechanism to remove diffused air beneath the HAE ceramic generated during constant-suction RS testing.

SAMPLE PREPARATION VIA IN-PLACE STATIC COMPACTION

The test soil used in this work classifies as SM soil (80% sand and 20% silt) according to the USCS. The soil was selected because of its local availability and poor gradation, which minimizes the effects of particle size/shape on menisci formation in the water phase, reducing the equalization time of pore fluids (air and water) during suction-controlled testing. Samples were prepared with a water content equivalent to a suction of 25 kPa according to the soil-water characteristic-curve (SWCC) shown in Figure 3. In this figure, data points represent actual experimental data, whereas solid and dashed lines represent best-fit curves using Van Genuchten (1980) and Fredlund and Xing (1994) model equations.

Ring-shaped specimens were directly compacted onto the lower annular platen of the cell via in-place static compaction. The upper platen was used to compress the loose soil-water mix until achieving the target density. A monotonic force is applied to the top platen by means of a triaxial loading frame, as shown in Figure 4. The samples were prepared in a single layer at a compaction displacement rate of 1.25 mm/min to minimize the potential for fabric variation throughout the specimen (Venkatarama 1993). Specimens were compacted at 95% of maximum Proctor dry density, $\gamma_{d\text{-max}}$ = 1.85 g/cm^3. After compaction, the final height and weight of the compacted sample were determined to verify achievement of the target dry unit weight.

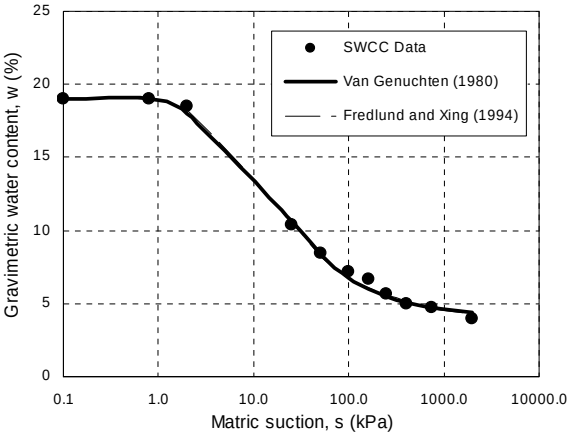

Figure 3. Soil-water characteristic curve for SM soil along with best-fit model curves

Figure 4. In-place static compaction of ring-shaped SM sample in triaxial frame

SUCTION-CONTROLLED RS TEST PROCEDURE

A series of two multi-stage suction-controlled RS tests were performed on compacted specimens of SM soil. A range of normal net stresses ($\sigma_n - u_a$) of 0, 25, and 75 kPa was chosen in order to reproduce normal stress states that are typically encountered in first-time landslides in shallow unsaturated soil slopes and embankments (Stark and Eid 1997). Suction-controlled RS tests were performed under constant suctions of 25 and 100 kPa. In both cases, the specimen was sheared at a displacement rate of 0.018 mm/min.

After full assemblage of the RS apparatus, as shown in Figure 1, a vertical load was monotonically applied via the upper annular platen to induce a 25 kPa normal stress on the specimen. Right after application of normal stress, and prior to shearing, the pore-air pressure was increased (via compressed air in the cell chamber) to achieve a desired suction state of 25 kPa via axis translation. Once equalization of pore-air and pore-water pressures was achieved, shearing was initiated. Shearing was continued until it was observed, from the shear stress readings, that a well-defined residual state had been reached. Shearing was then stopped and the normal stress on the specimen was further increased to 50 kPa. Pore-air pressure was kept constant at 25 kPa and shearing initiated until a well-defined residual state was observed. The process was repeated for a normal stress of 100 kPa.

Upon completion of the last stage, the applied torque and pore pressures were brought back to zero and the vertical stress was fully removed. The upper platen was taken off and the sheared surface of the soil carefully examined for significant features such as potential shear-band formation. The same procedure was repeated on a second SM soil specimen for constant suction of 100 kPa and normal net stresses ($\sigma_n - u_a$) of 0, 25, and 75 kPa.

ANALYSIS OF TEST RESULTS

Results from RS tests performed at suction s = 25 kPa are shown in Figure 5. Results from RS tests performed at suction s = 100 kPa are shown in Figure 6. Results are shown in terms of shear stress versus shear displacement response for different normal net stresses, as well as vertical displacement versus shear displacement response for different normal net stresses. As it is expected, the peak strength of the soil is critically influenced by the normal net stress level, with a considerable increase for ($\sigma_n - u_a$) = 75 kPa.

Regardless of induced suction level, compacted SM soil exhibits peak strength and considerable dilatancy under a low normal net stress ($\sigma_n - u_a$) of 0 kPa. This can be attributed to the dense nature of the sample initially achieved via static compaction (Figure 4). The response of the soil becomes more contractile as the normal net stress ($\sigma_n - u_a$) is increased to 25 and 75 kPa, which can be explained by the multi-stage testing scheme followed in this work, which induces a predefined failure surface in the sample before increasing the normal net stress ($\sigma_n - u_a$) to carry out the next shearing stage.

CONCLUDING REMARKS

Preliminary RS testing on compacted SM soil has shown that the newly developed RS apparatus is suitable for testing unsaturated soils under suction-controlled states via axis-translation technique. The core of the system was developed under U.S. National Science Foundation Award # 0626090. This support is gratefully acknowledged.

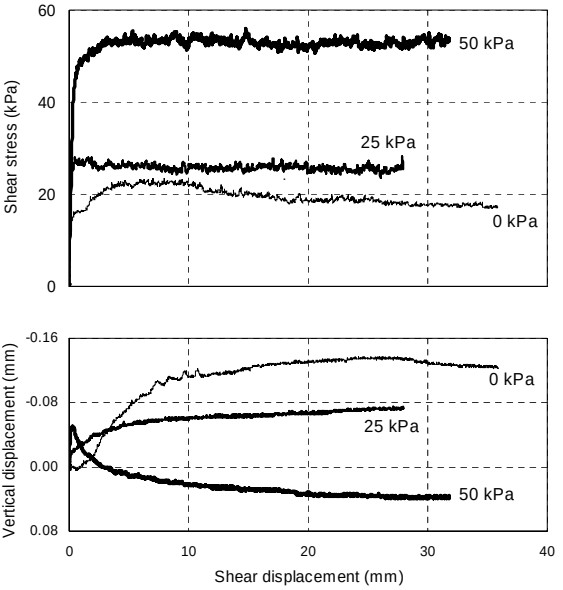

Figure 5. Suction-controlled RS tests on compacted SM soil at s = 25 kPa

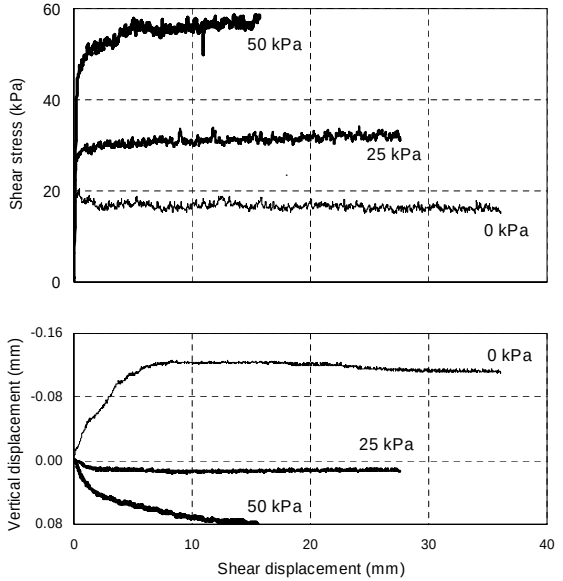

Figure 6. Suction-controlled RS tests on compacted SM soil at s = 100 kPa

REFERENCES

Alonso, E.E., Gens, A., and Josa, A. (1990). A constitutive model for partially saturated soils. Géotechnique, 40(3), 405-430.

Bromhead, E.N. (1979). A simple ring shear apparatus. Ground Engineering, 12 (5), 40-44.

Burland, J. B., and Ridley, A.M. (1996). The importance of suction in soil mechanics. Proceedings of the 12th Southeast Asian Geotechnical Conf., Kuala Lumpu, vol. 2, 27-49.

Cui, Y.J, and Delage, P. (1996). Yielding and plastic behavior of an unsaturated compacted silt. Géotechnique, 46 (2), 291-311.

Fredlund, D. (2006). Unsaturated soil mechanics in engineering practice. Journal of Geotechnical and Geoenviromental Engineering, 132(3), 286-321.

Fredlund, D.G., and Xing, A. (1994). Equations for the soil water characteristic curve. Canadian Geotechnical Journal, 31(3), 521-532.

Hoyos, L.R., and Macari, E.J. (2001). Development of a stress/suction-controlled true triaxial testing device for unsaturated soils. Geotechnical Testing Journal, ASTM, 24(1), 5-13.

Infante, J.A., Vanapalli, S.K., and Garga, V.K. (2007). Modified ring shear apparatus for unsaturated soil testing. Geotechnical Testing Journal, ASTM, 30(1), 1-9.

Stark, T.D., and Eid, H.T. (1997). Slope stability analyses in stiff fissured clays. Journal of Geotechnical and Geoenvironmental Engineering, 123(4), 335-343.

van Genuchten, M.T. (1980). A closed form equation for predicting the hydraulic conductivity of unsaturated soils. Soil Science Society of America Journal, 44, 892-898.

Vaunat, J., Amador, C., Romero, E., and Djeren-Maigre, I. (2006). Residual strength of a low plasticity clay at high suctions. Proceedings of the Fourth International Conference of Unsaturated Soils, vol. 1, 1279-1289.

Venkatarama, R.B., and Jagadish, K.S. (1993). The static compaction of soils. Géotechnique, 43(2), 337-341.

Wheeler, S.J., and Sivakumar, V. (1995). An elasto-plastic critical state framework for unsaturated soils. Géotechnique, 45(1), 35-53.

Modeling Unsaturated Soil Behavior Under Multiaxial Stress Paths Using a Refined Suction-Controlled Cubical Test Cell

L.R. Hoyos[1], D.D. Perez-Ruiz[2], and A.J. Puppala[3]

[1] Associate Professor, University of Texas at Arlington, Texas 76019, e-mail: lhoyos@uta.edu
[2] Associate Professor, Universidad Javeriana, Cali, Colombia, e-mail: diegoperezr@gmail.com
[3] Professor, University of Texas at Arlington, Texas 76019, e-mail: anand@uta.edu

ABSTRACT: This paper introduces a servo-controlled true triaxial (cubical) device that has been developed to test 3-in (7.5-cm) side, cubical specimens of unsaturated soil under controlled-suction states for a wide range of stress paths not achievable in a conventional cylindrical apparatus. The cell is a mixed-boundary type of device, with the specimen seated on top of a high-air-entry disk and between five flexible (latex) membranes on the remaining sides of the cube. The new cell is an upgraded, more elaborate version of the one previously reported by Hoyos et al. (2005), featuring two independent pore-air pressure and pore-water pressure control systems via a PVC-100-UNSAT pressure panel, as well as a fully computer-driven stress application/control system via a PCP-5000-UNSAT pressure panel. Suction states, $s = (u_a - u_w)$, are induced in the specimens via axis-translation technique. The technique is implemented by using the $s = u_a$ testing concept (i.e., $u_w = 0$). Results from a preliminary series of hydrostatic compression and triaxial compression tests are presented.

INTRODUCTION

Over the last few decades, the description of the stress-strain-strength behavior of unsaturated soils has been closely linked with efforts to isolate the relevant effective stress fields governing their mechanical response. The adoption of matric suction, $s = (u_a - u_w)$, and the excess of total stress over air pres-sure, $(\sigma - u_a)$, as the relevant stress state variables, have facilitated the modeling of key features of unsaturated soil behavior via suction-controlled oedometer, triaxial, and direct shear testing (Alonso et al. 1990, Wheeler and Sivakumar 1992, Fredlund and Rahardjo 1993). The majority of these devices, however, allow for the application of loads along limited paths and modes of deformation, such as one-dimensional, hydrostatic or axisymmetric loading.

In nature, pavement subgrades and shallow foundation soils well above the ground-water table may be subject to three-dimensional stress gradients due to changes in the stress state variables ($\sigma_{ij}-u_a\delta_{ij}$) and ($u_a - u_w)\delta_{ij}$, as illustrated in Figure 1. Therefore, accurate predictions of the stress-strain response of geosystems resting on unsaturated ground require that all the constitutive relations be valid for all stress paths that are likely to be experienced in the field. It is in this context that a true triaxial (cubical) cell, capable of inducing in the soil test specimens a wide range of simple-to-complex multiaxial stress paths under controlled-suction states, plays a fundamental role in a thorough stress-strain-strength characterization of this type of materials.

This paper describes a servo-controlled true triaxial (cubical) apparatus that has been developed to test 3-in (7.5-cm) side, cubical specimens of unsaturated soil under controlled-suction states for a wide range of stress paths that are not achievable in a conventional cylindrical apparatus. The cell is a mixed-boundary type of device, with the specimen seated on top of a high-air-entry disk and between five flexible (latex) membranes on the remaining sides of the cube. The new cell is an upgraded, more elaborate version of the apparatus previously reported by Hoyos et al. (2005), featuring two independent pore-air and pore-water pressure control systems, via a PVC-100-UNSAT pressure panel, and a fully computer-driven stress application and control system, via a PCP-5000-UNSAT pressure panel. Suction states, $s = (u_a - u_w)$, are induced in the specimens via the axis-translation technique. The technique is implemented by utilizing the $s = u_a$ testing concept ($u_w = 0$).

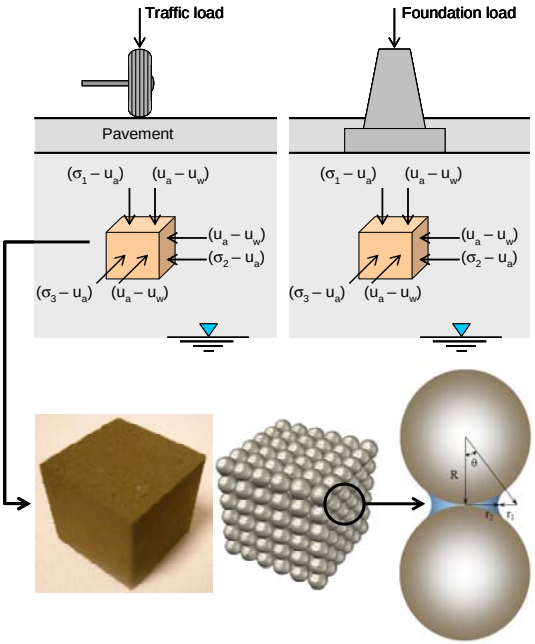

Figure 1. Idealization of unsaturated soil deposits subject to multiaxial stress gradients

PREVIOUS WORK

Hoyos and Macari (2001) reported a first attempt to test unsaturated soil specimens under suction-controlled multiaxial loading. The cell used, however, presented some important limitations, such as a highly corrosive steel frame, which caused occasional clogging of the HAE ceramic disk; and the use of hydraulic oil to pressurize the latex membranes in contact with the sample, which resulted in occasional damage of the membranes when exposed to hydraulic oil for extended periods of time.

Matsuoka et al. (2002) reported a rigid-boundary system that induces suction states in the specimens via negative pore-water pressure. This system also presented some limitations, including undesirable boundary effects due to rigid loading platens, reducing the capability of the cell to induce a wide range of stress paths; and the very use of negative pore-water pressure to induce suction states via HAE ceramics, which limits suction application to 100 kPa.

More recently, Hoyos et al. (2005) developed a new system similar to the one reported by Hoyos and Macari (2001), with a few enhanced features. However, the system still presents some important limitations, including low resolution of pressure transducers, which restricts load increments to a minimum of 1 psi (6.9 kPa); manual application of load increments, which limits the application of a continuous, ramped loading scheme; no real-time acquisition of soil deformation data from LVDTs; and occasional corrosion of springs attached to the LVDT extension rods when exposed to water over an extended period of time.

The true triaxial apparatus described herein is aimed at overcoming all of the above limitations, yielding a considerably enhanced performance with the inclusion of two fully servo-controlled systems for independent applications of external stresses and matric suction states on the test specimens.

A REFINED SUCTION-CONTROLLED TRUE TRIAXIAL CELL

In general, true triaxial devices can be classified into three major categories: rigid-boundary, flexible-boundary and mixed-boundary cells (Sture 1979). The apparatus presented in this paper is a mixed-boundary type of cell, with the specimen seating on top of a HAE ceramic disk and between five flexible membranes on the remaining sides of the cube. The cell consists mainly of a stainless steel frame featuring six pressure cavities to accommodate one top and four lateral flexible latex membranes, and a cubical base aluminum piece at the bottom assembly to house a HAE ceramic disk and four symmetrically spaced coarse porous stones, as shown in Figure 2.

The ceramic disk, with a 5-bar air-entry value, is saturated in place following a procedure similar to that suggested by Bishop and Henkel (1962). After saturation of the ceramic, the cubical specimen is gently slid in through one of the lateral cavities of the cubical frame, with the specimen ultimately sitting right on top of the saturated ceramic disk.

After setting of the compacted specimen into the inner cavity of the frame, the remaining five walls are assembled to the frame. The system does not require the use of LVDTs for monitoring soil deformation during testing.

Figure 2. Bottom wall assembly with sealed HAE ceramic and four coarse stones

Cubical latex membranes were prepared in the laboratory using Dow Corning silicone rubber on a custom-made mold placed in a vacuum chamber, as shown in Figure 3. This is a Silastic J-RTV type of rubber that yields high tear strength and low stiffness rubber membranes. Each membrane forms a pressure seal between the wall assembly and the reaction frame and provides an effective seal against the leaking of the pressurized fluid. The membranes transmit the water-based hydraulic pressure to the top and four lateral faces of the specimen. Figure 4 shows a typical lateral wall assembly, including a picture illustrating the stretchability of the latex in a clayey sand sample monotonically stressed to 35% vertical strain.

External hydraulic pressure is generated and controlled by a computer-driven Pressure Control Panel (PCP-5000-UNSAT), allowing independent control of major, intermediate, and minor principal stress. A computer-driven pressure volume control system (PVC-100-UNSAT) maintains a constant suction on the specimen and allows for determination of soil deformation in all three principal directions. In this panel, three Model DC 750-5000 sensors allows for real-time measurements of the positive (compression) and negative (extension) deformations experienced by the soil. Figure 5 shows a panoramic view of entire suction-controlled true triaxial test layout.

SAMPLE PREPARATION VIA STATIC COMPACTION

Test soil classifies as clayey sand (SP-SC) according to the USCS, with 70% poorly-graded sand and 30% low-plasticity clay. Cubical specimens were prepared via static compaction. The initial water content was kept at 10% while the target dry density was approximately 15.34 kN/m^3. A triaxial load frame is then used to apply a quasi-static axial load to the loose sample until achieving the target volume, as shown in Figure 6.

Figure 3. Custom-made mold and fabrication process for cubical latex membranes

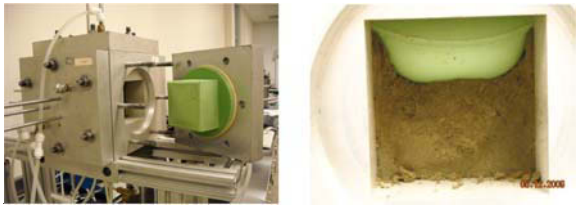

Figure 4. Typical lateral wall assembly and stretchability of cubical latex

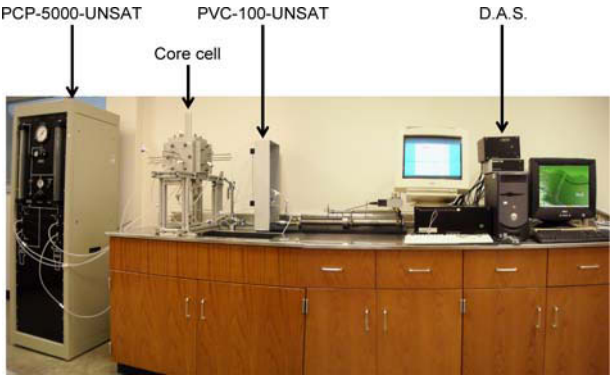

Figure 5. Panoramic view of entire suction-controlled true triaxial test layout

Figure 6. Static compaction process and typical statically-compacted specimen

Samples were prepared using a custom-made stainless steel mold, as shown in Figure 6. The mold is first filled with 761.5 g of SP-SC soil mixed with water to the target 10% moisture. The loose mixed is then compressed by the loading frame at a constant rate of 1.0 mm/min. Immediately after compaction, the specimen is gently extruded from the mold and transferred to the cubical cell. A photograph of a typical statically-compacted sample is also shown in Figure 6.

INFLUENCE OF COMPACTION DRY UNIT WEIGHT

A series of four drained (suction-controlled) hydrostatic compression (HC) tests were conducted at constant matric suction, $s = u_a = 100$ kPa, to experimentally determine the adequate compaction dry unit weight for SP-SC samples using static compaction. The intent was to reproduce identical samples with a relatively small preconsolidation pressure so that it was feasible to bring the test soil to a virgin state, hence inducing elasto-plastic deformations that would help identify the Loading-Collapse yield curve postulated by Alonso et al. (1990).

All four specimens were prepared using static compaction method. Although all samples were compacted at the same initial water content, w = 10%, each sample had enough solid mass to attain a different dry unit weight at the same total volume. The selected dry unit weights, γ_d = 19.18, 17.26, 16.30, and 15.34 kN/m^3, correspond to 100%, 90%, 85% and 80% of the maximum standard Proctor dry unit weight $\gamma_{d\text{-}max}$, respectively.

Figure 7 shows the variation of the specific volume, v = 1 + e, with neat mean stress, $p = (1/3)(\sigma_1 + \sigma_3) - u_a$, from the four suction-controlled HC tests. All tests were carried out from an initial net mean stress of 20 kPa to a final net mean stress of 800 kPa. Based on these results, a dry unit weight, γ_d = 15.34 kN/m^3, which corresponds to 80% of maximum standard Proctor dry unit weight $\gamma_{d\text{-}max}$, was found to yield lowest preconsolidation pressure.

It is also worth noting that the initial (elastic) portion of all v-p curves show a reasonably identical slope, including the rebound portion of the curve for γ_d = 15.34 kN/m^3. Statically compacted samples of SP-SC soil yield an average specific volume, v = 1+ e = 1.72, and an average degree of saturation, S = 37.5%.

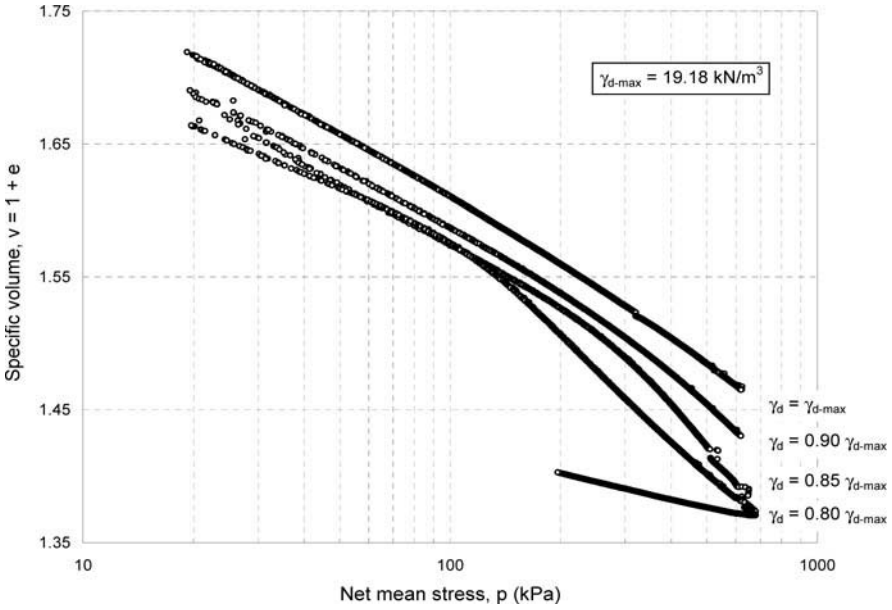

Figure 7. HC tests at s = 100 kPa on four statically compacted SP-SC specimens

RESPONSE UNDER TRIAXIAL COMPRESSION

Two triaxial compression (TC) tests were conducted at constant matric suction, $s = u_a = 200$ kPa, to assess the repeatability of test results and the suitability of the developed apparatus for testing unsaturated soil samples under suction-controlled conditions via axis-translation technique. Results from the two TC trial tests are shown in Figure 8, which shows reasonably identical trends from both tests. It is also observed that the cell is capable of reproducing the compressive nature (+) of the major principal strain and the extensive nature (–) of the minor and intermediate principal strains, as dictated by the loading scheme of the TC stress path.

CONCLUDING REMARKS

Preliminary testing on SP-SC soil has shown that the newly developed cell is suitable for testing unsaturated soils under suction-controlled conditions via axis-translation technique. The cell will play a fundamental role in the complete characterization of unsaturated soil behavior under multiaxial stress paths that are likely to be experienced in the field. On-going testing involves stress paths not achievable in a cylindrical cell, including simple shear. The core of the system was developed under U.S. National Science Foundation Award # 0216545. This support is gratefully acknowledged.

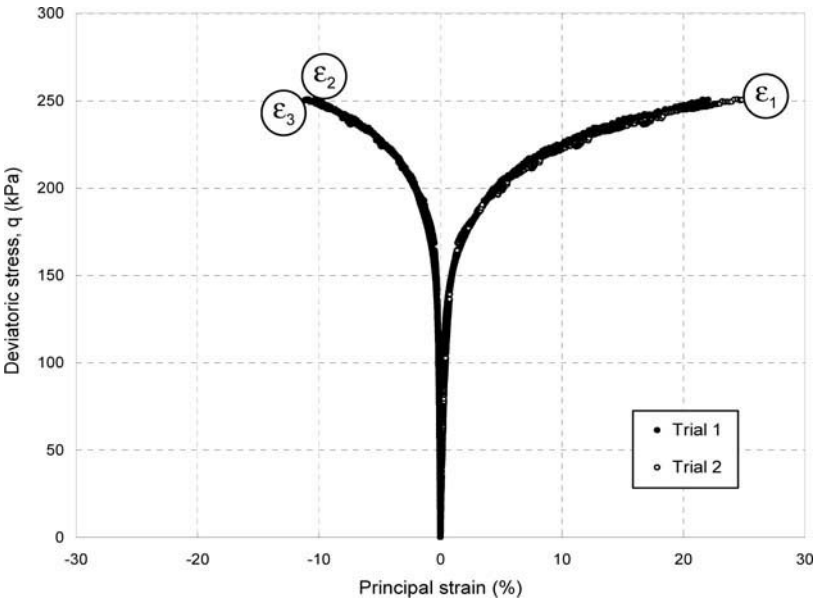

Figure 8. TC tests at s = 200 kPa on two statically compacted SP-SC specimens

REFERENCES

Alonso, E.E., Gens, A., and Josa, A. (1990). A constitutive model for partially saturated soils. Géotechnique, 40(3), 405-430.

Bishop, A.W., and Henkel, D.J. (1962). The measurement of soil properties in the triaxial test. 2nd ed., London, England: Edward Arnold, 227 pp.

Fredlund, D.G., and Rahardjo, H. (1993). Soil mechanics for unsaturated soils. John Wiley and Sons, Inc., NY.

Hoyos, L.R., Laikram, A., and Puppala, A.J. (2005). A novel true triaxial apparatus for testing unsaturated soils under suction-controlled multi-axial stress states. CD-Rom Proc., 16th International Conf. on Soil Mechanics and Geotechnical Engineering, September 12-16, 2005, Osaka, Japan, 387-390.

Hoyos, L.R., and Macari, E.J. (2001). Development of a stress/suction-controlled true triaxial testing device for un-saturated soils. Geotechnical Testing Journal, ASTM, 24(1), 5-13.

Matsuoka, H., Sun, D.A., Kogane, A., Fukuzawa, N., and Ichihara, W. (2002). Stress-strain behaviour of unsaturated soil in true triaxial tests. Canadian Geotechnical Journal, 39, 608-619.

Sture, S. (1979). Development of multiaxial cubical test device with pore-water pressure monitoring facilities. Rep. VPI-E-79.18, Dept. Civil Eng., Virginia Poly. Inst. & State U., Blacksburg, VA.

Wheeler, S.J., and Sivakumar, V. (1992). Development and application of a critical state model for unsaturated soils. Predictive Soil Mech., eds: G.T. Houlsby & A.N. Schofield, 709-728, London.

Effect of Saturation on Cyclic Volumetric Change of Compacted Silty Sands

E. Yee[1], P.M. Duku[2], and J.P. Stewart[3]

[1] Graduate Student, Department of Civil and Environmental Engineering, University of California, Los Angeles, USA, e-mail:mailericyee@ucla.edu
[2] Staff Engineer II, Fugro West Consultants, Ventura, California, USA
[3] Professor and Vice Chair, Department of Civil and Environmental Engineering, University of California, Los Angeles, USA, e-mail:jstewart@seas.ucla.edu

ABSTRACT: Seismic compression is the accumulation of contractive volumetric strains in unsaturated soils during earthquake loading. Cyclic simple shear tests were conducted on several unsaturated soil specimens to evaluate the role of low-plasticity fines content and the degree of saturation on vertical strains from seismic compression. Sands with low plasticity fines generally show larger vertical strains than clean sands and decreased vertical strains at intermediate saturations (S ~ 30%) relative to dry (S = 0%) and higher saturations (S ~ 60%). At saturation levels where vertical strains are minimized, the specimens have relatively high matric suction head, which maximizes the effective confining stress in the soil sample. Accordingly, it is postulated that saturation levels that give rise to high matric suction increase the moduli of the specimen, which in turn reduces volume change susceptibility.

INTRODUCTION

Unsaturated soils have a tendency to accumulate contractive volumetric strains under strong cyclic loading. This process typically manifests itself as soil settlement during strong earthquake shaking and is commonly known as seismic compression (Pyke et al. 1975, Stewart et al. 2001, 2004, Wartman et al. 2003, Tokimatsu 2008).

The state-of-practice for estimating settlements from seismic compression was originally defined by the simplified procedure of Tokimatsu and Seed (1987). A critical component of this procedure relates shear strain demand and number of strain cycles to volumetric strain; this component is referred to as a volumetric strain material model (VSMM). The VSMM in Tokimatsu and Seed (1987) was solely defined by laboratory test data from Silver and Seed (1971) for one clean sand material. Recognizing the need to expand the VSMM database for clean sands, Duku

et al. (2008) conducted numerous simple shear tests on sixteen materials. Their tests showed that volumetric strains decreased with increasing relative density and confining pressure and were not affected by saturation.

The database for seismic compression of sands with fines of varying plasticity is sparse. Whang et al. (2004) performed cyclic simple shear testing on four soils with high fines contents, FC = 40–54%, plasticity indices, PI = 2–15, and relative compactions of 84-96%. Their findings showed that compacted plastic soils exhibited lower seismic compression when compacted at high saturation (wet of line of optimums) than when compacted at lower saturations. Their tests also showed lower levels of seismic compression for clayey sands than for clean sands.

Whang et al. (2005) investigated the effects of density, saturation, and fines content on the seismic compression behavior of several synthetic non-plastic silty sands (fines were rock-flour). They found that intermediate levels of saturation, S ~ 30%, produced vertical strains that were less than samples with S > 60% and that increasing fines content increased vertical strains under constant relative compaction.

In the present work we extend the work of Whang et al. (2005) by utilizing relatively "natural" fines fractions, in the sense that they are derived from actual soil samples from the field and have modest (although small) plasticity. We vary the fines content and as-compacted degree of saturation of sands with these fines to investigate whether the levels of vertical strains and trends with FC and saturation observed by Whang et al. (2005) are confirmed for these more realistic soil minerologies.

LABORATORY TESTING

The soil materials tested were obtained from bulk samples of natural soils retrieved from three locations in southern California: an unspecified location in Orange County, downtown Los Angeles, and Santa Clarita Valley. To reflect the origin of these soils, they are referred to as Orange, Wilshire, and Newhall#2. The original Orange, Wilshire, and Newhall#2 soils had FC ~ 35, 22, and 14% respectively. For each soil, fine fractions were acquired by sieving the natural materials through the number 200 sieve. The coarse portion was taken from the material retained on the number 200 sieve after washing.

Cyclic simple shear testing was conducted on specimens reconstituted by mixing the host clean sand with different fractions of the native fines. This testing was performed using the UCLA Digitally Controlled Simple Shear device (Duku et al. 2007); the sample preparation and testing protocols are as described in Duku et al. (2008). Properties of the natural and reconstituted mixtures are shown in Table 1.

TEST RESULTS

Figures 1-3 show typical test results for specimens prepared to as-compacted saturations in the range of S ~ 0-60% on the vertical strain at 15 cycles of loading ($\varepsilon_{v,N=15}$) as a function of cyclic shear strain (γ_c). Results for the Orange, Wilshire, and Newhall#2 mixtures are shown in Figures 1-3, respectively. Figures 1(a) and 2(a)

show results for soil mixtures with FC = 20% compacted to a void ratio between 0.55 and 0.59. Whereas Figures 1(b) through 3(b) displays results for reconstituted soils with FC = 50% and void ratios in the range of 0.65 and 0.81.

Table 1. Soil properties for materials tested

Material	FC (%)	C_U	C_C	LL	PI
Natural Orange	35	–	–	21	0.7
Orange Mixtures	0	3.2	1.1	N/A	N/A
	10			18	NP
	20			19	NP
	35			21	0.3
	50				
	100			28	14
Natural Wilshire	22	–	–	19	3
Wilshire Mixtures	0	3.8	1.1	N/A	N/A
	10			16	NP
	20				
	35			20	7
	50			25	9
	100			41	16
Natural Newhall#2	14	7.8	1.1	19	NP
Newhall#2 Mixtures	0	3.6	0.9	N/A	N/A
	10			19	NP
	35			24	7
	50			28	8

N/A = Not Available
NP = Nonplastic

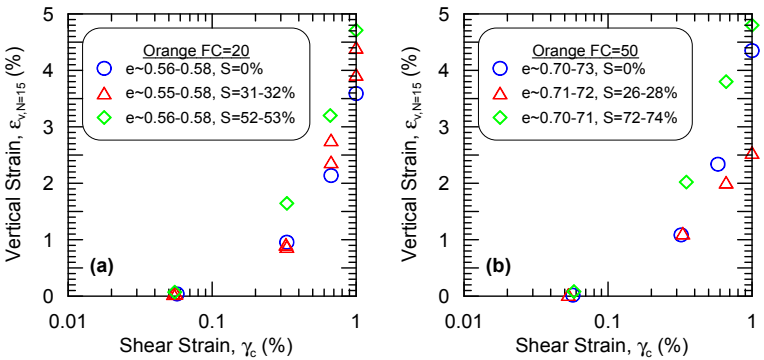

Figure 1. Saturation effects on Orange mixtures with: (a) FC = 20% and e~0.57, (b) FC = 50% and e~0.71

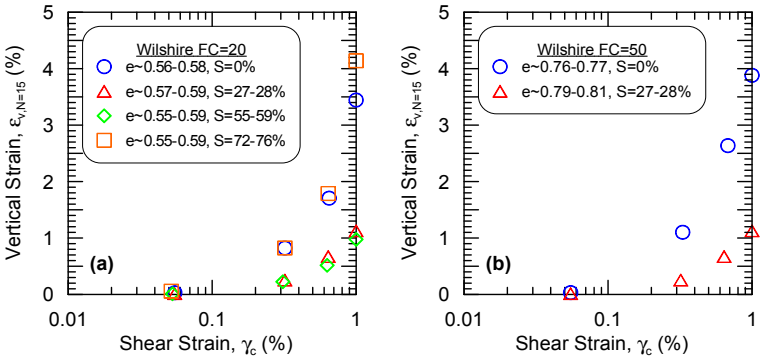

Figure 2. Saturation effects on Wilshire mixtures with: (a) FC = 20% and e~0.57, (b) FC = 50% and e~0.78

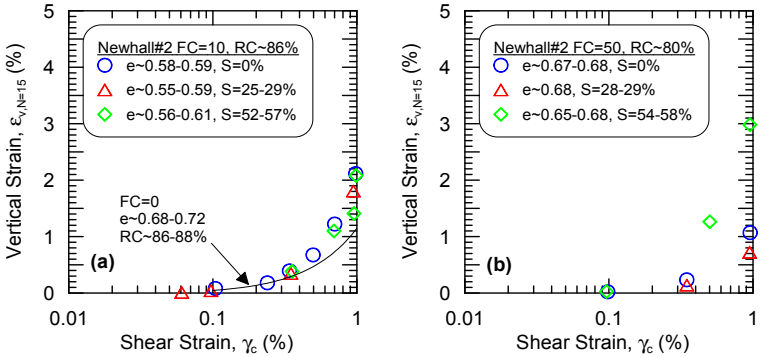

Figure 3. Saturation effects on Newhall#2 mixtures with: (a) FC = 10% and e~0.58, (b) FC = 50% and e~0.68

Effect of Fines Content

Our analysis of the effect of FC on seismic compression is incomplete, but some preliminary results are given here for the Newhall#2 material. Figure 3(a) compares the seismic compression of clean sand (black line) to the data for soils with FC = 20%. We take relative compaction by the modified Proctor standard as the density metric for the soils with fines and relative density as the metric for clean sands. The comparison in Figure 3(a) is made assuming the maximum dry density for analysis of RC matches that for D_R for the Newhall#2 clean sand material.

The results show that vertical strains for the soils with fines generally exceed those for clean sands. This is consistent with the results of Whang et al. (2005) for non-plastic fines.

Effect of Saturation

Figures 1-3 show that specimens of the Orange and Wilshire soils at high saturations (S ≥ 60%) generally experience vertical strains similar to specimens at S = 0%. However, for specimens at intermediate saturations (S ~ 30%), the vertical strains decrease relative to specimens at S = 0%.

To understand the role of saturation on seismic compression, matric suction tests were performed on partially saturated soil mixtures using the filter paper method (ASTM D5298-03). Typical matric suction test results are shown in Figure 4 for the Newhall#2 material. These figures show matric suction is higher at S = 30% than at S = 60% and also increases with FC. Since matric suction increases inter-particle stresses, the constrained modulus increases with matric suction, which in turn decreases the volume change potential of the soil. The effect of matric suction on the constrained modulus is also demonstrated in Figure 4.

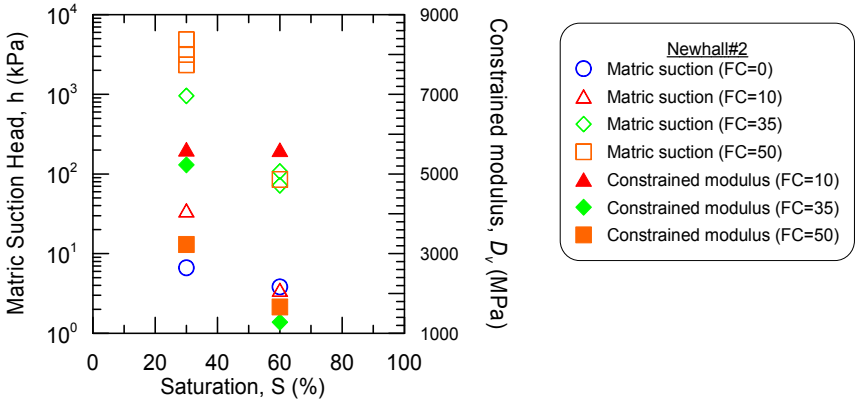

Figure 4. Effect of saturation on matric suction and constrained modulus for Newhall#2 mixtures

CONCLUSIONS

We have performed cyclic simple shear tests on low-plasticity silty sands with variable fines content (FC) to investigate the effects of FC and as-compacted saturation on vertical strain from seismic compression. We find a modest increase of settlement potential with increasing FC. We also find that modest saturations (approximately 30%) increase matric suction, which in turn increases constrained modulus. This decrease of volumetric compressibility is manifest by decreased seismic compression potential relative to dry specimens or specimens with relatively high saturation (and low matric suction). These trends are generally consistent with previous work on mixtures of rock flour and sands, although the compressibility of the present soils is considerably lower.

ACKNOWLEDGMENTS

We thank Priscilla Chui and Alexi Poulos for laboratory testing assistance. Support for this work was provided by the U.S. Geological Survey (USGS), Department of the Interior, under USGS award No. 05HQGR0050 and award No. 07HQGR0112. This support is gratefully acknowledged. The views and conclusions contained in this document are those of the authors and should not be interpreted as necessarily representing the official policies, either expressed or implied, of the U.S. Government.

REFERENCES

ASTM D5298-03 Standard test method for measurement of soil potential (suction) using filter paper, Annual Book of ASTM Standards, Section 4: Construction, Vol. 04.08, Soil and Rock, ASTM, Philadelphia.

Duku, P.M., Stewart, J.P., Whang, D.H., and Venugopal, R. (2007), Digitally controlled simple shear apparatus for dynamic soil testing, Geotech. Testing J., 30(5), 368-377.

Duku, P.M., Stewart, J.P., Whang, D.H., and Yee, E. (2008), Volumetric strains of clean sands subject to cyclic loads, J. Geotech. and Geoenv. Engrg., ASCE, 134(8), 1073-1085.

Pyke, R., Seed, H.B., and Chan, C.K. (1975), Settlement of sands under multidirectional shaking, J. Geotech. Engrg, ASCE, 101(4), 379-398.

Silver, M.L., and Seed, H.B. (1971), Volume changes in sands during cyclic loading, J. Soil Mech. and Foundations Div., ASCE, 97(9), 1171-1182.

Stewart J.P., Bray, J.D., McMahon, D.J., Smith, P.M., and Kropp, A.L. (2001), Seismic performance of hillside fills, J. Geotech. and Geoenv. Engrg., ASCE, 127(11), 905-919.

Stewart J.P., Smith P.M., Whang D.H., and Bray J.D. (2004), Seismic compression of two compacted earth fills shaken by the 1994 Northridge earthquake, J. Geotech. and Geoenv. Engrg., ASCE, 130(5), 461-476.

Tokimatsu, K. (2008), Geotechnical problems in the 2007 niigata-ken chuetsu-oki earthquake, Geotech. Eqk. Eng. Soil Dyn. IV, Sacramento, CA, May 18-22, 2008, 1-30.

Tokimatsu, K., and Seed, H.B. (1987), Evaluation of settlements in sand due to earthquake shaking, J. Geotech. Engrg., ASCE, 113(8), 861-878.

Wartman, J., Rodriguez-Marek, A., Repetto, P.C., Keefer, D.K, Rondinel, E. Zegarra-Pellane, J., and Baures, D. (2003), Ground failure Earthquake Spectra, 19(S1), 35–56.

Whang, D.H., Stewart, J.P., and Bray, J.D. (2004), Effect of compaction conditions on the seismic compression of compacted fill soils, Geotech. Testing J., 27 (4), 371-379.

Whang, D.H., Moyneur, M.S., Duku, P., and Stewart, J.P. (2005), Seismic compression behavior of nonplastic silty sands, Proc. Int. Sym. Adv. Experimental Unsaturated Soil Mech., A. Tarantino, E. Romero, and Y.J. Cui (eds.), Trento, Italy, June 27-29, A.A. Balkema Publishers, 257-263.

Wetting and Drying Unsaturated Soil Moisture Diffusivity Parameters

D. Mabirizi[1], and R.Bulut[2]

[1] Graduate Student, School of Civil and Environmental Engineering, Oklahoma State University, 207 Engineering South, Stillwater, OK 74078
[2] Assistant Professor, School of Civil and Environmental Engineering, Oklahoma State University, 207 Engineering South, Stillwater, OK 74078; e-mail:rifat.bulut@okstate.edu

ABSTRACT: Unsaturated soil moisture diffusivity parameter is important to variety of engineering applications, such as design and analysis of pavements, highway embankments and slopes, and shallow foundations. The unsaturated diffusivity coefficient controls transient moisture flow conditions within a soil in response to suctions or fluxes imposed at the boundaries of the soil mass. This research paper presents laboratory test results for wetting and drying unsaturated diffusion coefficients, and investigates the hysteresis effect between the wetting and drying processes on the measured parameters. Undisturbed soil specimens were obtained from a compacted highway embankment site in Oklahoma. Soil specimens were exposed to drying and wetting cycles, and the resulting wetting and drying coefficients were evaluated. The wetting diffusion coefficients were generally higher than the drying diffusion coefficients by factors between one and two.

INTRODUCTION

The unsaturated moisture diffusion coefficient controls transient moisture flow conditions within a soil mass in response to suctions or fluxes imposed at the boundaries of the mass. The flow of moisture through unsaturated soils is governed by the total suction gradient within the soil profile; with moisture traveling from regions of low total suctions to regions of high total suctions (Fredlund and Rahardjo 1993).

Mitchell (1979) proposed a very practical basis for characterizing unsaturated soil behavior. Mitchell showed that the rate at which water will move into the soil both vertically and horizontally can be determined using thermocouple psychrometers inserted into cylindrical soil specimens. Thermocouple psychrometers measure total suction changes over time as moisture evaporates from or infiltrates into the soil.

Fitting a theoretical solution to the suction data permits an estimate of the moisture diffusion coefficient. Laboratory methods based on Mitchell (1979) approach have the advantage of well-defined boundary conditions and permit moisture flow description using a single diffusivity parameter with a relatively high degree of confidence.

Nine undisturbed soil specimens, obtained from a compacted highway embankment site in Oklahoma, were tested to determine the wetting and drying diffusivity parameters. The drying and wetting testing method adopted in this study is based on the methodology proposed by Mitchell (1979) and subsequent improvements by Lytton et al. (2004) and Bulut et al. (2005) for the drying diffusion coefficient measurements. However, there are no cases in the literature to the knowledge of the authors where both the drying and wetting diffusion parameters were measured on the same soil samples. An evaluation of the effect of hysteresis on the diffusivity parameters associated with the drying and wetting of soil was also performed.

BACKGROUND

Mitchell (1979) reduced the general nonlinear diffusion equation into a linear one when total suction was expressed on a logarithmic scale, $u = \log|h|$ In this case the diffusion process is governed by a linear diffusion equation with the rate of diffusion controlled by a single diffusivity coefficient, α:

$$\frac{\partial u}{\partial t} = \alpha \frac{\partial^2 u}{\partial x^2} \tag{1}$$

where u is the total suction on logarithmic scale, h is the total suction, t is the time, and x is the distance. Equation 1 defines the distribution of suction throughout the soil body as a function of space and time. Mitchell (1979) considered a cylindrical soil specimen sealed along its curved surface and one end while the other end is left open to permit flow of moisture in or out of the specimen (Figure 1).

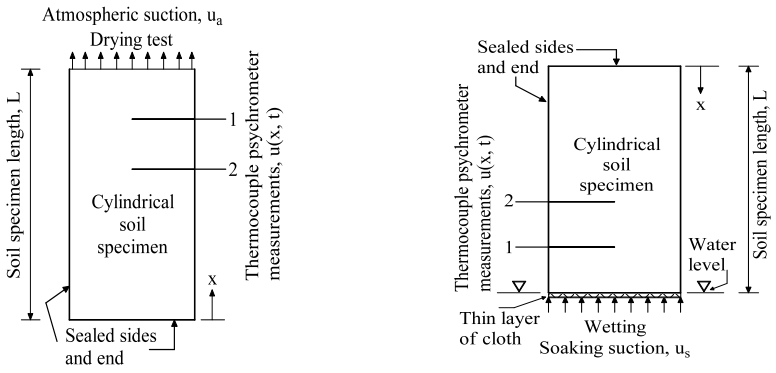

Figure 1. Boundary conditions for: (a) drying tests, (b) wetting tests

Mitchell (1979) derived two linear expressions from Equation 1 using the boundary conditions in Figure 1. Equation 2 was derived for the drying diffusion coefficient measurements using and Equation 3 was derived for the wetting diffusion coefficient measurements:

$$u(x,t) = u_a + \sum_{n=1}^{\infty} \frac{2(u_o - u_a)\sin z_n}{z_n + \sin z_n \cos z_n} \exp\left[\frac{z_n^2 \alpha t}{L^2}\right] \cos\left[\frac{z_n x}{L}\right] \quad (2)$$

where u_a is the atmospheric suction in the laboratory, u_o is the initial suction in the soil, α is the drying diffusion coefficient, t is the time, L is the sample length, x is the coordinate, z_n is the solution of $\cot z_n = z_n/h_eL$, and h_e is the evaporation coefficient. An evaporation coefficient $h_e = 0.54$ cm^{-1} was used in test data interpretation, based on previous work by Mitchell (1979).

$$u(x,t) = u_s + \frac{4(u_s - u_o)}{\pi} \sum_{n=1}^{\infty} \frac{(-1)^n}{2n-1} \exp\left[\frac{-(2n-1)^2 \pi^2 \alpha t}{4L^2}\right] \cos\left[\frac{(2n-1)\pi x}{2L}\right] \quad (3)$$

where u_s is the soaking (minimum) suction. Soaking suction of 1.75 log kPa was used in the diffusion coefficient measurements based on the previous work by Mitchell (1979). This level of suction is very low and representative of the suction energy in the soaking water.

Total suction as a function of space and time can be used to realistically characterize moisture flow through unsaturated soil mass by a single diffusivity parameter. This approach provides a very practical basis for simple, economical, and relatively rapid laboratory measurements of unsaturated soil moisture diffusivity characteristics.

LABORATORY MEASUREMENTS

Thermocouple psychrometers, with stainless steel screen shields were used to measure total suction in the soil. Before diffusion tests are performed, the psychrometers were calibrated using salt solutions having known water potential by immersing them in different concentrations of sodium chloride solutions. A plot of the millivolt output from the psychrometer versus water potential gives the calibration curve for the psychrometer. A datalogger was employed to record the total suctions from thermocouple psychrometer readings.

The drying testing method based on the methodology proposed by Mitchell (1979) was improved by Lytton et al. (2004) and Bulut et al. (2005) for the drying diffusion coefficient measurements. In this study, the drying testing equipment and method are modified for the measurement of wetting diffusivity parameters (Figure 2). The new equipment has enabled the measurements of drying and wetting parameters on the same soil specimens using total suction measurements with time. Temperature control is extremely important in total suction measurements (Bulut et al. 2005). The

water bath developed at Oklahoma State University is an important tool in maintaining the testing temperature of the specimens at relatively constant levels. This water bath can be used to perform drying and wetting coefficient measurements for up to ten samples at the same time. The testing room is maintained at 25±0.1 ^{o}C and a dehumidifier was used to control the relative humidity in the room. A typical diffusion test takes about seven to ten days to complete a drying and wetting cycle, depending on the soil texture and the initial suction level of the sample. Typical suction values with time on a soil specimen exposed to one drying and wetting cycle using the above testing procedure is depicted in Figure 3.

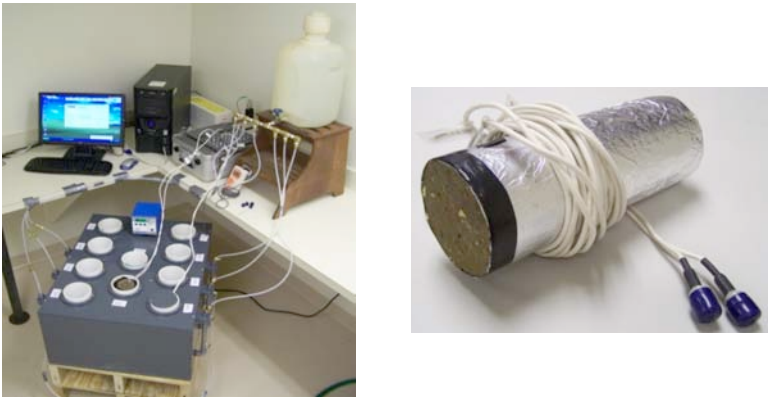

Figure 2. Wetting and drying diffusion test setup

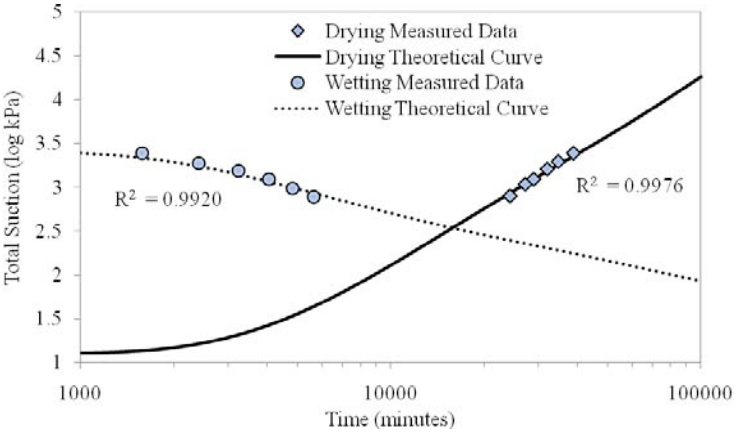

Figure 3. Theoretical versus measured total suction values with time

The filter paper method was also used to validate the initial total suction levels of the soil specimens. The testing procedure in Bulut et al. (2001) was adopted for the laboratory filter paper measurements. Schleicher and Schuell No. 589 – White Hard (WH) filter papers were used in the study. The use of the filter paper method is especially warranted for low suction levels at which the reliability of thermocouple psychrometers are questionable. This method gives relatively consistent measurements at low suctions compared to thermocouple psychrometer readings. The atmospheric suction in the laboratory was determined by measuring the relative humidity in the air using a digital thermo-hygrometer. The atmospheric suction was then calculated using Kelvin's equation (Fredlund and Rahardjo 1993).

TEST RESULTS

Nine undisturbed soil specimens, obtained from a compacted highway embankment site in Oklahoma, were tested to determine the wetting and drying diffusion coefficients. The soil specimens were obtained near the ground surface at shallower depths. The specimens had initial soil total suction values ranging from 1.12 to 2.45 log kPa, as determined by the filter paper method. The atmospheric suction in the testing room was relatively constant at 5.24 log kPa by running a dehumidifier during the course of the testing. Two psychrometers were used for each diffusion test and the suction values from psychrometer closest to the open end were used for data interpretation. The testing sequence started with the drying process to obtain the drying diffusivity coefficient and then the wetting process to obtain the wetting diffusivity coefficient. The drying and wetting diffusion coefficients for each sample were determined on the same soil specimen. The results are given in Table 1.

Table 1. Soil Moisture Wetting and Drying Diffusivity Parameters

Soil No.	Atterberg Limits		% Finer #200 Sieve (%)	[c]Drying Test			[c]Wetting Test		
	LL (%)	PL (%)		[a]u_o	$\alpha_{dry_2} \times 10^{-3}$ (cm^2/min)	[b]R^2	[a]u_o	$\alpha_{wet_2} \times 10^{-3}$ (cm^2/min)	[b]R^2
1	59.1	25.7	91.7	1.35	1.0158	0.9953	3.33	1.0026	0.9984
2	57.7	27.0	92.7	1.27	1.2816	0.9976	3.43	1.0158	0.9971
3	48.4	23.5	89.7	1.12	1.5837	0.9976	3.42	1.9316	0.9920
4	52.5	23.8	90.1	2.14	0.6316	0.9939	3.43	1.4474	0.9954
5	49.8	22.1	90.2	1.83	0.9368	0.9985	3.46	1.2421	0.9965
6	54.2	22.3	90.5	2.45	0.5211	0.9982	4.36	0.9526	0.9991
7	50.3	21.1	91.0	1.90	0.7895	0.9997	3.43	1.5263	0.9858
8	55.5	21.8	89.4	2.03	1.2421	0.9989	3.47	1.7789	0.9979
9	47.7	20.9	92.2	1.80	1.0526	0.9996	3.45	1.3874	0.9983

[a]u_o = Initial total suction (log kPa), [b]R^2 = Goodness of Fit values between measured and predicted total suctions, [c]Testing sequence: first performed drying test and then wetting test.

The drying diffusion measurements range from 0.5211×10^{-3} to 1.5837×10^{-3} cm^2/min while the wetting diffusion measurements are from 0.9526×10^{-3} to 1.9316×10^{-3} cm^2/min. The diffusivity measurements indicate that α_{wet} values are generally higher than α_{dry} values by factors ranging from 0.8 to 2.3. These differences are probably due to the formation of crack networks within the soil column, which lead to moisture migration paths that are much shorter than those that would exist if the soil mass behaves as an intact medium. Several small-size cracks were observed on the open end of the soil column during the drying process and those cracks were closing up at the end of the wetting process. Also, root-holes in the soil column caused by the vegetative influence create water migration paths thus contribute to the differences in the diffusion values.

CONCLUSIONS

Testing equipment developed for the drying and wetting diffusion coefficient measurements in the laboratory provides a strong tool to study the hysteresis between the drying and wetting process in a soil profile. The equipment can be used for running multiple tests at the same time under a controlled temperature environment. The wetting diffusivity parameters are generally higher than the drying diffusivity values. This approach provides a very simple framework for experimental measurement of diffusion properties on an economical and routine basis.

ACKNOWLEDGEMENTS

The authors are thankful and acknowledge the support provided by the Oklahoma Transportation Center and Oklahoma Department of Transportation.

REFERENCES

Bulut, R., Lytton, R.L., and Wary, W.K. (2001). Soil suction measurements by filter paper. Expansive Clay Soils and Vegetative Influence on Shallow Foundations (GSP 115), ASCE, Reston/VA: 243-261.

Bulut, R. and Wary, W.K (2005). Free energy of water suction in filter papers. ASTM Geotechnical Testing Journal, 28: 355-364.

Bulut, R., Aubeny, C.P., and Lytton, R.L. (2005).Unsaturated soil diffusivity measurements. Proceedings of an International Symposium on Advanced Experimental Unsaturated Soil Mechanics, Trento, Italy, June 27-29: 281-286.

Fredlund, D.G. and Rahardjo, H. (1993). Soil Mechanics for Unsaturated Soils, John Wiley and Sons Inc., New York.

Lytton, R.L., Aubeny, C.P, and Bulut, R. (2004). Design Procedure for Expansive Soils, FHWA/TX-05/0-4518-2, Texas Transportation Institute, College Station, Texas.

Mitchell, P.W. (1979). The Structural Analysis of Footings on Expansive Soils. Research Report No. 1, Kenneth W.G. Smith and Associates Pty. Ltd., Newton, South Australia.

Influence of Initial Water Content on the Collapsibility of Loess

M. Wang[1], X. Bai[2], and D. Frost[3]

[1] PhD Candidate, Taiyuan University of Technology, 79 West Yingze Street, Taiyuan, Shanxi, 030024 and Visiting Scholar, Georgia Institute of Technology, 210 Technology Circle, Savannah, GA 31407, e-mail: mwang43@mail.gatech.edu
[2] Professor and Dean, College of Architecture and Civil Engineering, Taiyuan University of Technology, 79 West Yingze Street, Taiyuan, Shanxi 030024, e-mail: bxhong@tyut.edu.cn
[3] Professor and Vice Provost, Georgia Institute of Technology, 210 Technology Circle, Savannah, GA 31407, e-mail: dfrost@ce.gatech.edu

ABSTRACT: Collapse of loess is the combined effect of a number of factors acting together. The water content is the most important of these factors. Based on a series of consolidation tests on Yuncheng loess, the influence of initial water content on the collapsibility of loess was investigated. As the initial water content increases, the compressibility of the loess increases, while the collapsibility coefficient, the peak collapsibility coefficient and the peak collapse pressure all decrease. Overall, the collapsibility of the loess decreases. Collapse will likely not occur if the initial water content yields a collapsibility coefficient of less than 0.015. In addition, scanning electron microscopy analysis indicated that the void area ratio of the loess specimens decreases as the initial water content increases, while the density of the loess increases and the collapsibility of the loess decreases.

INTRODUCTION

The collapsibility of loess is a measure of the degree to which a loess material with high strength and low compressibility at low water content loses strength or collapses when it is immersed in water or is even exposed to limited increases in water content (Xie 2001). Most accidents at collapsible loess sites are caused by the alteration of in-situ water content and the collapsibility of loess is closely associated with changes in water content. Accordingly, it is important to characterize the properties of loess as a function of changing water content (Zhang and Zhang 1995). Further, it is equally important to study the behavior of loess in the process of increasing and/or decreasing water content.

In this study, undisturbed loess samples from three different depths were taken by digging exploratory pits manually from a site in Yuncheng city in Shanxi province. After being cut, packed and sealed, the samples were sent to the laboratory to perform a series of tests to determine their physical and mechanical properties. The properties and grain size distribution of samples are shown in Table 1 and Table 2, respectively. All three samples are classified as sandy silts.

Table 1. Properties of loess

Sample	Water content	Unit weight	Dry unit weight	Void ratio	Saturation degree	Liquid limit	Plastic limit	Plastic index	Liquidity index
	ω	γ	γ_d	e	Sr	W_L	W_P	I_P	I_L
	%	kN/m^3	kN/m^3		%	%	%		
YC1	11.2	15.1	12.4	0.997	32.2	24.8	18.4	6.4	-1.12
YC2	12.8	15.2	11.0	0.998	34.6	26.0	19.2	6.8	-0.935
YC3	15.3	16.1	9.9	0.912	42.7	26.2	19.1	7.1	-0.54

Table 2. Grain size distribution of loess (%)

Sample	Sand particle	Silt particle (coarse)	Silt particle (fine)	Clay particle	Colloidal particle
	>50 μm	50-10 μm	10-5 μm	<5 μm	<2 μm
YC1	25.1	49.9	8.6	16.4	11.0
YC2	13.1	55.7	12.3	18.9	13.3
YC3	26.6	48.8	7.1	17.5	13.3

For each loess sample, five different initial water content specimens were prepared by increasing or decreasing the water content from the natural water content. Decreasing the water content was achieved by putting the specimen in a ring wrapped in plastic film into desiccators without water. The moisture in the specimen can thus be uniformly removed slowly to reduce the water content. The procedure of increasing the water content is to add the water into the specimen evenly by syringe, before putting the specimens wrapped in plastic film into desiccators with water for at least 24 hours. The total amount of water for addition into a specimen was injected in three equal increments. Five different initial water contents (a through e) were thus prepared for the three specimens YCI, YC2 and YC3 as shown in Table 3.

Table 3. Initial water content of loess

Sample	Depth (m)	Natural water content (%)	Initial water content (%)				
			a	b	c	d	e
YC1	3	11.2	11.2	15	18	22	25
YC2	8	12.8	12.8	15	18	22	25
YC3	14	15.3	12	15.3	18	22	25

The collapsibility of specimens with different initial water contents was tested using incremental consolidation tests. The applied pressures in the tests were 25, 50, 100, 200, 300, 400, 600, 800 and 1200 kPa. The deformation of the specimens was tested both under the initial water content and after being immersed in water. The collapsibility coefficient of the specimens was calculated from the difference in deformation of these specimens. The specimen to be immersed was loaded under a pressure of 50 kPa until deformation became steady. The specimen was then immersed in water and allowed to further deform until its deformation became steady again, before it was loaded incrementally to the remaining pressure levels.

Specimens with different initial water contents were impregnated with an epoxy resin to fix their structure. Each specimen was then cut to yield coupons which measured 20×20×5 mm for one of two observation planes, either a horizontal plane or a vertical plane. After grinding and polishing the appropriate surface of each coupon, they were placed under a scanning electron microscopy for observation.

Based on the consolidation test results, the relationship between pressure and deformation as well as between pressure and collapsibility coefficient for specimens with different initial water contents was quantified. Images of microstructure from specimens with different initial water contents were also captured using scanning electron microscopy and the void area ratios of the images were determined. Variations in the microstructure of the loess specimens as a function of different initial water content were identified.

COMPRESSIBILITY WITH DIFFERENT INITIAL WATER CONTENTS

The relationship between deformation and pressure (S-logP) for the three loess specimens at their natural water contents are shown in Figure 1. The deformation of the specimens at a given pressure decreases with increasing loess sample depth.

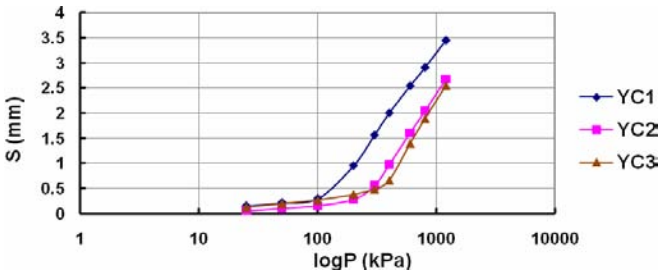

Figure 1. S-logP plot of YC samples from different depths and natural water content

The S-logP curves in Figure 2 indicate the relationship between pressure and deformation for the loess specimens with different initial water contents. The three groups of compression curves for specimens from different depths are similar in shape, however the magnitudes of the deformation vary.

For example, when the specimen is compressed under a lower pressure, the slope of the compression curve of YC1 (from a depth of 3 m) is bigger than that for YC3 (from a depth of 13 m), while YC2 (from a depth of 7 m) is intermediate between them. The increase in deformation for the shallower loess specimen is greater than for the deeper ones. When the pressure exceeds a particular value, (for YC1 it is about 300 kPa, for YC2, about 400 kPa, and for YC3, about 600 kPa,) the slope of each S-logP curve decreases. The pressure at which the deformation rate decreases, increases with increasing sample depth. Under the highest applied pressure of 1200 kPa, the largest deformation for YC1 at different water contents ranges from 3.4-4.5 mm, for YC2 from 2.6-3.8 mm, and for YC3 from 2.0-3.2 mm. The deformation decreases with increasing sample depth.

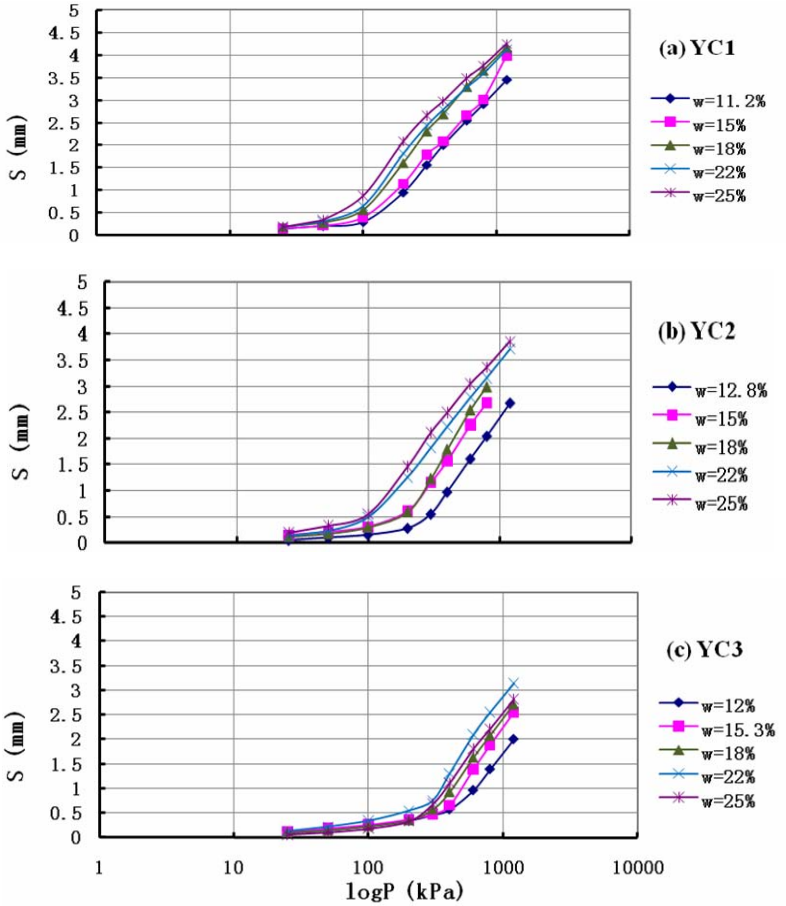

Figure 2. S-logP plot of YC samples with different initial water content

It can be seen in the S-logP curve of YC1 at different initial water contents (Fig. 2a) that the deformation changes with an increase in the initial water content. When the water content is smallest (11.2%), its compression curve is lowest in the group, while those at 15%, 18%, and 22% are higher in the sequence. The curve for the largest water content of 25% is highest within the group. The curves for YC2 and YC3 are similar. The deformation of the loess specimens increases with increasing initial water content.

The compression curves of specimens from different depths with similar initial water contents can be seen in Figure 3. In all five curve groups, YC1 samples from a depth of 3 m are always at the top of the groups, YC3 samples from the depth of 14 m are below the other curves. So whatever the initial water content is, the deformation of the specimens at a given pressure decreases with increasing loess sample depth.

As shown in the deformation curves of loess, the deformation increases with increasing pressure. The increase of deformation for shallower specimens is larger than for deeper specimens under lower pressures. The pressure at which deformation rate decreases from fast to slow, increases with specimens depth. The deformation of loess increases with increasing initial water content.

COLLAPSIBILITY COEFFICIENT WITH DIFFERENT INITIAL WATER CONTENTS

The collapsibility coefficient is defined as:

$$\delta_s = \frac{h_p - h_p'}{h_0} \tag{1}$$

where h_p is the height of the specimen at the initial water content, h_p' is the height of the specimen immersed in water and h_0 is the initial height of the specimen.

The relationship between collapsibility coefficient and pressure (δ_s-P) for Yuncheng loess specimens at their natural water content is shown in Figure 4. When the pressure is applied to the specimen, the collapsibility coefficient increases quickly with increasing pressure. When the pressure exceeds a certain value, the collapsibility begins to decrease. There is a peak in the collapse curve. The corresponding values on the x and y axes are the peak collapse pressure and peak collapsibility coefficient, respectively. With increasing sampling depth, peak collapsibility coefficient decreases and collapse pressure increases, and thus the collapsibility of the loess is reduced.

It can be seen from the P-δ_s plots for loess specimens from different depths (Fig. 5) that the curves for different initial water contents decrease with an increase in the initial water content and the collapsibility coefficient also decreases. For the collapse curve groups for samples from different depths, both the peak collapsibility coefficient and the peak collapse pressure change.

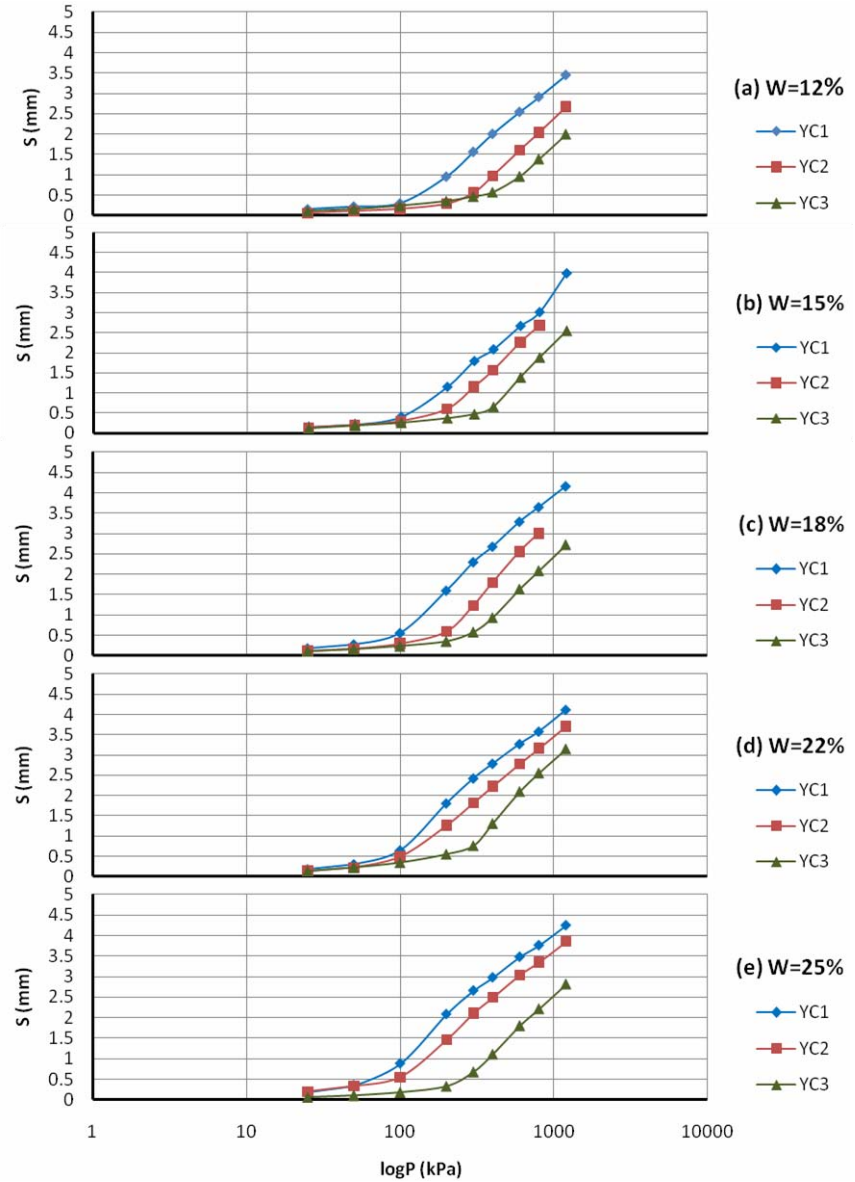

Figure 3. S-logP plots of YC samples from different depths and initial water content: (a) w = 12%, (b) w = 15%, (c) w = 18%, (d) w = 22%, (e) w = 25%

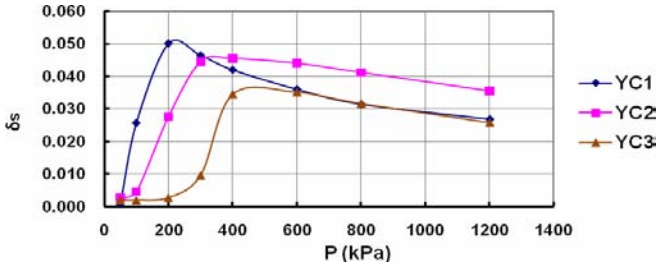

Figure 4. δ_s-P plot of YC samples from different depths and natural water content

With increasing initial water content, the peak collapsibility coefficient (δ_{smax}) decreases and the collapsibility of the loess is reduced. When δ_{smax} falls below 0.015, for example, all points on the curve for YC2 with an initial water content of w=25% have a δ_s value below 0.015. This means that when the initial water content of the loess specimen rises above a particular value, the specimen will not collapse, irrespective of the pressure applied to it. This value can be called the collapse limiting water content. If the initial water content is larger than the collapse limiting water content, collapse will not occur.

The peak collapse pressure exhibits a tendency to decrease with increasing initial water content, but it varies within a narrow range. With increasing initial water content, the peak collapse pressure for YC1 is about 200 kPa, for YC2 drops from about 350 kPa to about 250 kPa, and for YC3 drops from 600 kPa to 400 kPa with increasing initial water content. The peak collapse pressure becomes larger with the increase in sample depth and becomes smaller with increasing initial water content.

The collapsibility coefficient (δ_s) is an important parameter for characterizing loess. It is the difference in deformation between the specimen immersed in water until saturated and the specimen at the initial water content divided by the height of the sample. When the initial water content increases, the deformation of the specimen increases, but the deformation of the saturated specimen immersed in water is constant, so the collapsibility coefficient decreases as initial water content increases.

MICROSTRUCTURE WITH DIFFERENT INITIAL WATER CONTENT

Images were captured at nine evenly distributed locations on both horizontal and vertical planes from loess specimens with different initial water contents using scanning electron microscopy and were analyzed using a digital image analysis system. Table 4 summarizes the void area ratios of Yuncheng samples at their natural water contents. Figure 6 shows the variation in the void area ratios of specimens with different initial water contents. It can be seen in Figure 6 that the void area ratios of both horizontal and vertical planes declines as the initial water content increases. As the initial water content increases, the void area of the samples reduce, the density of the samples increase and the collapsibility of the loess decreases.

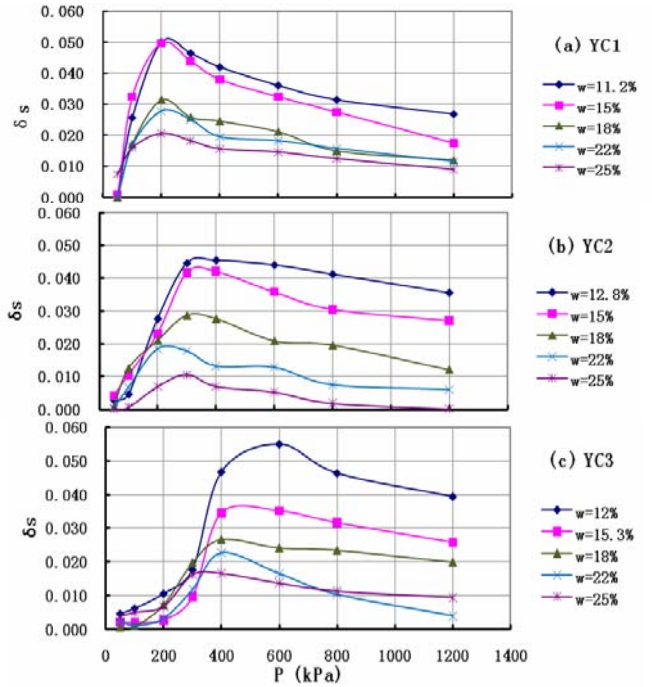

Figure 5. δ_s-P plots of YC samples with different initial water contents

The void area ratios at the natural water contents (Table 4) are smaller than those for samples at different initial water contents (Fig. 6). That is because the initial water content is increased by adding small quantities of deionized water into the undisturbed samples at the natural water contents. The added water dissolves soluble salts in the loess and increases the void area ratio of the samples (Bai et al. 2001). The microphotographs of loess specimens with different initial water contents are shown in Figure 7. The void area ratios of the images shown in the figure are similar to the average values for those specimens. As can be seen in the plots, the microstructure of the loess becomes denser as the initial water content increases.

Table 4. The void area ratio of loess with natural water content

Sample	Water content (%)	Plane	Void area ratio (%)
YC1	11.2%	H	0.465
		V	0.538
YC2	12.8%	H	0.543
		V	0.509
YC3	15.3%	H	0.492
		V	0.484

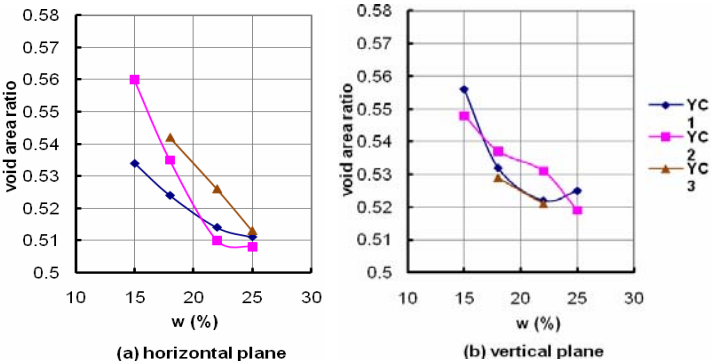

Figure 6. The void area ratio of loess with different initial water content

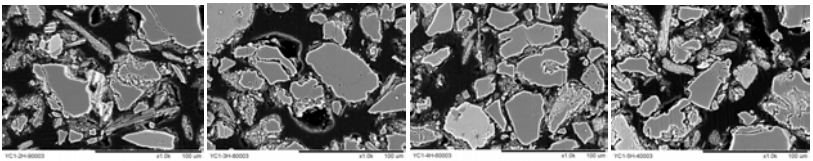

w = 15% w = 18% w = 22% w = 25%

Figure 7. Microphotograph of loess with different initial water contents

CONCLUSIONS

As the initial water content of the loess increases, the deformation of the specimen increases, the collapsibility coefficient decreases, the void area ratio in the microphotograph decreases, the microstructure of the specimen becomes denser and the collapsibility of the specimen decreases. When the initial water content is larger than the collapse limiting water content, collapse will not occur under any applied pressure level. Both the peak collapsibility coefficient and the peak collapse pressure decrease as the initial water content increases.

REFERENCES

Bai, X., Zhang, D. and Wang, M. (2001).The relationship between microstructure and collapsibility of Lucheng loess. Collapsibility Loess Research and Engineering, China Architecture and Building Press, 93-96.

Xie, D. (2001). Exploration of some new tendencies in research of loess soil mechanics. Chinese Journal of Geotechnical Engineering, 23(1), 3-13.

Zhang, W. and Zhang, S. (1995). Development of loess engineering properties research in China. Chinese Journal of Geotechnical Engineering, 17(6), 80-88.

Treatment of Collapsible Soils by Salts Using the Double Consolidation Method

K. Abbeche[1], O. Bahloul[1], T. Ayadat[2], and A. Bahloul[3]

[1] Civil Engineering Department, LARHYA, University of Batna, Avenue Chahid Boukhlouf, Batna 05000, Algeria
[2] Civil Engineering Department, University of Concordia, Sir George Williams Campus, 1515 St. atherine West, EV002. 139, Montreal Quebec, Canada H3G-2W1
[3] CGI Technical Services, 1612 Wedding Way, Redding, California, 96003 USA

ABSTRACT: Collapsible soils are unsaturated soils which present a potential for large deformation and a complete change to the whole particle structure after wetting, with or without loading. These soils are characterized with loose structures composed of silt to fine-sand-size particles. Collapsible soils are deposited in arid and semi-arid regions. Due to the expansion of human activities, these regions are occupied aggressively leading to the use of large quantities of water, which creates favorable conditions for soil collapses. Theses soil failures lead to severe damage and large distress to man-made structures. The objective of this experimental study is to illustrate that the mechanical resistance of collapsible soil can be improved. This study demonstrates that it is possible to minimize the collapse potential C_p to an acceptable level after chemical treatment with salts (ammonium sulfates $(NH_4)_2SO_4$ and potassium chlorides KCl) at different concentrations (i.e., 0.5, 1.0, 1.5 and 2.0 mole/liter) and under different compaction energies. The method used in this study is based on oedometric tests with variable normal stresses.

INTRODUCTION

The collapse of natural ground constitutes the origin of several engineering challenges, such as excessive settlement of civil and road construction throughout the world. The collapse phenomenon can occur in the case of natural soil (wind deposits, alluvial deposits or residual soils) as well as in a compacted material (artificial fill compacted in the dry side of the optimum Proctor). Generally, collapsible soils are defined as metastable soils that contain voids within their structures, with grain sizes ranging from silt to fine sand. In a dry state, these soils are generally characterized by a

relatively important mechanical resistance but in the presence of a flood with water, they collapse, producing deformations which may cause the ruin of structures.

The Algerian south-east is constituted in large part by collapsible soils. Also, that area is known for the construction of pipelines and various structures for the oil industry. Following significant recent distresses affecting the oil infrastructure, attention is needed to understand the collapse mechanisms and find the best techniques to mitigate and stabilize such soils. Experimental and theoretical studies are currently being carried out to understand the several uncertainties involved in the phenomenon of collapse. Review of the literature has revealed that the majority of the research was devoted to the collapse mechanism, identification methods, treatment and prediction Rollins et al. (1994), Cui et al. (1999), Abbeche (2005) and Ayadat et al. (2007).

Building on collapsible soils requires either designing structures which can withstand large ground movement or treating the soils to make them less sensitive to variation of the water content. In practice, several processes of stabilization are available (mechanical and thermal stabilizations, or by material addition) however, the chemical technique of stabilization by salts has been recently used. Kaufhold et al. (2009) and Shao-Chi et al. (2009). The choice of one of these processes depends on several parameters such as economic considerations, the nature of the ground to treat, the availability of materials to be used as well as the environmental conditions.

The purpose of the present study is to illustrate that it is possible to decrease the collapse potential to an acceptable level of a soil sample reconstituted in the laboratory after treatment by salts, while varying the energy of compaction and the vertical load.

MATERIALS, EQUIPMENT AND TESTS

Sand

The tests were carried out on soils reconstituted in the laboratory. The sand used in the sample reconstitution comes from the Liwa River, located in the region of Biskra, Algeria, and was screened through the 2mm sieve. Results of SEM (XL 30 ESEM) analyses and physical characteristics are summarized as follows: coefficient of uniformity $C_U = 3.13$, coefficient of curvature $C_C = 1.07$, sand equivalent SE = 87 %. Figure 1 reveals various size grains but primarily coarse sand (D > 200 µm) composed of silica and some impurities of clay and iron. The sand is made up of 90% of silica.

Kaolin

The fine grained soil (D < 80 µm) used in this study is extracted from the Debbagh area of Guelma, Algeria. The SEM analysis shows the composition indicated on Figure 2 with the following physical characteristics: Liquid limit LL = 67, Plastic limit PL = 39, Specific Gravity Gs = 2.7. Figure 2 indicates that most of the sample is composed of kaolin (more than 95% of the sample), generally lower than 80µm, with titanium, lime and manganese impurities.

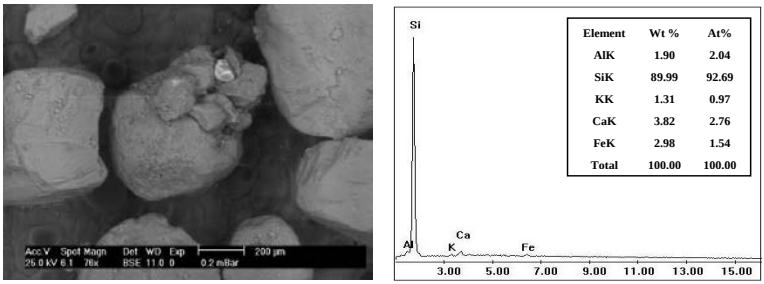

Figure 1. SEM (XL 30 ESEM) analysis of sand

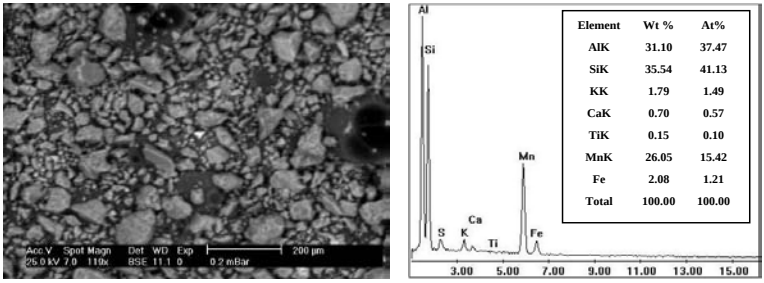

Figure 2. SEM (XL 30 ESEM) analysis of kaolin

Reconstituted Test Soil

The reconstituted soil sample is composed of 80% of sand and 20% of kaolin. The application of various criteria of collapse, as indicated by Lutenegger et al. (1988) and Abbeche et al. (2005), show that this material is collapsible. The SEM analysis reveals the composition presented in Figure 3.

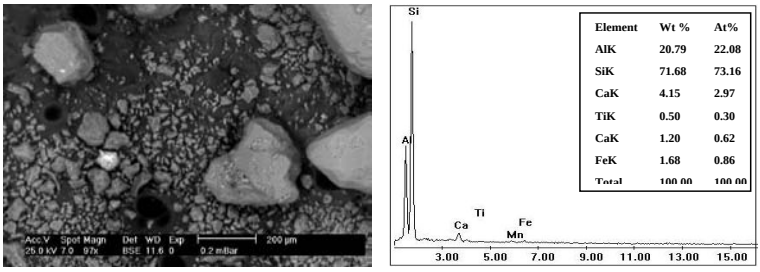

Figure 3. SEM (XL 30 ESEM) analysis of composite sample

Figure 3 reveals the presence of both coarse elements (D > 200 μm) which are siliceous sands, and fine elements (D < 80 μm) that represent the kaolin and titanium, manganese, lime and iron impurities. The reconstituted soil has a particle size distribution curve presented in Figure 4. Basic characteristics are given in Table 1.

Table 1. Properties of reconstituted soil sample

Material	Property
Reconstituted Soil (80% Sand + 20% Kaolin)	Coefficient of Uniformity, C_U = 5.13
	Coefficient of Curvature, C_C = 1.07
	Liquid Limit, LL = 28
	Plastic Limit, PL = 16
	Specific Gravity, G_S = 2.65
	Optimal Water Content, w_{opt} = 10.1%

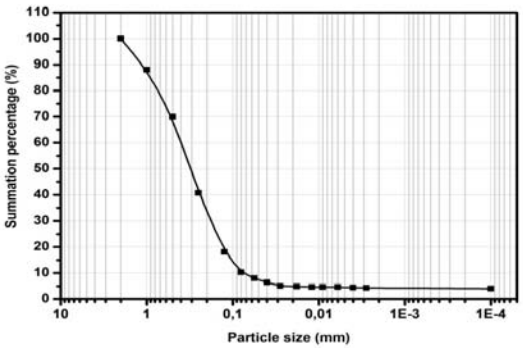

Figure 4. Particle size distribution curve of the composite sample

Equipment and Tests

The equipment used for the compaction of the sample was designed at the laboratory and is shown schematically in Figure 5: it is composed of a disc having a diameter slightly smaller than that of the ring, fixed at a guidance rod and a hammer in the shape of a disc. The 152g hammer falls along the rod with a drop of 15 cm and contacts the disc resulting in the compaction of sample in the oedometric ring, with the following compaction energy:

$$E_C = \left[\frac{\mathbf{n}.\mathbf{m}.\mathbf{g}.\mathbf{h}}{\mathbf{v}}\right] \text{ Joules/cm}^3 \quad (1)$$

where, Ec = compaction energy, n = number of drops, m = mass of disc (hammer), h = drop height, g = acceleration of gravity, v = volume of material before compaction.

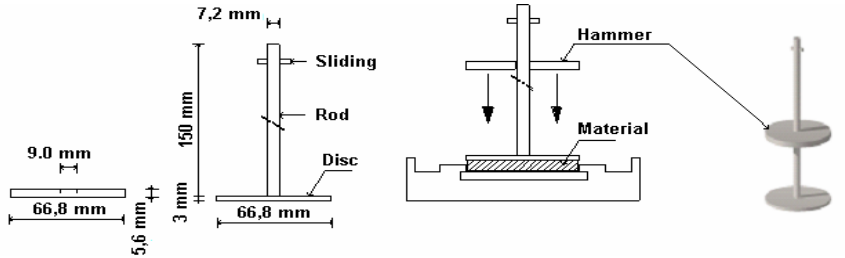

Figure 5. Compaction device

Oedometer Test Procedure

The concept is to reconstitute the soil in an oedometric mold with specific water content and dry density. The material is compacted in one layer because of the low thickness of the ring. Reconstituted soil exhibits good mechanical characteristics when it is compacted with a low initial water content (w_0 = 2, 4 and 6%). However, if moisture is introduced, even without additional load, the structure collapses and significant deformations occur. This behavior is illustrated in Figure 6, representing a typical curve of a double consolidation method for such soil. Jennings and Knight (1975) correlated the collapse potential C_p to the severity of foundation disorder (Table 2).

Table 2. Foundation disorder level based on collapse potential C_p (after Jennings and Knight 1975)

C_P (%)	Severity of Disorders
0 to 1	Minor disorders
1 to 5	Moderate disorders
5 to 10	Disorders
10 to 20	Severe disorders
› 20	Very severe disorders

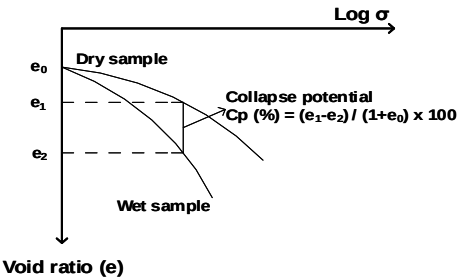

Figure 6. Typical oedometric curve for a collapsing soil

The salt solutions used for the soil treatment are potassium chloride (KCl) and ammonium sulfate (NH4)2SO4 with various concentrations (0.5, 1.0, 1.5 and 2.0 mole/liter). For this study, two collapse potentials C_p, before and after treatment, will be determined by the following formula based on the concept indicated in Figure 6:

$$C_p\,(\%) = \left[\frac{\Delta e}{e}\right] x100 \qquad (2)$$

where, Δe = variation of the void ratio between the dry sample and the saturated sample, and e_o = initial void ratio of the sample.

RESULTS AND ANALYSIS

From the results obtained in Figures 7 and 8, it is clear that collapse of soil without treatment correlates with the classification of Jennings and Knight (1975). Indeed, for various vertical stresses σ as well as for various compaction energies EC, the collapse potentials Cp vary from 0.98 to 12.40% for initial water content w0 = 2%; from 0.82 to 10.64% for initial water content w0 = 4%; and from 0.66 to 8.79% for an initial water content w0 = 6%. These results correspond to minor to severe disorders (table 2). It should be noted that the potential of collapse Cp decreases when initial water content increases. In the same way, Figures 7 and 8 clearly illustrate that for a given initial water content, the collapse potential Cp decreases by increasing the compaction energy, EC. These results agree with those of Lawton et al. (1989) and Abbeche et al. (2007 and 2009). It is observed that the reconstituted soil sample has a behavior similar to those encountered in situ, which justifies the experimental study.

Substantial reductions of the collapse potential Cp are obtained for soil sample treated with salt solutions such as potassium chloride KCl and ammonium sulfates (NH4)2SO4 at various concentrations. The collapse potential Cp is at its maximum for a vertical stress in the range of 400 kPa.

For a collapse potential at a vertical stress of 400 kPa, and for a low salt concentration 0.5 mole/liter, the reduction ratios of C_p vary from 12% to 30% and 3.5% to 12% for the salt solutions KCl and $(NH_4)_2SO_4$, respectively. For high concentrations 2 mole/liter, the reduction ratios of C_p vary from 62% to 68% and 40% to 60% for the salt solutions KCl and $(NH_4)_2SO_4$, respectively.

The collapse reduction ratio is related to the applied vertical stress, knowing that for low concentrations 0.5 mole/liter, this collapse reduction ratio varies from 8% to 26% and from 2% to 12% for a vertical constraint of 200 kPa, and for salt solutions KCl and $(NH_4)_2SO_4$, respectively; and it varies between 4% to 42% and 2% to 6% for the salt solutions KCl and $(NH_4)_2SO_4$, respectively; and for a vertical constraint of 800 kPa. For high salt concentrations 2 mole/liter, the collapse reduction ratio varies between 42% to 68% for KCl and between 39% and 50% for $(NH_4)_2SO_4$ for a vertical stress of 200 kPa. On the other hand for a vertical stress of 800 kPa, the values of the collapse reduction ratio vary between 17% to 67% for KCl and 9% to 37% for $(NH_4)_2SO_4$.

Lastly, it is noted that soil treatment by salt solutions KCl and $(NH_4)_2SO_4$ is affected by initial water content and the compaction energy.

Figure 7 shows clearly that the reduction ratio in C_p for a KCl solution concentration of 1.5 mole/liter converges closely with that of 2 mole/liter. Thus, the use of an optimal KCl solution concentration of 1.5 mole/liter provides a reasonably effective treatment.

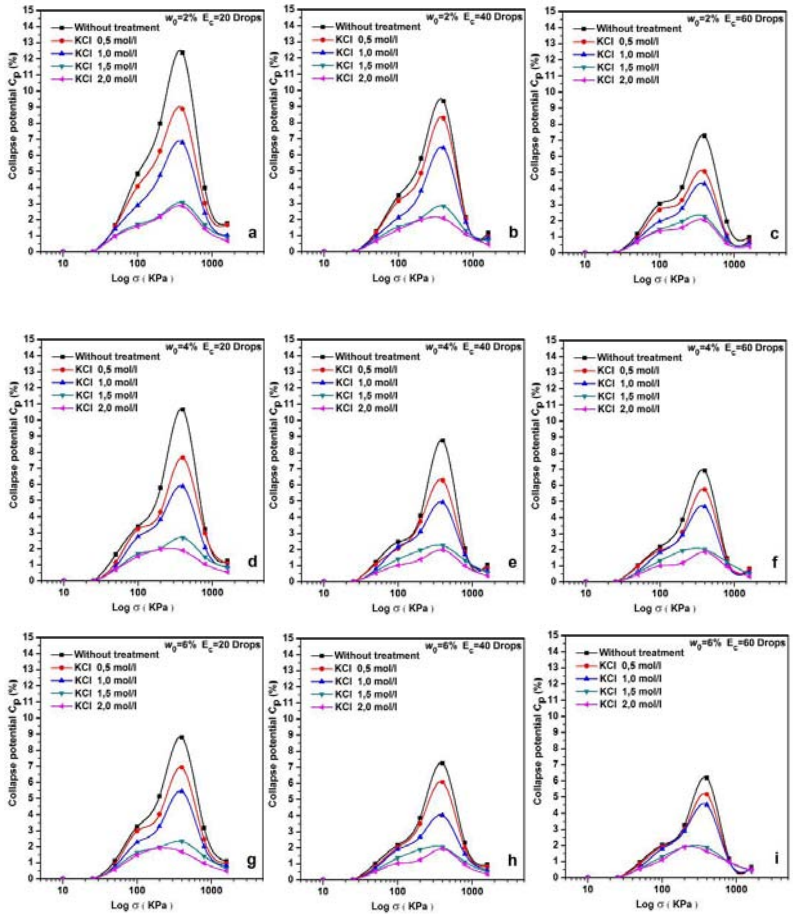

Figure 7. Variation of the collapse potential Cp vs. vertical load for various water contents and energies of compaction for treatment by KCl salt

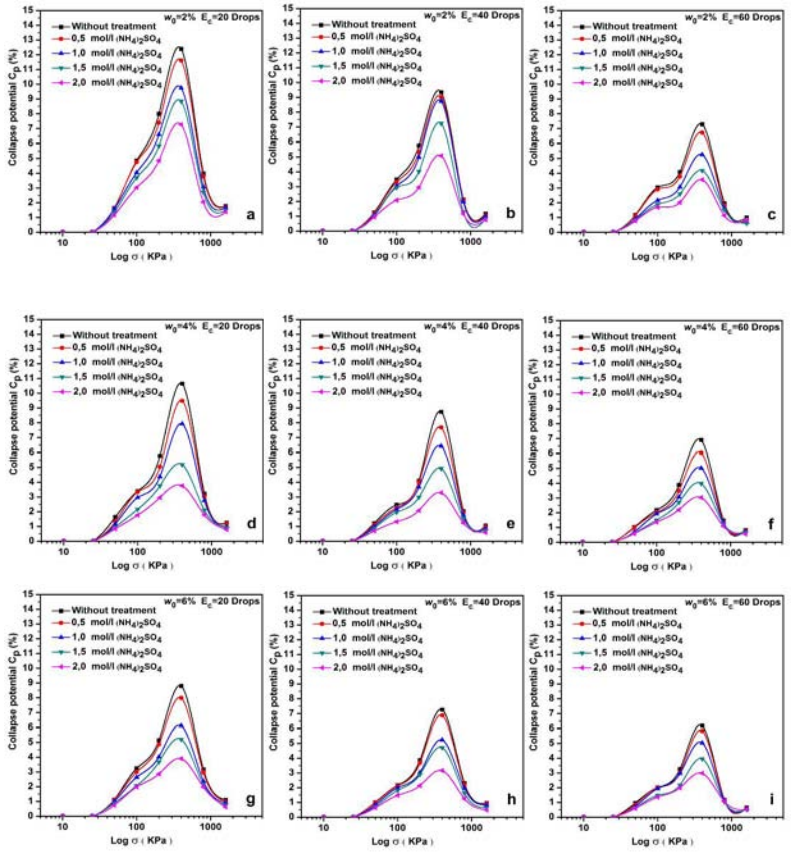

Figure 8. Variation of the collapse potential Cp vs. vertical load for various water contents and compaction energies for treatment by $(NH_4)_2SO_4$ salt

CONCLUSION

The collapse of soils is a very complex phenomenon with various numbers of intrinsic and environmental parameters. It is mainly caused by the rearrangement of the soil grains after moisture intrusion or flooding. However, a collapsible soil can be reconstituted at the laboratory, at varying densities, water contents, and soil gradations. The compressibility and consistency characteristics confirm that these materials have the characteristics of collapsible soils. First, the influence of certain parameters such as the water content and the compaction energy on the collapse potential was evaluated. Second, the obtained results show clearly that mineral salt has

a very strong effectiveness on reducing the collapse of soil. KCl proves to be the salt that has the most effect on reducing the rate of collapse C_P. A concentration in KCl of 1.5 mole/liter made it possible to reduce the rate of collapse C_P by about 60%.

The treatment method of collapsible soils depends on the thickness of the layer of soil to be treated. If the layer is less than 4m, it is economic to excavate and treat the soil with saline solutions and then recompact with adequate procedures. On the other hand, if the layer to treat is located at greater depth, the best treatment method is the injection of saline solutions.

Despite the results achieved by this study, it is necessary to note that when leaching of the salts occurs, the benefit of the treatment is reduced or removed leading to a reduction of the resistance of the soil. The lack of field data does not allow comments regarding the durability of the salt treatment. It should be noted that the site drainage is critical to mitigate or reduce the leaching process. This type of treatment is recommended where only minor to moderate amelioration of soil resistance is needed and where pre-saturation and pre-loading are not possible. Also, because these salts are relatively inexpensive, efficient at low concentration, and easy to incorporate, the treatment with salts is an affordable solution to consider and an economic alternative.

ACKNOWLEDGEMENTS

The authors would like to thank the members of CGI Technical Services for their contributions to this study.

REFERENCES

Abbeche, K. (2005). Etude de l'influence de la densité relative et l'indice de consistance sur le taux et l'amplitude de l'affaissement des sols. PhD Thesis University of Batna, Algeria.

Abbeche, K., Mokrani, L. and Boumekik, A. (2005). Contribution à l'identification des sols effondrables. Revue Française de Géotechnique.,110: 85-90

Abbeche, K., Hammoud, F. and Ayadat, T. (2007). Influence of relative density and clay fraction on soils collapse. Experimental Unsaturated Soil Mechanics, Springer Proceedings in Physics, 112: 3-9

Ayadat, T and Hanna, A. (2007). Identification of collapsible soils using the fall cone apparatus.Geotechnical Testing Journal., 30 (4).

Abbeche, K., Laouar, M., and Messaoud, F. (2009). Prediction of collapsing soil by the cone penetrometer and ultrasonic tests. International Symposium Unsat-Waste Shanghai, Chine.

Cui Y. J., Delage P., Schlosser F., and Wonarowcz M. (1999). Etude du comportement volumique d'un lœss du nord de la France. Xlléme Congrès européen de mécanique des sols et de géotechnique Amsterdam., 1: 337-342.

Jennings, J. E. and Knight, K. (1975). The additional settlement of foundation due to collapse of sandy soils on wetting. Proc. 4th Inter. Conf. on Soil Mechanics and Foundation Engineering., 1, pp 316-319

Kaufhold S., and Dohrman R. (2009) Stability of bentonites in salt solutions/sodium chloride. Applied Clay Science. 45: 171-177.

Lutenegger, A.J., and Saber R.T. (1988). Determination of collapse potential of soils. Geotechnical Testing J., 11, (4):173-178

Lawton E C,. Fragaszi R J., and James H. H. (1989). Collapse of compacted clayey sand. Journal of geotech. Eng. Div., ASCE, 155.(9): 1252-1267.

Rollins Kyle , M., and Wayne Rogers, G. (1994). Mitigation measures for small structures on collapsible alluvial soils. Journal of Geotechnical Engineering, 120, (9) Paper N° 1016.

Shao-Chi C., Chang-Yu O and Ming-Kuang W. (2009). Injection of saline solution to improve the electro-osmotic pressure and consolidation of foundation soil. Applied Clay Science, 44: 218-224.

Soil Water Characteristic Curve Parameters of Compacted Lateritic Soil Treated with Bagasse Ash

K.J. Osinubi[1], and A.O. Eberemu[2]

[1] Prof. Dept. of Civil Engrg. Ahmadu Bello University, Zaria.810001, Nigeria.
e-mail: kosinubi@yahoo.com
[2] Lecturer Dept. of Civil Engrg. Ahmadu Bello University, Zaria.810001, Nigeria.
e-mail: aeberemu@yahoo.com

ABSTRACT: Lateritic soil treated with up to 12% bagasse ash by dry weight of soil was prepared at -2, 0 and +2% of the optimum moisture content (OMC) and compacted with standard Proctor energy, for use as a suitable material in waste containment application. The treated soil was assessed to determine its soil water characteristic curve (SWCC) parameters that were used to predict the measured laboratory SWCC with Brooks - Corey (BC) and Van Genuchten (VG) models. VG n fitting parameter increased to a peak at OMC and thereafter decreased with higher molding water content, while α fitting parameter generally increased with higher molding water content. BC pore size distribution index (λ) increased with higher molding water content, while no clear trend was observed for air entry suction (ψ_a) with higher molding water content. VG n increased, while α decreased with higher bagasse ash content. Higher BC ψ_a and λ were obtained with higher bagasse ash content. BC model tends to over predict the volumetric water content (θ), particularly at low matric suction values, while VG model under predicts θ. Generally, the measured and predicted SWCC did not show great variation from each other but are fairly close.

INTRODUCTION

The purpose of the cover system in landfill is to prevent the generation of leachate by minimizing the amount of precipitation percolating through the waste during the inactive (post closure) period and provide containment and prevent physical dispersion by wind and water (Shackelford 1996). The hydraulic conductivity of unsaturated soils

is difficult to measure, partly due to its variability in the field as well as a very time-consuming process and very expensive.

The two common models for predicting unsaturated hydraulic conductivity from more easily measured parameters of the soil water characteristics curves (SWCC), using the saturated coefficient of permeability as an initial value are the Brooks - Corey (Brooks and Corey 1964) and Van Genuchten (Van Genuchten 1980) equations. The Brooks-Corey model is expressed as:

$$\Theta = \frac{\theta - \theta_r}{\theta_s - \theta_r} = \left(\frac{\psi_a}{\psi} \right)^{\lambda} \quad \psi \geq \psi_a$$

$$\Theta = 1 \text{ and } \theta = \theta_s \text{ where } \psi < \psi_a \tag{1}$$

where Θ is a normalized, dimensionless volumetric water content; and λ = a fitting parameter called the pore-size distribution index (Corey 1994) that is related to the slope of the curve and a function of the distribution of pores in the soil.

The Van Genuchten model is expressed as:

$$\Theta = \frac{\theta - \theta_r}{\theta_s - \theta_r} = \left\{ \frac{1}{\left[1 + (\alpha\psi)^n \right]} \right\}^m \tag{2}$$

where α, n and m are fitting parameters and m is equal to $1 - n^{-1}$. The parameter m, rotates the sloping portion of the curve. As m increases, the range of the curve between ψ_a and the knee (i.e., the point of inflection at the lower portion of the curve as it approaches a horizontal position) of the SWCC decreases. The parameter α is the pivot point of the curve and its value is related to the value of the air-entry suction. As α increases, the air-entry suction increases. The parameter n controls the slope of the SWCC about the pivot point, which occurs at normalized volumetric water content (Θ) of 0.5. As n increases, the sloping portion of the curve between ψ_a and the knee of the SWCC becomes steeper (Miller et al. 2002).

There exist little data in literature on the unsaturated hydraulic properties of compacted lateritic soil treated with bagasse ash for use in waste containment barrier applications. Consequently, the objectives of this study were to determine the soil water characteristic curve parameters of the compacted lateritic soil treated with bagasse ash and to use them to predict the measured laboratory soil water characteristic curves based on the Brooks - Corey (1964) and Van Genuchten (1980) curve fitting models.

MATERIALS AND METHODS

Soil

The soil used in this study is a naturally reddish-brown lateritic soil obtained by method of disturbed sampling from a borrow pit in Shika area of Zaria (Latitude $11^{o}15'$N and Longitude $7^{o}45'$E), Nigeria. Previous studies on soils from this area have shown that kaolinite is the dominant clay mineral (Osinubi 1998). The soil is classified as A-7-6 (10) according to AASHTO soil classification system (AASHTO 1986) and low plasticity clay (CL) according to the Unified Soil Classification System (ASTM 1992).

Bagasse Ash

The bagasse ash used in this study was reported by Osinubi and Mohammed (2005) to be pozzolanic based on its oxide composition. The ash passed through BS No. 200 sieve (75 μm aperture) was mixed with the soil to form four different soil - bagasse ash mixtures in stepped increment of 4% up to 12% by weight of dry soil.

Index Properties

Laboratory tests were conducted to determine the index properties of the natural soil and soil - bagasse ash mixtures in accordance with British Standards (BS 1990a, b).

Preparation of specimens

All soil samples mixed with 4, 8, and 12% bagasse ash by dry weight of soil were prepared at -2, 0 and +2% of the optimum moisture content (OMC) (i.e., from the dry to the wet side of the line of optimum). Compaction using the standard Proctor energy in accordance with BS 1377 (1990) was carried out. Specimens were then cored from the extruded samples with rings having inside diameters of 50 mm and heights of 50 mm. The samples were covered with caps at both ends. Prior to saturation, the caps were removed and samples contained in the stainless steel rings were placed in an immersion tank. Water was allowed to saturate the samples by capillary action which lasted for about 3 weeks. Full saturation was confirmed when water rose to the surface of the soil specimens.

Application of pressure

The specimens were subjected to pressures of 10, 30, 100, 500, 1000 and 1500 kPa, respectively. On completion of the test, the equipment was disassembled, the soil specimen removed and placed in an oven to determine its final gravimetric water content. All computations were based on the as compacted soil-volumes.

DISCUSSION OF TEST RESULTS

Index Properties

The index properties of the natural lateritic soil and lateritic soil – bagasse ash mixtures determined in accordance with BS 1377 (1990) are summarized in Table 1.

Table 1: Physical properties of the natural and stabilized soils

Property	Natural Soil	Bagasse Ash Content, %		
		4	8	12
Natural Moisture Content, %	6.5	-	-	-
Liquid Limit, %	42	39.5	37.3	34.3
Plastic Limit, %	18	19	23	25
Plasticity Index, %	24	20.5	14.3	9.3
Linear Shrinkage, %,	6	5.5	4.7	3.5
Percent Passing BS No. 200 sieve	56.71	60.1	64.4	65.52
AASHTO classification	A-7-6 (10)	-	-	-
USCS	CL	CL	CL	CL
Specific Gravity	2.61	2.53	2.44	2.35
MDD, Mg/m^3	1.75	1.72	1.71	1.67
OMC, %	16	17	18.3	19.8
pH	6.7	-	-	-
Colour	Reddish Brown	-	-	-
Dominant Clay Mineral	Kaolinite	-	-	-

Soil Water Characteristic Curve Parameters

The soil water characteristic curve parameters are examined by considering the effects of moulding water and bagasse ash contents on them.

Effect of Moulding Water Content on SWCC Parameters

The effect of moulding water content on the soil water characteristic curve parameters using Van Genuchten and Brooks - Corey models are shown in Figs 1 and 2, respectively. Van Genuchten n that increased and decreased with higher moulding water content recorded a peak value at the optimum moulding water content (see Figure 1). According to Tinjum et al. (1997) the n value controls the slope of the SWCC with a decrease in its value that is reflected by an increase in slope. Van Genuchten's α generally increased with higher compaction moulding water content (see Figure 1). It initially decreased slightly from the dry side up to the optimum before increasing on the wet side, indicating the greater difficulty in de-saturating the soils on the wet side of optimum since the micro scale pores with minimal void ratio is dominant.

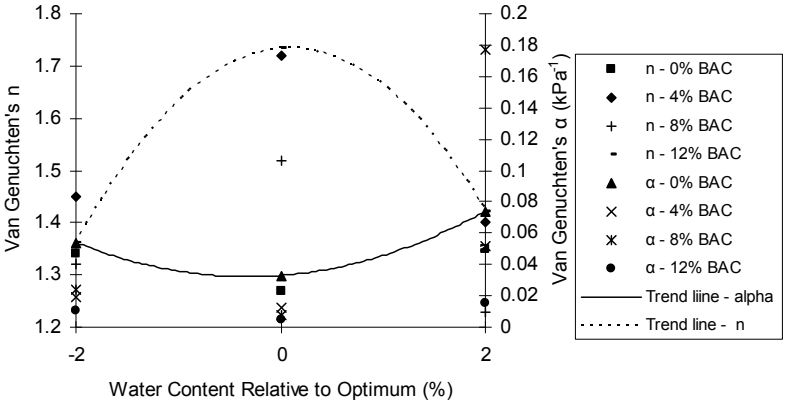

Figure 1. Variation of Van Genuchten n and α with water content relative to optimum

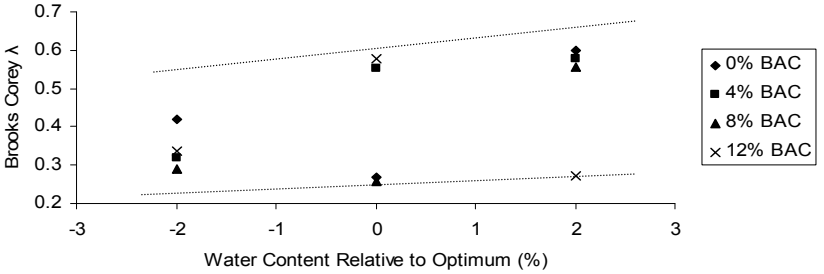

Figure 2a. Variation of Brooks - Corey's λ with water content relative to optimum

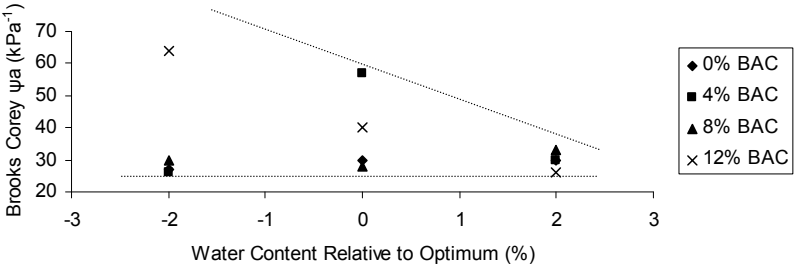

Figure 2b. Variation of Brooks - Corey ψ_a with water content relative to optimum

Brooks - Corey pore size distribution index (λ) generally increased with higher compaction moulding water content as shown in Figure 2a. There was a slight reduction from the dry side to the optimum before greater increase on the wet side which indicates the transformation in the pore sizes within the soil from the dry to wet side of compaction optimum. As the moulding water content increased, the macro scale pores that transited to the micro scale pores with minimal void ratio became dominant. No clear trend was observed for Brooks - Corey ψ_a with higher compaction moulding water content (see Figure 2b). Soils with smaller pores have higher air entry suction (ψ_a) while, soils with wider ranges of pore sizes exhibit greater changes in ψ_a (Hillel 1980, Fredlund and Rahardjo 1993) as the soil changes from macro scale pores to micro scale pores from the dry to wet side of optimum.

Effect of Bagasse Ash Content on SWCC Parameters

The variations of Van Genuchten parameters with bagasse ash content are shown in Figure 3. Van Genuchten n value (which controls the slope of the SWCC about the pivot point) increased while the slope of the SWCC decreased with higher bagasse ash content. The SWCC of specimens with higher bagasse ash treatments plotted above those with lower ash treatments which reflect as increase in Van Genuchten n values.

Van Genuchten α decreased with higher bagasse ash content. Optimum moisture content increased with higher bagasse ash content since more fines in the specimen with greater surface area required more water for reaction. This resulted in higher air entry suction characterized by smaller α requiring more suction to remove the water from the fabric of soil; since pore spaces were smaller and micro scale structure dominated.

Brooks - Corey's ψ_a increased with bagasse ash content. Higher bagasse ash treatment resulted in higher water content and higher air entry suction is required to desaturate the specimens as characterized by greater ψ_a values (see Figure 4). Brooks - Corey's λ increased with higher bagasse ash content as shown in Figure 4. According to Tinjum et al. (1997) soil with steeper SWCC is characterized by smaller λ as observed with increase in bagasse ash content on the SWCC generating λ.

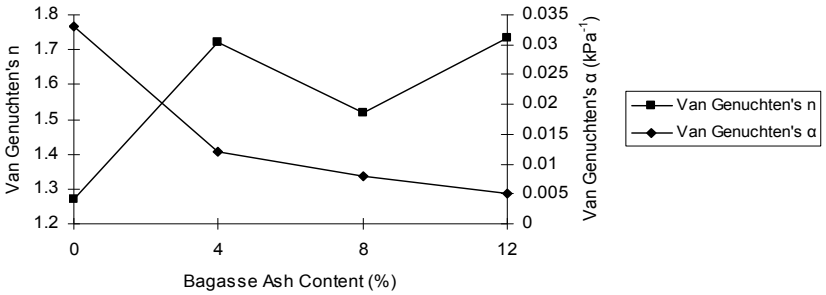

Figure 3. Variation of Van Genuchten's n and α with bagasse ash content

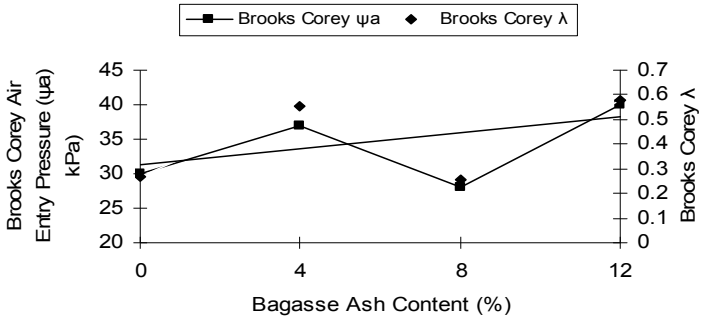

Figure 4. Variation of Brooks - Corey's ψ_a and Brooks - Corey's λ with bagasse ash content

Prediction of Soil Water Characteristics Curves

Brooks - Corey and Van Genuchten models expressed in eqs. (1) and (2), respectively, were used in conjunction with the SWCC fitting parameters generated from measured laboratory results to predict the SWCC. The predicted values were in turn compared with the SWCC obtained from measured soil water retention data. Plots of SWCCs predicted with measured laboratory curves at optimum moisture content for the various bagasse ash contents (BAC) are shown in Figure 5.

The plots show that Brooks - Corey model tends to over predict the volumetric water content (θ) particularly at low suction values, while Van Genuchten's model tends to under predict it. However, the values are close to those measured in the laboratory. Generally, residual volumetric water content (θ_r) values from measured laboratory data were lower than the predicted values in all bagasse ash treatments. Also, the measured and predicted SWCC did not show great variations from each other because measured and predicted θ values are fairly close. Similar results were obtained by Tinjum et al. (1997); Chiu and Shackelford (1994) as well as Nwaiwu (2004).

CONCLUSIONS

A reddish brown lateritic soil treated with up to 12% bagasse ash by dry weight of soil; prepared at -2, 0 and +2% of the optimum moisture content was compacted with standard Proctor energy, for use as a suitable material in waste containment application. The lateritic soil-bagasse ash mixtures were assessed to determine their soil water characteristic curve (SWCC) parameters as well as predict the measured laboratory SWCCs using parameters provided by the Brooks - Corey (BC) and Van Genuchten (VG) models.

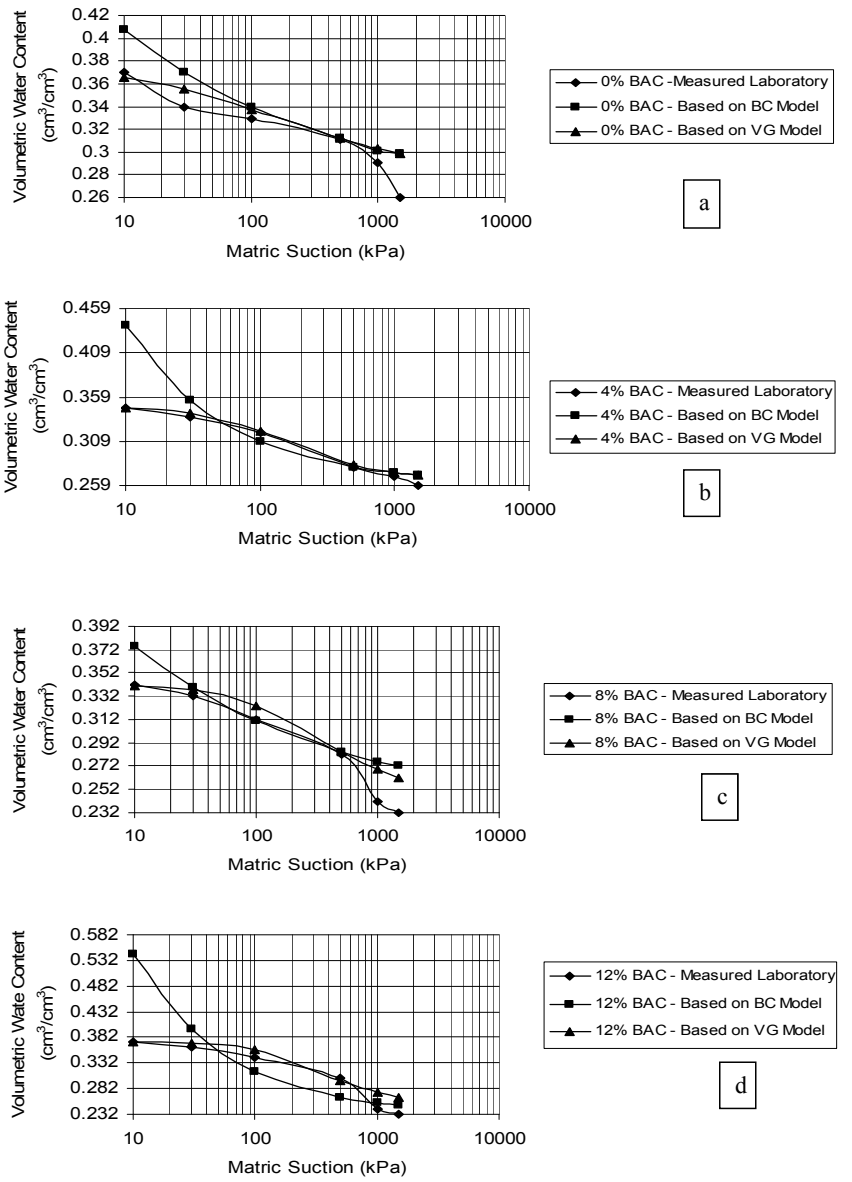

Figure 5. SWCC and curve fits at optimum moisture content for different bagasse ash contents: (a) 0% BAC, (b) 4% BAC, (c) 8% BAC, (d) 12% BAC

Van Genuchten n that increased and decreased with higher moulding water content recorded a peak value at the optimum moulding water content, while α increased with higher molding water content. Brooks - Corey pore size distribution index (λ) increased with higher molding water content. No clear pattern was observed for Brooks - Corey ψ_a with higher compaction moulding water content. VG n increased, while α decreased with higher bagasse ash content. Higher BC ψ_a and λ values were obtained with increased bagasse ash content.

BC model tends to over predict the volumetric water content (θ) particularly at low matric suction values, while VG model under predicts θ. Residual volumetric water content (θ_r) was lower for laboratory values compared to predicted values. Generally, the measured and predicted SWCC did not show great variation from each other being fairly close.

REFERENCES

AASHTO (1986). Standard specification for transportation materials and methods of sampling and testing, 14th Ed., Washington, D.C.

ASTM, (1992), Annual book of ASTM standards, Vol. 04.08, Philadelphia.

British Standard Institute. (1990a). "Methods of testing soils for civil engineering purposes." BS 1377, London.

British Standard Institute. (1990b). "Methods of tests for stabilized soils." BS 1924, London.

Brooks, R. H., and Corey, A. T. (1964). 'Hydraulic properties of porous medium.' Hydrology Paper No. 3. Civil Engrg. Dept, Colorado State Univ. Fort. Collins, Colorado.

Chiu, T. F. and Shackelford, C. D. (1998).'Unsaturated hydraulic conductivity of compacted sand-kaolin mixtures.' J. Geotech. and Geoenviron. Engrg., ASCE, 124(2), 160-170.

Fredlund, D. and Rahardjo, H. (1993). ' Soil Mechanics for Unsaturated Soils.' John Willey and Sons Inc. New York. N. Y.

Hillel, D. (1980). Fundamentals of Soil Physics. Academic Press, Inc., San Diego, California.

Miller, C. J, Yesiller N., Yaldo, K., Merayyan, S. (2002).'Impact of soil type and compaction conditions on soil water characteristics.' J. of Geotech. and Geoenvironmental Engrg. A.S.C.E. 128(9), 733-742.

Nwaiwu, C. M. O. (2004). 'Evaluation of compacted lateritic soils as hydraulic barriers in municipal solid waste containment systems'. Unpublished Ph.D. Dissertations. Ahmadu Bello University, Zaria, Nigeria

Osinubi, K. J. (1998). 'Influence of compactive efforts and compaction delays on lime treated soils.' J. of Transp. Engrg. A.S.C.E. 124(2), 149-155.

Osinubi K. J. and Mohammed, M. A.(2005). "Potentials of bagasse ash as pozzolans." Proceedings of the Nigerian Material Congress 2005 (NIMACON 2005). 17 – 19 Nov., Zaria, Nigeria. 41-45.

Shackelford, C. D. (1996). 'Geoenvironmental design consideration for tailing dams.' Proc. of the International Symp. On Seismic and Environmental Aspects of Dam Design: Earth, Concrete and Tailing Dams. Santiago, Chile, Oct. 14-18, Vol. 1.

Tinjum, J. M, Benson, C. H., Boltz, L. R. (1997). 'Soil water characteristics curves for compacted clay.' J. of Geotech. and Geoenvironmental Engrg. ASCE, 123(11), 1060-1069.

Van Genuchten, M.T. (1980). "A closed form equation for predicting the hydraulic conductivity of unsaturated soils." Soil Sci. Soc. Am. J., 44, 892-898.

Variations in Soil Water Characteristic Curves of Lateritic Soil Treated with Bentonite

K.J. Osinubi[1], and A.A. Amadi[2]

[1] Osinubi, K. J. Department of Civil Engineering, Ahmadu Bello University., Zaria 810001, Nigeria, e-mail: kosinubi@yahoo.com
[2] Amadi, A. A. Department of Civil Engineering, Federal University of Technology. Minna, Nigeria, e-mail: agapitusahamefule4@yahoo.com

ABSTRACT: Soil water characteristic curve (SWCC), which defines a soil's ability to store and release water as it is subjected to various soil suctions, is an important tool to estimate and interpret unsaturated sol property functions. The purpose of this study was to estimate SWCC data for lateritic soil - bentonite mixtures proposed as a barrier material in waste containment systems. Also, the effect of various compaction states, namely dry, optimum and wet moisture conditions, using standard Proctor energy on SWCCs of the mixtures was examined. The SWCCs were measured in the laboratory by sequential desorption of saturated compacted lateritic soil – bentonite mixtures using pressure plate extractors. The experimental SWCC data were fit to the Brooks – Corey and Van Genuchten parametric equations. Variations in SWCCs due to higher bentonite contents reflected in the fitting parameters of the two equations. For example, higher air entry pressures (ψ) were obtained for mixtures containing higher bentonite content when compacted wet of optimum water content.

INTRODUCTION

Lateritic soils are weathered surface deposits which occur in vast areas of tropical regions of the world (Magnien 1966, BRRI/Lyon 1971, Gidigasu 1975). Their availability and geotechnical properties make them potential natural materials for the construction of hazardous waste control systems (Osinubi and Nwaiwu 2006, Gabas et al. 2007). However, the predominance of non expanding 1:1 lattice clay minerals (i.e., kaolinite) that results in relatively high hydraulic conductivity values is a major setback in the use of this soil for such applications. Treatment with bentonite, which is a high swelling clay of the smectite mineral group that has montmorillonite as the

principal clay mineral, will improve the hydraulic performance of the soil as barrier material (Grim and Guven 1978, Daniel 1993, Gleason et al. 1997, Osinubi and Amadi 2009).

In designing the geotechnical components of compacted soil liners and covers for hazardous waste control systems, proper evaluation of the pathways for contaminant migration is required for flow and transport analyses (Benson and Khire 1995). In this regard, a full understanding of the geotechnical characteristics, particularly the unsaturated hydraulic properties, is needed for the assessment of the compacted soils because the barriers are frequently unsaturated (Khire et al. 1995, Chiu and Shackelford 1998, Miller et al. 2002). The relationship between the suction potential (ψ) and the volumetric water content (θ), termed the soil water characteristic curve (SWCC) is a fundamental tool in understanding the unsaturated behaviour of soils. Therefore, accurate calculation of the SWCC is important for better prediction of performance (Miller et al. 2002).

The aim of this study was to evaluate the influence of bentonite as well as the various compaction states (dry, optimum and wet moisture conditions) on the soil water characteristics of lateritic soil treated with bentonite. The mixture is proposed as barrier material in waste containment systems.

THEORETICAL BACKGROUND

Soil Water Retention Models

Numerous mathematical models have been used to simulate the SWCC experimental data. The soil water characteristic functions presented by Brooks and Corey (1964) and Van Genuchten (1980) were considered for use in this study.

The Brooks-Corey model, subsequently referred to as BC equation is given as:

$$\frac{\theta_w - \theta_r}{\theta_s - \theta_r} = \left(\frac{\psi_a}{\psi}\right)^{\lambda} \tag{1}$$

where, the optimized parameters are θ_r, ψ_a and λ. θ_r, θ_s are the residual and saturated water contents, respectively; ψ_a is the air entry value which is the matric suction when air starts to enter the largest pores in the soil, while λ is an empirical parameter representing the pore size distribution index and is related to the slope of the curve.

The Van Genuchten model is expressed as:

$$\frac{\theta_w - \theta_r}{\theta_s - \theta_r} = \frac{1}{\left[1 + \left(\frac{\psi}{\alpha}\right)^n\right]^m} \tag{2}$$

where, the optimized parameters are θ_r, α, n and m. θ_r, θ_s are as in BC equation, while the parameter α is related to the air entry value and the n parameter is related to pore size distribution of the soil that controls the slope of the SWCC, while m is related to asymmetry of the model curve.

MATERIALS AND METHODS

Soil

The lateritic soil used in this study is a natural reddish brown soil with inclusions of white mottles collected from a borrow pit in Shika – Zaria (Latitude 11°15' N and Longitude 7°45' E), Nigeria at depths between 1.5 and 2.0 m. It belongs to the group of ferruginous tropical soils derived from igneous and metamorphic rocks. In a study of soil samples from this borrow pit, Osinubi (1998) reported that kaolinite is the principal clay mineral in the soil.

Bentonite

The bentonite used in this study is in powdered form and was obtained from a major supplier in Lagos – Nigeria. It is representative of typical bentonite available for construction purposes as reported by Osinubi and Amadi (2009).

Preparation of Specimens

Five lateritic soil – bentonite mixtures containing 0, 2.5, 5, 7.5 and 10% bentonite by dry weight of soil, that represented soils with varying plasticity were investigated. Specimens of each mix were prepared at compaction water contents approximately 2% dry of optimum, near optimum water content and 2% wet of optimum water content using standard Proctor (SP) energy. Specimens for the test were first compacted in the SP compaction mould, extruded and a stainless steel ring with a beveled sharp cutting edge having inside diameter of 50 mm and height of 50 mm was used to core columns of soil from the specimens. These specimens were soaked and brought to full saturation before being subjected to pressure plate drying test.

Pressure Plate Drying

Pressure plate drying test was conducted to determine the relationships between volumetric water content and matric suction potentials in specimens subjected to pressures in the range 0.1 – 1500 kPa. Procedures followed were in accordance with ASTM D3152-72 (ASTM 1994).

The saturated soil specimens were placed in the pressure plate cell and pressure was applied to a predetermined value to induce matric suction. The test was terminated when the outflow stopped thus, indicating that specimens were in equilibrium with the applied matric suction. The specimens were removed from the cell and their volumetric water contents determined. The procedure was repeated to develop an entire soil water characteristic curve by subjecting the soil specimens to different pressures.

RESULTS AND DISCUSSION

Index Properties

The index properties of the natural lateritic soil and lateritc soil – bentonite mixtures determined following standard laboratory procedures outlined in BS 1377 (1990) are summarized in Table 1.

Table 1. Properties of natural lateritic soil and lateritic soil - bentonite mixtures

	Bentonite Content (%)				
Characteristics	0	2.5	5	7.5	10
Natural moisture content (%)	19.6	-	-	-	-
Liquid Limit (%)	42.2	48	49.5	53.5	57
Plasticity Index (%)	22.2	26.6	28.6	30.7	33.4
USCS Classification	CL	CL	CL	CH	CH
Specific Gravity	2.6	2.58	2.5	2.5	2.48
pH	6.7	7.2	7.4	7.6	7.9
Color	Reddish brown				
Dominant Clay Mineral	Kaolinite				
Maximum Dry Unit Weight (kN/m^3)	17	16.4	16.4	15.9	15.4
Optimum Moisture Content (%)	17.5	18.3	18.8	18.9	19.1

Soil Water Characteristic Curves

The measured SWCC data were fitted with Brooks – Corey and Van Genuchten functions defined by eqs. (1) and (2), respectively. Figs. 1 - 6 show fitted curves for the various bentonite treatments prepared dry, wet and at optimum moisture content using SP compactive effort.

The trend observed in the three compaction states is that the SWCCs plot in order of decreasing bentonite content with specimens having higher bentonite content being above those with lower bentonite fractions (see Figs 1 – 6). Generally, the volumetric water content (θ) increased with higher bentonite content. This was expected since the incorporation of bentonite increased the plasticity of the mixtures and therefore more water was retained at any given matric suction. It was also observed that the SWCCs are shallow for specimens with higher bentonite contents.

A summary of the curve fitting parameters namely, Van Genuchten's α and n as well as Brooks-Corey's ψ and λ determined by graphical procedures described by Van Genuchten (1980) are presented in Table 2. The value of parameter α of VG model decreased with higher bentonite content, which corresponds to higher air entry suction. Conversely, the second parameter, n increased with higher bentonite content in the range 1.0 - 1.78. Typically, soils with greater plasticity index have larger n values, which correspond to SWCC with shallow slope (Tinjum et al. 1997, Chiu and Shackelford 1998, Miller et al. 2002).

In the case of BC fitting parameters, ψ_a generally increased with higher bentonite content. As plasticity index increased due to higher bentonite content, the effective pore spaces became smaller resulting in higher air entry value, ψ_a.

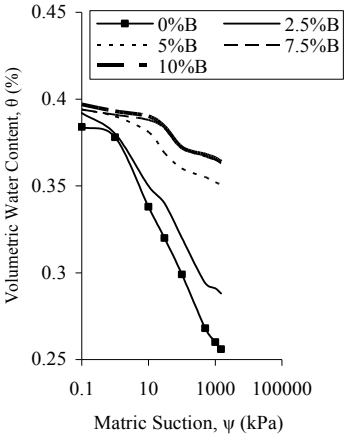

Figure 1. Fitted SWCCs based on VG functions for specimens compacted dry of optimum moisture content

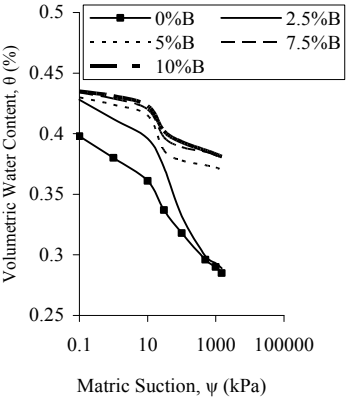

Figure 2. Fitted SWCCs based on VG functions for specimens compacted at optimum moisture content

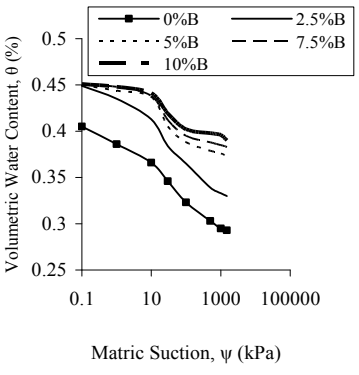

Figure 3. Fitted SWCCs based on VG functions for specimens compacted wet of optimum moisture content

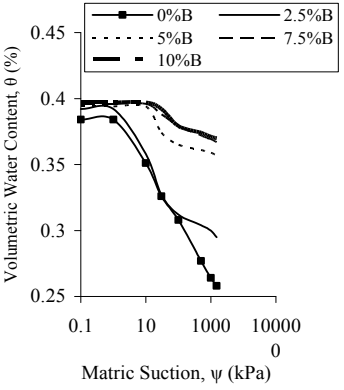

Figure 4. Fitted SWCCs based on BC functions for specimens compacted dry of optimum moisture content

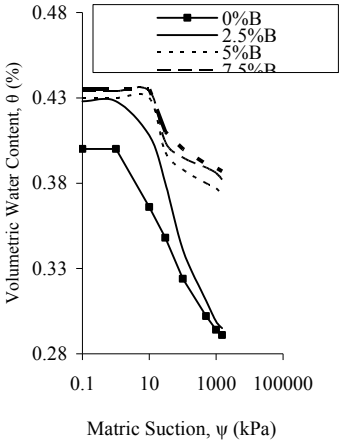

Figure 5. Fitted SWCCs based on BC functions for specimens compacted at optimum moisture content

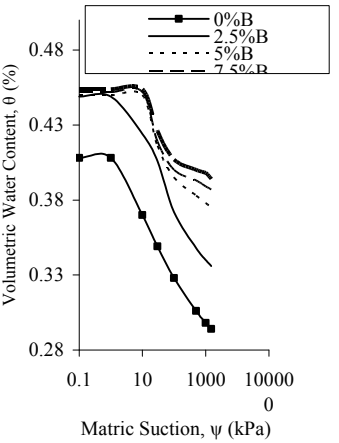

Figure 6. Fitted SWCCs based on BC functions for specimens compacted wet of optimum moisture content

Table 3. Soil water characteristic curve fitting parameters for the various soil mixtures

Model	Parameter	Soil Specimen	Compaction condition		
			Dry	Opt	Wet
VG	α	0%B	0.101	0.092	0.09
		2.5%B	0.085	0.065	0.055
		5%B	0.022	0.013	0.009
		7.5%B	0.009	0.008	0.007
		10%B	0.002	0.004	0.002
	n	0%B	1.41	1.291	1.22
		2.5%B	1.5	1.326	1.276
		5%B	1.566	1.340	1.30
		7.5%B	1.65	1.353	1.344
		10%B	1.67	1.40	1.389
BC	ψ_a	0%B	0.476	0.624	0.82
		2.5%B	3.10	3.24	3.66
		5%B	6.77	5.21	5.76
		7.5%B	6.8	6.39	6.91
		10%B	7.13	8.24	8.84
	λ	0%B	0.765	0.725	0.7
		2.5%B	0.564	0.542	0.538
		5%B	0.515	0.506	0.502
		7.5%B	0.48	0.475	0.47
		10%B	0.45	0.44	0.432

CONCLUSIONS

A residual lateritic soil treated with up to 10% bentonite by dry weight of soil was prepared at dry, optimum and wet moisture conditions and compacted with standard Proctor energy. The soil water characteristic curves of the specimens were measured and the data fitted with Brooks – Corey and Van Genuchten soil water characteristic curve functions. Based on the SWCC data, greater air entry suctions were obtained for specimens with higher bentonite contents when compacted wet of optimum moisture content. The results of the study show that accurate knowledge of the SWCCs for the various lateritic soil - bentonite mixtures is essential in order to examine the effects of bentonite treatment on the unsaturated hydraulic properties of the soil barrier which are employed in simulating fluid migration.

REFERENCES

ASTM. (1994). Standard test method for capillary-moisture relationships for fine-textured soils by pressure-membrane apparatus. Designation: D 3152-72,West Conshohocken, Pa.

Benson, C. H. and Khire, M. (1995). Earthen final covers for landfills in semi-arid and arid climates. In: R. J. Dunn and U. P. Singh (1995) Landfill Closures, Geotech. Special Publications, No. 53, ASCE, Reston, Va., 201-217.

Brooks, R. H. and Corey, A. T. (1964). Hydraulic properties of porous media. Colorado State University, Hydrology Paper No. 3, Fort Collins, Colorado.

BRRI/Lyon Associates (1971). Laterites and lateritic soils and other problem soils of Africa. An Engineering Study for USAID. AID/csd-2164, Baltimore, Md.

BS 1377 (1990). Method of Testing Soils for Civil Engineering Purposes, British Standards Institute, London.

Chiu, T. F. and Shackelford, C. D. (1998). Unsaturated hydraulic conductivity of compacted sand-kaolin mixtures. J. Geotech and Geoenviron. Eng., ASCE, 124 (2), 160-170.

Daniel, D. E. (ed.) (1993), Clay Liners Chapter 7, Geotechnical Practice for Waste Disposal, Chapman and Hall, London, 136 – 163.

Gabas, S. G., Boscov, M. E. G. and Sarkis, J. E. S. (2007). Cadmium and Lead Adsorption in a compacted lateritic soil. CD-ROM of presentations at the First International Conference on Environmental Research, Technology Policy ERTEP 2007, Ghana. 16 – 19th July. Session E3.18: State – of – the – Art Technologies for Environmental Performance and Protection, 1 – 12.

Gidigasu, M. D. (1975). The Formation and General Characteristics of Laterite Soils. Project Report SM No. 2, Building and Road Research Institute, Kumasi, Ghana.

Gleason, M. H., Daniel, D. E. and Eykholt, G. R.. (1997). Calcium and sodium bentonite for hydraulic containment applications. J. Geotech. and Geoenviron. Eng. ASCE, 123(5), 438 – 445.

Grim, R. and Guven, N. (1978). Bentonite: Geology, Mineralogy, Properties and Uses. Elsevier Science Publishing, N.Y.

Khire, M. V., Meerdink, J. S., Benson, C. H. and Bosscher, P. J. (1995). Unsaturated hydraulic conductivity and water balance predictions for earthen landfill final covers. Soil Suction Applications in Geotechnical Engineering Practice, W. K. Wray and S. L. Houston, eds., ASCE, 38 - 57.

Maigien, R. (1966). Review of Research on Laterites. Natural Resources Research IV, United Nations Educational Scientific and Cultural Organisaton, Paris.Miller, C.J., Yesiller, N.,

Osinubi, K. J. (1998). Permeability of lime treated laterite. J. Transp. Eng. ASCE, 124(5), 465 -469.

Osinubi, K. J. and Nwaiwu, C. M. O. (2006). Design of compacted lateritic soils liners and cover. J. Geotech and Geoenviron. Eng., ASCE, 132(2), 203 – 213.

Osinubi, K. J. and Amadi, A. A. (2009). Hydraulic performance of compacted lateritic soil – bentonite mixtures permeated with municipal solid waste landfill leachate. CD_ROM of presentations at Transportation Research Board (TRB) 88th Annual Meeting, 11 - 15th Jan., Washington D.C., U.S.A., 1 - 18.

Tinjum, J. M., Benson, C. H. and Blotz, L. R. (1997). Soil water characteristic curves for compacted clays J. Geotech and Geoenv. Eng., ASCE, 123(11), 1060-1069.

Yaldo, K. and Merayyan, S. (2002). Impact of soil type and compaction conditions on soil water characteristic. J. Geotech and Geoenv. Eng., ASCE, 128(9), 733-742.

Van Genuchten, M. Th. (1980). A closed-form equation for predicting the hydraulic conductivity of unsaturated soils, Soil Science Society of America J.,44, 892 - 898.

Analytical Solution of the Barcelona Basic Model

X. Zhang[1]

[1] Assistant Professor, Alaska University Transportation Center, Department of Civil and Environmental Engineering, University of Alaska Fairbanks, Fairbanks, AK99775,USA e-mail:ffxz3@uaf.edu

ABSTRACT: Alonso et al. (1990) proposed the first elasto-plastic model for unsaturated soils, which was subsequently called the Barcelona Basic Model (BBM). The BBM successfully explained many features of unsaturated soils and received extensive acceptance. At present, the BBM remains one of the fundamental elasto-plastic models for unsaturated soils. The original BBM was proposed in terms of an incremental formulation. Though the incremental formulation is useful for programming in the constitutive modeling, it is complicated for understanding soil behavior. This paper derives an analytical formulation of the BBM. Its significances in the constitutive modeling of unsaturated soils are also discussed.

INTRODUCTION

Alonso et al. (1990) proposed the first elasto-plastic model for unsaturated soils, which was subsequently called the Barcelona Basic Model (BBM). This model was based on the Modified Cam Clay Model (MCCM) for fully saturated soils, and was extended for unsaturated states through the introduction of the concept of the loading-collapse yield surface. The BBM successfully explained many features of unsaturated soils and received extensive acceptance. Since then many elasto-plastic models have been developed (Wheeler and Sivakumar 1995, Cui and Delage 1996, Bolzon et al. 1996). A review of the early constitutive models can be found in Wheeler and Karube (1996), Delage and Graham (1996), Gens (1996), Vaunat (2006), and Gens et al. (2006). Wheeler and Sivakumar (1995) pointed out that one of the fundamental assumptions made in the BBM is the existence of a unique four dimensional state boundary surface in the *v-p-q-s* space, where *p* is the net normal stress, *q* shear stress and *s* matric suction. They also experimentally verified the existence of the unique state boundary surface. However, no close-form solution was given and the

relationship between the yield surface and the state boundary surface was not clear at that time. Wheeler and Karube (1996) envisioned that "there is an inextricable link between the form of the normal compression lines in the *v: p* plane and the shape of the Loading/Collapse (LC) yield curve as it expands in the *s: p* plane" and pointed out that "in developing an elasto-plastic model, it is therefore only necessary to define either the changing shape of the yield curve as it expands or the form of the normal compression lines for different values of suction." Sheng et al. (2004) considered that all the existing models are variants of the BBM and the BBM remains one of the fundamental models for unsaturated soils. Consequently, a complete understanding of the BBM is very helpful in the constitutive modeling for unsaturated soils. The original BBM was proposed in terms of an incremental formulation. Though the incremental formulation is useful for programming in the constitutive modeling, it is complicated for understanding soil behavior. Zhang and Lytton (2009a and 2009b) proposed a Modified State Surface Approach (MSSA) and derived the analytic form for the BBM under isotropic conditions. This paper derives an analytical formulation for the four dimensional state boundary surfaces in the BBM based on the newly-developed MSSA. Its significances in the constitutive modeling of unsaturated soils are also discussed.

MODIFIED STATE SURFACE APPROACH AND THE BBM

Zhang and Lytton (2009a and 2009b) proposed a MSSA to study volume change of unsaturated soils. The MSSA was based upon the uniqueness of the state boundary surface under isotropic conditions. The concept of the MSSA can be explained by Figures 1 and 2. Figure 1 shows results of a typical isotropic loading-unloading compression test under constant suction for an unsaturated soil. The soil has an initial condition of point D, is elastically loaded to the initial yield point E and then plastically loaded to point V. It is followed by an elastic unloading to point D', then an elastic reloading from point D' to the new yield point V, and a plastic loading from V to F.

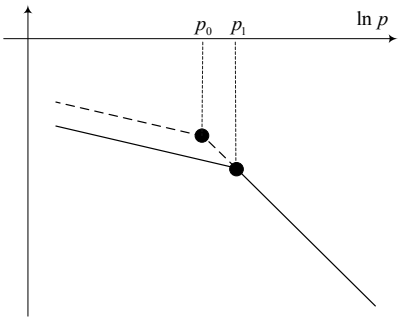

Figure 1. Typical variations of specific volume with net normal stress at constant suction

The following observation can be made from this process: (1) the plastic segment of the normal compression line (or the virgin consolidation line) always remains stationary in the *v-lnp* diagram; (2) the elastic segment of the normal compression line is movable. It remains stationary during elastic loading or unloading and move downwards parallel to the original elastic segment during plastic loading; and (3) the yield point is the intercept point of the elastic and plastic segments.

Figure 2 shows the situation when the same test results as shown in Figure 1 are plotted in the *v-p-s* space. Figure 2a shows the stress path in the *p-s* plane and the changes in the positions of the loading/collapse (LC) yield curve due to plastic loading from point E to V. Figure 2b shows the changes in the specific volume with the net normal stress for the test as shown in Figure 1 in the *v-p-s* space.

In the elastic zone, the volume change of the soil is stress path independent since all the behavior is recoverable. As long as the initial and final stress states are the same, volume change from D to E by taking different stress paths such as 1 and 2 will be same. As a result, the specific volume of the soil in the elastic zone should be able to be expressed as a surface in the *v-p-s* space when there is no plastic loading.

The boundary curve separating the elastic and plastic zones is the LC yield curve. Appling a load under constant suction from an arbitrary point on the LC yield curve, for example, point E, will cause plastic loading and the corresponding specific volume with net normal stress curve is the virgin consolidation line EVF as shown in Figures 1 and 2b. The above three observations still hold true in the *v-p-s* space. For example, the plastic segment EV(Y)F of the normal compression line always remains stationary in the *v-p-s* space. Since the suction at point E is arbitrary, it is concluded that there must be a stationary plastic surface BEHUXYZW in the *v-p-s* space. Similarly, the following conclusions can be made for the soil under isotropic conditions: (1) there is a plastic surface which always remains stationary in the *v-p-s* space for the soil; (2) there is a movable elastic surface in the *v-p-s* space for the soil. It re-mains stationary during elastic loading or unloading and move downwards parallel to the original elastic surface during plastic loading; and (3) the yield curve is the intercept point of the elastic and plastic surfaces.

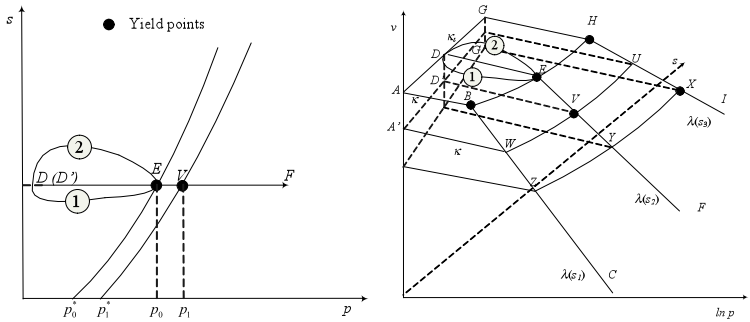

(a) Stress path (b) Soil responses to different loading paths

Figure 2. Relationship among Elastic Surface, Plastic Surface and Yield Curves

Zhang and Lytton (2009a and b) found that under isotropic conditions, the BBM consists of three surfaces, an elastic surface AHIF, a plastic collapsible soil surface JIFGB, and a plastic expansive soil surface HCJI as shown in Figure.3. Their mathematical expressions are as follows:

$$e^e = C_1 - \kappa \ln p - \kappa_s \ln\left(s + p_{at}\right) \text{(Elastic unloading/reloading surface)} \quad (1)$$

$$e = C_2 - \kappa_s \ln\left(\frac{s + p_{at}}{p_{at}}\right) - \lambda(s) \ln\left(\frac{p}{p^c}\right) \text{(Plastic collapsible surface)} \quad (2)$$

$$e = C_3 - \kappa \ln p - \lambda_s \ln\left(s + p_{at}\right) \text{(Plastic expansive surface)} \quad (3)$$

Where κ= slope of the unloading-reloading line associated to the mean net stress, κ_s = slope of the unloading-reloading line associated to soil suction, p_{at} = atmospheric pressure. The superscripts "e" represents the elastic change in the specific volume. $\lambda(s) = \lambda(0)\left[(1-r)\exp(-\beta s) + r\right]$; r = parameter con-trolling the slope of the virgin compression line, β= parameter controlling the slope of the virgin compression line for s≠0,$\lambda(0)$= slope of the virgin compression line associated with the mean net stress at saturation (s=0); p_c = reference stress, λs= slope of the virgin compression line associated with soil suction, and C_1, C_2 and C_3= constants. Eqs.1, 2, and 3 are mathematical expressions of the elastic surface AHIF, plastic collapsible soil surface JIFGB, and plastic expansive soil surface HCJI Figure.3, respectively. Note that Figure 3 was plotted in scale based on the real data of Case 3 in Alonso et al. (1990).

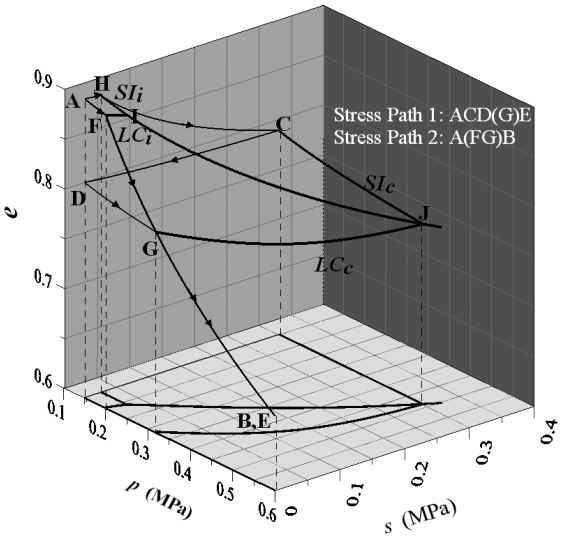

Figure 3. Surfaces used in the BBM (Zhang and Lytton 2009a)

DERIVATION OF STATE BOUNDARY SURAFCE FOR TRIAXIAL STRESS SATES IN THE BBM

Zhang and Lytton (2009a and b) explained all examples in the BBM using the above criteria and the approach was later named MSSA. The MSSA can be used to significantly simplify the constitutive modeling for unsaturated soils under isotropic conditions. It can also be extended to triaxial stress states for the constitutive modeling purpose. In the following sections, the analytical solutions for triaxial stress states in the BBM will be derived.

As discussed previously, the yield point in Figure 1 is the intercept point between the elastic and plastic segments of normal compression test under constant suction. The LC yield curve is the intercept curve between the elastic and plastic surfaces under isotropic conditions. Similarly, the yield surface as shown in Figure 4 should be intercept surface between the four dimensional state boundary surfaces in the *v-p-q-s* space and the elastic surface. Under isotropic conditions (*q=0*), the four dimensional state boundary surface in the *v-p-q-s* space becomes a three dimensional plastic surface in the *v-p-s* space as expressed by eq.2. Elastic surface is the same for isotropic conditions and triaxial conditions since shear will not cause any volumetric change. With the known elastic surface, the plastic surface in the *v-p-s* space as expressed by eq.2, and the yield surface in the *p-q-s* space as shown in Figure 4, it is possible to derive the close-form solution the four dimensional state boundary surface in the *v-p-q-s* space as described by Wheeler and Sivakuma (1995) as follows.

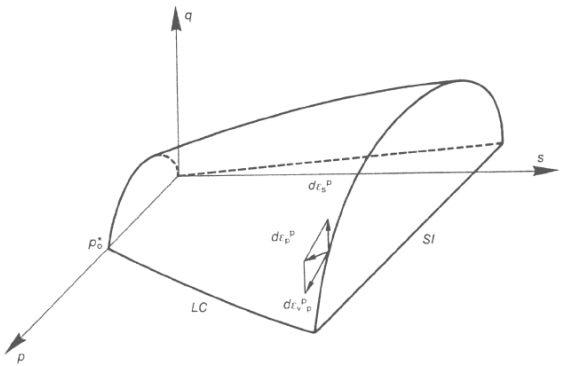

Figure 4. Three-dimensional view of yield surface in the *p-q-s* space in the BBM (Alonso et al. 1990)

The LC yield curve is the intercept curve between the elastic and plastic surfaces as expressed by eqs. 1 and 2, respectively. By making eq.1 equal to eq.2, the mathematical expression for the LC yield curve can be obtained as follows:

$$\ln\left(\frac{p_0}{p^c}\right)=\frac{C_2-C_1+\kappa\ln\left(p^c\right)+\kappa_s\ln\left(p_{at}\right)}{\lambda(s)-\kappa} \tag{4}$$

BBM as shown in Figure 4 has the following expression:

$$q^2 - M^2 (p + ks)(p_0 - p) = 0 \tag{5}$$

Rearranging eq. 5, one has

$$p_0 = p + \frac{q^2}{M^2 (p + ks)} \tag{6}$$

Combining eqs. 4 and 6, one has

$$p + \frac{q^2}{M^2 (p + ks)} = p^c \exp\left(\frac{C_2 - C_1 + \kappa \ln(p^c) + \kappa_s \ln(p_{at})}{\lambda(s) - \kappa} \right) \tag{7}$$

Rearranging eq. 1, one has

$$C_1 = e + \kappa \ln p + \kappa_s \ln(s + p_{at}) \tag{8}$$

Combining eqs. 7 and 8, one has

$$e = C_2 - \kappa \ln \frac{p}{p^c} - \kappa_s \ln\left(\frac{s + p_{at}}{p_{at}} \right) - (\lambda(s) - \kappa)\left[\ln\left(p + \frac{q^2}{M^2 (p + ks)} \right) - \ln p^c \right] \tag{9}$$

Eq.9 is the plastic surface in the *v-p-q-s* space for the BBM. Under isotropic conditions (*q = 0*), eq.9 becomes eq.2. The intercept of plastic (eq.9) and the elastic surface (eq.1) in the *v-p-q-s* space is the yield curve. By using the condition that eq.9 is equal to eq. 1, the yield surface in the *p-q-s* space is obtained, which is eq.5 or 6.

SIGNIFICANCE OF THE ANALYTIC SOLUTION IN THE CONSTITUTIVE MODELING OF UNSATUARTED SOIL BEHAVIOR

With the known analytic solution, the constitutive modeling of unsaturated soil behavior can be significantly simplified. Use of the analytic solution together with the MSSA will also improve the accuracy of the constitutive modeling as well as the other benefits. An example is used to demonstrate the author's viewpoint. Figure 5 shows the isotropic consolidation tests for a silt with a high plasticity at various suction levels (Thu et al. 2007).

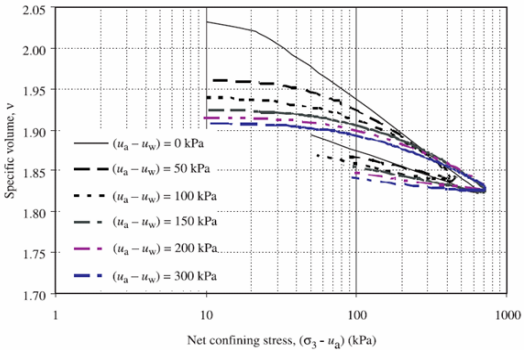

Figure 5. Isotropic consolidation tests for a silt with a high plasticity at various suction levels (Thu et al. 2007)

When the BBM is used to analyze the test results, usually the slopes of the virgin consolidation curves are calculated separately in order to calculate the model parameters β and r for the BBM, according to the equation $\lambda(s)=\lambda(0)\left[(1-r)\exp(-\beta s)+r\right]$. For the test results as shown in Figure 5, $\lambda(s)$ equals to 0.063, 0.057, 0.047, 0.043, and 0.040 for suction at 0, 50, 100, 150, and 200 kPa, respectively. At present, $\beta$and r are usually obtained by best-fitting equation $\lambda(s)=\lambda(0)\left[(1-r)\exp(-\beta s)+r\right]$ according to the method proposed in the Alonso et al. (1990), which are β= 13.39 MPa^{-1} and r= 0.742, respectively. This method will not give the best-fit for the experimental results since only the slopes of the isotropic virgin consolidation tests were used while the positions of these curves in the *v-lnp* diagram were not considered.

Zhang et al. (2008) re-analyzed the same results using the MSSA and found thatβ=13.39 MPa^{-1} and r=0.610 can give the best-fit of the test results. Figures 6 shows the comparison on prediction based on the analytic solution and the method proposed in the Alonso et al. (1990). It can be seen that the prediction based on the analytic solution fit the experimental results better.

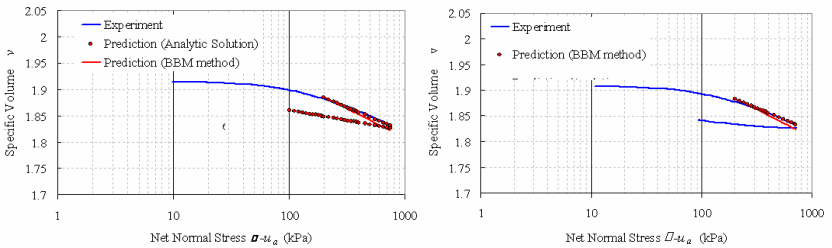

(a) s =200 kPa (b) s =200 kPa

Figure 6. Comparison on predictions based on the analytic solution and the method proposed in Alonso et al. (1990)

CONCLUSIONS

Based on the newly-developed MSSA, the analytical solution of the BBM under triaxial conditions is derived. An example is used to demonstrate the application of the analytic solution can provide better predictions for the same experimental results even when the same constitutive model is used.

REFERENCES

Bolzon, G., Schrefler, B. A., and Zienkiewicz, O. C. (1996). Elastoplastic soil constitutive laws generalised to partially saturated states. Geotechnique, 46(2), 279–289.

Cui, Y. J. and Delage, P. (1996). Yielding and Plastic Behaviour of an Unsaturated Compacted Silt. Geotechnique, 46(2), 291-311.

Delage, P. and Graham, I. (1996). State of the Art Report-Understanding the Behavior of Unsaturated Soils Requires Reliable conceptual models. Proceedings of 1st International Conference on Unsaturated Soils, Paris; 3, 1223-1256.

Gallipoli, D., Gens A, Sharma, R., and Vaunat, J. (2003). An elasto-plastic model for unsaturated soil incorporating the effects of suction and degree of saturation on mechanical behaviour. Geotechnique 53:123–135

Gens, A. (1996). Constitutive Modelling: Application to Compacted Soil. Proceedings of 1st International Conference on Unsaturated Soils, Paris; 3, 1179–1200.

Sheng, D., Sloan, S.W., and Gens, A. (2004). A constitutive model for unsaturated soils: thermomechanical and computational aspects. Comput. Mech. 33:453–465

Tamagnini R. (2004). An extended Cam-clay model for unsaturated soils with hydraulic hysteresis. Geotechnique 54:223–228.

Tarantino, A. and Tombolato, S. (2005). Coupling of hydraulic and mechanical behaviour in unsaturated compacted clay. Geotechnique 55(4), 307–317

Thu, T. M, Rahardjo, H., and Leong, E. C. (2007). Soil-water Characteristic Curve and Consolidation Behavior for a Compacted Silt. Canadian Geotechnical Journal, 44(3), 266-275.

Vaunat, J., Romero, E., and Jommi, C. (2000). An Elasto-plastic hydro-mechanical model for unsaturated soils. Experimental evidence and theoretic approaches in unsaturated soils (Eds. Tarantino, A. and Mancuso, C.), 121-138. Rotterdam: Balkema.

Wheeler, S. J. and Karube, D. (1996). State of the Art Report-Constitutive Modeling. Proceedings of 1st International Conference on Unsaturated Soils, Paris; 3, 1323-1356.

Wheeler, S.J., Sharma, R.S. and Buisson, M.S.R. (2003). Coupling of hydraulic hysteresis and stress-strain behavior in unsaturated soils. Geotechnique, 53(1), 41-54.

Wheeler, S. J. and Sivakumar, V. (1995). An Elasto-plastic Critical State Framework for Unsaturated Soil. Geotechnique, 45(1), 35-53.

Zhang X., Liu, J. and Li, P.(2008). New Method to Determine the Shapes of Yield Curves for Unsaturated Soils. Journal of Geotechnical and Geoenvironmental Engineering, ASCE (in press).

Zhang, X. and Lytton, R. L. (2009a). A Modified State Surface Approach on Unsaturated Soil Behavior Study (I) Basic Concept." Canadian Geotechnical Journal, 46(5), 536-552.

Zhang, X. and Lytton, R. L. (2009b). A Modified State Surface Approach on Unsaturated Soil Behavior Study (II) General Formulation" Canadian Geotechnical Journal, 46(5), 553-570.

Fundamentals of Unsaturated Soil Modelling: Have we got it right?

D. Sheng[1], and A. Zhou[2]

[1] Professor, Centre for Geotechnical and Materials Modelling, the University of Newcastle, Callaghan, 2308 Australia, e-mail: daichao.sheng@newcastle.edu.au
[2] PhD student, Centre for Geotechnical and Materials Modelling, the University of Newcastle, Callaghan, 2308 Australia, e-mail: annan.zhou@newcastle.edu.au

ABSTRACT: An unsaturated soil is not a special type of soil, rather a state of the soil. All soils can be unsaturated with water. There are many concepts specifically related to constitutive models for unsaturated soils, e.g., suction, net stress, apparent consolidation, loading-collapse yield surface, suction-increase yield surface, etc. These concepts are not always well understood and also seem to make unsaturated soils very special. This paper gives a critical review of these concepts, in an attempt to clarify some common confusion in constitutive modelling of unsaturated soils.

INTRODUCTION

Soils that are partially saturated with water are often referred to as unsaturated soils. It should be stressed that all soils can be unsaturated with water. An unsaturated soil is a state of the soil, rather than a special type of soil (Gens et al. 2006). Some soils may exhibit distinct volume, strength and flow characteristics when become unsaturated. For these soils, a change in the degree of saturation can cause significant changes in the volume, shear strength and permeability. Nevertheless, the distinct mechanical and hydraulic behaviour in unsaturated states is a form of material non-linearity and should be dealt with within a continuous framework. In other words, a constitutive model for a soil should represent the soil behaviour over the entire possible ranges of variations for pore pressures and stresses and should allow arbitrary changes of these quantities. The constitutive model should also recover well established principles when the soil becomes fully saturated.

Elastoplastic modelling of unsaturated soils started since the pioneering work of Alonso et al. (1990). Since then, a number of constitutive models have been proposed in the literature (see Gens 1996, Gens et al. 2006, and Sheng et al. 2008b for

reviews). Many concepts have been used in these models, for example, suction, net stress, effective stress, apparent consolidation, apparent tensile strength, loading-collapse yield surface, suction-increase yield surface. These concepts are not always well defined and sometimes can cause confusion. This paper presents a critical review of some common approaches used in the literature, in an attempt to clarify some confusion in constitutive modelling of unsaturated soils.

NET STRESS

Net stress is commonly used in unsaturated soil models. It is defined as

$$\bar{\sigma}_{ij} = \sigma_{ij} - \delta_{ij} u_{\mathrm{a}} \tag{1}$$

where $\bar{\sigma}_{ij}$ is the net stress tensor, σ_{ij} is the total stress tensor, δ_{ij} is the Kronecker delta, u_{a} is the pore air pressure. The net stress is sometimes considered to recover the effective stress for saturated soils where the suction (see below) becomes zero. It is often used in analysing the laboratory data, particularly those based on the axis-translation technique where the air pressure is not zero.

However, under natural ground conditions, the air pressure is usually atmospheric. In this case, the net stress is equivalent to the total stress, rather than the effective stress. Indeed, the so-called total stress in a dry sand is the difference between the absolute total stress and the atmospheric pore air pressure. Therefore, it is preferable to consider the pore air pressure as zero and the net stress as the total stress. More reasons for this consideration are discussed below.

The concept of net stress can be useful in interpreting experimental data based on axis-translation technique, if the technique is indeed valid for applying suction. In this case, the net stress is different from the total stress, as the pore air pressure is no longer zero.

SUCTION

The soil suction in the literature of unsaturated soil mechanics usually refers to the matric suction:

$$s = u_{\mathrm{a}} - u_{\mathrm{w}} \tag{2}$$

where s is the matric suction or also called the matrix suction, and u_{w} is the pore water pressure. The matric suction consists of two parts: the capillary and adsorptive potentials. When the pore water exists as capillary water at relatively high degrees of saturation, the capillary potential (ψ_{c}) is dominant in the matric suction $s = \psi_{\mathrm{c}} = u_{\mathrm{a}} - u_{\mathrm{w}}$. When the pore water exists as adsorbed water films in the soil at low degrees of saturation, the adsorptive potential (ψ_{a}) becomes dominant in the matric suction. In this case the true water pressure is not well defined. It is not unique at one material point and is dependent on the proximity to the particle surface. However an

apparent water pressure can be introduced: $u_w = u_a - \psi_a$, i.e. the apparent water pressure represents the negative adsorptive potential measured in excess of air pressure. When the air pressure is atmospheric (zero), the apparent water pressure is then the negative adsorptive potential. Such an apparent water pressure is then unique at one material point. With such a definition of u_w, the matric suction can be expressed as $s = u_a - u_w$ and can be used continuously for a relatively large range of saturation, from fully saturated to very dry states.

We also note that suction is a physically different quantity than stress. However, it is often treated as an additional stress state variable to form a stress space for establishing constitutive laws. This is very similar to choosing a coordinators system (e.g. x and t, with x being space coordinate and t being time) to describe a function. We also note that stress and suction have the same unit, which is why the two variables can be added together through dimensionless multiplies (e.g.χ, S_r or 1).

A confusing concept that is often cited in the literature is to treat zero suction as an equivalent to saturated states. This concept has two shortcomings. First, it does not differentiate suction levels that correspond to full saturation (S_r=1). A soil can be fully saturated over a range of positive to negative pore water pressures. Second, it does not provide a continuous treatment between positive and negative pore water pressures. In natural ground conditions where the pore air pressure remains constantly atmospheric, a better alternative would be to treat the atmospheric air pressure as zero and the suction as a negative pore water pressure for all saturated and unsaturated states. In this case, the suction becomes the negative pore water pressure and can vary between positive and negative values. Such an alternative will provide a continuous transition between saturated and unsaturated states.

YIELD STRESS AND SUCTION-INDUCED APPARENT CONSOLIDATION

In the literature of unsaturated soil mechanics, the yield stress of an unsaturated soil is usually assumed to be a function of soil suction. The concept of yield stress in classic elastoplasticity theory refers to the stress level that causes plastic deformation. Under isotropic stress states, the yield stress is also called the preconsolidation stress or preconsolidation pressure. For unsaturated soils, the yield net mean stress, denoted here by $\overline{p}_c$, is conventionally determined from isotropic compression curves obtained under constant suctions. These compression curves are usually plotted in the space of void ratio versus logarithmic mean stress. The initial portion of the curve is typically flatter than the ending portion of the curve, if the suction is larger than zero. Such a curve is then approximated by two straight lines, one representing the elastic unloading-reloading line and the other the elastoplastic normal compression line. The meeting point of the two lines is used to define the preconsolidation stress or yield stress (Figure 1a). The yield stress so determined is generally found to increase with increasing suction, irrespective of samples prepared from slurry or from compacted soils, leading to the so-called apparent consolidation concept and the loading-collapse yield surface that is widely used in constitutive models for unsaturated soils (Figure 1b).

The procedure outlined above for determining the yield stress for unsaturated soils suffers a significant shortcoming. To demonstrate this shortcoming, we should first realise that the isotropic compression curves shown in Figure 1 are typical to unsaturated soils air-dried from slurry (e.g. Jennings and Burland 1962) as well as to compacted soils. Because it is easier to understand the preconsolidation stress for a slurry soil than for a compacted soil, we use a slurry soil as an example here. Let us assume that the slurry soil was isotropically consolidated to Point F in Figure 2 and it has an air entry value indicated by the suction at Point C. Because of the effective stress principle for saturated soils, the initial elastic zone is then bounded by the two lines that go through points A and F and are inclined to horizontal by 45^o. The yield (preconsolidation) stress at suction of Point B is then zero. Drying this slurry soil under zero mean stress to suction at Point D will then cause plastic yielding, because part of the stress path (BD) is outside the initial elastic zone. Let us now isotropically compress the soil under the constant suction at Point D (i.e., stress path DE in Figure 2). According to the data by Jennings and Burland (1962) and Cunningham et al. (2003), the isotropic compression line in the space of void ratio against logarithmic mean stress will be curved, in a pattern as those shown in Figure 1a for s>0. However, the isotropic compression path (DE) is clearly outside the current elastic zone and the soil at point D is normally consolidated. Once the soil becomes unsaturated, the yield stress does not necessarily change with suction along the 45^o line (denoted by the dashed line). However, the new yield surface must go through the current stress point. Therefore, the isotropic compression path (DE) as well as the drying path from B to D is elastoplastic and does not involve a purely elastic portion as Figure 1 indicates, suggesting that the method for determining the yield stress in Figure 1 be incorrect. Indeed, the suction-induced apparent consolidation effect should refer to the increase of the preconsolidation stress at zero suction ($\overline{p}_c(0)$ moves from F to G as suction increases from B to D in Figure 2), not the preconsolidation stress at current suction.

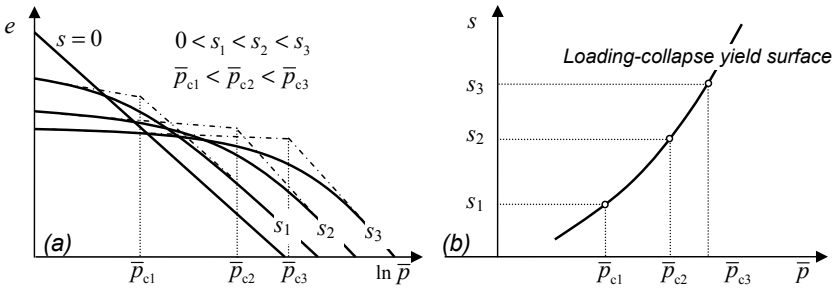

Figure 1. (a) Isotropic compression curves under constant suction (s), and (b) derived yield stresses

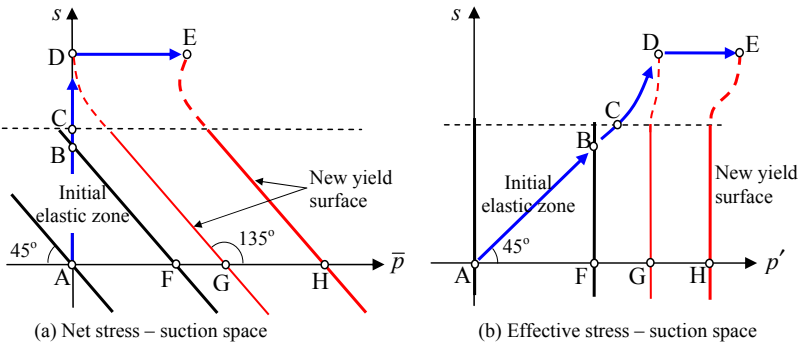

(a) Net stress – suction space (b) Effective stress – suction space

Figure 2. Evolution of elastic zone during drying and compression of slurry soil

The same analysis can be done in the effective stress – suction space (Figure 2b). In the effective stress space, the initial elastic zone for saturated states is bounded by two vertical lines going through A and F. The stress path for suction increase under constant net mean stress is inclined to horizontal by 45° in the saturated zone, but will drift away from the 45° line once the soil becomes unsaturated. As shown in Figure 2b, the soil will yield at point B and the stress path BCDE will again cause elastoplastic volume change.

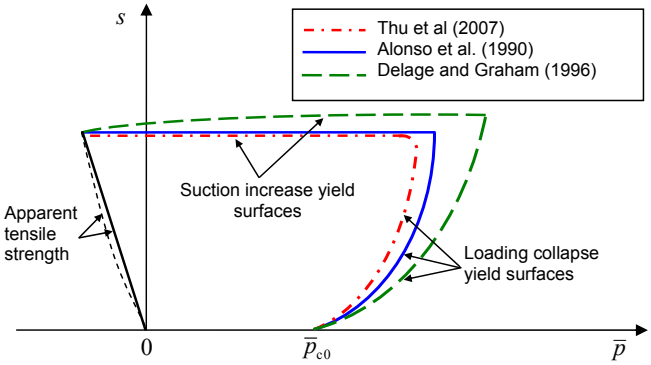

Figure 3. Yield stress variation with suction in existing models

In the literature, the yield stress variation with suction is a rather confusing point. Many models adopt three yield surfaces in the net stress – suction space, namely the loading-collapse yield surface, the suction-increase yield surface and the apparent tensile strength surface. Figure 3 shows some examples of these models (e.g. Alonso et al. 1990, Delage and Graham 1996, Thu et al. 2007). The loading-collapse yield

surface is used to model the volume collapse when an unsaturated soil is first loaded under constant suction and then wetted under constant stress. The suction-increase yield surface is used to capture the possible plastic volume change when an unsaturated soil is dried to a historically high suction. The apparent tensile strength surface defines the apparent tensile strength due to suction increase. Because of the incorrect interpretation of the yield stress in Figure 1b, these yield surfaces are usually defined by separate functions and are not related to each other. For example, setting the preconsolidation stress ($\overline{p}_{c0}$) to zero in the loading-collapse yield function does not lead to the apparent tensile strength function. The suction-increase yield surface is usually horizontal or gently sloped (Figure 3).

Recently Sheng et al. (2008a) showed the relationship between the loading-collapse surface, the apparent tensile strength surface and the suction-increase yield surface. In a new modelling approach proposed by Sheng et al. (2008a), the yield stress, apparent tensile strength and shear strength of an unsaturated soil are related to the relationship that defines the volume change caused by suction and mean stress changes. A specific model was proposed and it was referred to as the SFG model. An essential difference between the SFG model and the other elastoplastic models in the literature is that the former provides a consistent explanation of yield stress, apparent tensile strength, shear strength and suction-increase yield surface of unsaturated soils, both for soils air-dried from slurry and from compacted specimens. In the SFG model, the yield stress for a slurry soil that has never been consolidated or dried varies with suction in a unique function. This yield function also defines the apparent tensile strength surface in the stress – suction space (the curve through point A in Figure 4). The curve approaches the 45^{o} line as the suction becomes zero or negative (positive pore water pressure). Drying the slurry soil under constant stress (stress path AB) is somewhat equivalent to consolidating the soil, leading to the yield surface expansion to point B in Figure 4. Therefore, the suction-increase yielding is already included in the yield function and there is no need to define a separate function. If the unsaturated soil is then compressed under constant suction (stress path BC), the yield surface will evolve to that passing through point C in Figure 4. We note that the yield surface in the stress space represents the contours of the hardening parameter, which is usually the plastic volumetric strain for isotropic hardening materials. The stress path BC will then change the initial shape of the yield surface, because the plastic volumetric strain caused by the isotropic compression depends on the suction level. The loading-collapse yield function recovers the apparent tensile strength function when the preconsolidation stress at zero suction ($\overline{p}_{c0}$) is set to zero. All these yield surfaces are continuous and smooth in the stress – suction space. In addition, it was shown by Sheng et al. (2008a) that the apparent tensile strength function, the suction-increase yield function and the loading-collapse yield function are all derived from the volumetric model that defines the elastic and elastoplastic volume changes caused by stress and suction changes.

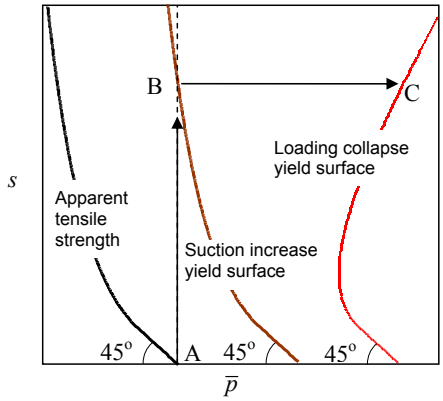

Figure 4. Yield stress variation with suction in the SFG model (Sheng et al. 2008a)

VOLUME CHANGE BEHAVIOUR

The volume change behaviour is one of the most fundamental properties for saturated and unsaturated soils. For unsaturated soils, it forms the base for the yield stress – suction relationship and the shear strength – suction relationship (Sheng et al. 2008a, Zhang and Lytton 2009). The volumetric model that defines the volume change caused by stress and suction changes should again be applicable to the entire range of possible pore pressures. A common starting point is the linear relationship between void ratio (e) and the logarithm effective mean stress ($\ln p'$) for a normally consolidated and saturated clay:

$$v = 1 + e = N - \lambda \ln p' = N - \lambda \ln (p - u_w) \tag{3}$$

where v is the specific volume, $\lambda$is the slope of the $v - \ln p'$ line, and N is the intercept on v axis when $\ln p'$=0.

We should note that equation (3) represents a line in the total stress space ($v - \ln p$) only if the pore water pressure is zero. If the pore water pressure were allowed to be kept at a negative value during the isotropic compression of the soil, equation (3) would predict a smooth curve in the $v - \ln p$ space, as shown by Figure 5. Indeed, these compression lines look very much like those for overconsolidated soils. However, the soil modelled by equation (3) is normally consolidated. The curvature of the normal compression lines is purely due to the feature of the logarithmic function. If the air entry suction for the soil in Figure 5 is larger than 100 kPa, the compression curves for s=10 and 100 kPa for the normally consolidated and saturated soil would take the shape as those in Figure 5. This is perhaps why the isotropic compression lines in Jennings and Burland (1962) and Cunningham et al. (2003) were curved for soils prepared from slurry states.

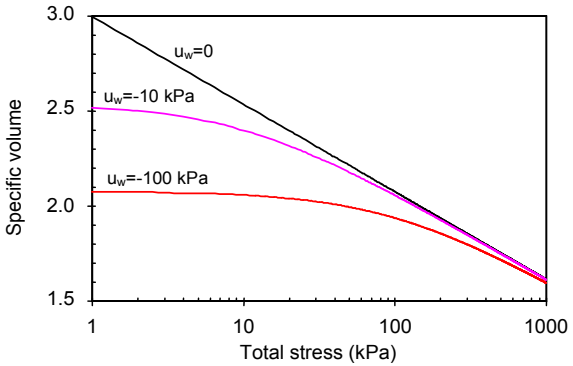

Figure 5. Normal compression lines for saturated clay under constant pore water pressures (λ=0.2, N=3)

Equation (3) can also be written in an incremental form:

$$\mathrm{d}v = -\lambda \frac{\mathrm{d}p}{p - u_\mathrm{w}} - \lambda \frac{\mathrm{d}(-u_\mathrm{w})}{p - u_\mathrm{w}} \tag{4}$$

The equation above clearly states that a change in pore water pressure has exactly the same effect on the volume of a saturated soil as an equal change in mean stress.

In the literature, equation (3) is extended to unsaturated states in one of the two approaches exclusively:

Approach A: Separate stress-suction (or the net stress and suction) approach.

Approach B: Combined stress-suction (or the effective stress) approach.

Approach A is perhaps first adopted by Coleman (1962) and is then used in many models such as Alonso et al. (1990), Wheeler and Sivakumar (1995), Cui and Delage (1995), and Vaunat et al. (2000). In this approach, the compressibility due to stress variation under constant suction is separated from the shrinkability due to suction variation under constant stress. A typical example is:

$$v = N - \lambda_\mathrm{vp} \ln \overline{p} - \lambda_\mathrm{vs} \ln \left(s + p_\mathrm{at} \right) \tag{5}$$

where λ_vp is the slope of an assumed $v - \ln \overline{p}$ line or the compressibility due to stress change λ_s is the slope of an assumed $v - \ln s$ line or the shrinkability due to suction change, and p_at is the atmospheric pressure and used to avoid the singularity when s=0.

The main advantage of equation (5) is that the volume changes caused by stress and suction changes can be dealt with separately. Experimental data also indicate that the two compressibilities λ_vp and λ_vs can be very different (Toll 1990, Figure 6). It is usually true that the shrinkability (λ_vs) decreases with increasing suction or decreasing degree of saturation. On the other hand, the compressibility (λ_p) can increase with decreasing degree of saturation, due to the structural changes during drying processes (Toll 1990, Gallipoli 2003).

There are a few confusing points about equation (5). First, equation (5) does not recover equation (3) when the soil becomes saturated. Second, the atmospheric pressure (p_{at}) makes the change of suction insignificant when $s<p_{at}$. Third, the suction-compressibility is independent of stress. Fourth, the volume change becomes undefined at the transition suction between saturated and unsaturated states. The third point contradicts with experimental data (e.g. Delage and Graham 1996). The and first and last points were two of the main reasons that some researchers turned to the effective stress approach instead of the net stress approach (Sheng et al. 2003a, 2003b, Pereira et al. 2005, Santagiuliana and Schrefler 2006). A simple numerical example will illustrate the problem associated with equation (5). Let a soil be compressed at the transition suction (s_{sa}) from mean stress 1 kPa to 100 kPa. Let the air pressure remain atmospheric. In the saturated zone, the volume change according to equation (3) would be:

$$\Delta v\big|_{s_{sa}^{-}} = -\lambda_{vp} \ln\left[\left(100+s_{sa}\right)/\left(1+s_{sa}\right)\right]$$

In the unsaturated zone, the volume change according to equation (5) would be:

$$\Delta v\big|_{s_{sa}^{+}} = -\lambda_{vp} \ln 100$$

These two volume changes can be very different.

In Approach B, suction and stress are combined into one single variable (effective stress) to define their effects on soil volume. A general form of the effective stress is:

$$p' = \overline{p} + f(s) = \overline{p} + f(S_r, s) \tag{6}$$

where f is either a function of suction or a function of suction and degree of saturation. Obviously such a definition of effective stress is very general and covers most of existing definitions in the literature. With such an effective stress, equation (3) is assumed to be valid for unsaturated states via the following form:

$$v = N - \lambda \ln p' = N - \lambda\,(s) \ln\left(\overline{p} + f(S_r, s)\right) \tag{7}$$

In equation (7), the coefficient λ is generally assumed to be a function of suction. However, the parameter N should generally be independent of suction. Otherwise, the volume of the soil would change even if the effective stress (p') was kept constant,

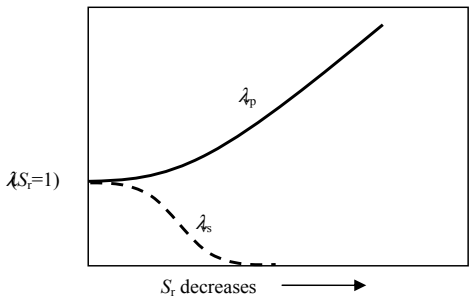

Figure 6. Variation of compressibilities with degree of saturation (after Toll 1990)

and an additional function would then be required to define the volume change caused by suction change under constant effective stress.

Equation (7) is widely used in the literature and in fact most models based on the effective stress approach adopt it as the volume change equation (Kohgo et al. 1993, Bolzon et al. 1996, Sheng et al. 2004, Li 2007, Sun et al. 2007a). If the function f is properly chosen, equation (7) should recover equation (3) when the soil becomes saturated. This is one of the greatest advantages of using an effective stress.

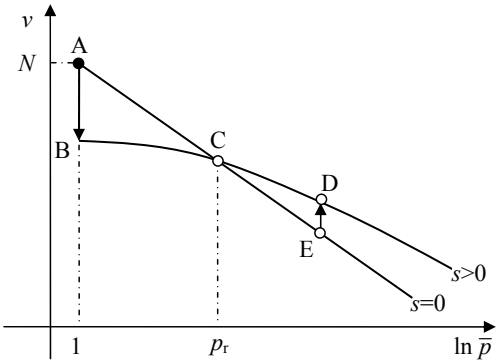

Figure 7. Normal compression lines according to the effective stress approach

However, there are a couple of issues with equation (7). The obvious issue is the difficulty in addressing the different compressibilities due to stress and suction changes, as shown in Figure 6. The second issue is related to a constraint on the compressibility λ Let a saturated slurry soil be dried from zero suction to an arbitrary suction under constant mean stress of 1 kPa, i.e. the stress path AB in Figure 6. As discussed above, this drying path is elastoplastic, not elastic. The volume of the soil then changes according to:

$$v_{\mathrm{B}} = N - \lambda(s)\ln\left(1 + f(s)\right) \tag{8}$$

Now let the soil be compressed under constant suction, i.e. stress path BC in Figure 7. The compression line will be curved in the v - $\ln \bar{p}$ space, due to the term $f(s)$. If the suction at point B is above the air entry value, this compression line is anticipated to intersect with the initial compression line for the saturated soil, as shown in Figure 7. Let the intersection be point C. The volume at point C is then:

$$v_{\mathrm{C}} = v_{\mathrm{B}} - \lambda(s)\ln\left(\frac{p_{\mathrm{r}} + f(s)}{1 + f(s)}\right) = N - \lambda(s)\ln\left(p_{\mathrm{r}} + f(s)\right) \tag{9}$$

Alternatively alone path AC the volume changes according to:

$$v_{\mathrm{C}} = N - \lambda(0)\ln\left(p_{\mathrm{r}} + f(0)\right) = N - \lambda(0)\ln p_{\mathrm{r}} \tag{10}$$

Therefore, we have

$$\frac{\lambda(s)}{\lambda(0)} = \frac{\ln p_r}{\ln\left(p_r + f(s)\right)} < 1 \tag{11}$$

We usually anticipate the effective stress increases with increasing suction, at least for low suction values. Therefore, we have: $\lambda(s) < \lambda(0)$, meaning that the slope of the compression line must decrease with increasing suction. Such a conclusion is however not supported by experimental data. In the data by Jennings and Burland (1962) for air-dry soils, the slope of the compression lines at different suctions (saturation) is more or less constant. In the data by Sivakumar and Wheeler (2000) for compacted soils, the slope of the compression lines increases somewhat with increasing suction. In addition, experimental data on collapse (e.g. Sun et al. 2007b) do not support an increasing collapse volume with increasing mean stress.

Another issue associated with equation (7) about the volume change during drying at high stresses. Let a saturated slurry soil be consolidated to a mean stress larger than $\overline{p}_r$ (say point E) and then dry the soil to the suction at point B. Because the volume change according to equation (7) is stress-path independent, the stress point at the end of the drying path ED must be on the compression curve BCD. Since the drying path is elastoplastic (not purely elastic), as shown in Figure 2, it is only possible to have a volume increase to research point D during the drying path ED. Clearly, this is not reasonable. Therefore, further research is required if equation (7) is adopted for the volume change, particularly in terms of explaining the collapse volume. Realising that the degree of saturation can increase during isotropic compression under constant suction, we note that a possible solution to some of the issues mentioned above is to have the slope λ as a function of the degree of saturation instead of suction. As such, $\lambda(S_r)$ can increase as S_r increases, even though $\lambda(S_r) \le \lambda(S_r = 1)$. Further exploration in this direction is worthwhile.

Sheng et al. (2008a) proposed a third way to model the volume change for unsaturated soils. The new model, referred to as the SFG model, represents a somewhat middle ground between Approach A and Approach B and is expressed in an incremental form as follows:

$$\mathrm{d}v = -\lambda_{vp}\frac{\mathrm{d}\overline{p}}{\overline{p} + f(s)} - \lambda_{vs}\frac{\mathrm{d}s}{\overline{p} + f(s)} \tag{12}$$

Like Approach A, equation (12) separates the compressibilities due to stress and suction changes. Like Approach B, it also recovers equation (3) when the soil becomes saturated. However, there is no constraint on parameter λ_{vp}. As a first approximation, λ_{vp} can be assumed to be independent of suction, as indicated by the data of Jennings and Burland (1962) for reconstituted soils. More realistically it should depend on suction and perhaps on degree of saturation as well. The data of Sivakumar and Wheeler (2000) shows λ_{vp} increases with increasing suction for compacted soils. Parameter λ_{vs} must equal λ_{vp} when the soil is fully saturated and it decreases with increasing suction. Sheng et al. (2008a) suggested the following function for λ_{vs}

$$\lambda_{vs} = \begin{cases} \lambda_{vp} & s \le s_{sa} \\ \lambda_{vp} \dfrac{s_{sa}+1}{s+1} & s > s_{sa} \end{cases} \tag{13}$$

where s_{sa} is the saturation suction which is the unique transition suction between saturated and unsaturated states (see Sheng et al. 2008a). We note that the number '1' in equation (13) is used to avoid the singularity when s_{sa}=0 and is not needed if s_{sa} is larger than zero:

$$\lambda_{vs} = \begin{cases} \lambda_{vp} & s \le s_{sa} \\ \lambda_{vp} \dfrac{s_{sa}}{s} & s > s_{sa} \end{cases} \tag{14}$$

The difference between equation (13) and (14) is minimal, but equation (14) is preferred to equation (13). Equation (14) can be applied as long as the transition suction is not absolutely zero. Both λ_{vp} and λ_{vs} vary with stress path and can take different values on a loading and unloading path respectively.

The function $f(s)$ in equation (12) can also take different forms. Sheng et al. (2008a) initially used the simplest form possible:

$$f(s) = s \tag{15}$$

Even with this simplest form, Zhou and Sheng (2009) showed that the SFG model is able to predict a good set of experimental data on volume change and shear strength, both for reconstituted soils prepared from slurry and for compacted soils.

An alternative form of $f(s)$ could be:

$$f(s) = S_r s \tag{16}$$

This equation would also guarantee the continuity between saturated and unsaturated states. More interestingly, both equations (15) and (16) lead to the same yield stress – suction and shear strength – suction relationships in the SFG model. However, the validity of equation (16) is yet to be tested against experimental data.

SHEAR STREHGTH

The shear strength is related to the apparent tensile strength function, which is related to the volume change equation (Sheng et al. 2008b). However, this relationship has been overlooked in most existing models for unsaturated soils. If the slope of the critical state line is assumed to be independent of suction, such as supported by experimental data by Toll (1990), the shear strength – suction relationship can indeed be derived from the volume change equation. In the case that the slope of the critical state line depends on suction, two equations are needed to define the shear strength – suction relationship: the volume change equation and the $M(s)$ function, with M being the slope of the critical state line in the deviator – mean stress space.

Fredlund et al. (1978) proposed the following relationship which conveniently

separates the shear strength due to stress from that due to suction:

$$\tau = \left[c' + (\sigma_n - u_a)\tan\phi'\right] + \left[(u_a - u_w)\tan\phi^b\right] = \bar{c} + (\sigma_n - u_a)\tan\phi' \tag{17}$$

where $\tau$is the shear strength, c' is the effective cohesion, σ_n is the normal stress on the failure plane, ϕ' is the effective friction angle of the soil, ϕ^b is the frictional angle due to suction, and $\bar{c}$ is the apparent cohesion due to suction.

In the case that ϕ' is independent of suction, the shear strength – suction relationship for unsaturated states is solely determined by the apparent tensile strength function $\bar{p}_0$. For example, in the SFG model, the apparent cohesion is

$$\bar{c} = -\bar{p}_0 \tan\phi' = \begin{cases} s\tan\phi' & s < s_{sa}, c' = 0 \\ \tan\phi'\left(s_{sa} + (s_{sa}+1)\ln\dfrac{s+1}{s_{sa}+1}\right) & s \geq s_{sa}, c' = 0 \end{cases} \tag{18}$$

This apparent cohesion can then be used to derive the friction angle ϕ^b due to suction.

CONCLUSIONS

This paper presents a critical review of some common concepts used in constitutive modelling of unsaturated soils. These concepts include net stress, matric suction, yield stress, apparent consolidation, apparent tensile strength, loading-collapse yield surface, volume change model, shear strength and effective stress. They are often used in the literature without clear definitions and can sometimes cause confusion. Realizing the fact that all soils can be partially saturated with water and partial saturation is a state of any soil, we can define these concepts in a more consistent way. For example, the matric suction can be understood as negative pore water pressure when the air pressure is atmospheric. The loading-collapse yield surface and the apparent tensile strength surface can be understood as the extension of the bounds of the elastic zone to the negative pore water pressures (or the extension of the bounding surfaces to the negative pore water pressures in a bounding surface model). A constitutive model for a soil should therefore cover all possible ranges of stress and pore pressures variations.

REFERENCES

Alonso, E. E., Gens, A., and Josa, A. (1990). "A constitutive model for partially saturated soils". Geotechnique, 40(3): 405-430.

Bolzon, G., Schrefler, B. A. and Zienkiewicz, O. C. (1996). "Elastoplastic soil constitutive laws generalised to partially saturated states". Géotechnique, 46(2): 279-289.

Cui, Y. J. and Delage, P. (1996). "Yielding and plastic behaviour of an unsaturated compacted silt". Geotechnique, 46(2): 291–311.

Cunningham, M. R., Ridley, A. M., Dineen, K., and Burland, J. B. (2003). "The mechanical behaviour of a reconstituted unsaturated silty clay". Geotechnique, 53(2): 183-194.

Delage, P., and Graham, J. (1996)."State of the art report - Understanding the behavior of unsaturated soils requires reliable conceptual models". In: Unsaturated Soils (Proc. 1st Int Conf on Unsaturated Soils, Alonso EE and Delage P, eds), Balkema, Rotterdam, vol.3, pp. 1223-1256.

Fredlund, D. G., Morgenstern, N. R., and Widger, A. (1978). "Shear strength of unsaturated soils". Canadian Geotechnical Journal, 15: 313-321.

Gens, A. (1996)."Constitutive modelling: application to compacted soils." In: Unsaturated Soils (Proc. 1st Int Conf on Unsaturated Soils, Alonso EE and Delage P, eds), Balkema, Rotterdam, vol.3, pp. 1179-1200.

Gens, A., Sánchez, M., and Sheng, D. (2006). "On constitutive modelling of unsaturated soils". Acta Geotechnica, 1(3): 137-147.

Jennings, J. E. B., and Burland, J. B. (1962). "Limitations to the use of effective stresses in partly saturated soils". Geotechnique, 12(1): 125-144.

Kohgo, Y., Nakano, M. and Miyazaki, T. (1993). "Theoretical aspects of constitutive modelling for unsaturated soils". Soils and Foundations, 33(4): 49-63.

Li, X. S. (2007). "Thermodynamics-based constitutive framework for unsaturated soils, 2: A basic triaxial model". Géotechnique, 57(5): 423-435.

Pereira, J. M., Wong, H., Dubujet, P. and Dangla, P. (2005). "Adaptation of existing behaviour models to unsaturated states: Application to CJS model". International Journal for Numerical and Analytical Methods in Geomechanics, 29(15): 1127-1155.

Santagiuliana, R., and Schrefler, B. A. (2006). "Enhancing the Bolzon-Schrefler-Zienkiewicz constitutive model for partially saturated soil". Transport Porous Media, Vol. 65(1): 1-30.

Sheng, D., Fredlund, D. G., and Gens, A. (2008a). "A new modelling approach for unsaturated soils using independent stress variables". Canadian Geotechnical Journal, 45(4): 511-534.

Sheng, D., Gens, A., Fredlund, D. G., and Sloan, S. W. (2008b). "Unsaturated soils: From constitutive modelling to numerical algorithms". Computers and Geotechnics, 35(6): 810-824.

Sheng, D., Sloan, S. W., Gens, A., and Smith, D. W. (2003a). "Finite element formulation and algorithms for unsaturated soils. Part I: Theory". International Journal for Numerical and Analytical Methods in Geomechanics, 27(9): 745-765.

Sheng, D., Sloan, S. W., Gens, A., and Smith, D. W. (2003b). "Finite element formulation and algorithms for unsaturated soils. Part II: Verification and application". International Journal for Numerical and Analytical Methods in Geomechanics, 27(9): 767-790.

Sheng, D., Sloan, S. W. and Gens, A. (2004). "A constitutive model for unsaturated soils: thermomechanical and computational aspects". Computational Mechanics, 33(6): 453-465.

Sivakumar, V., and Wheeler, S. J. (2000). "Influence of compaction procedure on the mechanical behaviour of an unsaturated compacted clay. Part 1: Wetting and isotropic compression". Geotechnique, 50(4): 359-368.

Sun, D. A., Sheng, D., and Xu, X. F. (2007a). "Collapse behaviour of unsaturated compacted soil". Canadian Geotechnical Journal, 44: 673-686.

Sun, D. A, Sheng, D. and Sloan, S.W. (2007b). "Elastoplastic modelling of hydraulic and stress-strain behaviour of unsaturated soil". Mechanics of Materials, 39: 212-221.

Thu, T. M., Rahardjo, H., and Leong, E. C. (2007). "Critical state behavior of a compacted silt specimen". Soils and Foundations, 47(4): 749-755.

Toll, D. G. (1990). "A framework for unsaturated soil behaviour". Geotechnique, 40(1): 31-44.

Vaunat, J., Romero, E. and Jommi, C. (2000). "An elastoplastic hydromechanical model for unsaturated soils". Experimental Evidence and Theoretical Approaches in Unsaturated Soils, Proc. of Int. Workshop on Unsaturated Soil (Tarantino A and Mancuso C, eds), Balkema, Rotterdam, 121-138.

Wheeler, S. J. and Sivakumar, V. (1995). "An elasto-plastic critical state framework for unsaturated soil". Géotechnique, 45(1): 35-53.

Zhang, X. and Lytton, R. L. (2009a). "Modified state-surface approach to unsaturated soil behaviour study. Part I: Basic concept". Canadian Geotechnical Journal, 46(5): 536-552.

Zhang, X. and Lytton, R. L. (2009b). "Modified state-surface approach to unsaturated soil behaviour study. Part II: General formulation". Canadian Geotechnical Journal, 46(5): 553-570.

Zhou, A. N., and Sheng, D. (2009). "Yield stress, volume change and shear strength behaviour of unsaturated soils: Validation of the SFG model". Canadian Geotechnical Journal, 46(9): 1034-1045.

Elastoplastic Modelling of Hydraulic and Mechanical Behaviour of Unsaturated Expansive Soils

W. Sun[1], D. Sun[2], and J. Li[3]

[1] Department of Civil Engineering, Shanghai University, 149 Yanchang Road, Shanghai 200072, China, e-mail: wjsun@shu.edu.cn
[2] Department of Civil Engineering, Shanghai University, 149 Yanchang Road, Shanghai 200072, China, e-mail: sundean@shu.edu.cn
[3] School of Civil, Environmental and Chemical Engineering, RMIT University, GPO Box 2476V, Melbourne, VIC 3001 Australia, e-mail: jie.li@rmit.edu.au

ABSTRACT: The Barcelona Expansive Model (BExM) for unsaturated expansive soils is complicated and the micro parameters and the coupling function from micro-structural strain to macro-structural strain are difficult to be determined. This paper presents an elastoplastic constitutive model from the macroscopic observation for predicting the hydraulic and mechanical behaviour of unsaturated expansive soils. The model predictions are performed on the results of triaxial tests on compacted unsaturated expansive clay available in the literature. The comparisons between measured and predicted results indicate that the model offers great potential for quantitatively predicting the hydraulic and mechanical behaviour of unsaturated expansive soils.

INTRODUCTION

Since the Barcelona Basic Model (BBM) was published by Alonso et al. (1990), a number of elastoplastic constitutive models for unsaturated soil have been proposed. Although these models can describe most basic mechanical response of non-expansive unsaturated soil including collapse phenomenon, they cannot predict the mechanical behaviour of unsaturated expansive soil. Gens and Alonso (1992) presented a framework for describing the mechanical behaviour of unsaturated expansive soil. Alonso et al. (1999) presented the Barcelona Expansive Model (BExM) in which two levels of structure were considered. The behaviour of the macrostructure follows the BBM, and that of the microstructure is adopted from the framework proposed by Gens and Alonso (1992). In the BExM, the micro parameters and the coupling function from micro-structural strain to macro-structural strain are difficult to be determined. Moreover, the models can only predict the strength and stress-strain behaviour without incorporating the water retention behaviour.

In this research, an elastoplastic constitutive model has been developed, based on the existing hydro-mechanic elastoplastic model for non-expansive unsaturated soil (Sun et al. 2007), for predicting the hydraulic and mechanical behaviour of unsaturated expansive soil. It takes into account the coupled effect of the degree of saturation and the void ratio.

HYDRO-MECHANICAL ELASTOPLASTIC MODEL

The stress-state variables employed in the model are the 'average skeleton stress' tensor $\sigma_{ij}^{'}$ and the suction s, and the strain state variables are the soil skeleton strain tensor ε_{ij} and the degree of saturation S_r. The tensor $\sigma_{ij}^{'}$ is defined as

$$\sigma_{ij}^{'} = \sigma_{ij} - u_a \delta_{ij} + S_r s \delta_{ij} \tag{1}$$

where σ_{ij} is the total stress tensor, u_a the pore-air pressure, and δ_{ij} the Kronecker delta.

The water-retention curves of unsaturated expansive soils at different constant void ratios are given in Figure. 1, which are similar to those used for non-expansive soils (Sun et al. 2007). The water- retention curves can be rewritten as

$$\mathrm{d}S_r = -\lambda_{se}\,\mathrm{d}e - \beta\frac{\mathrm{d}s}{s} \tag{2}$$

where λ_{se} is the slope of the $S_r - e$ curve under constant suction larger than the air-entry value(Sun et al. 2007), and

$$\beta = \begin{cases} \kappa_s & \text{Scanning curve} \\ \lambda_{sr} & \text{Main drying/wetting curve} \end{cases} \tag{3}$$

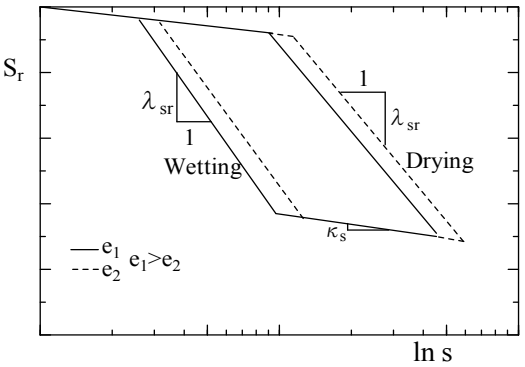

Figure 1. Water retention curve of expansive soil at different constant void ratios

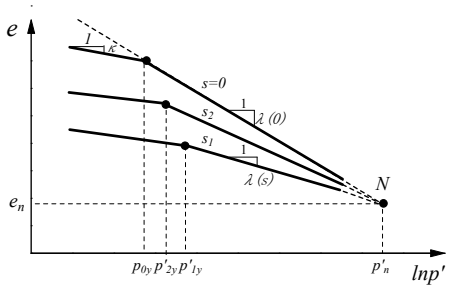

Figure 2. Sketch of compression curves of expansive soils

in which, κ_s and λ_{sr} are the slopes of the scanning curve, the main drying or wetting curves on a plot of S_r against ln$s$.

Figure 2 shows the sketch of compression curves of expansive soil. κ is the swelling index, and $\lambda(0)$, $\lambda(s_1)$ and $\lambda(s_2)$ are the slopes of normal compression lines of saturated soil and unsaturated soils with suction s_1, s_2 respectively, p_{0y}, p'_{1y} and p'_{2y} are the initial yield stresses for saturated soil and unsaturated soils with suction s_1, s_2. From Figure 2 it can be seen that the yield stress increases with increasing suction, which has the same tendency with LC curve in the BBM. However, the compression curve is located down with increasing suction, which is different from the BBM.

The specimens with the same initial state are wetted or dried to different target suctions and then are compressed under constant suctions. The initial yield curve (IYC) is a curve in the $s-p'$ plane combining the initial yield stresses, which expresses the increase of the initial yield stress with increasing suction. It is similar in form with LC curve of the BBM, and is defined as

$$\frac{p_y^{'}}{p_n^{'}}=\left(\frac{p_{0y}}{p_n^{'}}\right)^{\frac{\lambda(0)-k}{\lambda(0)[(1+r)e^{\alpha\cdot s}-r]-k}} \tag{4}$$

where $p_y^{'}$ is the initial yield stress for unsaturated expansive soil with suction s; $p_n^{'}$ is an isotropic stress at which no swelling or collapse occurs when suction is decreased; r and α are the material parameters.

The IYC is used to judge whether the specimen reaches the yield state. When the stress state is inside the IYC, the specimen is under the elastic state; when the stress state reaches the IYC, the elastoplastic deformation takes place and can be obtained by using the concept of the Equivalent Void Ratio Curve (EVRC).

A line is drawn at the elastoplastic stage of compression curves in Figure 3(a). The plastic void ratios at different suctions are the same in the line. It can be seen that the average skeleton stress increases with decreasing suction. In order to describe this trend, the concept of equivalent void ratio curve (EVRC) is introduced. When the stress state is inside the IYC, the EVRC is the line paralleled to p' axis at suction s; when the stress state reaches the IYC, the EVRC can be defined by

$$p_y^{'} = p_n^{'}(\frac{p_{0y}}{p_n^{'}})^{\frac{\lambda(0)-\kappa}{\lambda(s)-\kappa}} \tag{5}$$

$$\lambda(s) = \lambda(0)\cdot[(1-\xi)\cdot e^{(-\tau)\cdot s} + \xi] \tag{6}$$

where ξ and τ are the parameters for identifying the change of $\lambda(s)$ with suction s.

A simple constitutive model for isotropic stress states is presented here. Differentiating Eq.(1) gives the increment of the 'average skeleton stress':

$$dp' = dp + S_r ds + s dS_r \tag{7}$$

where p is a mean net stress.

Substituting Eq.(2) into Eq.(7) gives

$$dp' = dp + S_r ds + s(-\lambda_{se} de - \beta \frac{ds}{s}) \tag{8}$$

where de is the elastic deformation under constant suction, that is

$$de = -\frac{\kappa \cdot dp'}{p'} \tag{9}$$

Substituting Eq.(9) into Eq.(8) and re-arranging gives

$$dp' = \frac{dp + (S_r - \beta)ds}{p' - \lambda_{se}\kappa s} p' \tag{10}$$

When the initial 'average skeleton stress' $p' = p_{net} + s_1 \cdot S_r$ with suction s_1 is less than the corresponding initial yield stress $p_y^{'}$, the strain increment consists of the elastic strain increment caused by the change of the 'average skeleton stress' ($p' : p'_1 \rightarrow p'_2$) and the plastic strain increment caused by the change of suction ($s : s_1 \rightarrow s_2$), as shown in Figure 3.

The elastic volumetric strain increment caused by p' is given by

$$d\varepsilon_v^e = \frac{\kappa dp'}{(1+e)p'} \tag{11}$$

The plastic volumetric strain increment caused by s can be written as

$$de^p = e^p(s_2) - e^p(s_1) = (\kappa - \lambda(s_2))\cdot \ln\frac{p_y^{'}(s_2)}{p_n^{'}} - (\kappa - \lambda(s_1))\cdot \ln\frac{p_y^{'}(s_1)}{p_n^{'}} \tag{12}$$

Given the increment of the net stress and suction, volumetric strain increment can be calculated by Eqs.(10), (11) and (12), and the increment in S_r can be obtained by

$$dS_r = (dp' - dp - S_r ds)/s \tag{13}$$

After the initial state reaches IYC as shown in Figure 3, the plastic strain increment caused by the changes in 'average skeleton stress' ($p' : p'_3 \rightarrow p'_4$) and suction ($s : s_1 \rightarrow s_2$) is described by

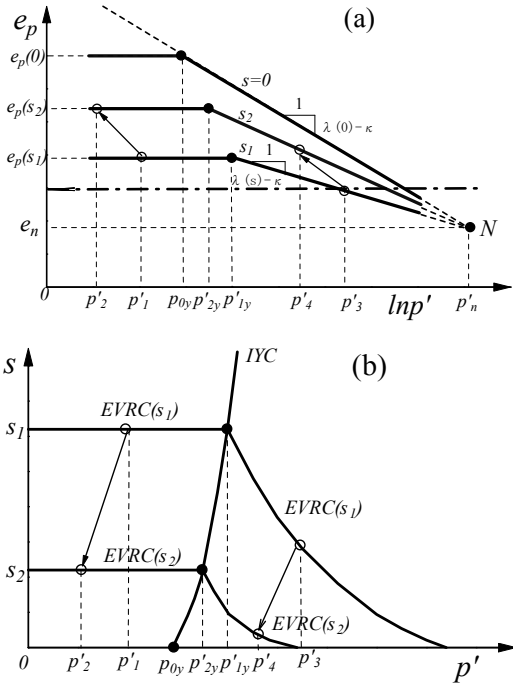

Figure 3. Sketch of the model for isotropic stress state

$$d\varepsilon_v^p = \frac{(\lambda(0)-\kappa)dp_{0y}}{(1+e)p_{0y}} \tag{14}$$

From Eq.(5),

$$dp'_y = \frac{\partial p'_y}{\partial p_{0y}} dp_{0y} + \frac{\partial p'_y}{\partial s} ds \tag{15}$$

Substituting Eq.(15) into Eq.(14) gives

$$d\varepsilon_v^p = \frac{\lambda(0)-\kappa}{(1+e)p_{0y}} (dp'_y - \frac{\partial p'_y}{\partial s} ds) / \frac{\partial p'_y}{\partial p_{0y}} \tag{16}$$

During the elastoplastic deformation stage the increments in $p_y^{'}$ is given by differentiating Eq.(1) according to

$$dp_y^{'} = dp_y + S_r ds + s dS_r \tag{17}$$

where p_y is an isotropic net stress in elastoplastic range. Substituting Eqs.(2), (11) and (16) into Eq.(17) and re-arranging gives

$$dp_y^{'} = \frac{dp_y + B ds}{(1-A)p_y^{'} - \lambda_{se} s \kappa} p_y^{'} \tag{18}$$

where $A = \lambda_{se} s(\lambda(0) - \kappa)/(p_{0y} \frac{\partial p_y^{'}}{\partial p_{0y}})$; $B = S_r - \beta - A\frac{\partial p_y^{'}}{\partial s}$

Given the increment of the net stress and suction, when $dp_y^{'} > 0$, volumetric strain increment can be calculated by Eqs. (11) and (16) with Eq.(18); when $dp^{'} = 0$, volumetric strain increment can be calculated by Eqs. (11) and (12) with Eq.(10), and the increment in the degree of saturation can be calculated by

$$dS_r = (dp_y^{'} - dp_y - S_r ds)/s \tag{19}$$

The model for isotropic stress can be extended to general stress by following Sun et al. (2007).

The proposed constitutive model for unsaturated expansive soils requires 12 model parameters which can all be determined from element tests. The parameters $\lambda(0)$ and κ can be obtained from the result of isotropic compression test on saturated soil with a loading-unloading-reloading cycle. The four parameters related with the IYC are r, α, p_{0y} and $p_n^{'}$ and two parameters about the compression index $\lambda(s)$ are ξ and τ, which can be determined from the results of isotropic compression tests at different constant suctions. There are three parameters to describe the water retention behavior, i.e. λ_{sr}, κ_s and S_{rw}^{0}, which are determined by the measured water-retention curve. The parameter λ_{se} reflects the hydraulic and mechanical coupling behavior, and is determined by plotting e against S_r from results of isotropic compression test on unsaturated soil at a constant suction.

MODEL PREDICTIONS VERSUS EXPERIMENTAL RESULTS

Zhan (2003) conducted a series of triaxial tests on compacted unsaturated expansive clay using a suction-controlled double-cell triaxial apparatus. Five tests (RST5, RUT7, RUT8, RUT9 and RUT10) were selected to verify the proposed model. The stress path of RST5 test was: wetting specimen to saturation first and then carrying out an isotropic compression to the maximum stress of 400kPa. The other four tests were the isotropic compression tests on unsaturated expansive soils with target suctions of 25, 50, 100 and 200 kPa respectively. After wetting tests, the specimens were compressed to the maximum stress of 200 kPa. The water-retention curve of unsaturated expansive soil is depicted as shown in Figure 4(a). Figure 4(b) shows the $S_r - e$ relation of an isotropic compression test on the expansive soil at different constant suctions. Based on the experimental data in Zhan (2003), the relevant model parameters used for predicting the stress-strain relation and water retention behavior of the expansive soil were determined as follows:

$\lambda(0) = 0.11$, $k = 0.02$, $r = -2.76$, $\alpha = -1.11$, $p_{0y} = 60$kPa, $p_n^{'} = 300$kPa, $\xi = 0.3489$, $\tau = 0.0294$kPa^{-1}, $\lambda_{sr} = 0.1$, $k_s = 0.03$, $S_{rw}^{0} = 45.1\%$, $\lambda_{se} = 0.83$.

The parameters λ_{sr}, κ_s and S^0_{rw} can be determined by the water-retention curve in Figure 4(a) and λ_{se} by the S_r-e relationship in Figure 4(b).

For the wetting tests under a constant isotropic net stress of 20 kPa (Figure 5), the suctions of four specimens (RUT7, RUT8, RUT9 and RUT10) were decreased from an initial suction of 540 kPa to the target suctions of 25 kPa, 50 kPa, 100 kPa and 200 kPa respectively. Figure 5 shows the changes in void ratio and the degree of saturation before and after the wetting tests and its prediction. From the predicted results in Figure 5(b), it can be seen that at the initial stage of suction decrease the changes in the saturation degree trend to be the same for the four tests, while when the suctions decrease at smaller than 100kPa, the increase tendency of the saturation degree of RUT7 and RUT8 specimens is more obvious. It can be analyzed from the water-retention curve shown in Figure 4(a). When the suction decreases to 100kPa during the wetting, the wetting curve changes from the scanning curve to the main wetting curve. The comparison between predicted (Pred.) and measured (Exp.) results indicates that the coupled model provides good description of the changing process of void ratio and the degree of saturation during wetting at constant net stress.

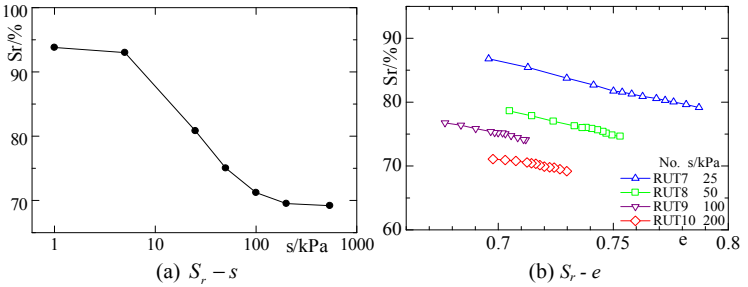

Figure 4. Water-retention behavior of unsaturated expansive soil

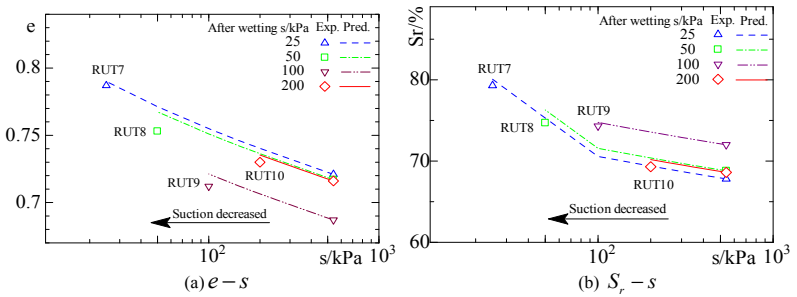

Figure 5. Changes in void ratio and degree of saturation during wetting

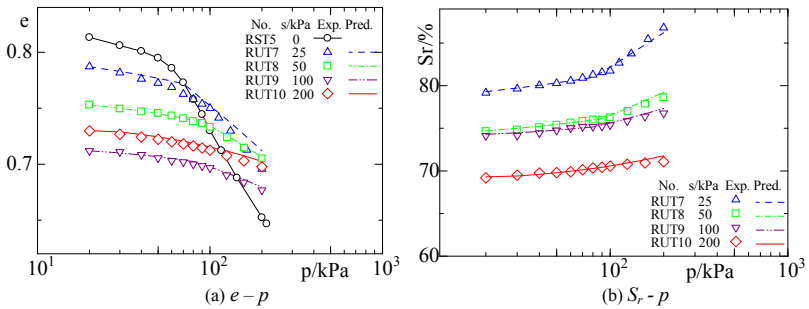

Figure 6. Changes in void ratio and degree of saturation during compression under constant suctions

Figure 6 shows the changes in void ratio and degree of saturation during compression under constant suctions. From the predicted results in Figure 6, it can be seen that the specimens behave from the elastic state to the elastoplastic state during increasing isotropic net stress. With the increase in suction, the yield stress gradually increases, and the compression index gradually decreases. It shows that the predicted results have the consistency with the test results. At the same time, the coupled model can also predict that the degree of saturation increases with increasing the isotropic net stress even at constant suctions, which cannot be predicted by the BExM.

CONCLUSIONS

This paper presented a hydro-mechanical coupled elastoplastic model for expansive unsaturated soils from the macroscopic observation based on the existing hydro-mechanic elastoplastic model for non-expansive unsaturated soil. The model takes into consideration the coupled effect of the degree of saturation on the mechanical behavior and void ratio on the water-retention behavior. The predicted results compare very well with the experimental results published in the literature, which include the swelling tests under constant net stresses and isotropic compression tests under constant suctions. This research has shown that the proposed model offers great potential for quantitatively predicting the hydraulic and mechanical behaviour of unsaturated expansive soil.

ACKNOWLEDGMENTS

The authors appreciate the support of the Research Fund for the Doctoral Program of Higher Education of China (Grant No. 20093108110017).

REFERENCES

Alonso, E.E., Gens. A. and Josa, A. (1990). "A constitutive model for partially saturated soils." Geotechnique, Vol. 40 (3), 405-430.

Alonso, E.E., Vaunat, J. and Gens, A. (1999). "Modelling the mechanical behaviour of expansive clays." Engineering Geology, 54, 173-183.

Gens, A. and Alonso, E.E. (1992). "A framework for the behaviour of unsaturated clay." Canadian Geotechnical Journal, 29, 1013-1032.

Sun, D.A., Sheng, D.C. and Sloan, S.W. (2007). "Elastoplastic modelling of hydraulic and stress-strain behaviour of unsaturated compacted soils." Mechanics of Materials, 39(3), 212-221.

Zhan, L. T. (2003). "Field and laboratory study of an unsaturated expansive soil associated expansive soil associated with rain-induced slope instability." Ph. D. Dissertation, Hong Kong University of Science and Technology, 302-354.

Effect of Slope Terrain on Distribution of Matric Suction in Unsaturated Slopes Subjected to Rainfall

Ch. Fan[1], and Ch. Hsiao[2]

[1] Associate Professor, Dept. of Construction Engrg., National Kaohsiung First University of Science and Technology, Taiwan, R.O.C. 2, Jhuoyue Rd., Nanzih District, Kaohsiung City, Taiwan, R.O.C.; e-mail: ccfan@ccms.nkfust.edu.tw
[2] Graduate Student, Dept. of Construction Engrg., National Kaohsiung First University of Science and Technology, Taiwan, R.O.C.

ABSTRACT: This paper presents a field experimental study on the influence of slope terrain on the distribution of matric suction of the soil in unsaturated slopes subjected to rainfall. Instrumentation and testing programs were carried out in a slope with different terrains, i.e. planar slopes, gullied slopes, and ridge-like slopes. The matric suctions of the soil at a depth greater than 1.2m were measured using jet-filled tensiometers, and those less than 0.9m were measured using the filter paper method. The matric suctions of the soil along the depth in the slope were measured prior to and after the rainfall event, and data in two major rainfall events (accumulated precipitations with small and large amount) were presented. Major findings concluded from this research are: (1) the matric suctions of the soil at shallow depths in gullied slopes in dry season are significantly less than those in planar slopes and ridge-like slopes, and those in ridge-like slopes are slightly greater than those in planar slopes; (2) the amount of drop in the matric suctions of the soil in gullied slopes is considerably small compared with that in planar and ridge-like slopes; (3) after the rainfall event, the matric suctions of the soil at the shallow depth in the ridge-like slope are considerably greater than those in the planar and gullied slopes no matter what the amount of the accumulated precipitation is; (4) the influence of the rainfall with a low accumulated precipitation on the behavior of the matric suction of the soil in different slope terrains is similar to that with a high accumulated precipitation.

INTRODUCTION

Soils are usually treated as dry or fully saturated materials in the conventional analysis of slope stability. However, it is not the case in natural or man-made slopes. Soils at the shallow depth experience drying and wetting processes in dry and rainy seasons.

The soil moisture content in the slope may go through unsaturated and saturated conditions, particularly at the shallow depth of the slope. The mechanics of unsaturated soils plays an important role in the stability of the slope. The mechanical properties of the soil at the shallow depth, normally less than 3-4 m, may govern the occurrence of shallow slope failures, especially as the slope is subjected to rainfall activity. Drying and wetting processes affect the soil moisture content significantly in the slope. Infiltration of surface runoff during or after a rainfall event results in a reduction in the matric suction of the soil, and the shear strength of unsaturated soils relies on the matric suction of the soil considerably (Fredlund and Rahardjo 1993). The mechanism of changes of the soil matric suction due to the rainfall activity plays an important role in the failure of slopes (Au 1998). The influence of the rainfall on the distribution of the soil matric suction is governed by the antecedent climate conditions, e.g. duration of dry season and temperature. Additionally, infiltration of surface runoff induced by rainfall results in the development of wetting front and affects the potential depth of slope failures. Past investigation and research on landslide susceptibility showed that the frequency of landslides increased as the distance to drainage line decreased (Dai and Lee 2001). The flow of the surface runoff strongly relies on the topography, especially the terrain of the slope. Slopes running through valley or gully work as a drainage channel after prolonged heavy rains and obviously collect more surface runoff than other types of slope terrains. Past researches (Gasmo et al. 2000, Collins and Znidarcic 2004) showed that slope failures were governed not only by the strength characteristics, but also by the hydraulic characteristics of the soil in the slope. The behavior of the soil moisture content and the matric suction of unsaturated soil slopes subjected to rainfall are obviously affected by slope terrains. The shear strength of unsaturated soils in slopes with different terrains is different as it is subjected to rainfall.

This paper aims to investigate the behavior of the matric suction of the soil in different slope terrains, i.e. planar slopes, slopes running through a gully (gullied slopes), and ridge-like slopes, subjected to rainfall. Instrumentation and monitoring programs on the matric suction of unsaturated soils in the slope were carried out for different slope terrains in this study.

MATERIALS AND METHODS

Test Site

The test site, a fill slope covered with grass, is located at the campus of the National First University of Science and Technology, Kaohsiung city, Taiwan, as shown in Figure 1. Area of the test site is about 80 m×30 m. The soil at the test site is consisted of silty clay with occasional sandy materials, and is classified as CL. Dry unit weight of the soil ranges from 16.2 kN/m^3 to 17.2 kN/m^3. Liquid limit and plastic index of the clayey soil are in a range from 22 to 30 and from 15 to 20, respectively, based on the test procedure of ASTM Test Designation D-4318.

The orientation of the slope is north-south and dips toward east. There are three different slope terrains at the site, namely planar slopes, ridge-like slopes, and gullied slopes. The length and the slope gradient of the ridge-like slope are about 23 m and 30°, respectively; the length and the slope gradient of the planar slope are about

20m and 37°, respectively; the length and the slope gradient of the gullied slope are about 18 m and 30°, respectively. The longitudinal cross-section of the planar slope is shown in Figure 2, and the transverse cross-sections of the ridge-like slopes and the gullied slope are shown in Figs. 3 and 4, respectively. The data collected in the rainfall events of Nov. 24-29, 2007 (the accumulated precipitation is 55 mm, representing a low-level rainfall activity) and May 28-June 6, 2008 (the accumulated precipitation is 371 mm, representing a high-level rainfall activity) are presented and discussed in this paper.

Measurement of Matric Suction

Matric suctions of the soil at a depth of 1.2m, 1.5m, and 2.7m were measured using jet-filled tensiometers, manufactured by Soil-Moisture Inc., and those at depths of 0.15m, 0.6m, and 0.9m were measured using the filter paper method because matric suctions at the shallow depth were expected to be high and jet-filled tensiometers were only capable of measuring the matric suction up to 90kPa. Depths of instrumentations and tests are shown in Figure 2. The matric suctions of the soil along the depth at about the mid-height of the slope were measured prior to and after the rainfall event.

Measurement of the matric suction of the soil using the filter paper method is based on the procedure of ASTM 5298-94. The diameter of filter paper (Whatman No.42) is 5.5cm. Glass containers with a volume of 120 ml were used to contain the soil specimen and filter papers. The contact method proposed in the ASTM procedure was used to estimate the matric suction of the soil. The calibration formula recommended by the procedure of ASTM 5298-94 were used to calculate the matric suction of the soil and given as

$$\log\psi = 5.327 - 0.0779\omega_f \quad (\omega_f < 45.3\%) \tag{1}$$

$$\log\psi = 2.412 - 0.0135\omega_f \quad (\omega_f >= 45.3\%) \tag{2}$$

where ψ(kPa) is the matric suction of the soil; ω_f is the moisture content of the filter paper.

Figure 1. Picture of the test site

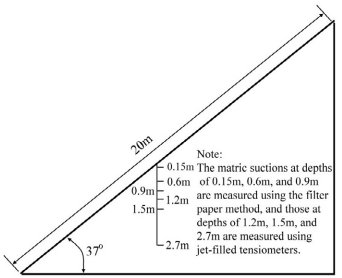

Figure 2. Longitudinal cross-section of the planar slope and the depths of instrumentation

RESULTS AND DISCUSSION

Time History of Matric Suction

Time histories of the matric suction of the soil at various depths measured at the middle part of the ridge-like, planar, and gullied slopes from July, 2007 to June, 2008 are shown in Figs. 5, 6, and 7, respectively. The period of June thru October is the major months of rainfall activities at the region of the test site. The matric suctions of the soil at shallow depths decrease significantly after the rainfall activities, and it increases progressively due to evaporation in the following dry season. The magnitude of the matric suction and its variation with time are different in various slope terrains. In general, rainfall activities result in a considerable decrease on the matric suction of the soil at a depth less than about 1.2 m for planar and ridge-like slopes, however, the extent of the wetting front relies on the amount of the accumulated precipitation.

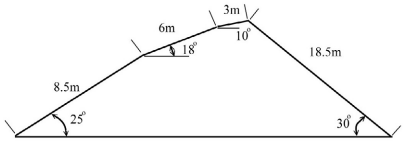

Figure 3. Transverse cross-section of the ridge-like slope

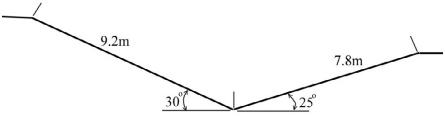

Figure 4. Transverse cross-section of the gullied slope

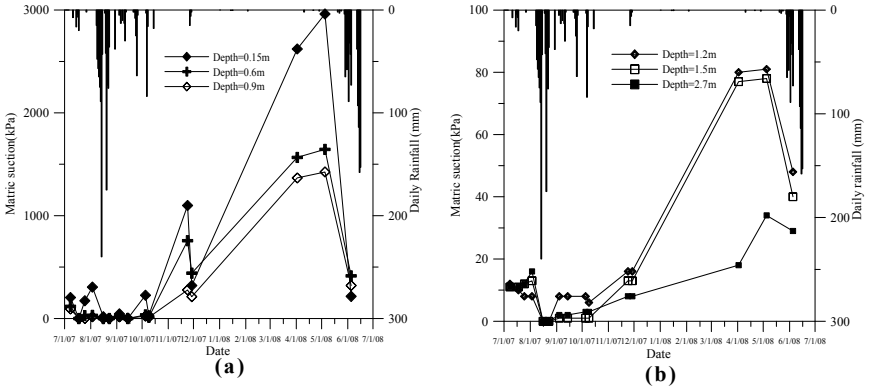

Figure 5. Time history of the matric suction of the soil measured in the ridge-like slope: (a) depth = 0.15m-0.9m, (b) depth = 1.2m-2.7m

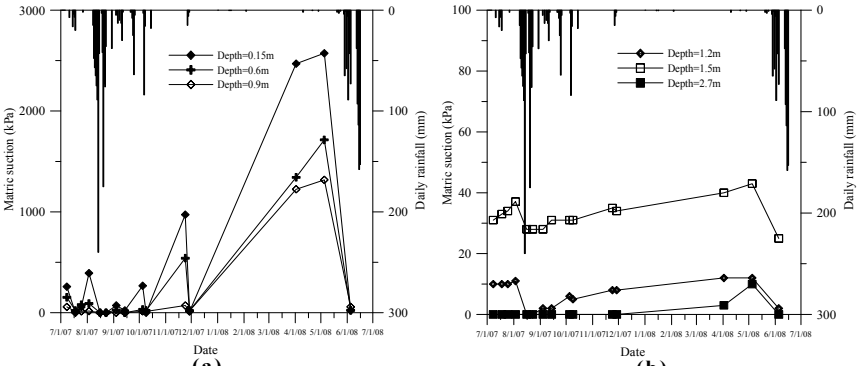

Figure 6. Time history of the matric suction of the soil measured in the planar slope: (a) depth = 0.15m-0.9m, (b) depth = 1.2m-2.7m

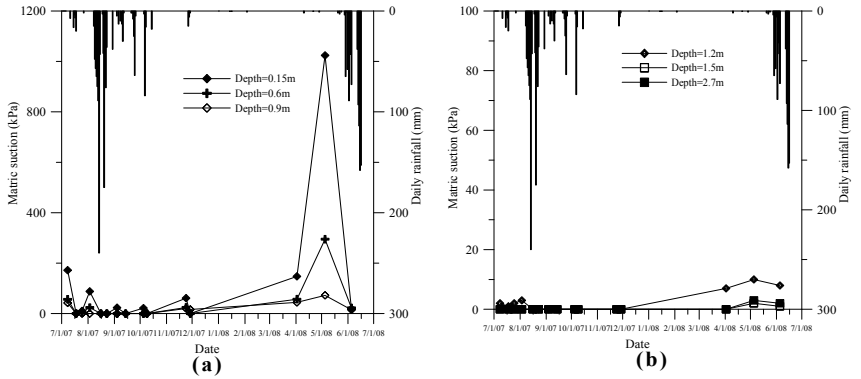

Figure 7. Time history of the matric suction of the soil measured in the gullied slope: (a) depth = 0.15m-0.9m, (b) depth = 1.2m-2.7m

The pattern of the variation of the matric suction of the soil at various depths with time in the planar slope is similar to that in the ridge-like slope. The matric suction of the soil at a depth of 0.15 m in the ridge-like and planar slopes reached up to about 1000 kPa and 2500 kPa due to evaporation of 43 days and 150 days, respectively, in dry season, and it reduces to nearly null following a heavy rainfall event. The matric suctions of the soil at depths greater than 1.2 m were all less than 100 kPa in the ridge-like and planar slopes before and after the rainfall event. The matric suctions of the soil at depths greater than 0.9 m measured in the gullied slope were all less than 100 kPa during the period of one-year field experiment, including dry and rainy seasons. The surface runoff in gullied slopes is considerably greater than that in planar and ridge-like slopes in a given rainfall event under the same geological and slope gradient conditions.

The influence of precipitation on the soil in gullied slopes in terms of the soil moisture content and the extent of wetting front may be anticipated to be high compared with those in planar and ridge-like slopes. In gullied slopes, the matric suctions of the soil at depths greater than 1.2 m were all less than 10 kPa in any season (dry and rainy), and the matric suction of the soil at the depth less than 0.6 m can reach about 300-1000 kPa in dry season lasting for about 5 months. In dry season, the matric suctions of the soil measured in the gullied slope were considerably less than those in the planar and ridge-like slopes, and this behavior may be attributed to the following reason: the soil moisture contents in gullied slopes at shallow depths (less than about 1.5 m in this study) are noticeably greater than those in planar and ridge-like slopes in dry season based on the monitored data, which is not presented in this paper. Thus, slope topography strongly affects the variation of the matric suction of the soil with time in dry season and after the rainfall activities based on the monitored data.

Distribution of the Matric Suction of the Soil with Depth

The distributions of the matric suction of the soil along the depth in the ridge-like, planar, and gullied slopes prior to and after the rainfall event of Nov. 24-29, 2007 (an accumulated precipitation of 55 mm) are shown in Figure 8(a). Prior to the rainfall event of Nov. 24-29, 2007, dry conditions last for 43 days. The matric suctions of the soil in the ridge-like and planar slopes were considerably greater than those in the gullied slope before the rainfall activity, and the matric suctions of the soil decreased with the depth. The matric suctions of the soil at a depth of 0.15 m in the ridge-like, planar, and gullied slopes reached up to 1100 kPa, 970 kPa, and 61 kPa, respectively, after a dry period of 43 days. The matric suctions of the soil at the shallow depth of the ridge-like slope were slightly greater than those of the planar slope. After the rainfall event, the matric suctions of the soil at shallow depths in the gullied slope and in the planar slope reduce to nearly null and low amount (<20 kPa), respectively. However, the matric suctions of the soil at shallow depths (<1 m) in the ridge-like slope were still greater than about 200 kPa after the rainfall event, and the maximum matric suction (=440 kPa) of the soil was located at a depth of 0.6 m in the ridge-like slope. In addition, the amount of drop in the matric suction of the soil along the depth after the rainfall event occurred on Nov. 24-29, 2007 is shown in Figure 8(b). The amount of drop in the matric suctions of the soil in the planar slope was slightly greater than those in the ridge-like slope. The amount of drop in the matric suctions of the soil at shallow depths in the gullied slope was considerably small due to low matric suctions prior to the rainfall event, and the values were considerably less than those in planar and ridge-like slopes.

The distributions of the matric suction of the soil along the depth in the ridge-like, planar, and gullied slopes prior to and after the rainfall event of May 28-June 6, 2008 (an accumulated precipitation of 371 mm) are shown in Figure 9(a). Prior to the rainfall event of May 28-June 6, 2008, dry conditions last for 150 days. The behavior of the distributions of the matric suction of the soil in the ridge-like, planar, and gullied slopes in this rainfall event (representing a high-level accumulated precipitation) is similar to that in the rainfall event of Nov. 24-29, 2007 (representing a low-level accumulated precipitation). The matric suctions of the soil at shallow depths (<1 m) prior to the rainfall event of May 28-June 6, 2008 were noticeably greater than those of

Nov. 24-29, 2007 because the period of the dry season prior to the rainfall event of May 28-June 6, 2008 is longer than that of Nov. 24-29, 2007. The matric suctions of the soil at a depth of 0.15 m in the ridge-like, planar, and gullied slopes reached up to 2960 kPa, 2570 kPa, and 1020 kPa, respectively, after a dry period of 150 days. It is of interest to note that the matric suctions of the soil at shallow depths in the ridge-like slope after an accumulated precipitation of 371 mm were close to those after an accumulated precipitation of 55 mm (rainfall event of Nov. 24-29, 2007). In addition, the amount of drop in the matric suction of the soil along the depth after the rainfall event occurred on May 28- June 6, 2008 is shown in Figure 9(b). The influence of the rainfall with an accumulated precipitation of 371 mm on the pattern of the soil matric suction with the depth after the rainfall event in different slope terrains, especially the ridge-like slope, is similar to that with an accumulated precipitation of 55 mm. The amount of drop in soil matric suction after the rainfall event of May 28-June 6, 2008 in three different slope terrains was considerably greater than that after the rainfall event of Nov. 24-29, 2007 because the antecedent dry season for the rainfall event of May 28-June 6, 2008 is about 100 days longer than that of Nov. 24-29, 2007.

A number of conclusions can be drawn through the measured results presented herein: (1) the matric suctions of the soil in gullied slopes in dry season are considerably low compared with those in planar and ridge-like slopes; (2) the amount of drop in the matric suctions of the soil at shallow depths in the gullied slope is considerably small due to low matric suctions prior to the rainfall event; (3) the matric suctions of the soil at shallow depths in the ridge-like slope after a high accumulated precipitation are close to those after a low accumulated precipitation; (4) the influence of the rainfall with a low accumulated precipitation on the behavior of the matric suction of the soil in different slope terrains is similar to that with a high accumulated precipitation; (5) after the rainfall event, the matric suctions of the soil at shallow depths in the ridge-like slope are considerably greater than those in the planar and gullied slopes no matter what the amount of the accumulated precipitation is.

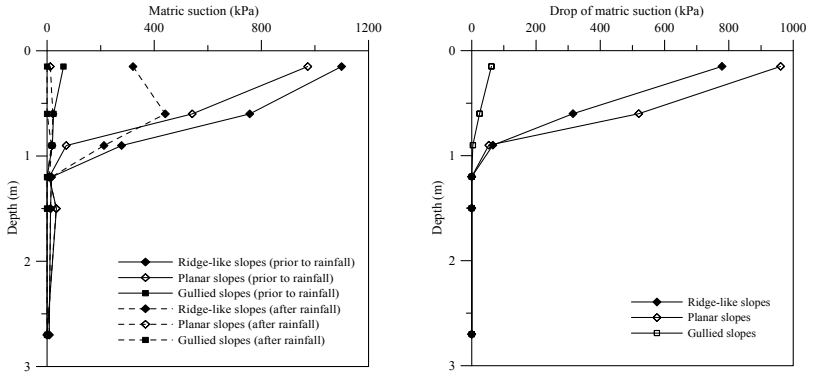

(a) **(b)**

Figure 8. Distributions of the soil matric suction along the depth in the rainfall event of Nov. 24-29, 2007: (a) the matric suction prior to and after the rainfall event, (b) drop of matric suction after the rainfall event

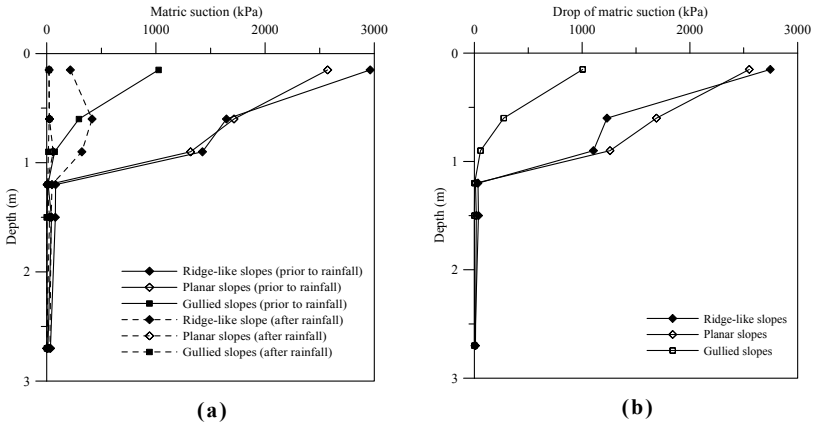

Figure 9. Distributions of the matric suction of the soil along the depth in the rainfall event of May 28-June 6, 2008: (a) the matric suction prior to and after the rainfall event, (b) drop of matric suction after the rainfall event

CONCLUSIONS

This paper presented a field experimental study on the influence of slope terrain on the distribution of the matric suction of the soil for unsaturated slopes subjected to rainfall. Instrumentation of tensiometers and testing program were carried out in three types of slope terrains, namely planar slopes, ridge-like slopes, and gullied slopes. The test program was carried out from July of 2007 thru June of 2008. Matric suctions of the soil along the depth in the slope were measured prior to and after the rainfall event, and data in the rainfall event of low and high accumulated precipitations were reported and discussed in this paper.

Major findings summarized from this research are: (1) the matric suction of the soil at a depth less than 1.2 m is considerably reduced after the rainfall event; (2) the matric suctions of the soil at shallow depths (<1 m) in gullied slopes in dry season are significantly less than those in planar and ridge-like slopes, and the matric suctions of the soil at shallow depths in ridge-like slopes are slightly greater than those in planar slopes; (3) after the rainfall event, the matric suctions of the soil at shallow depths in the ridge-like slope are noticeably greater than those in the planar and gullied slopes no matter what the amount of the accumulated precipitation is; (4) the amount of drop in the matric suctions of the soil in the gullied slope after the rainfall is considerably small due to low matric suctions prior to the rainfall event; (5) the matric suctions of the soil at shallow depths in the ridge-like slope after a high accumulated precipitation are close to those after a low accumulated precipitation; (6) for a given rainfall event, the amount of drop in the matric suction of the soil at shallow depths in planar slopes is slightly greater than that in ridge-like slopes.

REFERENCES

Au, S.W.C. (1998). Rain-induced slope instability in Hong Kong", Engineering Geology, 51, 1-36.

Collins, B.D., Znidarcic, D. (2004). Stability analyses of rainfall induced landslides, Journal of Geotechnical and Geoenvironmental Engineering, 130, 362–372.

Dai, F.C., and Lee, C.F. (2001). Terrain-based mapping of landslide susceptibility using a geographical information system: A case study. Canadian Geotechnical Journal, 38(5), 911-923.

Fredlund, D. G. and Rahardjo, H. (1993). Soil Mechanics for Unsaturated Soils, John Wiley & Sons, New York.

Gasmo, J.M., Rahardjo, H., Leong, E.C. (2000). Infiltration effects on stability of a residual soil slope, Computers and Geotechnics, 26, 145–165.

Lumb, P.B. (1975). Slope failures in Hong Kong. Q.J. Engineering Geology, 8, 31-65.

Ng, C.W.W., Zhan, L.T., Bao, C.G., Frelund, D.G., Gong, B.W. (2003). Performance of an unsaturated expansive soil slope subjected to artificial rainfall infiltration, Geotechnique, 53(2), 143-157.

Three-dimensional Slope Stability Analysis of Unsaturated Soil Slopes Subject to Reservoir Water Level Fluctuations

Ch. Yong[1], L. Defu[1], W. Shimei[1], and T. Dongfang[1]

[1] China Three Gorges University, Key Laboratory of Geological Hazards of Three Gorges Reservoir Area , Ministry of Education, Daxue Road, Yichang, Hubei 443002, China

ABSTRACT: Water infiltration is an important actor causing a bank slope failure, and the development of unsaturated soils mechanics has provided a new theoretical basis and corresponding analysis method for studying the effects on slope stability of reservoir water infiltration. The three-dimensional terrain and structure of slope are also the essential influencing factors in its stability analysis.

In the paper, the pore water pressure fields are computed by simulation of unsaturated seepage to ascertain the stress and strain distributions of three-dimensional slope based on the constitutive model of unsaturated soils, then the contribution of matric suction to shear strength is considered and three-dimensional stability analysis methods of unsaturated soils slope are performed to evaluate the safety factor (Fs). Taking Xietan landslide in Three Gorges reservoir area as the example, the result shows that its deformation and stability are seriously affected by reservoir water level change, and variation rules of slope stability are consistent with the dispatch of reservoir water.

INTRODUCTION

Many soils near the valley surface are unsaturated, during the reservoir water level fluctuations, water infiltrating into soil have a great impacts on the slope body. The earliest study of the impacts of the reservoir infiltrating level changes on the slope stability could be dated back to 1960s (Morgenstern 1963). Delightful achievements has made in recent 20 years (Duncan 1990, Massimo and Nicola 1999, Liao et al 2005, Liu et al 2005). Most of them emphasized on the ascertainment of the slope transient seepage field owing to reservoir water infiltration and pointed out that the change of soils physical, mechanical characteristics, the variation in reservoir water level and the seepage force are all the main factors affecting slope instability.

In this paper, the numerical methods are introduced into the unsaturated seepage, FE calculation and slope stability analysis. Then Xietan landslide in Three

Gorges Reservoir area is taken as the example, combined with the annual dispatch of reservoir water level, the stability variation is computed and analyzed based on the water level fluctuation.

UNITED METHOD OF SLOPE RUNOFF AND UNSATURATED SEEPAGE

The united method is a cooperative solving analysis, which is according to the equal relationship between the change of slope runoff and the boundary flux of seepage. The finite element expression of this coupling model is shown as (Tian et al 2009):

$$[N]\{\frac{\partial \phi}{\partial t}\} + [M]\{\phi\} = \{R\} \tag{1}$$

where $[M]$, $[N]$, and $\{R\}$ can be defined as: $m_{ij} = \int_e k_i \left(w_i \frac{\partial w_j}{\partial l} \right) dl + \iint_e [B_i]^T [k][B_j] ds$, $n_{ij} = \int_\Gamma (w_i w_j) dl + \iint_e C N_i N_j ds$, $r_i = \int_\Gamma (I \cos\alpha_i - f) w_i dl - \int_\Gamma N_i v_n dl = \int_\Gamma I \cos\alpha_i dl$, respectively, and k is the permeability coefficient of unsaturated soil, ϕ_i is the node hydraulic pressure, w is the interpolation basic function, N_i is the interpolating shape function of element, I is the rainfall intensity, f is the infiltration rate, α is the slope angle, v is the flow rate, $C = \frac{\partial \theta}{\partial h} = \rho_w g \frac{\partial \theta}{\partial (u_a - u_w)}$ can be defined by the soil-water characteristic curve.

THE FEM BASE ON MOHR-COULOMB MODEL OF UNSATURATED SOILS

The pore water pressure can be achieved by above unsaturated seepage, and the negative pressure is considered as suction. The Mohr-Coulomb yield function of unsaturated soils is:

$$F(\sigma) = \frac{1}{3} I_1 \sin\varphi + \sqrt{J_2} (\cos\theta_\sigma - \frac{1}{\sqrt{3}} \sin\theta_\sigma \sin\varphi) - (c + s \cdot tg\varphi_b) \cdot \cos\varphi \tag{2}$$

with c being the effective saturated cohesion, φ the effective saturated friction angle, s the matric suction, φ_b the friction angle accounting for the matric suction contribution to shear strength, $\boldsymbol{I}_1$ is the primary stress invariant, and $\boldsymbol{J}_2$, $\boldsymbol{J}_3$ are respectively second and third invariants of deviatoric stress, θ_σ is essentially similar to the Lode angle.

THREE-DIMENSIONAL STABILITY OF UNSATURATED SOILS SLOPE

Based on the FE analysis, the stress fields of slope are ascertained, and the safety factor (Fs) can be confirmed from the stress level of sliding zone. The center point location of elements are averaged from the coordinates of eight nodes at first; then the

six stress components of center points are computed from the stress of eight Gauss points through the interpolation technique (Zhen 2004).

According to the strength criterion of unsaturated soil proposed by Fredlund, when a node is in a critical state, the first principal stress can be described as:

$$\sigma_{1f} = \sigma_3 \tan^2(45^0 + \frac{\varphi}{2}) + 2 \cdot (c + s \cdot \tan \varphi_b) \tan(45^0 + \frac{\varphi}{2}) \quad (3)$$

and the stress level of this node is:

$$S = \frac{(\sigma_1 - \sigma_3)}{(\sigma_{1f} - \sigma_3)} \quad (4)$$

where σ_{1f}–σ_3 the diameter of Mohr's stress circle at critical state.

By this means, the stress level of each element's center points are confirmed, and the volumes of each element are defined as the weight function, thus, the safety factor along the sliding zone is:

$$F_s = \frac{\sum V_i}{\sum \left[\frac{\sigma_1 - \sigma_3}{\sigma_{1f} - \sigma_3}\right]_i \cdot V_i} \quad (5)$$

ANALYSIS OF XIETAN LANDSLIDE FOR WATER LEVEL FLUCTUATIONS

The Xietan landslide is located on the left bank of Yangtze River, about 36 km upstream from the Three Gorges Dam (Figure 1). The landslide is situated in a broad V-shape river valley. The gentle front extrudes to Yangtze River, like a tongue tip, and the back edge boundary is the intersection of steep and gentle region, like a circular chair. The area of landslide is about $2.1\times10^5 m^2$ and volume is about $6.24\times10^6 m^3$.

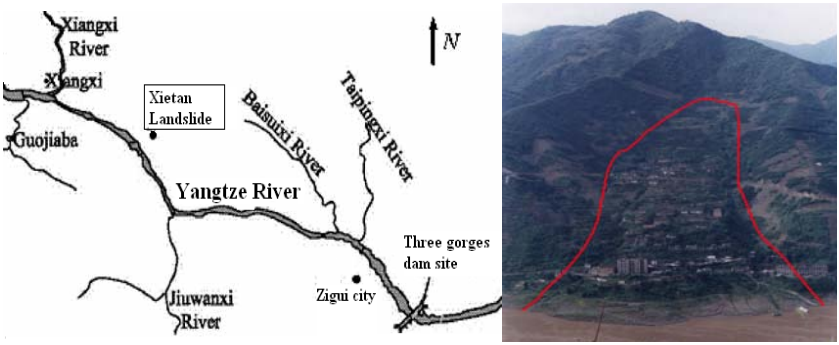

Figure 1. Location and front view of Xietan landslide

The Xietan landslide is composed of sliding mass, sliding zone and bed rock. The sliding mass consists of loose deposits and colluvial deposits from the back mountain, the sliding zone is mainly filling with gravel soil, and the bed rock is intact. According to geological data of Xietan landslide, three-dimensional calculation mesh is built and described as Figure 2, and on the middle section of model, six observation points are set between 130 and 175 m in sliding zone. The material parameters are list in Table 1.

Table 1 Mechanical parameters and penetration property of each material

Material number	E (kPa)	v	ρ sat (kN/m^3)	ρ (kN/m^3)	c (kPa)	φ (^{0})	φ^b (^{0})	k_s (m/d)	W_0 (%)	w_{sat} (%)
1	15×10^3	0.35	22.5	20.7	23.0	25.0	17.0	1.03	12.8	25
2	10×10^3	0.35	21.5	20.8	15.2	15.0	12.0	1.5×10^{-1}	11.4	27
3	800×10^3	0.25	23.5	23.5	500.0	38.0	–	4.5×10^{-6}	0.6	2.0

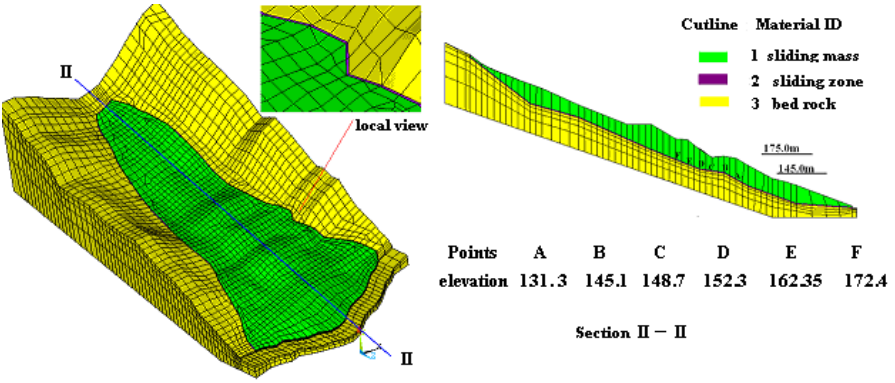

Figure 2. Three-dimensional mesh and profiling definition of Xietan landslide

According to the dispatch in Figure 3, water level is fluctuated from 145 to 175 m from the end of September to May of next year. The seepage calculation is begun at the end of September, and the water level elevates to 175 m in next 40 days and persists 175 m for 60 days, then drops down to and lasts 145 m during the following 110 days.

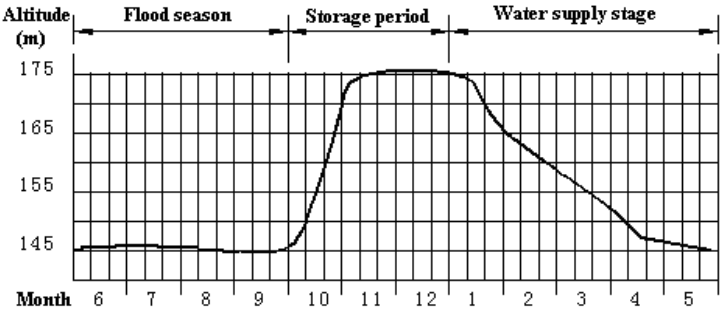

Figure 3. Annual dispatch of Three Gorges reservoir water level

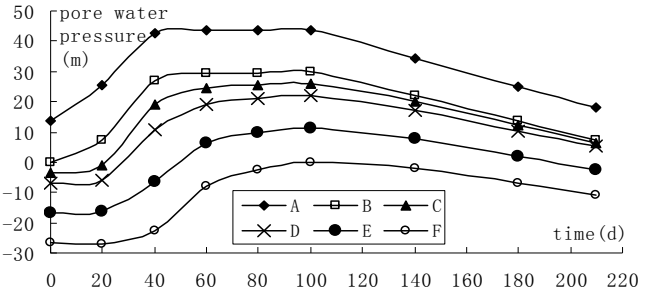

Figure 4. Variation of pore water pressure at six observation points

To ascertain the influence of reservoir water level fluctuation on the sliding zone, which exists with a certain depth, six observation points are paid more attention to study the variation rules of their pore water pressure. Figure 4 shows the variation rules of pore water pressure are accordant with the changes of reservoir water level, however, the former shows some lag.

The variation rule of slope safety factor along with the reservoir water level fluctuation is shown in Figure 5. It shows (a) the safety factor reduced gradually when the reservoir water level increased steadily; (b) the safety factor still reduced during the level persisting 175 m, but the decreasing rate was less than that of the beginning. This resulted from the positive pore water pressure also increased slowly due to the reservoir water infiltration. (c) The safety factor dropped to the minimum at the beginning of drawdown, at this moment, the saturation was not enough changes, and the moisture inside the slope infiltrate outwards because of the reservoir level is dropping rapidly, which is worst to the slope stability. (d) Along with the reservoir level lowering gradually to 145 m, the safety factor increased owing to the pore water pressure decreasing, but it was still less than that of the initial calculation point where the level was also 145 m.

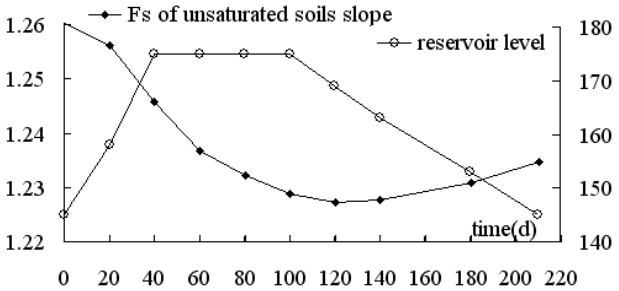

Figure 5. Variation in slope stability factor of safety with dispatch of reservoir water level

CONCLUSIONS

This study presents a set of method system to analyze the influence of reservoir water level fluctuation on the stability of unsaturated soils slope, and the following conclusions can be drawn:

1. Based on the results of three-dimensional unsaturated seepage analysis, the variation rules of pore water pressure of six observation points are accordant with the change of reservoir level, and compared to their changes, the pore water pressure shows some hysteresis at different degree.
2. According to the three-dimensional stability analysis of unsaturated soils slope, the safety factor of Xietan landslide is acutely affected by the reservoir level fluctuation, especially at the beginning of rapid drawdown, the factor drops to the minimum.
3. In the paper, the studies are focused on the influence of reservoir water level, but its fluctuation range is only 30 m, so the change range of safety factor is 1.225 to 1.26. Once rainfall infiltration occurs at this time, the moisture content of slope soil must increase rapidly, and the safety factor must decrease in a greater degree even the destruction and instability may occur.

ACKNOWLEDGMENTS

The research is financially supported by the Key Project of Nature Science Foundation of China (50839004).

REFERENCES

Duncan, Wright, Wong. (1990). Slope stability during rapid draw down. In: Proceeding of the H. Bolton seed memorial symposium. 2; 253-272.

Liao Hongjian, Sheng Qian, Gao Shihang, Xu Zhiping. (2005). Influence of drawdown of reservoir water level on landslide stability. Chinese Journal of Rock Mechanics and Engineering, 24(19): 3454-3458.

Massimo, Nicola. (1999). Stability of stream banks formed in partially saturated soils and effects of negative pore water pressures. Geomorphology, 26, 253 -277.

Morgenstern. (1963). Stability charts for earth slopes during rapid drawdown. Geotechnique, 13:121-131.

Liu Xinxi, Xia Yuanyou, Lian Cao, Zhang Kaipeng. (2005). Research on method of landslide stability valuation during sudden drawdown of reservoir level. Rock and Soil Mechanics, 26(9):1427-1436.

Tian Dongfang, Liu Defu, Wang Shimei, Chen Yong, Xiao Shirong. (2009). Coupling numerical analysis of unsaturated seepage and stress fields for soil slope. Rock and Soil Mechanics, 30(3): 810-814.

Zheng Hong, Liu Defu, Luo Xianqi (2004). Determination of potential slide line of slopes based on deformation analysis. Chinese Journal of Rock Mechanics and Engineering, 23(5): 709-716.

Effect of Environmental Conditions on Stability of an Unsaturated Soil Slope

Z. Zhang[1], W. Cui[2], and R. Guo[3]

[1] School of Highway, Chang' University, Xi'an, Shanxi, China, 710064, e-mail: zzg663@yahoo.com.cn
[2] School of Civil Engineering, Tianjin University, Tianjin, China, 300072, e-mail: superoasis@163.com
[3] Tsinghua University, Beijing, 100084, China, e-mail: guorh@tsinghua.edu.cn

ABSTRACT: The effect of negative pore-water pressure (suction) is often ignored in slope stability analyses. Based on the theory of infiltration and seepage through an unsaturated soil system, transient numerical analyses for an engineering case of slope instability, caused by the loss of soil suction under the condition of continuous rainfall, are conducted. The results of the analysis show that the unsaturated soil suction has an important effect on the stability of the unsaturated slope. The suction profile depends on the magnitude of the flux, frequency, duration of rainfall and evapotranspiration. In most cases, the simultaneous effect of several factors must be considered in assessing the magnitude of soil suction. The paper highlights the importance of monitoring soil suction in engineering practice for slope stability purposes.

INTRODUCTION

The effect of suction on the stability of slopes has become an important topic in geotechnical engineering. Specific case histories have shown examples where these failures were related to a loss of soil suction caused by local weather conditions. Wu et al. (2004) analyzed the important effect of suction on the stability of slopes, and the conclusions had a guiding significance in the analysis of slope stability under rainfall conditions. Chen et al. (2001) examined the stability of an unsaturated soil slope under transient piezometric conditions, and concluded that the loss of soil suction was an

important factor in causing slope failure. Zhang et al.(2004) studied the effects of the magnitude and duration of rain flux and the saturated coefficient of permeability on soil suction by using numerical analysis, and found that these factors significantly influence soil suction patterns. James et al. (2004) presented an engineering case history analyzed by finite element method. The results showed that the decrease of shear strength caused by the loss of soil suction was the main reason for the slope failure. In the field of theoretical research, the unsaturated soil mechanics framework postulated by Fredlund (2006) is widely applied in engineering practice and academia, and can be considered as the theoretical basis for the stability analysis of unsaturated soil slopes. However, the effects of environmental conditions, such as rainfall frequency, rainfall amount, rainfall duration, evaporation, among others, on soil suction and unsaturated soil strength need further investigations from both theoretical and practical standpoints.

In this paper, the failure of an unsaturated soil slope in a highway engineering project has been analyzed using Fredlund's (2006) unsaturated soil mechanics theory, identifying the key failure mechanisms. The effects of the predominant environmental conditions on the stability of the unsaturated soil slope are also discussed.

THEORY OF SEEPAGE THROUGH UNSATURATED MEDIA

Water Flow

Based on continuity considerations and Darcy's law, the governing partial differential equation for two-dimensional transient flow through an unsaturated soil media can be formulated as follows (Fredlund 1976):

$$\frac{\partial}{\partial x}\left(k_x \frac{\partial h}{\partial x}\right)+\frac{\partial}{\partial y}\left(k_y \frac{\partial h}{\partial y}\right)= m_2^w \rho_w g \frac{\partial h}{\partial t} \tag{1}$$

where k_x is the coefficient of permeability in the x direction, k_y is the coefficient of permeability in the y direction, and, m_2^w is the water storage coefficient. In this equation, the three soil parameters, k_x, k_y, and m_2^w, are functions of the negative pore pressure.

Unsaturated Soil Property Functions Related to Seepage

The soil-water characteristic curve (SWCC) is a relationship between water content and suction in the soil, either for drying or wetting conditions. In this paper, the Fredlund's (2006) equation with a correction factor C, equal to 1, is used as follows:

$$\theta_w = \frac{\theta_s}{\left\{\ln\left[e + \left(\frac{\psi}{a}\right)^n\right]\right\}^m} \tag{2}$$

where θ_s is the saturated volumetric water content, e is the natural base of logarithms, ψ is the soil suction, a is the matric suction at the SWCC's inflection point and is closely related to the air-entry value of the soil, m is a fitting parameter related to residual water content, and, n is the slope of the soil-water characteristic curve at the inflection point.

One of the three main methods available to predict the unsaturated hydraulic conductivity function from a volumetric water content function is the one proposed by Fredlund(1976), whose governing equation is as follows:

$$k_w = k_s \frac{\sum_{i=j}^{N} \frac{\theta(e^y) - \theta(\psi)}{e^{yi}} \theta'(e^{yi})}{\sum_{i=1}^{N} \frac{\theta(e^y) - \theta_s}{e^{yi}} \theta'(e^{yi})} \tag{3}$$

where k_s is the measured saturated conductivity, θ is the volumetric water content, y is a dummy variable of integration representing the logarithm of negative pore-water pressure, j is the least negative pore-water pressure to be described by the final function, N is the maximum negative pore-water pressure to be described by the final function, ψ is the suction corresponding to the jth interval, and, θ' is the first derivative, and can be obtained through eq. (2).

AN ENGINEERING CASE HISTORY

Overview

The highway project concerning this paper is located in a semiarid zone of China. In 2004, after several rainfalls, a slope failure occurred in the K412+100 section. The slide mass was shallow, reaching a maximum depth of approximately 4.0m. There are three distinctive soil layers in situ. The main soil parameters are summarized in Table 1. The first layer consists of silty clay of Quaternary system, and the maximum depth is about 20m. The second layer consists of weathered sandstone, featuring an irregular profile and a maximum depth of 4.0m. The third layer consists of grayish, slightly weathered argillaceous sandstone of Triassic system.

Table 1. Soil parameters

Soil	Cohesion	Friction angle	Shear strength	Density (kN/m^3)	Remarks
Silty clay	34 kPa	20.5°		17.1	Plastic state
Weathered sandstone			170 kPa	16.8	Good permeability
Argillaceous sandstone			170 kPa	16.8	Slightly weathered

Numerical Modeling and Boundary Conditions

The model stratigraphy used for the numerical analysis is shown Figure1. Based on the measured grain-size distribution curve, the SWCC for the soil in the study area was determined using Fredlund's SWCC model in eq. (1) with the following parameters: $a = 100$, $n = 2$, and $m = 1$. The associated hydraulic conductivity functions were estimated using eq. (3), with a saturated hydraulic conductivity value for silty clay of 1.8×10^{-4} m/day.

Figure 2 shows the typical SWCC and hydraulic conductivity function used in the model shown in Figure 1. The weathered sandstone and the argillaceous sandstone are both assumed to remain saturated and, hence, the nonlinear portion of their respective SWCC functions is not used in the analysis.

Average saturated hydraulic conductivity values, 6.8×10^{-2} m/day and 2.0×10^{-5} m/day, were determined from field tests for weathered sandstone and argillaceous sandstone, respectively, and were used in the analysis.

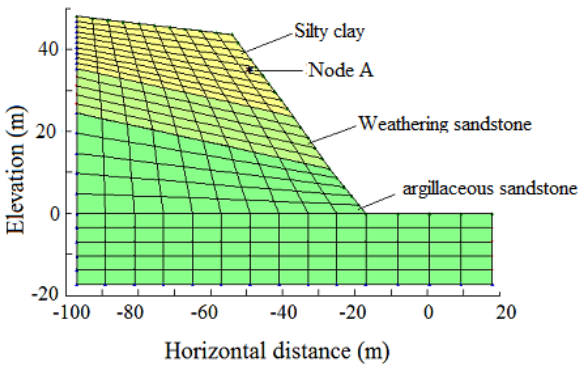

Figure 1. Model stratigraphy used for numerical analysis

The selected boundary conditions for the section shown in Figure 1 includes a *no-flow* boundary along the bottom of the spatial domain, indicating that flow through the cross section at the base was assumed to be horizontal. The left boundary for the slightly weathered sandstone is assigned a *no-flow* condition, because the lateral flow in the low permeability layers would be negligible compared with the flow resulting from the higher permeability of the weathered sandstone. A positive flux boundary condition is assigned to the weathered sandstone at the left boundary to act as a groundwater recharge. The right boundary of the domain incorporates a constant head value based on water table. An environmental flux boundary adjusted for potential seepage exiting on the ground surface is assigned to the slope face. This boundary condition includes a number of environmental factors that predominate at near-surface locations. The environmental flux boundary function includes both evapotranspiration during periods with no rainfall and infiltration during rainfall events. The flux function is determined from relevant rainfall and temperature data obtained from weather stations. Infiltration during rainfall events includes precipitation, evapotranspiration, and runoff based on the return period of the event. The infiltration was calculated based on the following relationship:

$$I = P - E - aP \tag{4}$$

where I is the infiltration, P is the precipitation, E is the evapotranspiration calculated using Meyer's (1944) approach, and, a is a runoff coefficient based on the return period T_R. Many factors affect the magnitude of evapo-transpiration E. In this paper, the equation proposed by Meyer (1944) was used, which is expressed as follows:

$$E = 0.0106(1 + 0.1u)(e_s - e_a)2.54 \tag{5}$$

where E is evaporation, u is the wind speed, e_s is the saturated water vapor pressure, and, e_a is the actual water vapor pressure.

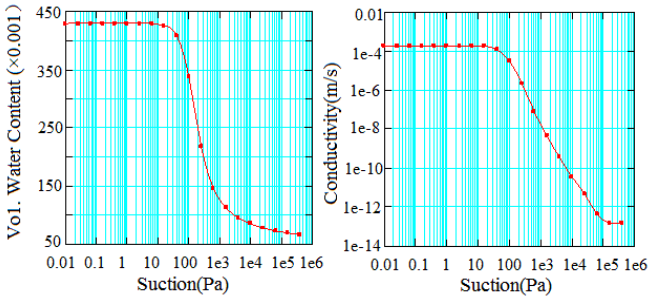

Figure 2. Soil-water characteristic curves and hydraulic conductivity functions for silty clay

The time interval used for the analysis is two months during the slope failure. Figure 3 shows the environmental flux boundary function that is used in the numerical model. Information about intensity, duration and frequency of rainfall can be obtained from these records. For the most part, the slope face was subjected to a negative flux or drying. There were several occasions, however, where rainfall events are large enough to create a positive flux that is, infiltration into the slope (Figure 3).

Results and Analysis

Figure 4 shows the change in soil suction with time for a variety of environmental flux boundary conditions for node A (Figure1) near the ground surface. It can be seen that one rainfall induces a loss in soils suction, although pore-water pressure still remains at a negative value. Soil suction decreases to virtually zero after four consecutive rainfall events. Suction continues to increase steadily afterwards, with only a slight decrease during the last rainfall event shown in the record. This indicates that soil suction is not only associated with rainfall intensity, but also with rainfall frequency and duration.

Figures 5 and 6 show the pore-water pressure contours throughout the slope right after the continuous-rainfall time interval (28 day) and at the end of the recording period (64 day), respectively. It is observed that the soil suction values in the slope after continuous rainfalls are negligible. At the end of the recording period, soil suction values in the upper layers reach a maximum value of 60 kPa.

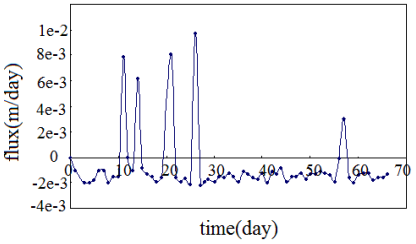

Figure 3. Environmental conditions

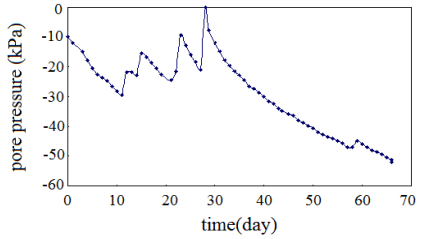

Figure 4. Variation of suction with time

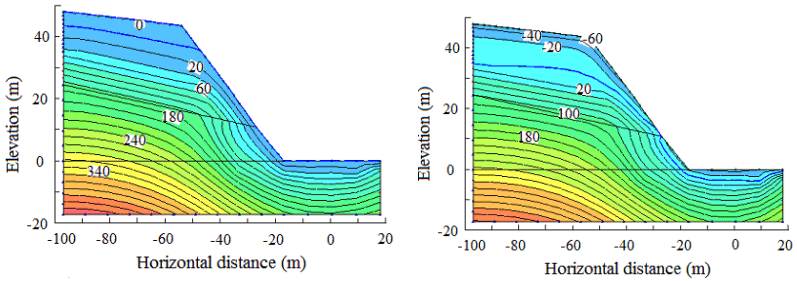

(a). 28 days **(b). 64 days**

Figure 5. Pore-water pressure distribution after 28 and 64 days

The modeled pore-water pressure distributions in Figure 5 were imported into a Limit Equilibrium slope stability application to examine the variation of the factor of safety during the entire period. Figure 6 shows these results in terms of change in factor of safety with time in days. Even though there were three rainfall events within the first 23 days recorded, the calculated factors of safety still remain significantly above 1.0. Right after the end of the continuous-rainfall time interval, i.e., at the 28th day, the soil suction in the slope virtually disappears and the factor of safety decreases to nearly 1.0. The factor of safety suggests that slope movements could have occurred.

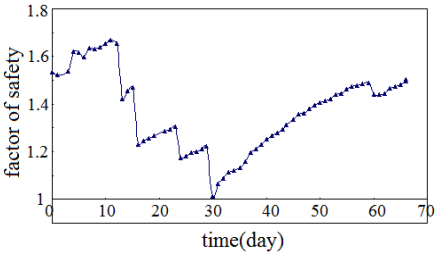

Figure 6. Variation of factor of safety with time

The analysis suggests that the stability of the unsaturated soil slope is closely related to changes in soil suction, with suction having a positive effect in maintaining the stability of the slope. Shallow failures of the slope are not likely to occur when the soil suction is relatively large. The effect of key environmental factors on the stability of the slope is mainly manifested through the influence they exert on the magnitude of soil suction throughout the slope profile.

CONCLUSIONS

Based on the unsaturated soil theory, this paper presents the analysis of a engineering case, and discusses the effect of the environmental conditions on stability of the unsaturated soil slope. The key observations can be summarized as follows:

Soil suction plays an important role to keep stability of the unsaturated soil slope. Infiltration of rainfall into a soil profile reduces the soil suction, thereby reducing factor of the safety in the slope.

Soil suction is dominated by the environmental conditions that can be appropriately modeled using known theories, and the environmental conditions include: rainfall intensity, duration, frequency of the rainfall, environmental temperature, and wind speed. Continuous rainfall can lead to continuous decrease of total tendency of soil suction.

For the engineering case analyzed in this paper, continuous rainfall is the key factor leading to slope failure. Based on the analytical results in this paper, an assumption can be obtained: if the rain interval is longer, or rainfall intensity is smaller, it is said if the process is long enough to recover soil suction, the slope failure could not happen.

In engineering practice, for the unsaturated soil slope, the monitor of soil suction must be strengthened to obtain the important data to help us to estimate whether the slope can keep stability or not.

REFERENCES

Frelund D.G. (2006). Unsaturated soil mechanics in engineering practice. Journal of Geotechnical and Geoenvironmental Engineering, 132(3), 286-321.

Frelund D.G. and Morgenstern N.R. (1976). Constitutive relations for volume change in unsaturated soils. Canadian Geotechnical Journal, 13, 261-276.

J. A.Blaz, N.J. Ferreira, J.G. (2004). Effects of near-surface environmental conditions on instability of an unsaturated soil slope. Canadian Geotechnical Journal, 41, 1111-1126.

J. Wu, C. Wang, and G. Li (2004). Influence of matric suction in unsaturated soils on slope stability. Rock and Soil Mechanics, 25(5), 732-736. (in Chinese).

L.L. Zhang, D.G.Fredlund, and L.M. Zhang (2004). Numerical study of soil conditions under which matric suction can be maintained.. Canadian Geotechnical Journal, 41,569-582.

Meyer A.F. Evaporation from lakes and reservoirs. Minnesota Resources Commission, St.Paul, Minn, 1944.

S. Chen, and S. Chen. (2001). Stability analysis of unsaturated soil slope considering rainfall infiltration. Rock and Soil Mechanics, 22(4),447-450. (in Chinese).

Failure Mechanism of Unsaturated Volcanic Slopes due to Rainfall and Freeze-thaw Actions

S. Kawamura[1], S. Miura[2], and T. Ishikawa[3]

[1] Assistant Professor, Graduate School of Engineering, Muroran Institute of Technology, 27-1, Mizumoto -cho, Muroran, 050-8585, Japan, e-mail: skawamur@mmm.muroran-it.ac.jp
[2] Professor, Graduate School of Engineering, Hokkaido University, Kita 13, Nishi 8, Sapporo, 060-8628, Japan, e-mail: s-miura@eng.hokudai.ac.jp
[3] Associate Professor, Ditto, e-mail: t-ishika@eng.hokudai.ac.jp

ABSTRACT: Collapse of volcanic slopes induced by rainfall has been frequently induced in Hokkaido, Japan, especially the middle southern area. It has been known that volcanic slopes in Hokkaido have a strong potential to cause such failure. The objective of this study is to reveal failure mechanism of volcanic slopes caused by both rainfall and freeze-thaw actions. A series of model tests was performed on volcanic slopes having several moisture contents. In particular, the effect of freeze-thaw actions on mechanical behavior at failure was investigated detailedly.

INTRODUCTION

Recently the earthquakes and heavy rainfalls in Hokkaido generated the most serious damage in the ground, the cut and embankment slopes, which composed of volcanic soils. For example, the slope failure of residential embankment due to the 1993 Kushiro-oki earthquake (JSSMFE 1994) and the failure of cut slope in the Hokkaido expressway in spring season, 1999 (Ito et al. 2008).

Figure 1 shows two types of failure mode for slope in cold region (Toya 1992). As shown in the figure, the surface slope failure is due to forming a frozen layer such as an impermeable layer in spring season and is due to softening of the slope by freeze-thaw actions in summer season. In previous studies (e.g. Kawamura et al. 2009), the effect of existence of frozen layer on failure mechanism of volcanic slopes was revealed on experimental approach. In this study, the effect of freeze-thaw actions on failure mechanism of volcanic slope during rainfall was elucidated in detail.

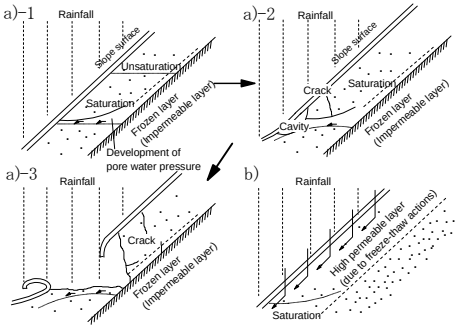

Figure 1. Failure modes in cold region: (a) in spring season, (b) in summer season

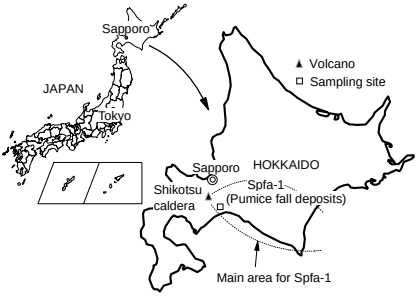

Figure 2. Location of sampling site

Table 1. Index properties of Kashiwabara volcanic soil

Sample name	ρ_s (g/cm^3)	$\rho_{d\ in\ situ}$ (g/cm^3)	$\rho_{d\ max}$ (g/cm^3)	$\rho_{d\ min}$ (g/cm^3)	D_{50} (mm)	U_c	F_c (%)
Kashiwabara	2.34	0.53	0.553	0.352	1.3	3.1	1.3
Toyoura sand	2.68	-	1.633	1.371	0.18	1.5	0

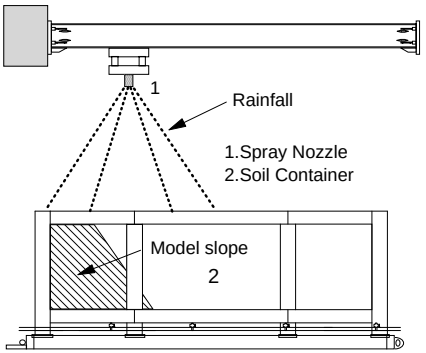

Figure 3. Cross sectional view of apparatus and measurement devices

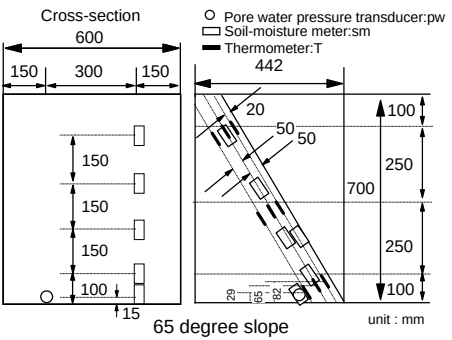

Figure 4. Model shape and the setting

TEST MATERIALS AND TEST PROCEDURES

Volcanic coarse-grained soil which was sampled from the ejecta of Shikotsu caldera in Hokkaido was used in this study. Sampling site is shown in Figure 2. This sample is hereafter referred to as Kashiwabara volcanic soil. The index property of sample is shown in Table 1, compared to that of Toyoura sand. As shown in Table 1, a finer content is less than 1.3%. A low value of dry density is also shown in the sample, because constituent particle is very porous and high crushable. The details of mechanical behavior of Kashiwabara volcanic soil have been also reported by Miura et al. (1996).

Figure 3 depicts the whole view of apparatus used in rainfall testing. The soil container was 2,000mm in length, 700mm in depth and 600mm in width, and its front wall was made of a reinforced glass to observe deformation with failure.

Model slopes were constructed by tamping the volcanic soil so as to be the desired density (ρ_d=0.48g/cm^3, and its variation in density is within 5%) of which constituent particle was not broken by tamping under initial water contents. The desired initial moisture content of model slope was w_0 =20, 40, 55, 60 and 70%. Thereafter, the slope surface was carefully cut to the angle of 65^o (relative to the horizontal) using a straight edge so as to free from disturbance of the surface. After the model slope was constructed, the surface of slope was made to freeze up by dry ice during 8 hours and was basically thawed in 20^{o}C (the period of thawing was 12 hours). According to this procedure, the frozen layer of thickness of 80 mm was formed in the model slope. The details of slope construction have been described by Kawamura et al. (2009).

Rainfall intensity was 100 mm/hr and was accurately simulated by using a spray-nozzle. The rainfall from the slope bottom was forcibly drained by a pump.

During the rainfall testing, the changes in deformation behavior, saturation degree and temperature were monitored using digital video cameras, soil moisture meters and thermocouple sensors, respectively. In particular, the deformation behavior was estimated according to the particle image velocimetry (PIV) analysis (White et al. 2003). Pore water pressure was similarly monitored, however its value was very small and its behavior at the slope failure was not sensitive as compared with the soil moisture behavior (e.g. Kawamura et al. 2007). Therefore, the behavior of deformation and saturation was illustrated in this study. Figure 4 shows typical slope shape and the setting positions of measurement devices.

For all model tests, the variation in initial saturation degree for each position was within around 5% because there was no difference in failure mechanism. A series of rainfall model tests was performed until 3 hours or slope failure. According to the preliminary test (Kawamura et al. 2007), since slope failure was rapidly developed after shear strain of 4-6% was induced at the peak of saturation degree, the mechanical behavior at shear strain of 4-6% was regarded as that at failure.

TEST RESULTS AND DISCUSSIONS

Figure 5 (a) and (b) show the changes in normalized saturation degree during rainfall test after freeze-thaw action, compared to that without freeze-thaw action. In the figures, the degree is normalized by its initial value Sr_0. In the figures, Sr_0 at sm6 indicated a high

value. This reason was that sm6 was set to 15mm from the bottom and its area became a high saturation due to the effect of seepage water. Each saturation degree is gradually increasing and is suddenly decreasing after failure (see black symbol). It is also noted that there is the difference of elapsed time until failure between both cases. For example, the elapsed time subjected to freeze-thaw action is 9 times faster than that without its action.

In order to more clarify the influence of freeze-thaw action on mechanical behavior of model slope, Figure 6 (a) and (b) illustrate the deformation behavior during freeze-thaw action and the change in density after freeze action. In the figures, the shear strain increases with freezing, and its vector becomes approximately perpendicular to the surface during freeze action, and changes downward during thaw action. The variation in density can be also confirmed, as shown in the photograph. For the reason, it can be said that mechanical behavior in the slope is remarkably affected by freeze-thaw action.

Similarly, the effect of the number of freeze-thaw cycles on deformation behaviour was investigated herein. Yamaki et al.(2009) reported that the number of freeze-thaw cycles is 6 times during winter season (from December 8, 2007 to April 1, 2008) in Sapporo Hokkaido, Japan, and indicated that the reduction ratio of shear modulus of the volcanic ground due to the increase of freeze-thaw cycle becomes a steady state at around 2 times of freeze-thaw action. In this study, therefore, 2 cycles of freeze-thaw action were adopted.

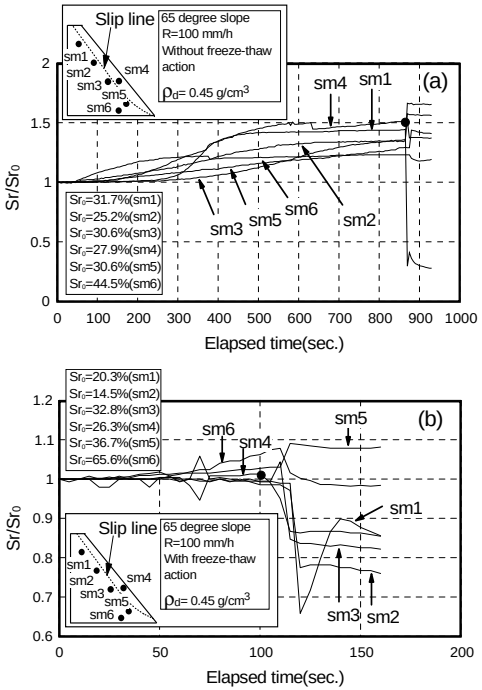

Figure 5. Changes in normalized saturation degree during rainfall test: (a) without freeze-thaw action, (b) with freeze-thaw action

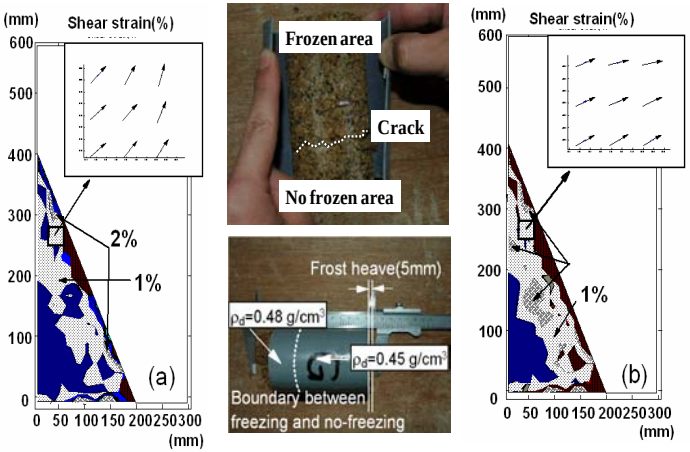

Figure 6. Changes in deformation behavior during freeze-thaw action: (a) during freeze action, (b) during thaw action

For the tests on the model slope subjected to 2 times of freeze-thaw action, the change in vertical strain $\Delta\varepsilon_{vi}$ during freeze actions becomes gradually smaller with the increase of freeze-thaw action, where *i* denotes the number of freeze-thaw cycles (see Figures 7). The schematic of the changes in vector in the slope during freeze-thaw sequence is also depicted in Figure 8. The similar tendency of which vertical strain decreases with the increase of freeze-thaw cycle has been indicated for results of element test on volcanic soil (Yamaki et al. 2009). These facts imply that the deformation changes from perpendicular to gravity direction during freezing and thawing and its effect is predominant at 1st cycle for the model test.

In order to obtain a better understanding, the comparison of the depths of slip line and of frozen layer is shown in Figure 9. It is found from this figure that these depths are almost the same for each case. Therefore, the surface slope failure may be predicted if the depth of frozen area in the slope can be estimated by monitoring in the field.

Figures 10 (a)-(d) show the changes in volumetric strain during freeze-thaw sequence, where contraction was expressed as a minus (-). In the figures, the dilatancy of around surface indicates the contractive tendency (-) for the initial stage of 1st cycle (see figure (a)), and changes from contraction to expansion during thaw action (see figures (b) and (c)). For 2nd cycle, the behavior is almost the same as that after thaw action of 1st cycle (see Figure (c) and (d)). From the results, it can be said that such volcanic slope subjected to freeze-thaw actions has already been the plastic equilibrium state. Therefore, if the change in dilatancy of slope is estimated, the influence of freeze-thaw actions on surface slope failure can be evaluated.

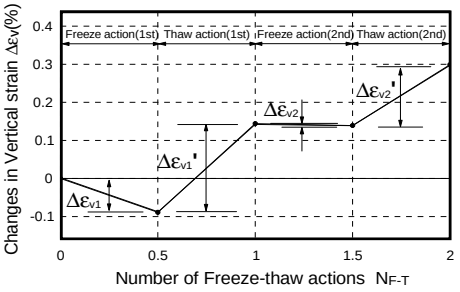

Figure 7. Change in vertical strain during freeze-thaw sequence

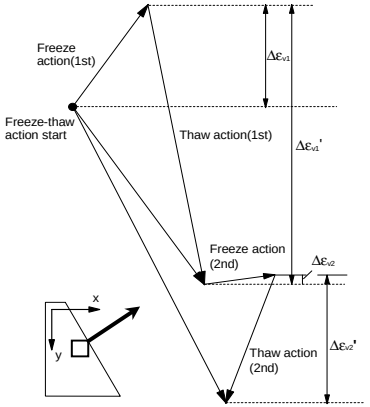

Figure 8. Schematic of the changes in vector in the slope after freeze-thaw actions

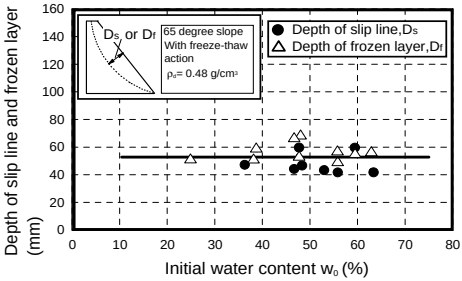

Figure 9. Comparison of the depths of slip line and frozen layer

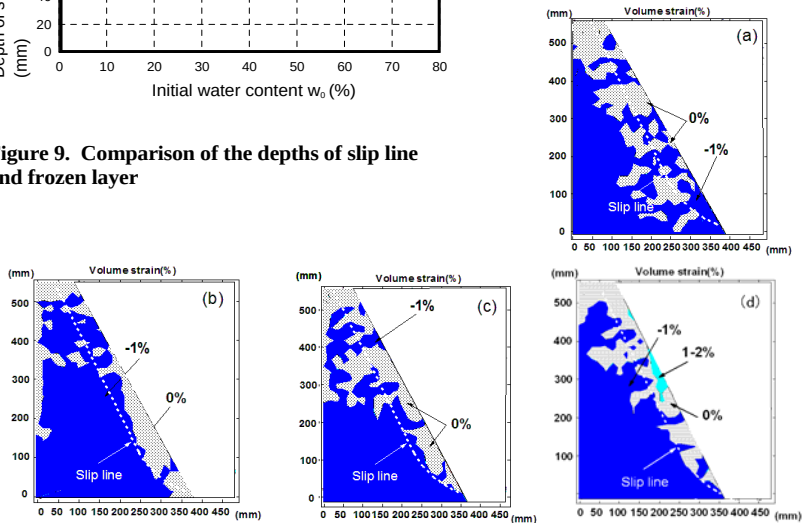

Figure 10. Changes in volumetric strain: (a) after 2hours (1st cycle), (b) after freezing (1st cycle), (c) after thawing (1st cycle), (d) after thawing (2nd cycle)

CONCLUSIONS

On the basis of the consideration on the limited number of model testing, the following conclusions were derived.

1. The increase of saturation degree is one of the causes of surface failure on volcanic slope.
2. The softening of the slope by freeze-thaw action is important for evaluating the stability of volcanic slope; in particular, its effect on mechanical behavior becomes lower with the increase of cycles of freeze-thaw action.
3. Volcanic slope subjected to freeze-thaw actions has already been the plastic equilibrium state. Therefore, if the change in dilatancy of slope is estimated, the influence of freeze-thaw actions on surface slope failure can be evaluated.

REFERENCES

Ito, Y., Shimura, K. and Watanabe, T. (2008) Recent landslide disaster in Hokkaido. Proceedings of 30th memorial symposium, Hokkaido branch, The Japan Landslide Society, Hokkaido: 37-56. (In Japanese).

JSSMFE (1994) The disaster report of the 1993 Kushiro-oki Earthquake and Notohanto-oki Earthquake. The 1993 Earthquake Disaster Committee. (In Japanese).

Kawamura, S., Kohata, K. and Ino, H. (2007) Rainfall-induced slope failure of volcanic coarse-grained soil in Hokkaido. Proceedings of 13th Asian regional conference on Soil Mechanics and Geotechnical Engineering, ISSMGE, Kolkata: 931- 934.

Kawamura, S., Miura, S., Ishikawa, T., and Ino, H. (2009) Failure mechanism of volcanic slope due to rainfall and freeze-thaw action. Proceedings of International Symposium on Prediction and Simulation Methods for Geohazard Mitigation. IS-Kyoto 2009, Kyoto: 25-31.

Miura, S., Yagi, K and Kawamura, S. (1996) Static and cyclic shear behavior and particle crushing of volcanic coarse grained soils in Hokkaido. Journal of Geotechnical Engineering, JSCE, III-36(547): 159-170. (In Japanese).

Toya, K. (1992): “The soil protection for volcanic soil in Doo high way road (between Noboribetsu and Shiraoi).” Proceedings of panel discussion on volcanic soils, Hokkaido branch, JSSMFE, Hokkaido: 89-98. (In Japanese)

White, D. G., Take, W. A. and Bolton, M. D. (2003) Soil deformation measurement using particle image velocimetry (PIV) and photogrammetry. Geotechnique, 53(7), 619-631.

Yamaki, M., Miura, S. and Yokohama, S. (2009) Effect of freeze-thaw sequence on deformation properties of crushable volcanic soil. Journal of Geotechnical Engineering, JSCE, III-65(1): 321-333. (In Japanese).

Centrifuge Model Tests of Slopes with Weak Layer under Rainfall

R. Wang[1], G. Zhang[2], and J.M. Zhang[3]

[1] Graduate Student, State Key Laboratory of Hydroscience and Engineering, Tsinghua University, China
[2] Associate Professor, State Key Laboratory of Hydroscience and Engineering, Tsinghua University, China
[3] Professor, State Key Laboratory of Hydroscience and Engineering, Tsinghua University, China

ABSTRACT: Failures of soil slopes are often triggered by rainfall, and weak layers tend to accelerate the failure process significantly. Centrifuge model tests were conducted to investigate the behavior of cohesive soil slopes with weak layer under rainfall conditions. Deformation process and change in soil suction were observed and recorded during the tests. Comparison between soil suction and strain showed that the rainfall infiltration, the decrease of suction and the increase of strain correspond in time. The analysis of displacement showed that dislocation zones appeared in the slopes during the rain precipitation process. The rainfall induced a discontinuous dislocation zone in the slope with a weak layer, and a continuous one in the homogeneous slope.

INTRODUCTION

Rainfall is reported to be a major cause of soil slope failures which claims the lives of thousands around the world (Moriwaki et al. 2004). Thus, many studies have been dedicated to this subject (e.g. Tohari et al. 2007; Rahardjo et al. 2007).

Previous studies showed that rainfall can reduce the stability level of slopes significantly (Xiao et al. 2007). Field studies in Hongkong indicated that the rainfall infiltration leads to the decrease in soil suction and a drop in soil strength (Li et al. 2003). Laboratory model test results showed that the slope profile, initial moisture content and soil infiltration rate are all highly influential to the failure modes (Tohari et al. 2007).

Most investigations were conducted on homogeneous slopes under rainfall conditions; few have touched upon heterogeneous slopes. It is widely accepted that most slopes have heterogeneous properties, and the weak layers within slopes have a significant impact on their stability during rainfall (e.g. Al-Homoud et al. 1997).

This paper describes two sets of centrifuge model tests of rainfall on

heterogeneous and homogeneous slopes. Deformation process and change in soil suction were observed and measured during the tests. Based on the test results, this paper looks into the characteristics of a slope with weak layer under rainfall condition.

TEST APPARATUSES

The tests were conducted using the geotechnical centrifuge of Tsinghua University (TH-50gt).The model tank used in the tests possesses a maximum inner dimension of 495×200×500mm. The frame and base of the tank are made of aluminum alloy. Trapezium shaped lucite plate was installed on both lateral sides of the tank. A rainfall generator, developed by Tsinghua University, was employed to simulate uniform rainfall in the tests. The UMS T5 tensionmeter with an accuracy of $\pm$0.5kPa was used to monitor the soil suction. Due to its small dimensions, it is highly suitable for centrifuge tests which requires minimal disturbance of the soil. The "GIAS-c" (GeoImage Analysis System for centrifuge) was used to measure the displacement of model slopes with an accuracy of sub-pixel (Zhang et al. 2009).

TEST DETAILS

The cohesive soil used for the slopes was acquired from Nongzhanguan subway station in Beijing, China. The soil has a specific gravity of 2.71. The effective particle size (D_{10}) and uniformity coefficient (D_{60}/D_{10}) of the soil are 0.003 mm and 16.7.

Montmorillonite powder was mixed with filter paper shreds to simulate the material that forms weak layers. Montmorillonite exhibits significant softening due to saturation, while filter paper shreds offer the high permeability desired for the weak layer.

Two types of slopes, homogeneous and heterogeneous, were used in the tests. The heterogeneous slope included a highly permeable water softening layer.

The soil moisture and dry density of the homogeneous slope were 15.1% and 1.50 g/cm^3. The moisture of soil and weak layer of the heterogeneous slope were 18.2% and 45.2%; the dry density of soil and weak layer were 1.48 g/cm^3 and 1.10 g/cm^3.

Figure.1 shows the profile of the slope and a rectangular coordinate system for the convenience of analysis. The model slope was constructed by placing horizontal layers of soil across the whole tank; the soil was then compacted to reach the designed dry density.

T5 tensiometers were buried in the slope to monitor and record the fluctuation in soil suction (Figure.1), and the sensors were numbered as S1, S2 and S3, respectively.

After the installation of the model on the centrifuge machine, the centrifugal acceleration was gradually increased to 50g-level. Once the deformation of the slope stabilized at 50g-level, the rainfall simulator was started. The rainfall intensity in the tests was around 1mm/min, and persisted till failure.

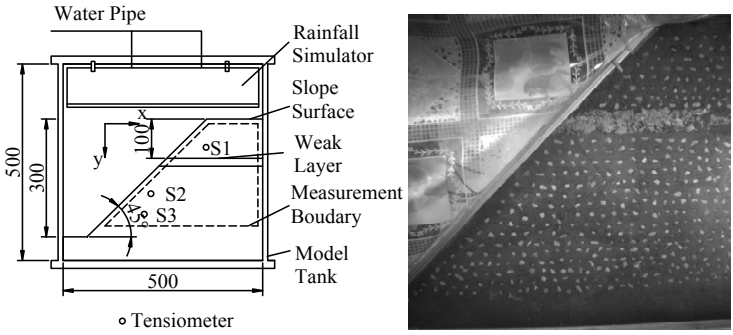

Figure 1. Diagram and photo of test models

FAILURE PRECESS OF SLOPES

For the homogeneous slope, hardly any displacement can be observed in the slope before rainfall reached 7 mm. From 7 mm rainfall onward, the horizontal displacement towards the toe of the slope began to accumulate, reaching 3-4 mm at the surface of the slope. The displacement increased as rainfall infiltrates. After 16mm rainfall, a 40 mm deep tension crack appeared on the surface of the slope. Upon the appearance of the crack, soil below the crack slid towards the toe of the slope rapidly, signaling failure of the slope. The slope failed through a shallow non-circular slide, with the slip surface starting at the crack and ending at the toe of the slope (Figure.2).

For the slope with a weak layer, the deformation and failure process displays distinct characteristics from the homogeneous slope. Before 6 mm rainfall, displacement was rather small apart from the weak layer. From 6 mm to 15 mm rainfall, soil displacement became significant and was observed in a larger area deeper into the surface. During this stage, evident surface erosion can be seen; a crack also appeared on the top of the slope. After 15 mm rainfall, the slope failed through a shallow non-circular slide, with the slip surface starting at the crack and ending at the weak layer (Figure.2).

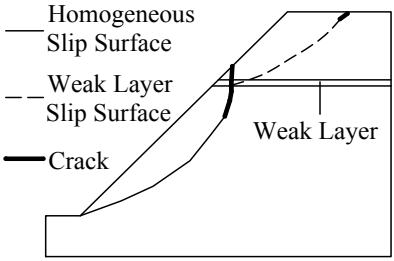

Figure 2. Failure mode of test slopes

SOIL SUCTION CHANGE IN COMPARISON WITH DEFORMATION

For both slopes, the recorded soil suction exhibits similar characteristics, which goes through a rapid decreasing process, but differ in time. Figure.3 shows the soil suction of S2 point in both slopes. For the slope with a weak layer, soil suction stays stable around 15 kPa before 10 mm rainfall and swiftly drops to 4 kPa after 10 mm rainfall. Suction steadies at 3 kPa after 17 mm rainfall. Whereas, the drop in suction occurs later for the homogeneous slope, which starts to drop after 13 mm rainfall and stables at 7 kPa after 25 mm rainfall. It can be concluded that the weak layer causes rainfall to infiltrate rapidly into the slope, thus the inflexion on the suction curve occurs earlier.

In both tests, the recorded soil suction experiences a stable-decrease-stable process. Since soil suction and moisture content are negatively correlated, the decrease in suction corresponds to the increase in moisture content at the test points, meaning that the rainfall has reached these points. The rise in moisture content decreases the modulus of the soil, which in turn leads to greater deformation. To further clarify the relationship between the change in soil suction and the deformation process, the horizontal strain at the points where the sensors are placed were analyzed.

Horizontal strain of a square element with side length of 1 cm is obtained according to the finite element method according to the measured displacement. The horizontal strain of S2 point in the slope with a weak layer is analyzed and compared with the suction-rainfall curve (Figure.4). It can be seen that the horizontal strain increases drastically after 9 mm rainfall. This coincides with the inflexion on the suction-rainfall curve, indicating that deformation at one point in the slope caused by rainfall is closely related with the change in soil suction at the point.

Thus, it is not difficult to conclude that when rainfall infiltrates to a point in the slope, as the soil suction of the point decreases, the strain increases significantly. Suggesting infiltration of rainfall, decrease of suction, and increase of strain correspond in time. Using this relationship of these three factors, the moment that rainfall reaches any point in the slope can be deduced from the inflexion of the point's strain-rainfall curve. This means that the infiltration field of the slope under rainfall can be determined via the strain field of the slope, which is obtained through analysis of the displacement field.

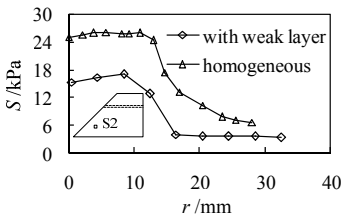

Figure 3. Soil suction change measured in the tests (*r*, rainfall; *S*, suction)

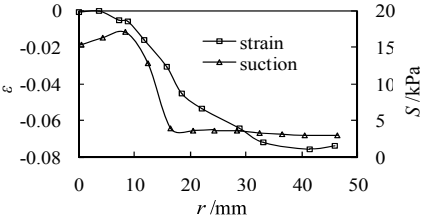

Figure 4. Strain-rainfall curve and suction-rainfall curve at S2. (ε, strain)

DEFORMATION CHARACTERISTICS OF SLOPES WITH WEAK LAYER

The displacement distribution in the slopes is looked into to further clarify the characteristics and patterns of the deformation process of slopes with a weak layer,. This analysis is only conducted on stages between 7-16 mm and 6-15 mm rainfall in homogeneous and heterogeneous slopes, to represent the deformation process.

In the slope with a weak layer, the horizontal displacement of the slope on horizontal lines at 10 mm intervals from the top to the bottom is analyzed. Figure.5 shows the displacement distribution on five different altitudes, three lines are above the weak layer, two are under the layer. It should be noted that the third is on the top edge of the weak layer (y=158 mm) and the fourth is on the bottom edge (y=189 mm). It is easy to see that each horizontal displacement distribution curve consists of a section of high gradient. Through connecting these inflexions of the curves on different altitudes (dashed lines in Figure.5), a zone can be outlined to have a high displacement gradient (Figure.6), indicating that the soil within this zone experienced significant deformation. Thus, this zone is defined as the dislocation zone; the boundary of this zone is defined as W (near surface) and N (inner boundary), respectively. It is easy to see that the dislocation zone becomes discontinuous at the weak layer. The dislocation zone below the weak layer develops deeper into the slope than the zone above the weak layer.

The same analysis is conducted on the homogeneous slope. The dislocation zone of the homogeneous slope runs through the slope from top to toe continuously, which is significantly different from that of the heterogeneous slope (Figure.5). These analyses indicate that the discontinuous characteristic of the dislocation zone in the slope with weak layer is caused by the existence of the weak layer. Due to its high permeability and significant softening at saturation, rain infiltrates deeper into the slope at the weak layer and causes more deformation, which leads to the dislocation zone below the layer to reach deeper into the slope.

CONCLUSIONS

Two sets of centrifuge model tests were conducted to investigate the behavior of cohesive soil slopes with weak layers under rainfall condition, including one homogeneous slope test and one with a weak layer.

Observation of the failure process showed that the slope with a weak layer experienced a shallow non-circular slide with the slip surface ending at the weak layer, while the slip surface of the homogeneous slope reached the toe of the slope.

The recorded soil suction decreased rapidly during rainfall. The infiltration field of the slope under rainfall can be determined via the strain field of the slope.

Analysis on the displacement distribution of the slopes showed that the slope with a weak layer exhibited discontinuous dislocation zones, while the homogeneous slope yielded a continuous dislocation zone.

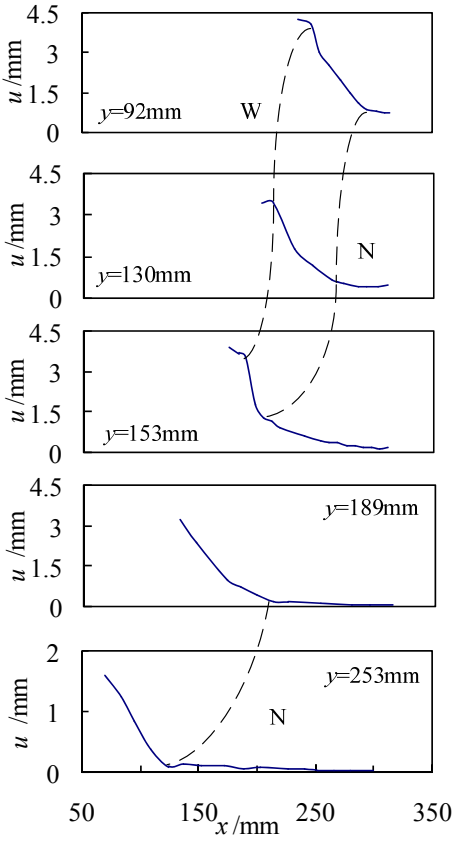

Figure 5. Horizontal displacement distribution in the slope with a weak layer

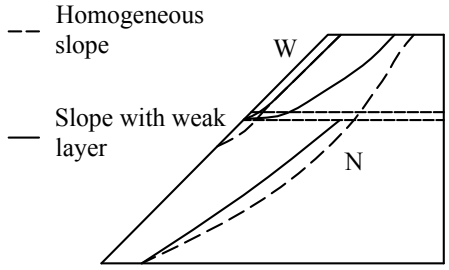

Figure 6. Dislocation zones in the two tests

ACKNOWLEDGMENTS

The study is supported by National Basic Research Program of China (973 Program) (2007CB714108) and National Natural Science Foundation of China (50823005).

REFERENCES

Al-Homoud, A.S. and Tubeileh, T.K. (1998). Analysis and remedies of landslides of cut slopes due to the presence of weak cohesive layers within stronger formations. Environmental Geology, 33(4), 299-311.

Li, A.G, Yue, Z.Q., Tham, L.G. and Lee, C.F. (2003). Soil moisture and suction measurement and its effect on slope stability. Chinese Journal of Geotechnical Engineering,25 (03), 278-281. (in Chinese).

Qian, J., Zhang, G., Zhang, J.M. and Lee, C.F. (2009). Rainfall centrifuge model tests of cohesive soil slopes. Journal of Tsinghua University (Science and Technology), 49(6), 813-817. (in Chinese).

Rahardjo, H., Ong, T. H., Rezaur, R. B. and Leong, E. C. (2007). Factors controlling instability of homogeneous soil slopes under rainfall. Journal of Geotechnical and Geoenvironmental Engineering,133(12),1532-1543.

Okura, Y., Kitahara, H., Ochiai, H., Sammori, T. and Kawanami, A. (2002). Landslide fluidization process by flume experiments. Engineering Geology, 66(1-2), 65-78.

Tohari, A., Nishigaki M., and Komatsu, M. (2007). Laboratory rainfall-induced slope failure with moisture content measurement. Journal of Geotechnical and Geoenvironmental Engineering, 133(5),575-587.

Xiao, H, Wang, J. and Shan, X. (2007). Comprehensive evaluation of slope stability under rain infiltrating. Resources and Industries, 9(04),117-120. (in Chinese).

Zhang, G., Hu, Y. and Zhang, J.M. (2009). New image analysis-based displacement measurement system for geotechnical centrifuge modeling tests. Measurement, 42(1), 87-96.

Development of Shrinkage Model for Clays Based on Moisture Variation

A. Sabnis[1], I. Abdallah[2], S. Nazarian[3], and A. Puppala[4]

[1] Graduate Engineer, Fugro Consultants Inc., 8613 Cross Park Dr., Austin, TX 78754; e-mail: asabnis@fugro.com
[2] Associate Director, Center for Transportation Infrastructure Systems, UTEP, e: mail: emadn@utep.edu
[3] Director, Center for Transportation Infrastructure Systems, UTEP, e-mail: nazarian@utep.edu
[4] Professor, University of Texas at Arlington, Texas 76019, e-mail: anand@uta.edu

ABSTRACT: The low-volume road pavement systems on high plasticity index (high PI) clay subgrades are perceived to fail prematurely by some highway agencies. The most common distress, at least in Texas, is longitudinal shrinkage cracking. Several models have been developed to estimate the shrinkage characteristics of various types of clays from their index properties. The process of estimating the shrinkage strain, modulus and tensile strength from index properties of clays is presented in this paper. The estimation of these parameters from their index properties can be reasonably carried out.

INTRODUCTION

A survey of pavement engineers in Texas by Wanyan et al. (2008) indicated that low volume road flexible pavements constructed on high plasticity index (high PI) clay subgrades fail prematurely primarily because of the highly variable properties of these clays due to moisture fluctuation throughout the year. At least in Texas, the most prevalent cause of this premature failure is reported as longitudinal cracking. Unfortunately, most current pavement design procedures do not account for this mode of failure. It is therefore, important to improve the design and laboratory procedures to evaluate clayey subgrades and then design pavements accordingly to extend the life expectancies of these roads. A part of the study focused on modifying laboratory tests and evaluating stiffness and deformation properties of high PI clays as a function of moisture content as discussed below.

In the summer months, the subgrade dries out with time. Such loss of moisture results in significant increase in the strength and stiffness (modulus) of the clay, which

has a positive impact on the load carrying capacity of pavements. However, the increase in stiffness results in the increase in the brittleness of the clays. The loss of moisture also contributes to the shrinkage of these clays. This tendency to shrink, along with the increase in the brittleness, causes longitudinal cracks that will propagate to the surface of the road (Uzan et al. 1972). These cracks, sometimes an in. or more wide, act as conduit for water to penetrate more rapidly in the subgrade, causing a vicious circle of continuous damage to pavements. To practically implement Uzan's approach, the variations in shrinkage strain, modulus and tensile strength of clays with moisture content are needed.

Based on this discussion, the focus of this paper is to investigate the changes in the behavior of high-PI clays with change in moisture content. Six clays were selected from six districts in Texas. Specimens from these six clays were prepared at their respective optimum moisture contents and subjected to drying. Changes in the modulus and shrinkage strains of these specimens were monitored daily until constant moisture contents were achieved (up to a month). Since for most actual projects, this testing time is perceived as excessive, models based on the laboratory data were developed to estimate the shrinkage strains, modulus and tensile strength as a function of moisture content and index properties of clays. In this paper, the results and process for the shrinkage strains are extensively discussed. Due to space limitations, the models for modulus and tensile strength are introduced without detail. The detail related to these models can be found in Sabnis et al. (2008).

LABORATORY TESTING

The classification, Atterberg limits, optimum moisture content (OMC) and the maximum dry unit weight (DUW) of each clay are summarized in Table 1. Four subgrades are classified as high-PI and two as low-PI clays. The current Texas and a number of other highway agencies practice consists of compacting clayey specimens nominally to a diameter of 4 in. and a height of 6 in. in four lifts using a kneading compactor. Several problems were observed with this process. The specimens sometimes separate at the interface of the layers during the drying phase. It was not uncommon that the specimens failed at the interface of the lifts during strength tests. The most suitable method was a modification of the static compaction based on the AASHTO T-307 for preparing the fine-grained soil specimens.

The drying of the specimen was carried out using a conventional oven at 104^{O}F. The specimen was removed from the oven every 24 hrs, was weighed, its length and diameter were measured, and its modulus was with the free-free resonant column device (Nazarian et al. 2003). The procedure was repeated until the decrease in weight in two consecutive days was about 0.1%.

Figure 1 shows typical results from drying a specimen. Typical variations in moisture content and seismic modulus (referred to simply as modulus hereafter) with time for one specimen are shown in Figure 1a. The variations in the vertical, lateral and volumetric shrinkage strains with time measured on the same specimen are shown in Figure 1b. The dimensions, modulus and moisture content become typically reasonably constant after 10 to 15 days.

Table 1 –Classification and index properties of subgrades

Clay	Gradation, %				Classification		Atterberg Limits			OMC, %	DUW, pcf
	Gravel	Sand	Silt	Clay	USCS	AASHTO	LL	PL	PI		
1	0	37	42	21	CL	A-6	30	14	17	16.5	112
2	0	12	43	44	CH	A-7-6	58	22	26	21.0	92
3	0	11	37	52	CH	A-7-5	61	32	29	24.0	91
4	0	13	40	47	CL	A-7-6	45	14	31	19.5	98
5	0	10	42	45	CH	A-7-6	54	21	35	20.0	99
6	0	9	45	46	CH	A-7-6	60	24	36	23.0	92

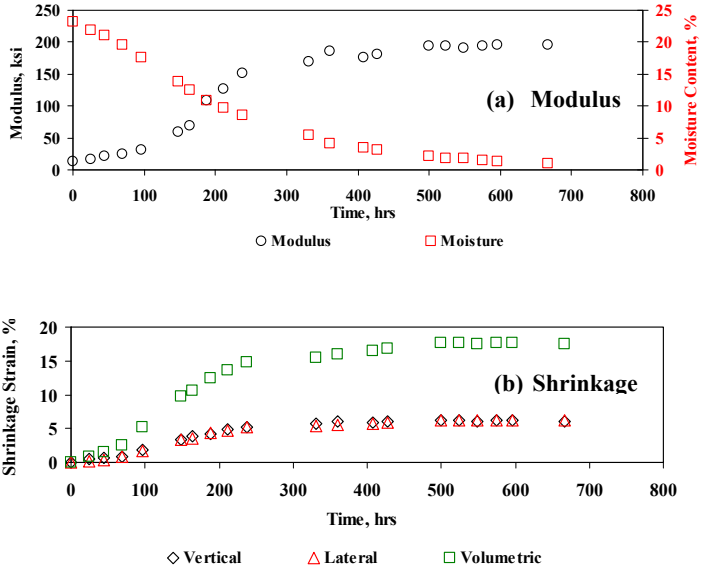

Figure 1. Typical changes in clay properties with time

The final moduli were 6 to 15 times the corresponding initial moduli for the high-PI clays, and about 30 times for the low-PI clays. The high-PI clays shrank drastically more than the low PI clays. The maximum horizontal and vertical shrinkage strains were 5 to 6% for the high PI clays and just 1 to 2% for the low PI clays.

MODEL DEVELOPMENT

To develop generalized models, the moisture contents were first normalized. The normalized moisture content (NMC) is defined as:

$$NMC = \frac{Individual\ Moisture\ Content}{OMC} \tag{1}$$

The relationships between the shrinkage strain, ε_s, and normalized moisture content, NMC, show a distinct trend as presented in Figure 2. Shrinkage strains increase rapidly until NMC is decreased to 0.4 after which, they are almost constant. Based on extensive curve fitting analysis, the following relationship was selected:

$$\varepsilon_s = [A(1 - NMC)^2]^n \tag{2}$$

where A is the parameter constant obtained from curve fitting. The value for n turned out to be close to unity for the vertical and lateral shrinkage. Figure 2 also shows that the best fit curves obtained using Eq. 2 follow the measured data quite well with R^2 values close to 1.

The parameters A obtained for all clays were then correlated to readily available index properties of the clays. A linear best fit curve was developed between each Parameter A and a given index property. The slope, intercept and R^2 for each set of parameters are shown in Table 2. The OMC and PI are generally correlated more favorably with Parameter A.

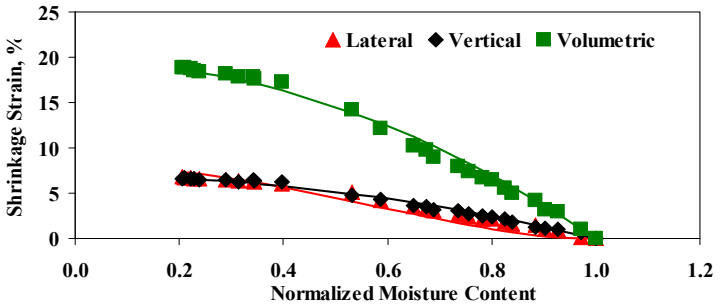

Figure 2. Variations in shrinkage strains with normalized moisture content

Since all four index parameters are commonly known, the following model is proposed to combine the information from all or any of these index parameters:

$$A^* = \frac{(A_{PI} \times W_{A\text{-}PI} + A_{LL} \times W_{A\text{-}LL} + A_{OMC} \times W_{A\text{-}OMC} + A_{DUW} \times W_{A\text{-}DUW})}{(W_{A\text{-}PI} + W_{A\text{-}LL} + W_{A\text{-}OMC} + W_{A\text{-}DUW})} \tag{3}$$

where A_i is A obtained from one of the four selected index parameters (i.e. PI, LL, OMC or DUW) and W_i is the weighting factor for index parameter i. The weight factors in Eq. 3, are calculated using

$$W_i = \frac{G_i}{\sum G_i} \tag{4}$$

where G_i, as reported in Table 2, is simply the product of R^2 value and a weighting multiplication factor, F. Parameter F of 4, 2 and 1 are proposed, if the R^2 value is greater than 0.8, between 0.6 and 0.8 and less than 0.6, respectively. This global A* can then be used in Eq. 2 to calculate shrinkage strains. If one or more of the index properties are not available, their corresponding term in Eq. 3 can be simply omitted. Sabnis et al. (2008) validated this model using a clay material not used in the development of the model. The model predictions were within 10% of the experimental results.

Figure 3 shows a typical relationship between normalized modulus, (E_n, modulus at a given moisture content divided by modulus at OMC), and NMC. A relationship in the following form was selected to predict modulus:

$$E_n = e^{(B-C\times NMC^2)} \tag{5}$$

where B and C are the parameters obtained from curve fitting. Eq. 5 describes the data quite well. Correlation studies between subgrade index properties and B and C are reported by Sabnis et al. (2008).

The indirect tensile strength (IDTS) tests were performed at six different moisture contents, from optimum to dry conditions, on each clay. The variations in the IDT strengths and normalized moisture contents for all clays except one, as shown in Figure 4, follow a unique trend with approximately 25 psi peak strength under dry condition which decreases smoothly to approximately 5 psi at OMC. To build in conservatism in the model, the results from the outlier material were excluded from curve-fitting process. The mathematical relationship to estimate subgrade tensile strength is in the form of:

$$\sigma_t = 35.7e^{-2.779\times NMC} \quad (R^2=0.89) \tag{6}$$

SUMMARY CONCLUSION AND RECOMMENDATION

In this paper, models that can be used to predict shrinkage strains and modulus at different moisture levels based on index properties of the clay materials are presented. The laboratory testing, relationship between shrinkage strains and moisture content, and finally connecting those relationships to the index properties of soil were discussed. These models, especially the lateral shrinkage strain model, can be used in pavement analysis tool to identify the thresholds of moisture change levels that initialize and propagate subgrade cracking.

Table 2. Relationships between parameter A and index properties of subgrades

Index Property	Mode	Parameter – A				
		Intercept	Slope	R^2	F	G
Plasticity Index (PI)	Vertical	0.25	-2.46	0.82	4	3.29
	Lateral	0.06	0.55	0.92	4	3.70
	Volumetric	0.58	-3.16	0.85	4	3.41
Liquid Limit (LL)	Vertical	0.13	-2.24	0.79	2	1.59
	Lateral	0.03	0.65	0.85	4	3.42
	Volumetric	0.30	-2.45	0.83	4	3.31
Optimum Moisture Content (OMC)	Vertical	0.48	-5.43	0.84	4	3.35
	Lateral	0.14	-0.58	0.87	4	3.49
	Volumetric	1.12	-9.96	0.89	4	3.58
Maximum Dry Unit Weight (DUW)	Vertical	-0.15	19.45	0.57	1	0.57
	Lateral	-0.04	6.32	0.68	2	1.36
	Volumetric	-0.35	48.25	0.62	2	1.23

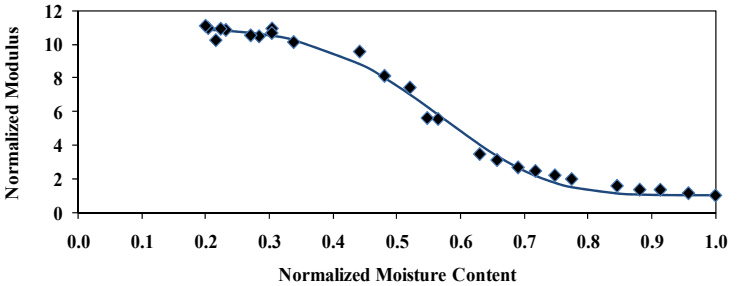

Figure 3. Normalized modulus variations with normalized moisture content

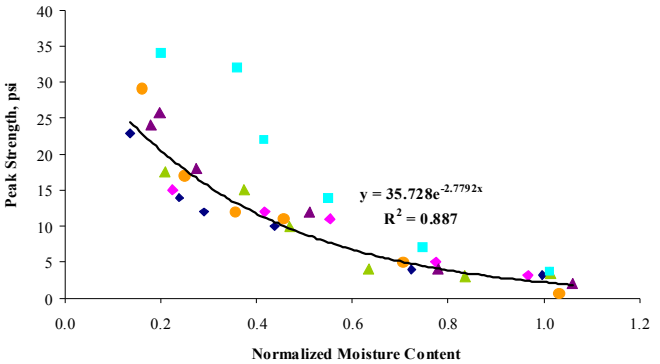

Figure 4. Tensile strengths of clays at different normalized moisture content

ACKNOWLEDGEMENT

The authors would like to thank the Texas Department of Transportation for sponsoring this project and especially the districts that contributed and assisted in this study.

REFERENCES

Nazarian, S., and Yuan, D. (2003). Comprehensive Mechanistic-based Quality Control of Flexible Pavements with NDT Methods. Non-Destructive Testing in Civil Engineering, Center for Highway Materials Research, The University of Texas at El Paso.

Sabnis, A., Abdallah, I., Pacheco, L. Nazarian, S., and Puppala, A., (2008). Impact of Moisture Variation on Strength and Deformation of Clays, Research Report No. 0-5430-01, Center for Transportation Infrastructure Systems, The University of Texas at El Paso, El Paso, Texas.

Uzan J., Livneh, M. and Shklarsky, E., (1972). Cracking Mechanism of Flexible Pavements, Transportation Engineering Journal, Proceedings of the American Society of Civil Engineers, February, pp. 17-36

Wanyan, Y., Manosuthkij, T., Abdallah, I., Nazarian, S., and Puppala, A., (2008). Expert System Design Guide for Lower Classification Roads over High PI Clays, Research Report No. 0-5430-02, Center for Transportation Infrastructure Systems, The University of Texas at El Paso, El Paso, Texas.

Slope Stability Analysis of Railway Embankments Considering the Effects of Vegetation and Capillarity

R. Katzenbach[1], and A. Werner[2]

[1] Director of the Institute of Geotechnics, Technische Universität Darmstadt, Petersenstrasse 13, 64287, Darmstadt, Germany, e-mail: katzenbach@geotechnik.tu-darmstadt.de
[2] Research assistant, Institute of Geotechnics, Technische Universität Darmstadt, Petersenstrasse 13, 64287 Darmstadt, Germany, e-,mail: werner@geotechnik.tu-darmstadt.de

ABSTRACT: It is well known that vegetation influences slope stability in following ways: (1) By mechanical reinforcement from the plant roots; (2) by increasing in soil suction or reduction of pore water pressure; (3) by surcharge from the weight of trees; and (4) by "wind throwing." The main beneficial effect includes root reinforcement. Roots increase the shear strength of soil primarily by transferring shear stresses that develop in the soil matrix into tensile resistance in the roots via interface friction along the imbedded roots.

INTRODUCTION

Results of stability analysis carried out on historical railway embankments of sandy soil with steep slopes demonstrate that the application of conventional calculation methods theoretically yields instability of the embankments (Katzenbach and Werner 2005). The computed factors of safety range between 0.9 and 1.1.

By the use of the concept of Experimental Statics it is however possible, to verify the true stability of the embankment, i.e. considering the effect of vegetation.

To analyze the contributions of vegetation, one needs to think of its mechanical, hydrological and biological role (Coppin and Richards 1990, Gray and Sotir 1996). The mechanical contributions arise from the interactions of the roots system of the plant with the slope (= root reinforcement). The hydrological mechanisms are those processes of water use and movement in the slope when living plants exists in the soil for growth. The vegetation contributes to slope stability by soil moisture depletion from interception and transpiration, too.

This paper presents results of experimental studies focused on the quantitative determination of the root tensile strength and the increase in soil shear strength due to

root systems. In the research we focus on soil materials consisting of fine-grained material. In order to quantify the contribution of roots to soil mechanical properties, direct shear test on undisturbed samples of rootless soil and soil with roots, respectively, were carried out. Furthermore this paper presents some measurements of matric suction at a historical railway embankment.

EXPERIMENTAL INVESTIGATION OF THE ROOT-SOLI-INTERACTION

Roots embedded in soil form a composite material consisting of fibers of relatively high tensile strength. This is analogous to the reinforced soil system, where a soil is stabilized by the inclusion of metallic, synthetic or natural materials. The shear strength of the rooted soil mass is enhanced due to the presence of a root matrix. The mechanical effect of the roots is to enhance the stress and resistance to sliding and increase the strength of the soil/root mass through the binding action of roots in the fiber/soil composite; the soil friction angle remains unchanged, as shown in Figure 1. Failure occurs either by pull-out that is slipping due to bond failure, or rupture, that is tension failure.

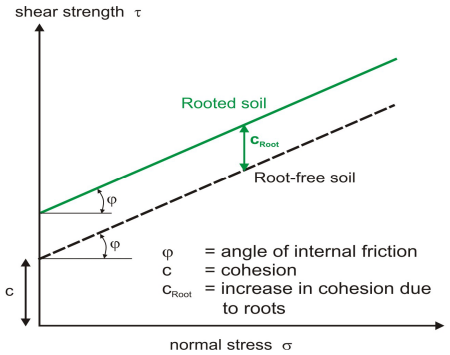

Figure 1. Effect of root reinforcement on shear strength of soil

Tensile Strength

The tensile strength of the considered roots was determined by testing root systems in the laboratory with the new testing apparatus at the Institute and Laboratory of Geotechnics (Figure 2). The tensile strength is dependent on the diameter, the water content and the age of the roots.

The roots were held at each end by specially developed clamps bonded with cork. The tested roots were up to 10 cm long with diameters in the range 2-12 mm. The constant tensile force was applied by a motor and the extension measurements made using a displacement transducer.

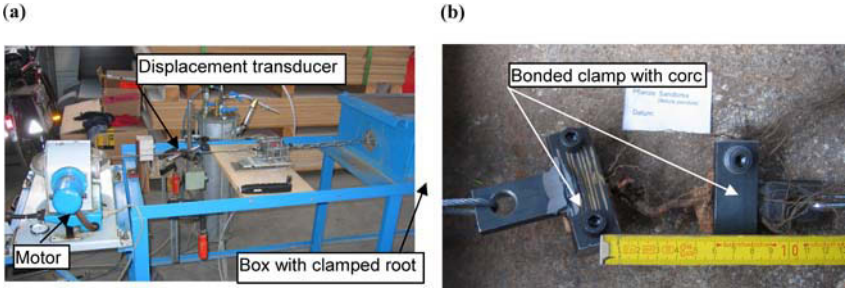

Figure 2. (a) View of testing apparatus, (b) Clamped birch root

Results of one study with birch roots are summarized in Figure 3; all show tensile strength decreasing with increasing root size for diameters. Most of the birch roots, especially with smaller diameter ruptured directly at the clamp. Some ruptured in the middle between the clamps or the bark is pulled off the roots.

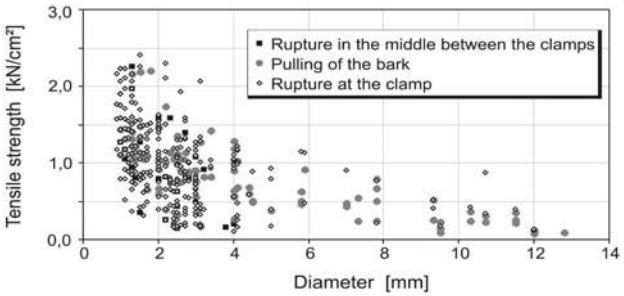

Figure 3. Influence of root diameter on tensile strength of birch roots

Shear Strength

The influence of root reinforcement on shear strength is determined by direct shear tests in the field and in the laboratory on sandy soil. Below we determined the reinforcing effect of young European birch (*Betula pendula*) and maple (*Acer platanoides*) roots on soil shear strength. Some tests were carried out at rootless soil specimens, too.

A schematic drawing of the shear apparatus is shown in Figure 4b. The shear box is square in plan (25 cm × 25 cm) and divided into two horizontally rigid halves. The shearing force was applied by one hydraulic jack that acted on the lower half. Instrumentation was designed to measure the horizontal displacements induced by hydraulic jack and the vertical displacements in the soil specimen. The normal load is kept constant during testing and is measured by a pressure transducer, as well. The shear box equipment allows displacements of 80 mm.

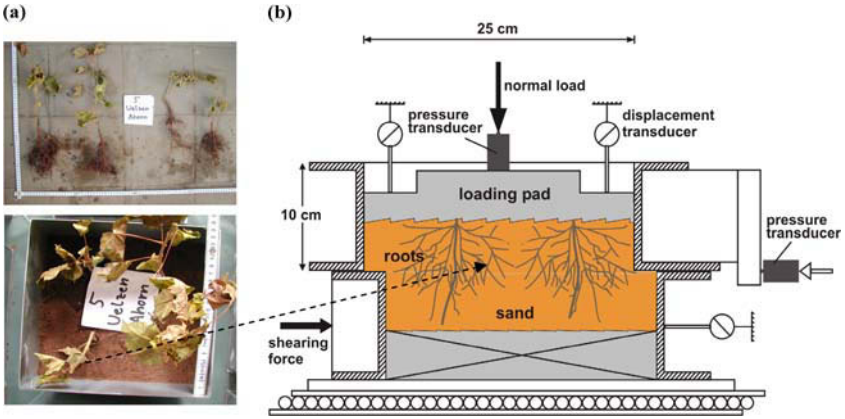

Figure 4. (a) Maple saplings in testing-boxes, (b) Schematic drawing of the shear apparatus (25×25 cm)

For the investigation in the laboratory there are planted birch (Betula pendula) and maple (Acer platanoides) saplings in testing-boxes (Figure 5a) one respectively two years before starting the test series. After each test, the roots were collected and the diameter of the roots was measured in the shear plane. The diameter of a main maple root increases i.e. from 5.1mm to 9.4mm, which means about 80% during two years. The root area ratio (RAR) (A_r/A) was determined in the range of 0.27-0.35 %. Figure 5a shows the roots during planting and Figure 5b after testing, i.e. two years later.

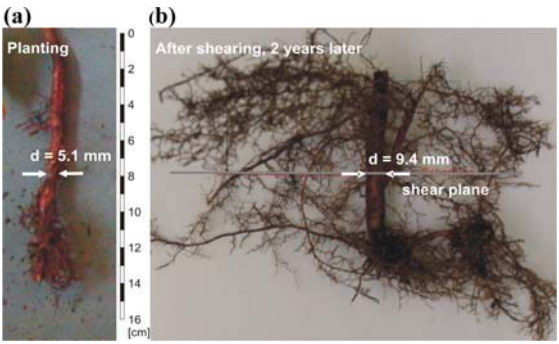

Figure 5. (a) Maple root planting, (b) Maple root after shearing

After completion of each test, the soil in the shear box was excavated by hand to expose the roots system. The exposed maple root system of one plant is shown in Figure 5b. This root does not failed in tension.

The normal stress applied was small, ranging from 25 to 75 kN/m². The shear parameters for the rootless soil result in ϕ = 32-34.7° and c'= 0-2.4 kN/m² depending on the water content. The angle of friction ϕ for the reinforced soil was found between 33.7° and 35.4° and the cohesion c_{Root} was found between 3.5 kN/m² and 6.3 kN/m². The results are shown in Figure 6.

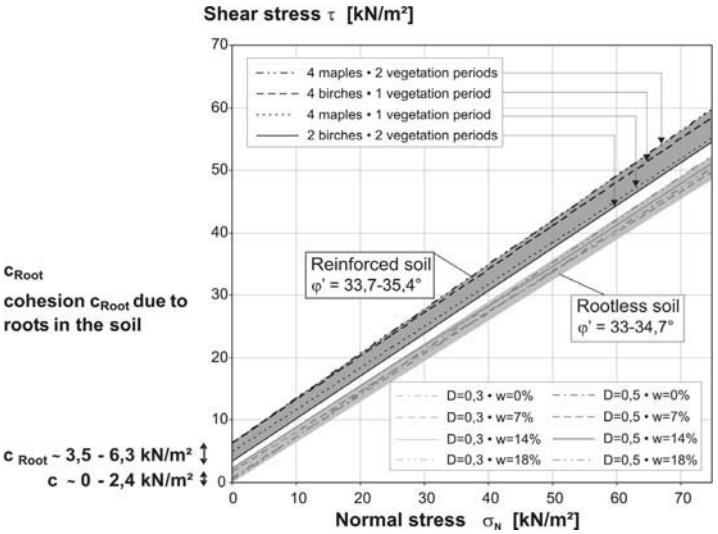

Figure 6. Influence of root reinforcement on shear strength of sand

The results of the own experimental shear tests and further studies documented in the literature are shown in Figure 7. The variation in shear strength increase ΔSR (=c_{Root}: cohesion due to roots) with root area ratio (AR/A) is essentially linear for most soil-fiber or soil-roots systems for values of (AR/A) less than 1 or 2 percent.

With the exception of the Douglas fir and spruce-hemlock data, all curves were plotted from the results of direct shear tests. The former were calculated from root area ratio data and root tensile strength data using a theoretical fiber model and equation (Gray and Leiser 1982).

SOIL MOISTURE

The first mention of soil suction in slope stability studies was made by Terzaghi (1950). Since then, many field works have been undertaken to study the effect of matric suction on slope stability (Öberg 1995). When the matric suction values have to be taken into account in stability analysis the results become more concordant with the existing steep configurations and observed sliding activities, than the results obtained by conventional stability analysis.

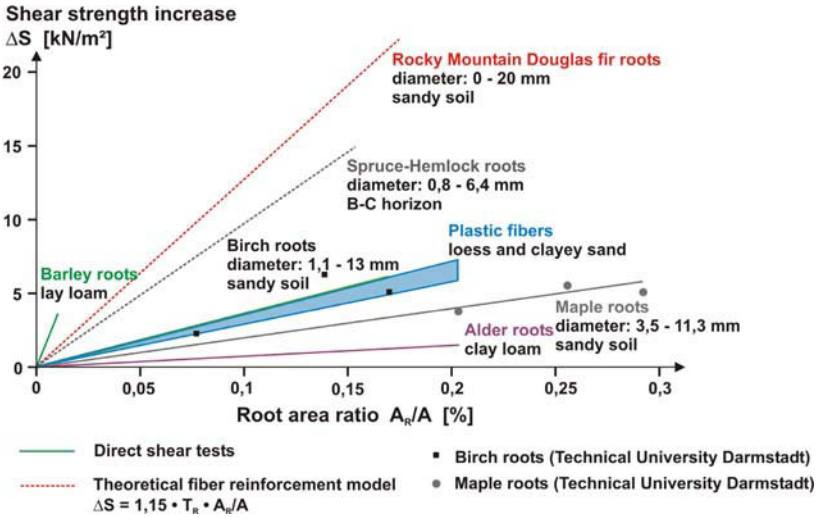

Figure 7. Examples of shear strength increases from root or fiber reinforcement of various soils

Matric Suction Measurements at the Railway Embankment

The matric suction profile in the historical railway embankment is studied by using tensiometers installed in the unsaturated fill. The investigated embankments were built towards the end of 19th century. The embankments are 4 m to 10 m high with slope angles βup to 40°. The investigated earth embankments are abundantly covered at the slopes as well as the crests with vegetation, i.e. by trees and shrubs of various types. The groundwater level is located at the bottom of the slope.

A total of 21 tensiometer (Tensio 151 with a measuring range between +20 and –85 kPa) were installed in the embankment at different depths to study the matric suction profile ranging from the dam crest to the dam base both. The tensiometers were fit in the center of the dam and along the slope in order that the influence of vegetation, i.e. the depth of the root zone z_r (Figure 9) and the influence of water (evaporation, precipitation), could be identified. At each depth three tensiometers are installed. Furthermore 7 TDR Trime IT (Time Domain Reflectometry)-probes are located at the same depths (Figure 8). The volumetric water content can be measured in the range between 0 and 95 % with the TDR-probes.

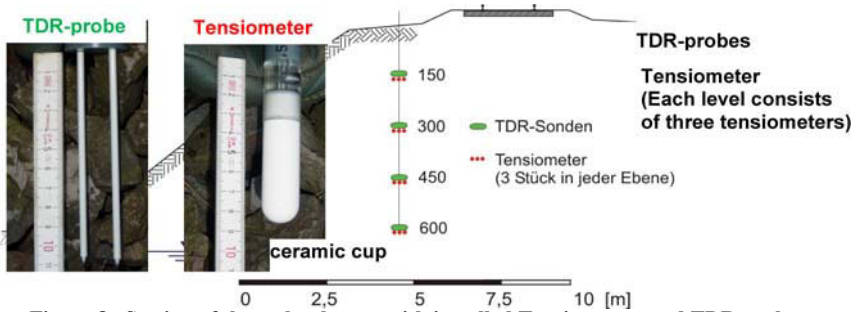

Figure 8. Section of the embankment with installed Tensiometers and TDR probes

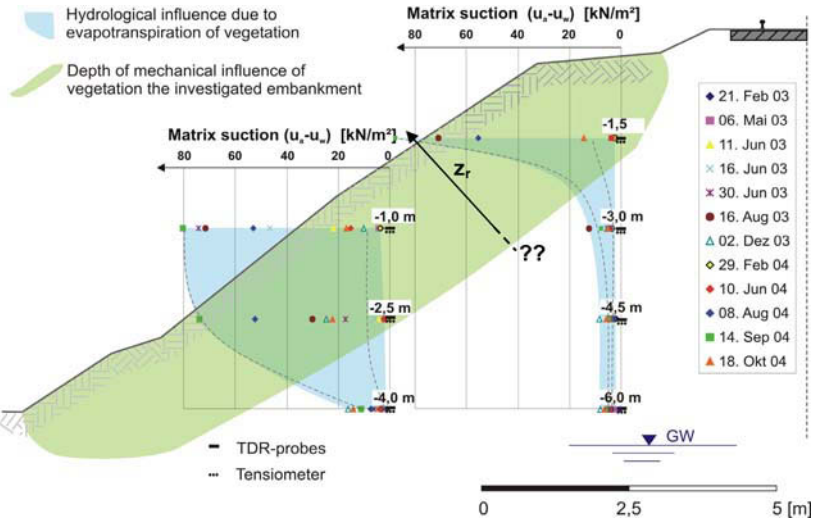

Figure 9. Results from suction measurements

During monitoring between February 2003 and October 2004 the matrix suction changed during the winter and summer months where trees and shrubs are growing. In the summer months the matrix suction reaches quite often the upper limit of the tensiometers of 80 kPa in depth up to 2.5 m below surface. In the winter months the matrix suction is rather constant at about 3 to 8 kPa. The seasonal variation of the matrix suction is marked by the blue area.

Furthermore it is possible to identify the depth of mechanical influence, where roots reinforce the soil, bind soil particles together and thereby increase the soil strength. The positive effect of mechanical reinforcement to slope stability has no seasonal variation.

CONCLUSIONS

A series of shear tests were performed to investigate the stabilizing mechanical effects of vegetation on slope stability. It is possible to verify the positive effect of young birch and maple roots in sandy soil due to our experimental studies. The cohesion c_{Root} was found between 3.5 kN/m² and 6.3 kN/m² for the reinforced sandy soil.

The soil suction profile in the embankment at the test side was studied by using tensiometers and TDR-probes. The results show the influence of vegetation, i.e. the depth of the root zones z_r and the influence of water (evaporation, precipitation) during the summer and winter months. The seasonal variation of the pore pressure followed the expected seasonal trend with the largest suctions (negative pore pressures) developing in the summer months. In the area up to 2.5 m below ground surface constant suctions up to 8 kPa were observed during the observation period.

In summary the magnitude of the mechanical reinforcement effect of vegetation is quite complex and a function of density, tensile strength, bond strength, length and diameter of roots, soil moisture etc.

The further long-term research activity has to be updating the conventional calculation methods for slope stability in an interdisciplinary cooperation of civil engineers, geodetic engineers, geologists, hydrologists and biologists considering the effects of vegetation.

REFERENCES

Coppin, N.J. and Richards, I.G. (1990). Use of vegetation in civil engineering. Butterworths, London.

Gray, D.H. and Leiser, A.T. (1982). Biotechnical slope protection and erosion control. Van Nostrand Reinhold Co., New York.

Gray, D.H. and Sotir, R.B. (1996). Biotechnical and soil bioengineering slope stabilization. John Wiley & Sons, Inc.

Katzenbach, R. and Werner, A. (2005). Experimental studies for the increase of slope stability of historical embankments due to the effects of capillarity and vegetation. 16th Internat. Conference on Soil Mechanics and Geotechnical Engineering, Osaka.

Öberg, A.-L. (1995). Negative pore pressures – seasonal variation and importance in slope stability analysis. Unsaturated Soils: 907-913.

Terzaghi, K. (1950). Mechanism of landslides. Application of Geology to Engineering Practice, Geological Society of America, Berkley Volume: 83-123.

Stabilization of Embankment on Expansive Soil – A Case Study

R. Katti[1], U. Kulkarni[2], A. Katti[3], and R. Kulkarni[4]

[1] Professor Emeritus, IIT, Mumbai, India, e-mail: kattirk@yahoo.co.in
[2] Proprietor, Noble Geo-Structs Mumbai - 81, India, e-mail: udayk@noblegeostructs.com
[3] Professor and principal, Datta Meghe College of Engineering, India, e-mail: kattianand8@yahoo.com
[4] Project coordinator, Noble Geo-Structs, Mumbai-81, India, rkulkarni@noblegeostructs.com

ABSTRACT: Longitudinal cracks often develop along the slope of embankments on shrink-swell soils due to continuous saturation. The presence of montmorillonite clay mineral in the soil sample considered for the study, exhibited binary phenomenon. Charge distribution in the montmorillonite clay mineral indicates the presence of both expansion and expansion preventing bonding forces in the same mineral structure. The study presents the use of Cohesive Non-Swelling Layer technology to reduce the formation of cracks. Structures constructed with this technology have shown superior performance for more than thirty seven years.

INTRODUCTION

Embankment constructed with expansive soil had exhibited longitudinal cracks along the slope upon continued wetting for laying turf. Continued transverse movement in the soil mass initiated the longitudinal crack propagation. The surface cracks were seen to be manifestation of the shallow slip circle failures. For inducing slope stability in the soil mass the objective of the study was to: arrest the deterioration of the shear strength under continued soil wetting; understand the behaviour of expansive soil in different moisture regimes through inspection of atomic structure of the mineral ingredients of expansive soil; understand the atomic structure of hydroxides; and devise methods of application of lime into the expansive soil matrix.

Generally, expansive soil deposits in this region, exhibit high swelling pressure of the order of 30 t/m^2 to more than 150 t/m^2, and heave of the order of 10 cm to more than 30 cm and undergo loss of shear strength when wet. They show no volume change properties within a shallow depth of 1 m to 1.5 m as seen in Figure 1 (Katti et al. 1969, 1987, 2002, and 2005).

IDENTIFICATION OF MONTMORILLONITE TYPE CLAY

The expansive soil deposits exhibit binary phenomenon: (i) active zone of 1 m to 1.5 m thick, and followed by (ii) constant volume zone. From X-ray, differential thermal analysis (DTA), gravimetric and chemical analysis tests it was inferred that the clay fraction is expanding lattice montmorillonite a 3 layer clay mineral.

A unit cell of montmorillonite is made of alumina octahedral layer sandwiched between two silica tetrahedral layers. Magnitude of this unit is around 14 A^o to 20 A^o in the 'c' direction. Number of such units in the 'c' direction in a 2μx2μx2μ clay particle would be around 1000 to 1428, and number of cleavages would be one less. Thus these cleavages can cause displacement in the 'c' direction of the order of 3.796 μ to 2666 μ (4 layers of water molecules can enter) due to adsorbed water, and the adsorbed water can also go around the external surface of the particle.

To measure interaction between dipolar nature of water and soil particles in the soil water system cohesion and or suction are adopted as measure by research workers which are nothing else but indirect measure of resultant Coulombian electrical charge forces existing on internal and external surfaces of clay minerals in particular and surfaces of soil particles in general (Grim 1953, Steve et al. 2005, Kalpana et al. 2005, Katti et al. 2000, Katti 1969, Katti et al. 2002). Thus, Katti's realised that such phenomenon can only take place if adequate Coulombian forces are also present.

DEFINITION OF MONTMORILLONITE CLAY

Any soil that contains expanding lattice in the clay fraction is called montmorillonite clay. This clay exhibits swelling and swelling pressure when it comes in contact with dipolar nature of water and loses shear strength. Based on this micro particle model is put forward. Swelling pressure or stress vs. swelling is given in Figure 2.

The Figures 3, 4 and 5 show surface and bottom unit cell layer between two cleavages, unit cell inter layer between Si and Al and between Al and Si. This clearly indicates atoms jointly shared by tetrahedral layer and octahedral layer. This is helpful in estimating equivalent Coulombic charges |e| on the inter layer surfaces, external surfaces, edges and corners, etc., as seen in Figure 6.

Table 1. Charges |e|*

Layer	Surface	Edges	Corner
Top	12|e|	a = 2|e|, b = 1|e|	one |e|
Si-Al Interface	7|e|	a = 2|e|	one |e|
Al-Si Interface	7|e|	a = 2|e|, b = 1|e|	one |e|
Bottom	12|e|	a = 2|e|, b = 1|e|	one |e|

*$e = 6.5 \times 10^{-10}$ ESU, $e/m = 1.7589 \times 10^{11}$ Coulomb per kilogram = 5.273×10^{17} ESU per gram. (That is why e is expressed as modulus, which serves the limited objective dealing with ratio.)

During rains, some of the bonds are broken and results in heave. In the field normally cells are aggregated and bonded, i.e. they are in compacted state when exposed to atmosphere.

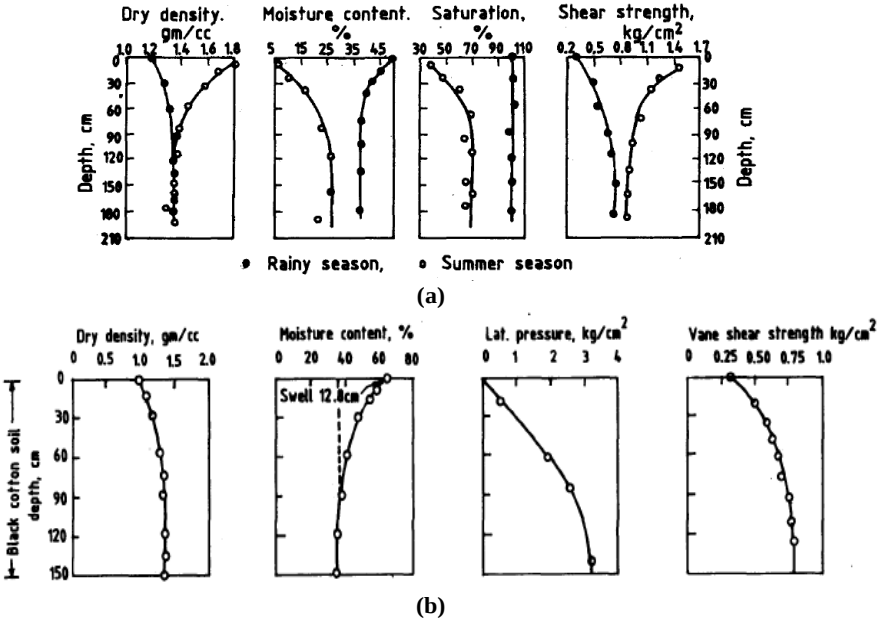

Figure 1. Results of: (a) field studies on expansive black cotton soil during summer and rainy season, (b) large scale model test

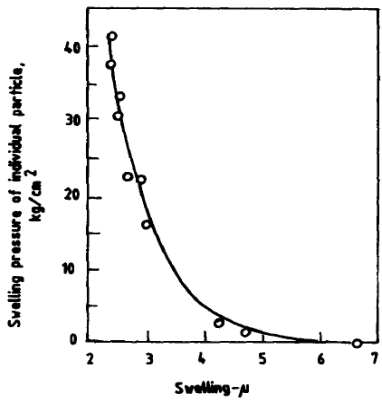

Figure 2. Micro particle model – Relation between swelling pressure of individual particle and swelling

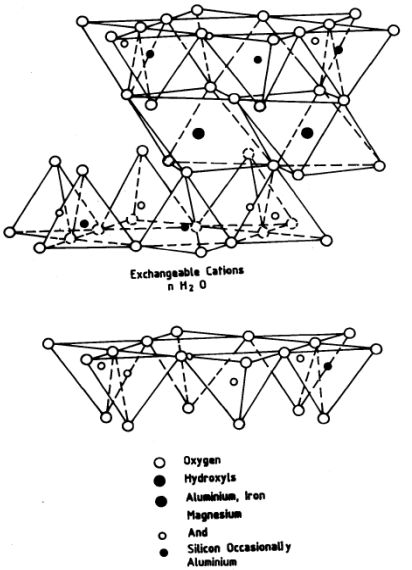

Figure 3. Diagrammatic sketch of montmorillonite: (a) after Hoffman, Endell and Wilm; (b) after Edelman and Faveje

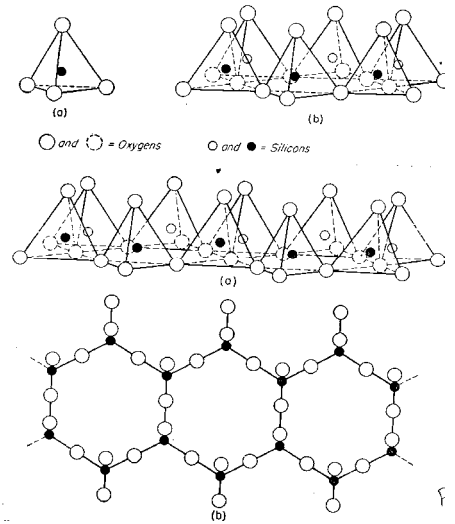

Figure 4. Diagrammatic sketch of: (a) single silica tetrahedron, (b) sheet structure of tetrahedron arranged in a hexagonal network, (a1) double chain of silica tetrahedron in perspective, (b1) projected on the plane of the tetrahedron

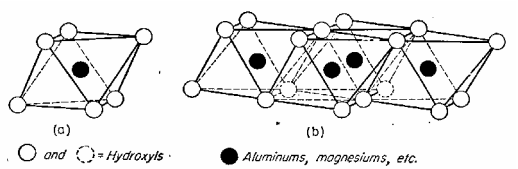

Figure 5. Diagrammatic sketch of: (a) single tetrahedral unit, (b) sheet structure of octahedral sheet

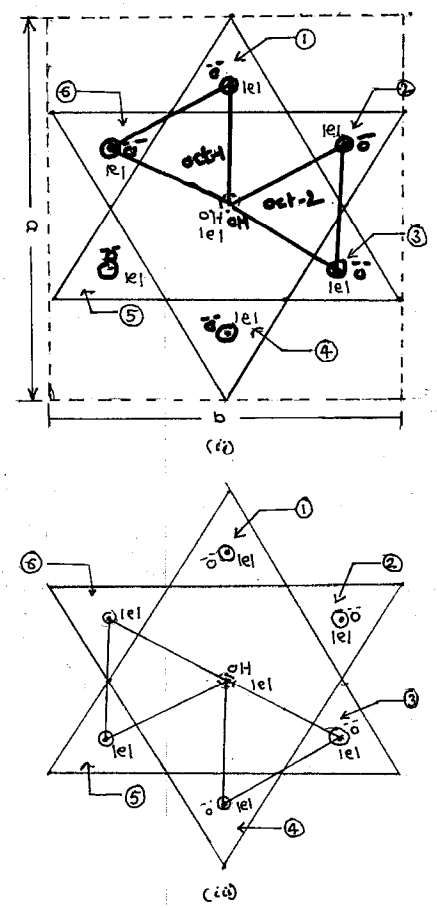

Figure 6. Diagrams showing atoms having unbalanced electrical charges n |e|: (i) at surface of unit cell of montmorillonite clay mineral, (ii) between Si and Al inter/intra layers, (iii) between Al and Si bottom layers

SECTION OF THE EMBANKMENT

The typical cross section of the embankment in the problem area is shown in Figure 7. The bottom width of the embankment is 26 m and the top width is 2 m. The reduced level of the embankment at the base is about 102.5m and at the top is about 106 m. The embankment is circular in plan and having length of 132 m.

Figure 7. Section of embankment

ENGINEERING PROPERTIES OF EXPANSIVE SOIL

The back fill consists of black expansive soil being the locally available material. This soil in general has following properties: Gravel 11%, Sand 10%, Silt 37%, Clay 41%, Liquid limit 54%, Plastic limit 27%, Free swell 140%, Swelling pressure 1.25 kg/cm^2.

STRATIGRAPHY

The following stratigraphy was observed from the geotechnical investigation. The top horizon consists of black cotton soil. It starts at R.L. 101.97 and extends up to R.L. 99.97. The standard penetration test (SPT) conducted shows N value of 11. This is followed by yellowish silty clay from R.L. 99.97 and R.L. 95.96. SPT conducted shows as N value 14. Below the silty clay, completely weathered rock is seen between R.L. 95.96 and R.L. 91.97. Slightly weathered rock is seen between R.L. 91.97 and R.L. 87.97. The core recovery ranges between 12% and 43% and RQD ranges between 0% and 20%. Lastly, fresh amygdaloidal basalt is encountered from R.L. 87.97. The core recovery is 81% and RQD is 28%.

PROBABLE FAILURE MECHANISM

Probable failure mechanism apparently is seen to owe excessive lateral deformation related to swelling of soil. Expansive soils swell on wetting during watering by sprinkler for gardening purpose. The soil has a tendency to undergo swelling upon wetting due to inherent montmorillonite clay mineral constituents. The swelling pressure magnitude is of much higher value in comparison with the gravitational active earth pressure. The related deformations are also of much higher magnitude. The lateral push from the back fill has triggered movement of embankment. There is also accompanied drop in shear strength during swelling process.

LIME STABILIZATION

The addition of lime produces stabilizing effect on expansive soil. When lime is added to soil two effects are observed:

- The plasticity index reduces from 27% to 21% and shrinkage limit increases from 14% to 16%. Thus the shrink swell properties are altered.
- The time dependent Pozzolanic reaction induces cementing and hardening properties in the expansive soils.

STABILITY OF SLOPE

Table 2 summarizes the results from slope stability analyses.

Table 2. Slope analysis

Case	Cohesion, c (t/m^2)	Angle of Shear Resistance, ϕ (degrees)	Unit weight, γ (t/m^3)	Factor of Safety
Dry Slope	6.0	15	1.8	9.44
	6.0	15	1.8	
	6.0	15	1.8	
Fully Swollen Slope	0.2	0	1.5	0.55
	2.5	5	1.8	
	6.0	20	1.8	
After Treatment Slope	1.8	2.5	0.0	3.69
	1.8	2.5	5.0	
	1.8	6	20.0	

DISTRESS NOTICED

The slopes are in distress and following are observations:

- Top surface of the embankment shows downward movement at the edges.
- The top of embankment has pronounced level difference behind the turrets.
- There are longitudinal cracks parallel to slope signalling incipient failure of slope.
- Progressively more and more soil slopes are showing signs of distress.

PROCEDURE FOR STABILIZATION

- Lime stabilization over a constant volume depth of 2m below slope was adopted for slope stabilization.
- Triangular spacing at 1 m c/c was adopted for grouting of lime.
- Lime grout was prepared by mixing two bags (30 kg each) in 200 litres of water.
- The diameter of the drill hole was selected to be 75 mm.
- The Katni lime with CaO content greater than 70 % was used.
- The hole was to act as reinforcement filled with lime and sand.

EFFICACY

Area is now continuously saturated after lime stabilization and no further distress is seen.

CONCLUSIONS

CNS is a phenomenon arising out of combination of Coulombian and Newtonian forces. Any system of material capable of developing this phenomenon may be designated as CNS. Both Newtonian and Coulombian forces alter H-O-H in the Montmorillonite structure and possess high shear strength. The CNS Technology has with stood 37-year seasonal cycles and proved to be a viable construction technology for construction expansive soils. Results from small test predictions are in considerable variance with field reality; as such tests are not properly simulated to account for exponential variations. In this case, lime stabilized black cotton soil acted as CNS layer.

REFERENCES

Grim, R. E., (1953). Clay Mineralogy; McGraw-Hill New York.

Handy, R. L., Turgut, D. (1987). Swelling Pressure vs. D-Spacing of Montmorillonite, 6th International conference on expansive clays, organized by TC-6 ISSMFE and CBIandP, New Delhi, India.

Katti, R.K., Katti, D.R., and Katti, A.R. (2005). Primer on construction in expansive black cotton soil deposits with C.N.S.L. C.N.S.

Katti, K., and Katti, D.R. (2006). Relationship of swelling pressure on silica-water interaction in Montmorillonite. American Chemical Society, 532-537.

Katti, R.K., Lal, R.K., Fotedar, S.K., and Kulkarni, S.K. (1969). Depth effect in expansive clays. Proceedings 2nd Int. Res. Engineering Conference, College Station Texas, (USA), 362-373.

Katti, R.K. (1987). Cohesion approach to mechanics of expansive soil media. Behaviour of Saturated Expansive Soil and Control Methods 2nd edition, TC-6 committee, ISSMFE and CBI and P New Delhi India.

Levin, S. (1946). On the interaction of colloidal particles, Part1, Particular application to parallel plates, in swelling and shrinkage, general discussion, Faraday Society (ed.) Gurniand and Jackson, London, 102-117.

Maron, S.H., Prutton, C. F. (1976). Principles of Physical Chemistry. 4th Edition, Amerind Publishing Co. pvt. LTD. New Delhi India

Subbarao, K. (2001). Construction Practices In Expansive Soils, IGC 2001 Indore.

Steven, R.S., Katti, D.R., Ghosh, P., and Katti, K. (2005). Evolution of mechanical response of sodium montmorillonite interlayer with increasing hydration by molecular dynamics. American Chemical Society, Published on Web 07/20/2005 Langmuir.

An Empirical Method for Predicting Foundation Heave Rate in Expansive Soil

J.D. Nelson[1], D.D. Overton[2], and K. Chao[3]

[1] Professor Emeritus, Colorado State University and Principal Geotechnical Engineer, Engineering Analytics, Inc., 1600 Specht Point Road, Suite 209, Fort Collins, Colorado, USA 80525; e-mail:jnelson@enganalytics.com
[2] Principal Geotechnical Engineer, Engineering Analytics, Inc., 1600 Specht Point Road, Suite 209, Fort Collins, Colorado, USA 80525; e-mail: doverton@enganalytics.com
[3] Senior Geotechnical Engineer, Engineering Analytics, Inc., 1600 Specht Point Road, Suite 209, Fort Collins, Colorado, USA 80525; e-mail: gchao@enganalytics.com

ABSTRACT: Predicted values for free-field heave and foundation movement are basic parameters for the design of foundation systems for buildings sited on expansive soil. Current design procedures generally incorporate only the maximum predicted heave that will occur at a site. This can introduce an impractical design situation when the depth of potential heave and the associated heave is large. Under some site conditions the design life of the structure may be less than the time required for the entire amount of predicted heave to occur. In such cases, it is desired to consider the rate of heave and the amount of heave to be expected at the end of the design life. This paper presents a methodology for extending observed heave data accumulated over a period of time in order to predict the progression of heave with time. The methodology incorporates curve fitting of survey data to a hyperbolic function. The method of analysis is validated and demonstrated using actual data accumulated over a period of several years on a large building that was constructed with a drilled pier foundation. The results show that in that case future movement of the foundation could be accurately predicted.

INTRODUCTION

Free-field heave is a basic parameter for design of slab-on-grade floors, and is also used in the design of pier and grade beam foundation systems for buildings. Current technology generally bases the design on the amount of predicted heave that will ultimately occur at a site. When large values of heave are predicted, the depth of potential heave may be very deep, and the time required for the full wetting of the foundation soils down to the depth of potential heave may exceed the design life of the structure.

Oftentimes an elevation survey of slabs and/or foundations is conducted for a structure. The change of the heave with time can be valuable data for predicting future heave over time. This paper introduces a hyperbolic curve fitting technique for predicting the change of heave with time if only several years of survey data is available. The hyperbolic fitting technique was verified using actual data accumulated over a period of approximate 3 years on a large building having a pier foundation. The results of the heave analysis demonstrate that future movement of the foundation system can be accurately predicted.

PREDICTION OF HEAVE WITH TIME

A method for prediction of ultimate free-field heave using oedometer test data was originally developed by the U.S. Army Corps of Engineers (1983). A similar methodology was developed to account for constant-volume swell pressure in Nelson and Miller (1992). Fredlund and Rahardjo (1993) presented a similar method for heave prediction. A refinement of that method is presented in Nelson, et al. (2006).

In order to predict the amount of heave that will occur at a particular time, it is necessary to know what zone of soil has been wetted by that time, and the expansive nature of that soil. Chao et al. (2006) conducted analyses of the migration of the wetting front using the computer program VADOSE/W Version 6.20 (GEO-SLOPE 2006). Typical results of the water migration simulation for a hypothetical case are shown in Figure 1. The example was analyzed for a cross section with 3.0 meters of clay over claystone bedrock. Analyses were performed for a site with good surface drainage migration within 1.5 meters of the house and a 10% slope away from the house for the first 3.0 meters. In the model, irrigation was applied to the lawn surface beyond 1.5 meters of the house in addition to precipitation. Figure 1 indicates that the depth of wetting continues to increase throughout the design life of the structure.

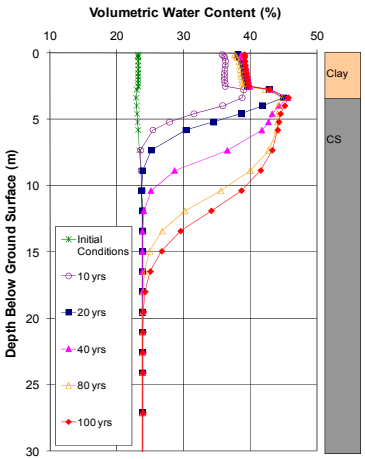

Figure1. Variation of water content profiles throughout 100 years (Chao et al. 2006)

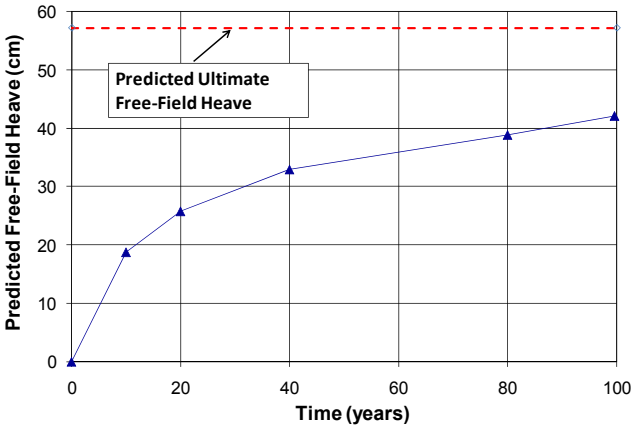

Figure 2. Computed Heave vs. time for the hypothetical case (Chao et al. 2006)

The clay and claystone were assumed to have a percent swell of 4% and 6% and a swelling pressure of 480 and 720 kPa, respectively. The ultimate free-field heave was calculated to be 57.2 cm using the procedure outlined in Nelson, et al. (2006). The change of heave with time was calculated using the volumetric water content profiles obtained from Figure 1, a relationship between water content and percent swell developed by Chao (2007), and the ultimate free-field heave calculated above. The computed heave is shown as a function of time in Figure 2.

PREDICTION OF HEAVE WITH TIME USING A HYPERBOLIC CURVE FITTING TECHNIQUE

In some cases, elevation survey results are available for heaving slabs and/or foundations of a structure. It is desired to be able to predict from those results the maximum amount of movement that will occur over the design life of the structure. The shape of the curve for the computed heave as a function of time as shown in Figure 2 suggests that a hyperbolic equation will represent the data well. The following section will discuss the application of such an equation to the data.

Methodology

It is proposed that the change of heave with time will fit a hyperbolic equation of the form:

$$\rho = \frac{t}{a + bt} \tag{1}$$

where:

ρ	=	heave since the time of construction
a and b	=	curve parameters.
t	=	the time since movement began

From Equation (1), as t approaches infinity the limit of ρ is 1/b. This would represent the ultimate heave.

Equation (1) can be rewritten in the form:

$$t/\rho = a + b\,t \tag{2}$$

Since t/ρ is a linear function of t, the curve parameters a and b can be determined from the intercept and the slope of a plot of t/ρ vs. t.

Example of Heave Prediction using the Hyperbolic Curve Fitting Technique

The hyperbolic curve fitting technique is demonstrated using the assumed survey data shown in Figure 3. The survey data shown in Figure 3 were plotted in the form of Equation (2) as shown in Figure 4. The values of a and b are shown in Figure 4. Figure 5 shows the plotted survey data and the slab heave predicted by Equation (1) using the parameters determined in Figure 4.

CASE STUDY USING THE HYPERBOLIC CURVE FITTING TECHNIQUE

The hyperbolic curve fitting technique was used to predict pier heave as a function of time in the case of a manufacturing building located in Colorado. The building was founded on 45 to 107-cm diameter piers with a depth of 7 meters. The bottom of the piers is approximately 13.4 meters below exterior final grade. Movement of the piers and structural floors was initially observed during construction and prior to the occupancy of the building. Individual piers had heaved as much as 28 cm within the first six years of being constructed.

Analyses of the pier heave were performed using the procedures outlined by Nelson and Miller (1992). The pier diameter and minimum dead load for the structures were obtained from the soils report. Using the solution for pier movement in an elastic medium as presented in Nelson and Miller (1992), and the laboratory test data, predicting ultimate heave of the existing piers were calculated to be approximately 40 cm (Overton, et al. 2007).

The initial elevation survey of the foundation piers was performed in July 1995. Follow-up surveys were performed on a semi-annual basis. From the time that the initial survey was made until the time that the analysis was conducted, individual piers had heaved up to 10.8 cm. The maximum estimated total heave that had occurred since construction of the building was approximately 25 to 28 cm. Figure 6 shows the observed heave as a function of time for selected piers.

Based on pier movement patterns, it was assumed that the first pier movement of piers E6, D7, and D8 was observed in September 1992. In order to extrapolate these data to predict the maximum movement that these piers will exhibit, it was assumed that the heave versus time data fits the hyperbolic equation. Plotting the survey data in the form of Equation (2), the parameters a and b were calculated to be 24.043 days/cm and 0.0259 cm^{-1}, respectively.

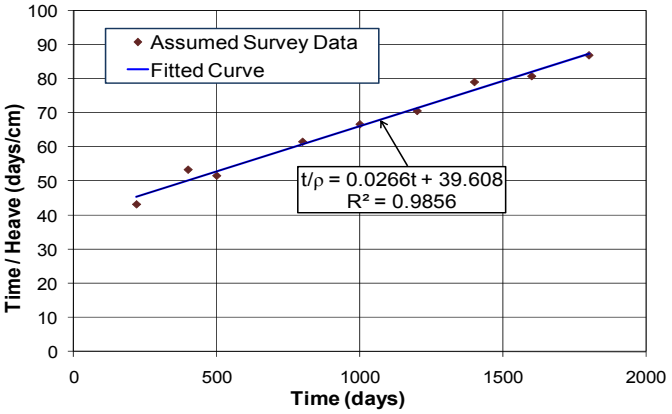

Figure 3. Example of assumed survey data

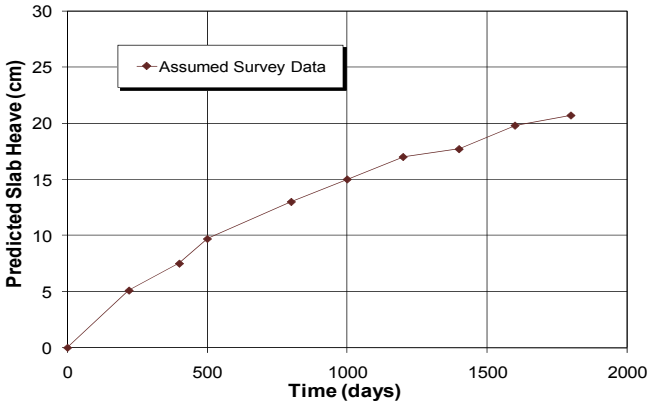

Figure 4. Plot of time/heave vs. time

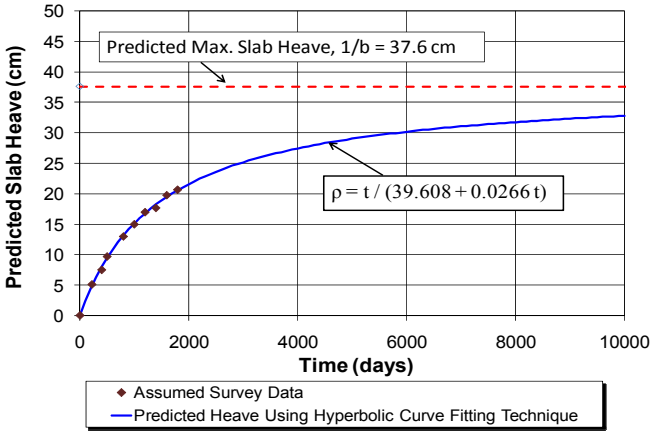

Figure 5. Predicted slab heave using the hyperbolic curve fitting technique

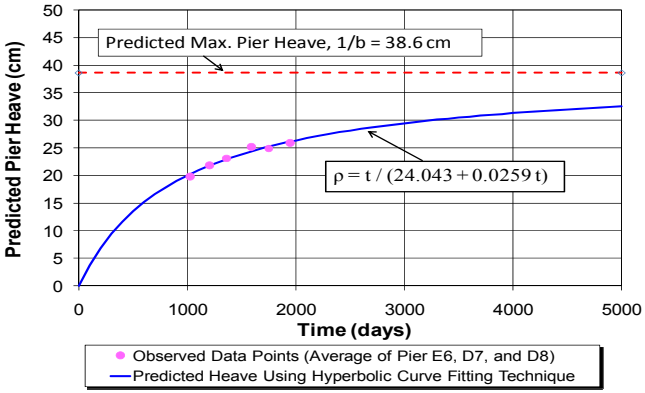

Figure 6. Pier heave as a function of time for Piers E6, D7, and D8

Figure 6 shows the pier heave predicted by Equation (1) using the a and b parameters along with the observed pier heave values obtained from the survey. For the data shown in Figure 6, the maximum value of movement of piers E6, D7, and D8 would be equal to 38.6 cm (1/b = 1/0.0259). This value agrees well with the pier movement of 40 cm predicted using the procedures outlined by Nelson and Miller (1992).

CONCLUSIONS

Fitting observed survey data to the hyperbolic equation provided a means of extending observed heave into the future using the observed survey data. The hyperbolic curve fitting technique was demonstrated using the actual survey data collected at the manufacturing building. Figure 6 indicates that using observed data collected over a period of less than 3 years provided reasonable accuracy for heave prediction. It is shown in Figure 6 that the predicted heave using the hyperbolic curve fitting technique agrees well with the pier heave prediction using Nelson and Miller (1992).

REFERENCES

Chao, K.C. (2007). Design Principles for Foundations on Expansive Soils. Dissertation submitted in partial requirement for the Ph.D. Degree, Colorado State University, Fort Collins, Colorado.

Chao, K. C., Overton, D. D., and Nelson, J. D. (2006). The Effects of Site Conditions on the Predicted Time Rate of Heave. Proceedings of the Fourth International Conference on Unsaturated Soils. Carefree, Arizona. April, 2086 – 2097.

Durkee, D. B. (2000). Active Zone and Edge Moisture Variation Distance in Expansive Soils. Dissertation submitted in partial requirement for the Ph.D. Degree, Colorado State University, Fort Collins, Colorado.

Fredlund, D. G. and Rahardjo, H. (1993). Soil Mechanics for Unsaturated Soil. John Wiley & Son, Inc., New York, NY.

GEO-SLOPE International, Ltd. (2006). GEO-STUDIO VADOSE/W Software Package for Seepage Analysis, Version 6.20. Calgary, Alberta, Canada.

Nelson, J. D. and D. J. Miller. (1992). Expansive Soils: Problems and Practice in Foundation and Pavement Engineering. John Wiley and Sons.

Nelson, J. D., Overton, D. D., and Durkee, D. B. (2001). Depth of Wetting and the Active Zone. Expansive Clay Soils and Vegetative Influence on Shallow Foundations, ASCE, Houston, Texas. 95 – 109.

Nelson, J. D., Reichler, D. K., and Cumbers, J. M. (2006). Parameters for Heave Prediction by Oedometer Tests. Proceedings of the Fourth International Conference on Unsaturated Soils. Carefree, Arizona. April, 951 – 961.

Overton, D. D., Chao, K. C., and Nelson, J. D. (2006). Time Rate of Heave Prediction for Expansive Soils. GeoCongress 2006, ASCE, Atlanta. 1 – 6.

Overton, D. D., Chao, K. C., and Nelson, J. D. (2007) Heave Distress of a Manufacturing Building. Proceedings of the Geo-Denver 2007 Conference, Denver, Colorado. February.

USA, Army Corp of Engineers. (1983). Technical Manual TM 5-818-7, Foundations in Expansive Soils. September 1.

Effect of Water Sources on Water Migration in the Vadose Zone

K. Chao[1], D.D. Overton[2], and J.D. Nelson[3]

[1] Senior Geotechnical Engineer, Engineering Analytics, Inc., 1600 Specht Point Road, Suite 209, Fort Collins, Colorado, USA 80525; e-mail: gchao@enganalytics.com
[2] Principal Geotechnical Engineer, Engineering Analytics, Inc., 1600 Specht Point Road, Suite 209, Fort Collins, Colorado, USA 80525; e-mail: doverton@enganalytics.com
[3] Professor Emeritus, Colorado State University and Principal Geotechnical Engineer, Engineering Analytics, Inc., 1600 Specht Point Road, Suite 209, Fort Collins, Colorado, USA 80525; e-mail: jnelson@enganalytics.com

ABSTRACT: This paper evaluates the effect of precipitation events, irrigation practice, and deep wetting from underground sources on migration of water in soils and bedrock. The water migration analyses were conducted using the VADOSE/W software for the TRACON building at Denver International Airport, Denver, Colorado, USA. Measurements of water content and density from surface nuclear gauge tubes installed around the building were used to calibrate and validate input parameters and boundary conditions specified in the VADOSE/W models. Long-term water migration within the soils and bedrock was evaluated for the cases with various water sources. It was concluded that the presence of deep water bearing stratum and irrigation on the lawn can be significant in the migration of the wetting front within the soils and bedrock.

INTRODUCTION

Free-field heave is a basic parameter for performance prediction of a slab-on-grade floor as well as a pier and grade beam systems. An important factor in computation of predicted free-field heave is the migration of the wetting front during the design life of a structure. A conservative analysis is to assume that the entire depth of potential heave is wetted. The depth of potential heave is defined as the depth to which the overburden vertical stress equals the swelling pressure of the soil (Nelson et al. 2001). Instead of using the depth of the potential heave for heave prediction, a rigorous water migration analysis can be performed to analyze the actual depth of wetting in soils during the design life of a structure.

Water migration analyses were conducted to evaluate the rate of movement of the wetting front at the TRACON building. The TRACON building is located at approximately 2 km south of Denver International Airport Terminals, Denver, Colorado, USA. Measurements of water content and density from surface nuclear gauge tubes installed around the building have been taken from June 2000 to August 2006 and the data was used to calibrate and validate input parameters and boundary conditions specified in the seepage models.

This paper considers the effect of precipitation events, irrigation practice, and deep wetting from underground sources on the pattern and rate of the wetting front movement during the design life of the TRACON building. Each of these conditions may have a significant influence on the migration of the wetting front to the subsoils.

ANALYSES OF ZONE OF WETTING

Analyses of the migration of the wetting front were conducted using the computer program VADOSE/W Version 6.20 (GEO-SLOPE 2006). The water migration analyses were performed for a soil profile having natural climate with no irrigation. The design life of the TRACON building was reported to be 50 years. The TRACON building was constructed in the year 1991. Therefore, the migration of soil water was modeled up to the year 2040.

The effect of precipitation events, irrigation practice, and deep wetting from underground sources on the rate of movement of the wetting front was evaluated in this study. Seepage analyses were conducted to evaluate the migration of soil water for the average, highest, and lowest annual precipitation events. The effect of lawn irrigation was also evaluated in this study. The irrigation was applied in the months of April through October at a rate of 130% of the turf grass water requirement (Mecham 2005).

Modeling Procedure

The water migration analyses were performed in four steps.

1. Initial Water Content Profiles – The subsurface nuclear gauge readings for May 2001 were input as initial water content profiles. The values of water content obtained from the deep benchmark were also input into the models for the deeper portions of the soil profile.
2. Model Calibration – The soil water characteristic curves (SWCCs) for the weathered claystone and claystone were measured in the laboratory. The SWCCs and hydraulic conductivity functions for the other soils including the silty clay fill, silty clay, coal, and sandstone bedrock were initially estimated using the soil database program SoilVision, Version 4.14 (SoilVision 2006). The SWCCs and hydraulic conductivity functions for these materials were then adjusted until the model results matched the observed water content data from May 2001 to June 2004.
3. Model Validation – Validation refers to comparing the measured response of the system (subsurface nuclear gauge data) with the results of the computational

model. This demonstrates that the model is consistent in predicting measured data. The validation of the model was performed by comparing the model output with nuclear gauge data for August 2006 at the modeling locations.

4. Long-Term Water Migration Simulations – The migration of soil water for the soil profiles was simulated from the year 2006 to 2040.

Climate Data Specified in the Models

Three cases of annual precipitation events including (1) average precipitation year, (2) highest precipitation year, and (3) lowest precipitation year were specified in the VADOSE models. The average annual precipitation at the Denver Airport weather station was 390 mm for the years 1949 to 2005. Climatic data from the years 1975, 1989, 1992, and 1998 with corresponding annual precipitation of 394, 393, 398, and 405 mm were repeated sequentially in the seepage models for the case representing average precipitation.

The years with the highest and lowest annual precipitation are 1967 and 2002, respectively. The annual precipitation value for the year 1967 was approximately 52% more than the average precipitation value, and the annual precipitation value for the year 2002 was approximately 51% less than the average value. Thus, climate data from the years 1967 ± 2 years and 2002 ± 2 years were repeated in the seepage models for the cases of the highest and lowest precipitation years, respectively.

Material Properties Used in the Models

The boring logs indicate that the soils at the site consisted of a layer of silty clay fill, underlain by silty clay, weathered claystone, claystone, coal, and sandstone bedrock. The soil parameters for these soils are summarized in Table 1. The soil parameters for the materials shown in Table 1 were obtained from the laboratory testing, the SoilVision database, calibrated values, or assumed values.

Table 1. Summary of soil parameters used in the seepage analyses

Soil Type	Saturated Hydraulic Conductivity (cm/sec)	K_h/K_v Ratio	Porosity
Silty Clay Fill	1.6×10^{-6} (1)	1 (4)	0.40 (1)
Silty Clay	1.0×10^{-6} (2)	1 (4)	0.40 (1)
Weathered Claystone	3.6×10^{-7} (3)	10 (4)	0.46 (2)
Claystone	8.5×10^{-8} (3)	10 (4)	0.46 (2)
Coal	5.0×10^{-4} (3)	10 (4)	0.48 (1)
Sandstone	1.5×10^{-5} (1)	10 (4)	0.44 (1)

(1) SoilVision Database
(2) Laboratory data (Chao 2007)
(3) Calibrated values
(4) Assumed values

Results of the Analyses

Model calibration

Figure 1 presents the predicted volumetric water content computed by VADOSE/W and the measured water content data in June 2004. Given the accuracy of the predicted water content distribution, the models were considered calibrated and were used for the model validation process.

Model validation

Figure 2 presents the comparison between the predicted and measured volumetric water content profiles at the location with the climate data only. In general, there is a good agreement between the predicted water content distribution and the measured data demonstrating model consistency and validation with respect to the data set used.

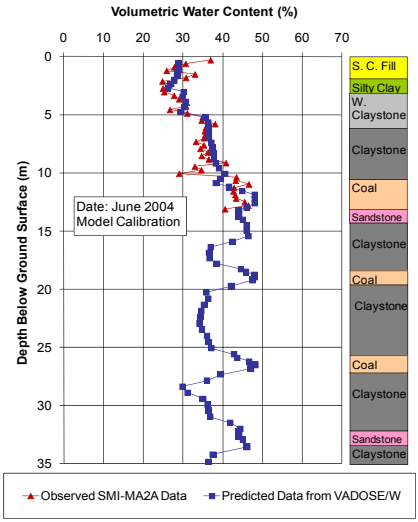

Figure 1. Measured and predicted water content profiles in June 2004

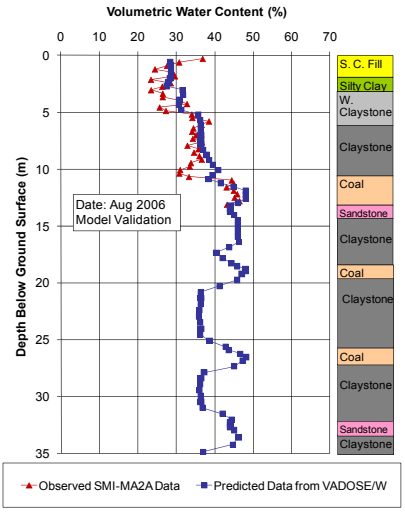

Figure 2. Measured and predicted water content profiles in August 2006

Long-Term Water Migration Simulations

Average precipitation year

Figure 3 shows the predicted water content profiles through the year 2040 for the average precipitation year. Figure 3 indicates that water will continue to migrate within the soils and bedrock through the year 2040. Of particular interest is the fact that it

appears that water migrates upward and downward from the coal seams and sandstone layers.

Highest precipitation year

Figure 4 presents the predicted water content profiles through the year 2040 for the case of the highest precipitation year. Water is shown to migrate in a much faster rate within the soils and bedrock through the year 2040, compared to that for the case of the average precipitation year. It is predicted that the entire bedrock below the top first coal layer could be saturated after approximately 2015.

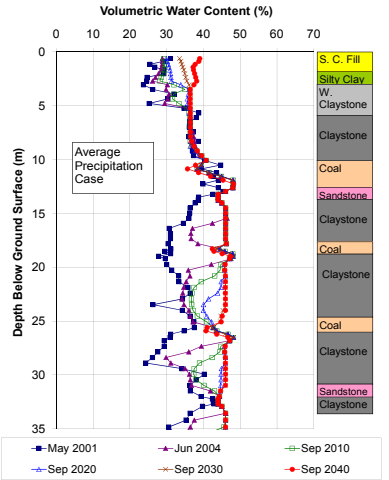

Figure 3. Predicted long-term water content profiles – average precipitation case

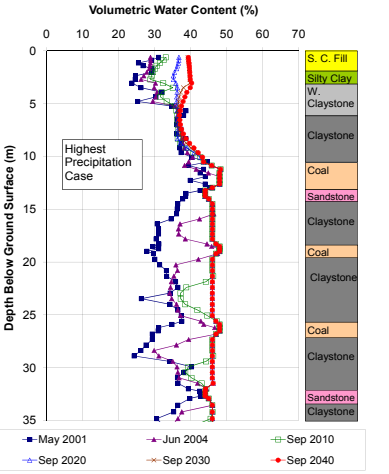

Figure 4. Predicted long-term water content profiles – highest precipitation case

Lowest precipitation year

The predicted water content profiles through the year 2040 for the case of the lowest precipitation year are shown in Figure 5. Figure 5 indicates that water migrates at about the same rate within the soils and bedrock as that for the average precipitation case. Comparing Figures 3 and 5 indicates that there is little difference in the water content profiles, except in the bedrock layer close to the upper coal seam. The entire bedrock could still be saturated through the year 2040 for both cases. The results of the VADOSE/W modeling demonstrate that the primary source of water for the overlying claystone bedrock is the coal seams rather than the precipitation. Consequently, the presence of a deep water bearing stratum is significant in the migration of the wetting front within soils and bedrock.

Average precipitation year plus irrigation

The predicted water content profiles through the year 2040 for the case of the average precipitation year plus irrigation are shown in Figure 6. Review of Figures 3 and 6 indicates that the water content for the case of the average precipitation year plus irrigation is significantly greater than that for the case of the average precipitation year.

CONCLUSIONS

The results of the water migration analyses show that depth of wetting will continue to increase through the design life of the structure. It appears that water migrates upward and downward from the coal seams and sandstone layers. The presence of a deep water bearing stratum is a significant source of water. Therefore, it is necessary for engineers to identify any deep water bearing stratum during the design process. Also, irrigation has a significant influence on the migration of the wetting front within soils and bedrock. It is not uncommon for irrigation amounts to be greatly in excess of that needed by the lawn, and thus the wetting front could migrate significantly even more than predicted.

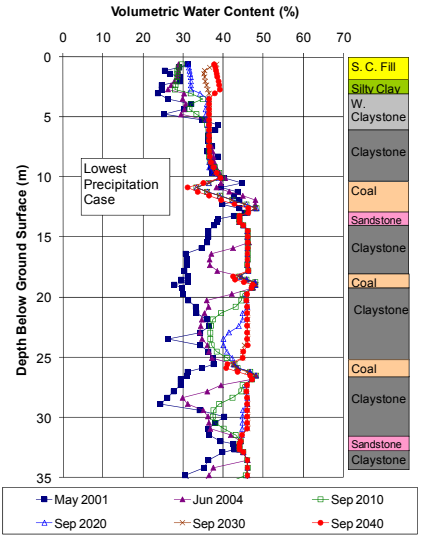

Figure 5. Predicted long-term water content profiles – lowest precipitation case

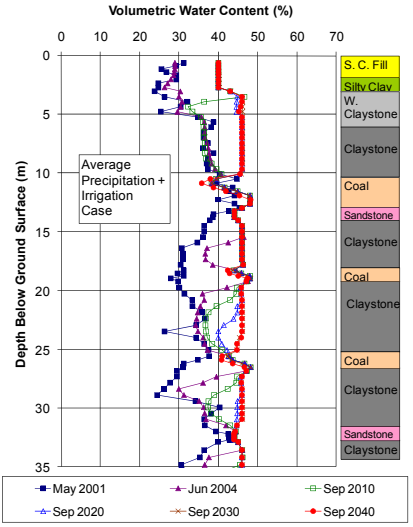

Figure 6. Predicted long-term water content profiles – average precipitation plus irrigation case

REFERENCES

Chao, K.C. (2007). Design Principles for Foundations on Expansive Soils. Dissertation submitted in partial requirement for the Ph.D. Degree, Colorado State University, Fort Collins, Colorado.

GEO-SLOPE International, Ltd. (2006). GEO-STUDIO VADOSE/W Software Package for Seepage Analysis, Version 6.20. Calgary, Alberta, Canada.

Mecham, B. (2005). Beautiful Hardy Lawn. Northern Colorado Water Conservancy District. Berthoud, Colorado.

Nelson, J. D., Overton, D. D., and Durkee, D. B. (2001). Depth of Wetting and the Active Zone. Expansive Clay Soils and Vegetative Influence on Shallow Foundations, ASCE, Houston, Texas. 95 – 109.

SoilVision Systems Ltd. (2006). SoilVision Software, Version 4.0. Saskatoon, Saskatchewan, Canada.

Signal Processing of Water Level Fluctuations in a Sloping Sandy Beach Modeled in a Laboratory Wave Canal

Y. Wang[1], R. Ababou[1], and M. Marcoux[1]

[1] Institut de Mécanique des Fluides de Toulouse (IMFT), Groupe d'Etude sur les Milieux Poreux (GEMP), UMR 5502 CNRS/INPT/UPS, Allée du Professeur Camille Soula, 31400 Toulouse, France, e-mails: wang@imft.fr , ababou@imft.fr, marcoux@imft.fr

ABSTRACT: In coastal processes, the strong water movements due to short periodic waves (such as sea swell) can induce irregular water level fluctuations in the swash zone and within the sandy beach. In this paper, the measured water level fluctuations in a wave canal with a sloping sand beach were analyzed by using seven capacitive sensors. Fourier spectrum and multi-resolution wavelet analyses were used to study these water level fluctuations. Several dominant periods for the entry water level were identified with Fourier analysis. The corresponding amplitudes and phases were obtained by wavelet analysis. A simplified (bimodal) Fourier approximation was then determined for the irregular water level fluctuations, with a good agreement with the original signals, which, therefore, could be used as the entry condition for numerical simulations.

INTRODUCTION

Beach groundwater interacting with tides, waves and swash is a complex and dynamic system. Groundwater fluctuations driven by oceanic oscillations enhance water exchange between the ocean and coastal aquifer. Interaction between swash dynamics and groundwater may also be important with regard to onshore sediment transport and beach profile evolution. There is currently limited understanding of how the beach groundwater system responds to oceanic forcing at various frequencies.

A "wave-beach" experiment was conducted in a large-scale water wave canal equipped with a wave generator (CIEM flume, Barcelona, Spain). The experiment was part of a European project, namely, the HYDRALAB-SANDS project, undertaken by the HYDRALAB laboratory in Barcelona, Spain, in collaboration with the OTE group of the IMFT laboratory in Toulouse, France. The experiment was initially designed to

measure the erosion of the swash zone in a sandy beach, with periodic water level oscillations.

This work focuses on a related problem, namely, the effect of surface water waves and swash zone phenomena on the subsurface oscillations in the sandy porous medium, and the possible interactions between surface and the subsurface oscillations. In this experiment, the water level fluctuations H(t) in the sloping sandy beach were measured by seven capacitive sensors: $H_i(t)$ denotes water level fluctuations measured by the *i*-th sensor.

This paper presents an analysis of these measured water level fluctuations $H_i(t)$ in the sloping sandy beach by Fourier spectrum and multi-resolution wavelet methods, using signal analysis tools previously developed by the IMFT/GEMP group (Fatmi 2009).

DESCRIPTION OF EXPERIMENTAL MODEL

A 100m long, 3m wide, and 5m high water-wave canal was used in this study. At the back end of the canal, a mechanical wave generator was designed with adjustable period and amplitude. For this experiment, the period was about 4 seconds, and the maximum amplitude was about 0.9m. The weighted average diameter D_{50} of sand grains was 0.25mm. The beach slope was 1/15.

As shown in Figs. 1 and 2, seven capacitive sensors were installed at intervals of about 1.5m in the beach slope in order to measure groundwater level fluctuations at different locations. In particular, sensor No.1 was placed near the still water/beach boundary to measure the water level fluctuations corresponding to the entry condition of the model.

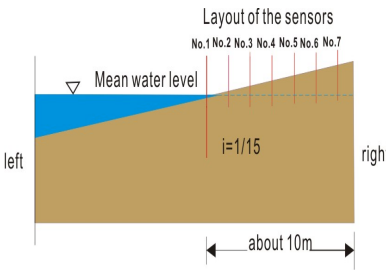

Figure 1. Test layout showing capacitive sensors installed in the swash zone. (Sensor N°1 is closest to the free water.)

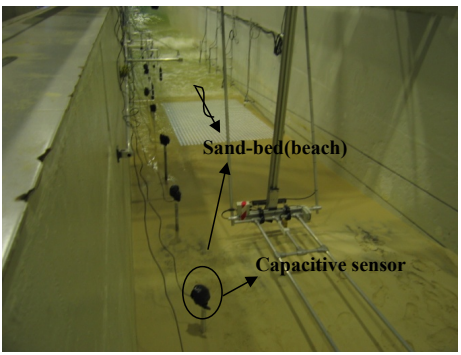

Figure 2. Photo of the sand beach with capacitive sensors/micro-piezometers at the HYDRALAB wave canal in Barcelona. (Incoming water waves are visible in the rear.)

MEASURED WATER LEVELS, H(t)

Water level measurements at the capacitive sensors began from the static initial water level (step 1 in Fig. 3), then lasted for about 30 minutes corresponding to water level fluctuations forced by the wave generator (step 2 in Fig. 3), and finally ended during the draining phase (step 3 in Fig. 3). The measured water levels H(t) shown in Figure 3 correspond to just one test.

The measurement results show clearly two effects: the spatial decaying of the amplitudes away from the shore, and the filtering out of the shortest periods (i.e., the system behaves as a low-pass filter of water fluctuations). Furthermore, the signals away from the shore, that is, $H_5(t)$, $H_6(t)$, and $H_7(t)$, exhibit a very different behavior from those closer to the shore.

The net increase of the mean groundwater level in these sensors may be caused by the sloping beach favoring vertical infiltration/drainage, and swash zone run-up, as observed in other coastal processes (Turner 1997).

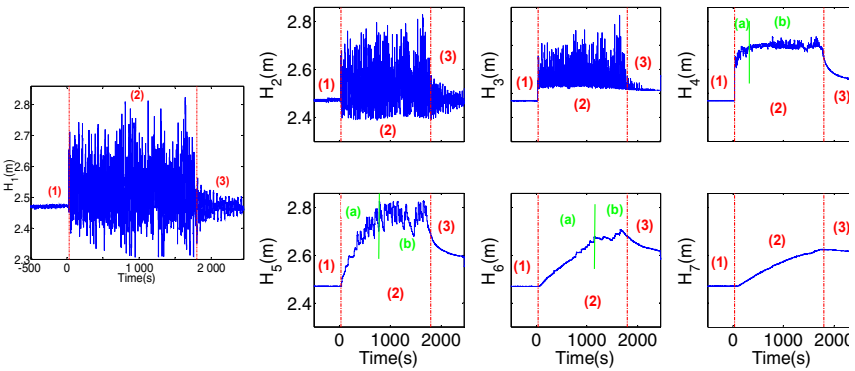

Figure 3. Water levels $H_i(t)$ versus time at each sensor. (Test 1: 18-March-2008.)

SIGNAL PROCESSING OF WATER LEVEL FLUCTUATIONS

Analysis of Sensor No.1: Entry Boundary Condition

Water level fluctuations at sensor No.1 (H_1) reflect surface water levels and can be considered as the entry boundary condition with respect to all the other *subsurface* sensors. The regular periodic wave with period, T = 4 seconds, produced at the wave generator seems much less regular when it arrives at Sensor No.1 in the swash zone (see Figs. 4 and 5). To simplify such complex signals, the dominant periods of $H_1(t)$ need to be extracted. Accordingly, the following bimodal Fourier approximation for water level signal $H_1(t)$ was chosen:

$$H_1(t) = H_0 + A_1 \sin(\omega_1 t + \varphi_1) + A_2 \sin(\omega_2 t + \varphi_2) \quad (1)$$

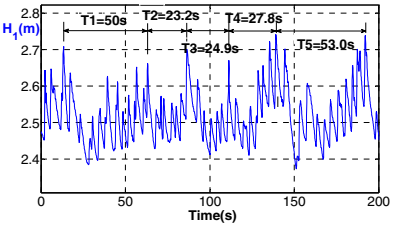

Figure 4. Evolution of water level H_1(m) – original signals

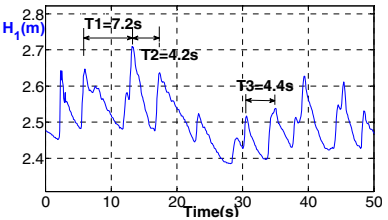

Figure 5. Magnified evolution of water level H_1(m) – original signals

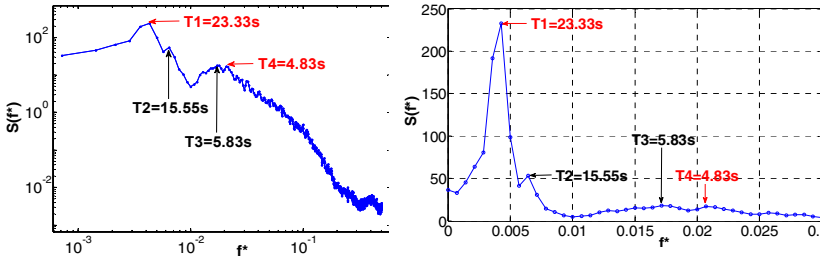

Figure 6: Reduced frequency spectrum of the water level fluctuations H_1(t)

To obtain the dominant periods, the Fourier method was used to analyze the original signals of H_1(t) in frequency space. The results are plotted in Figure 6.

From Figure 6, it can be noticed that the period $T_1 = 23.33$s prevails among the H_1(t) signals. There are also three other periods which play important roles. So far, the period $T_1 = 23.33$s is considered as the result of the size of the wave canal (the signals measured after the wave generator has been stopped were analyzed independently and the same results were obtained). On the other hand, period $T_4 = 4.83$s is obviously close to the wave generator period ($T_0 = 4$s).

Then the orthogonal multi-resolution wavelet analysis was used to verify the results of Fourier analysis and to obtain the corresponding amplitudes and phases for the dominant periodic waves. In Figure 7, it can be seen that the sum of the dyadic wavelet component C7 and the dyadic wavelet component C5, agree well with the original signal. After that, the amplitudes (defined as the 90% confidence band) of the wavelet components C7 and C5 can be obtained as follows: $A_{C7} = 1.64\sigma_{C7} = 0.0672\ m$ and $A_{C5} = 1.64\sigma_{C5} = 0.0524\ m$ (C5 and C7 are shown in Fig. 8).

Concerning the phases, they can be directly measured from Figure 8**.** A simple method was used at first, namely: $\varphi = 2\pi(t_n^* - 0)/T$, where t_n^* is the first 0-crossing of the signal (this method will be revised, with a statistical identification of the phase, at a later stage of this investigation). This yields the following: $\varphi_{C7} = 0.238\ rad$, and $\varphi_{C5} = 0.982\ rad$.

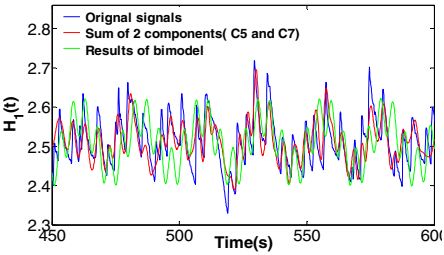

Figure 7. Wavelet analysis of signal $H_1(t)$: comparison of original signal, bimodal Fourier signal, and 2-component wavelet

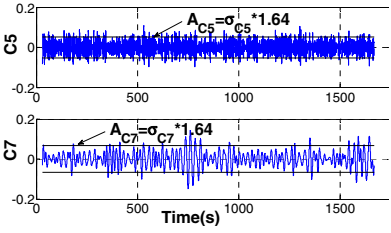

Figure 8. Wavelet analysis of signal $H_1(t)$: the dyadic components C7 and C5

At this point, all of the coefficients for the analytical bimodal Fourier model of equation (1) have been obtained, as summarized in Table 1. Figure 7 demonstrates that this 'analytical model' can be considered a reasonably good approximation to the original signal, which is confirmed by wavelet analysis.

Table 1 Coefficients of 'analytical' bimodal approximation

Coefficients	H_0**(m)**	T_1**(s)**	A_1**(m)**	φ_1**(rad)**
Values	2.5112	24	0.0672	0.238
Coefficients	-	T_2**(s)**	A_2**(m)**	φ_2**(rad)**
Values	-	4.83	0.0524	0.982
Methods	Average of the original signals	Fourier	Wavelet	Wavelet

Analysis of Sensor No.7: Groundwater

The water in the tube of the capacitive sensor No. 7, the farthest sensor from the swash zone, is thought to be a direct measurement of 'groundwater'. From Figure 9**,** it can be seen that signal $H_7(t)$ is totally different from $H_1(t)$: signal $H_7(t)$ clearly exhibits a slowly increasing stage (water filling) and a descending stage (water draining). The Fourier method is not directly suited for this type of strongly non-periodic and nonergodic signals (Convay 2000). Instead, a moving average filter is first used to remove the nonlinear trend, and then, Fourier is used to analyze the residual of the original signal.

The reduced Fourier spectra versus reduced frequencies of the detrended $H_7(t)$ are shown in Figure 10. It can be seen that all the small period waves have disappeared and the remaining dominant period is T1 = 171s, which is seven times longer than that of the $H_1(t)$ signal (T1 = 24s).

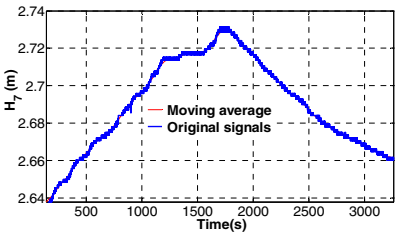

Figure 9. Original signals $H_7(t)$ and its moving average

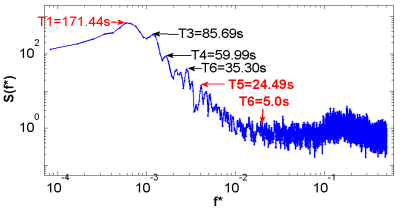

Figure 10. Reduced spectra of the residues of $H_7(t)$

Analysis of Other Sensors: Between Swash Zone and Deep Groundwater

Due to complex water level fluctuations and strong erosion in the swash zone, at the end of the series of wave generation tests (9 days), the static free water boundary arrived at the position of sensor No.3. For sensors No. 2, 3, and 4, the Fourier method was directly used to analyze their original signals (as for sensor No.1). The results are very similar to those of sensor No.1. On the other hand, for sensors No. 5 and No. 6, Fourier analyses of 'detrended' signals (moving averages) yield results similar to those of sensor No.7.

CONCLUSIONS AND FUTURE WORK

The experiment was especially designed to measure the erosion of the swash zone in a sandy beach, with periodic oscillations of water levels, using a wave generator. In this work, a related problem has been studied, namely, the effects of surface water waves and swash zone processes on subsurface water in the sand beach, and the possible interactions between surface and subsurface oscillations.

The artificial beach of the canal with subsurface sensors (micro-piezometers) has been instrumented to measure groundwater level fluctuations, and the signal processing techniques towards this goal have been used. The results obtained so far, with spectral frequency methods and multi-resolution wavelet analyses, appear quite promising. In particular, two important periods, and their corresponding amplitudes and phases at the entry boundary, were identified. A bimodal Fourier approximation of the signal was proposed. This yields a simplified version of the observed irregular water level fluctuations $H_1(t)$, which shows good agreement with the original signals, which, hence, can be used as the entry condition for numerical simulations.

In addition, numerical simulations are currently being implemented in order to complement the experimental water level signal analyses and to compare them with various water flow models (a preliminary version of modeling results was presented in Wang et al. 2008). The numerical models being used for these comparisons include:

(1) A 2D plane flow model based on the vertically averaged Dupuit-Boussinesq equation for unconfined groundwater flow (with fluctuating boundary conditions);
(2) A 3D variably saturated flow model based on a generalized Richards' equation.

ACKNOWLEDGMENTS

This research has been conducted through a collaborative effort on a long wave canal experiment (HYDRALAB-SANDS, Barcelona, Spain), also in collaboration with the OTE group of the IMFT laboratory (D. Astruc, O. Eiff et al., Toulouse, France).

REFERENCES

Conway P., D. Frame, A spectral analysis of New Zealand output gaps using Fourier and wavelet techniques. Reserve Bank of New Zealand, DP2000/06.

Turner.I. L., B.P. Coates, R.I. Acworth (1997), Tides, waves and the super-elevation of groundwater at the coast. Journal of Coastal Research, 13(1), 46-60.

Fatmi H. (2009). Méthodologie d'analyse des signaux et caractérisation hydrogéologique: application aux chroniques de données obtenues aux laboratoires souterrains du Mont Terri, Tournemire et Meuse/Haute-Marne, PhD thesis, INP Toulouse, 248, (Chap.4: pp.46-66).

Wang Y., R. Ababou, M. Marcoux (2008). Oscillatory Flows through Porous Media: Free Surface Hydraulics, Wave Propagation, and Capillarity. Proc. IAHR-GW2008, Internat. Assoc. Hydraulics Research: Internat. Ground Water Sympos., Istanbul, Turkey, June 2008.

Non-Destructive Measurements of Unsaturated Seepage Flow Using Surface Ground-Penetrating Radar

Y. Takeshita[1], S. Morikami[2], T. Yamashita[3], S. Kuroda[4], T. Morii[5], and M. Inoue[6]

[1] Professor, Graduate School of Environmental Science, Okayama University, Okayama, 700-8530, Japan; yujitake@cc.okayama-u.ac.jp
[2] Engineer, Obayasi Corporation, Tokyo, 108-8502, Japan
[3] Graduate student, Graduate School of Environmental Science, Okayama University, Okayama, 700-8530, Japan
[4] Researcher, National Institute for Rural Engineering, Ibaraki, 305-8069, Japan
[5] Professor, Faculty of Agriculture, Niigata University, Niigata 950-2181, Japan
[6] Professor, Arid Land Research Center, Tottori University, Tottori 680-0001, Japan

ABSTRACT: Surface ground-penetrating radar (GPR) was assessed as a non-destructive method to measure the temporal and spatial variability of unsaturated seepage flow under uniform wetting conditions on a homogeneous sandy soil. GPR profile survey with 400MHz antenna was conducted. GPR reflected wave from advancing wetting front during uniform field infiltration experiments was used to map the wetting front depth variability with time. The dielectric constant of soil measured by vertical soil moisture probe below the ground surface was used as standard measures of soil moisture to compare with the GPR estimated unsaturated seepage flow behavior. The utility of our proposed GPR profile survey was demonstrated by using numerical seepage flow FEM analysis of field infiltration experiments. There was good agreement between computed and measured wetted zone movements in two-dimensional unsaturated seepage flow. Traceability of the wetting front depth variability with time was found by GPR profile survey.

INTRODUCTION

Measuring unsaturated seepage flow behavior is the most common form of vadose zone monitoring. For the rainfall-induced slope failures or the levee failures caused by seepage, it is important to monitor groundwater tables or soil water content profiles over time. This necessitates a non-destructive measurement that can be made repeatedly. Recently, there has been a considerable amount of research on the use of

surface ground-penetrating radar (GPR) to detect buried objects and geological structures and to measure soil water content. GPR has been identified and tested as a non-intrusive geophysical method (Huisman 2001, Galagedara et al. 2003). GPR has a couple of advantages over the intrusive soil moisture sensors and tensiometers in unsaturated soils. GPR system offers a simple approach for in-situ determination of unsaturated seepage flow behaviors or soil water content profiles and a completely non-destructive measurement.

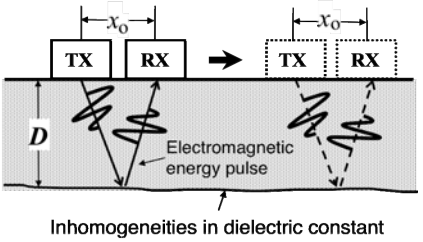

Figure 1. Schematic diagram of GPR profile survey

In this paper, the potential of surface GPR for measuring unsaturated seepage flow in sandy soils was evaluated. It is shown from field infiltration experiments performed in homogeneous unsaturated dune sands. The temporal and spatial variations of the wetting front caused by two-dimensional unsaturated seepage flow under uniform infiltration were measured non-destructively by using GPR profile survey. GPR estimated wetting front depth variability with time are assessed by comparison to computed unsaturated seepage flow behaviors and measured soil moisture content values. Traceability of the wetting front depth variability with time was found by GPR profile survey.

MATERIALS AND METHODS

Ground-Penetrating Radar

The GPR technique is based on the propagation of an electromagnetic energy pulse into the subsurface from a transmitting antenna at radio frequencies between 10 and 1000 MHz. When the radiated energy encounters inhomogeneities in the dielectric properties of the subsurface, some energy is reflected back to the radar antenna and some is transmitted downward to deeper material. Inhomogeneities of the dielectric properties of the soil are present in most hydrogeologic settings and are determined primarily by water content, dissolved minerals, and expansive clay and heavy-mineral content in the subsurface material.

Figure 1 illustrates the schematic diagram of GPR profile survey mode with the antennas on the surface. A receiver on the surface detects reflections of the energy pulse that occur where the radio wave velocity changes. The record shows the total

travel time for a signal to pass through the subsurface, reflect from an inhomogeneity, and return to the surface. The depth D to the reflector is approximated from the two-way travel time for the electromagnetic wave to propagate vertically downward and back to the surface.

$$D = \frac{\sqrt{(TV)^2 - x_o^2}}{2} \tag{1}$$

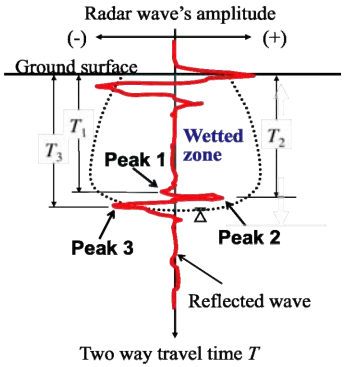

Figure 2. Illustration of relationship between radar wave's amplitude and two way travel time measured by GPR for unsaturated seepage flow

where T = two-way travel time; V = electromagnetic wave velocity in the medium; and x_o = the antenna separation (spacing between transmitter and receiver).

GPR measurements are based on transmission or reflection of an electromagnetic wave in the studied medium. Electromagnetic wave propagation velocity depends on the dielectric constant of the medium and its spatial variations; electromagnetic wave velocity varies from 0.3m/ns in air to 0.055 to 0.17m/ns in soils (Reynolds 1997). The relative dielectric constant ε_r is the ratio between the dielectric constant of the medium and that of the air. The electromagnetic wave velocity in the medium is expressed as

$$V = \frac{c}{\sqrt{\varepsilon_r}} \tag{2}$$

where c = the speed of light in the air (= 3×10^8 m/s).

Water content is the main factor of the dielectric variations observed in unsaturated soils. GPR profile survey was used to trace the wetting front of wetted zone coursed by unsaturated seepage flow. If x_o is negligible small compared with D in Figure 1, Equation 3 is derived from Equations 1 and 2. Two-way travel times of GPR measurements were converted to depths using Equation 3.

$$D = \frac{Tc}{2\sqrt{\varepsilon_r}} \tag{3}$$

An accurate determination for the travel time of reflected wave from GPR waveform data is very important to search the reflection from unsaturated seepage flow. An individual error is also occurred when the peak of waveform is decided. The relationship between radar wave's amplitude and two way travel time measured by

Table 1. Properties of Tottori dune sand for infiltration experiments

Dry density (g/cm^3)	Field saturated volumetric water content	Initial volumetric water content	Field saturated hydraulic conductivity (cm/s)	Coefficient of uniformity	D_{10} (mm)
1.48	0.38	0.03 - 0.06	2.0×10^{-2}	2.05	0.2

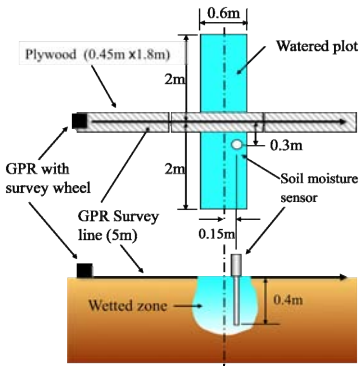

Figure 3. Field layout of infiltration experiments

GPR profile survey for unsaturated seepage flow is illustrated in Figure 2. The major reflection event visible in Figure 2 at three peaks (Peak 1 to Peak 3) is assumed to represent the wetting front of unsaturated seepage flow. In this study, these three peaks are picked as typical reflected wave peaks for the wetting front.

Field experiments

The Arid Land Research Center of Tottori University, Tottori, Japan, which has a well-drained homogeneous dune sand soil profile, was selected for this filed experiment. The properties of Tottori dune sand are listed in Table 1. Schematic diagram of infiltration experiments are shown in Figure 3. The uniform infiltration experiments were performed on a flat 4m×0.6m area.

The uniform infiltration was provided by using a water spray. One uniform infiltration work was conducted for 5 minutes at 0.0159m^3/min. and subsequently infiltration was interrupted for 3 minutes. GPR profile survey was performed while infiltration was suspended. A series of the uniform infiltration and GPR survey work was conducted continuously ten times.

Transient behavior of the wetting front caused by two-dimensional vertical unsaturated seepage flow from the uniform infiltration was non-destructive measured by using GPR profile survey. A vertically installed soil moisture sensor (Delta-T devices Inc. Profile prove type PR1/4) was used to measure dielectric constant at 4 different depths from 0.1 to 0.4m below the ground surface within a vertical unsaturated seepage flow. The GPR data were acquired with a Geophysical Survey Systems Inc. SIR-3000 system using 400MHz antennas with survey wheel.

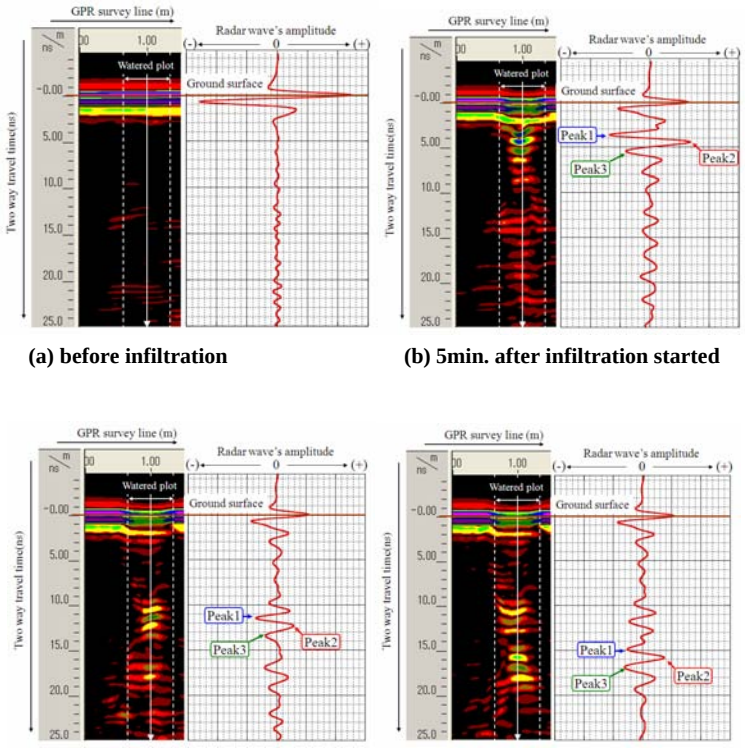

(a) before infiltration **(b) 5min. after infiltration started**

(c) 37min. after infiltration started **(d) 53min. after infiltration started**

Figure 4. Tomographic images under GPR profile survey line and reflected wave forms in the center of the watered plot

RESULTS AND DISCUSSION

GPR Tomographic Image of Unsaturated seepage flow

The tomographic images of the transient wetted zone variation of two dimensional unsaturated seepage flow were produced by GPR profile survey. Measured GPR tomographic images before infiltration examination and also 5, 37, 53minutes after infiltration started are shown in Figures 4. The major reflection event visible in

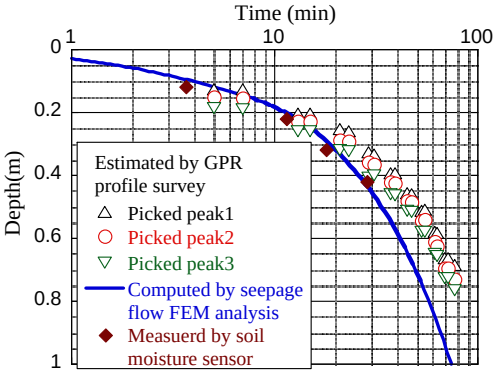

Figure 5. Comparison of the wetting front depths between GPR estimation and the seepage flow FEM computation

Figure 4(b), 4(c) and 4(d) at the watered plot is assumed to represent the vertical seepage flow. It is considered that the transient wetted zone variation of unsaturated seepage flow can be evaluated qualitatively by continuous GPR profile survey.

GPR Estimated Wetting Front Depth Variability with Time

Measured GPR waveforms before infiltration examination and also 5, 37, 53minutes after infiltration started are shown in Figure 4. Amplitude peaks of the reflected wavelet were picked manually at the three peaks (Peak 1 to Peak 3) in this Figure. Two-way travel times at these picked peaks were converted to depths of the wetting front by using Equation 3 respectively. GPR-estimated temporal and spatial variations of the wetting front were analyzed by using a numerical unsaturated seepage flow FEM analysis (HYDRUS-2D, Rassam et al. 2003). Figure 5 shows comparison of transient behavior of wetting front depths between GPR estimation and the FEM computation. The difference of wetting front depth estimated by GPR due to picked peak 1 to 3 is about 7cm. Traceability of the wetting front depth variability with time was found by GPR profile survey.

CONCLUSIONS

This study examined the potential of surface ground-penetrating radar (GPR) for measuring unsaturated seepage flow in sandy soils. It is shown from field infiltration experiments performed in homogeneous unsaturated dune sands. GPR estimated wetting front depth variability with time are assessed by comparison to FEM computed unsaturated seepage flow behaviors and measured soil moisture content values. The following are conducted;

1. The tomographic images of the transient wetted zone variation of two dimensional unsaturated seepage flow can be produced by GPR. The transient wetted zone variation of unsaturated seepage flow can be evaluated qualitatively by continuous GPR profile survey.
2. The temporal and spatial variations of the wetting front caused by two-dimensional unsaturated seepage flow under uniform infiltration can be measured non-destructively by using GPR. Traceability of the wetting front depth variability with time was found by GPR profile survey.
3. GPR profile survey offers a fast and non-destructive way for measuring the unsaturated seepage flow and may be a useful tool for low-cost mapping the transient behavior of wetting front for in-situ permeability tests.

ACKNOLEDGEMENTS

This work was supported by KAKENHI (Grant-in-Aid for Scientific Research (A)18206051 and (B)20360212) made by the Ministry of Education, Science, Sports and Culture of Japan, and by the Joint Research Grant made by the Arid Land Research Center, Tottori Univ., Japan.

REFERENCES

Galagedara, L.W., Parkin, G.W. and Redman, J.D. (2003). An analysis of the ground-penetrating radar direct ground wave method for soil water content measurement. Hydrological Processes, 17: 3615-3628.

Huisman, J.A., Sperl, C., Bouten, W. and Verstraten, J.M. (2001). Soil water content measurements at different scales: Accuracy of time domain reflectometry and ground penetrating radar. Journal of Hydrology, (245): 48-58.

Rassam, D., Simunek, J. and van Genuchten M. Th. (2003). Modelling variably saturated flow with HYDRUS-2D. International Ground-water Modeling Center.

Reynolds, J.M. (1997). An introduction to applied and environmental geophysics, chapter12, Ground penetrating radar. John Wiley & Sons: 682-777.

Unified Solutions for Unsaturated Soil Shear Strength and Active Earth Pressure

Ch. Zhang[1], J. Zhao[2], Q. Zhang[1], and F. Xu[3]

[1] Key Laboratory of Geotechnical and Underground Engineering of Ministry of Education, Tongji University, Shanghai 200092, P.R. China. Tel: 0086-21-65985249, e-mail:zcg1016@163.com
[2] School of Civil Engineering, Chang'an University, Xi'an 710061, P.R. China. Tel: 0086-29-82337238, e-mail:zhaojh@chd.edu.cn
[3] Shanghai No.1 Municipal Engineering Co. Ltd., Shanghai 200083, P.R. China. Tel: 0086-21-65988771, e-mail:afei362@citiz.net

ABSTRACT: The unified solution for shear strength for unsaturated soil in terms of two independent state stress variables is presented based on both Unified Strength Theory (UST) and Fredlund's shear strength theory for unsaturated soil, which can be especially versatile in reflecting the effect of intermediate principal stress. Considering different distributions of matric suction, the unified solution of active earth pressure for unsaturated soil is deduced, which could avoid some shortages of Rankine's active earth pressure. The influence of the intermediate principal stress and matric suction on the active earth pressure is also investigated. It is shown that the active earth pressure decreases significantly with an increase in the unified strength theory parameter or matric suction.

INTRODUCTION

Unsaturated soils are widely distributed worldwide. The shear strength for unsaturated soil is used in many geotechnical engineering problems such as earth pressure, slope stability and bearing capacity (Lu and Likos 2004). Fredlund and Rahardjo (1993) formulated an extended Mohr-Coulomb (M-C) criterion to describe the shear strength behavior of unsaturated soil in terms of two independent state stress variables, which are net normal stress (σ-u_a) and matric suction (u_a-u_w), where u_a is pore-air pressure and u_w is pore-water pressure. As is well known, the M-C criterion does not take into account the influence of intermediate principal stress, which is more conservative for engineering design. Many existing results for earth pressure are merely based on the M-C criterion and for saturated soil. More and more evidences have been accumulating

to indicate that the intermediate principal stress σ_2 does influence the soil strength in many instances (Houston et al. 2008, Matsuoka et al. 2002). The Unified Strength Theory (UST) takes into account the effects of all stress components on the yield or failure of materials, which can reflects the different effects of intermediate principal stress under various stress states for various materials fully (Yu 1998). The UST is a simple linear function, and it is easy to apply to the analytical solutions and to be used for engineering design.

The objective of this paper is to develop the unified solutions of shear strength and active earth pressure for unsaturated soil considering the effects of intermediate principal stress and matric suction. With two different distributions of matric suction, the influences of intermediate principal stress and matric suction on the active earth pressure are discussed through an engineering example.

THE UNIFIED STRENGTH THEORY

The UST was proposed by Yu in 1990s, which was developed based on an orthogonal octahedron of a twin-shear element model. In terms of principal stresses, the UST is expressed in term of shear strength parameters (cohesion c and internal friction angle φ) as (Yu 1998)

$$F=\sigma_1-\frac{1-\sin\varphi}{(1+b)(1+\sin\varphi)}(b\sigma_2+\sigma_3)=\frac{2c\cos\varphi}{1+\sin\varphi},\quad \sigma_2\le\frac{\sigma_1+\sigma_3}{2}+\frac{\sigma_1-\sigma_3}{2}\sin\varphi \quad (1a)$$

$$F'=\frac{1}{1+b}(\sigma_1+b\sigma_2)-\frac{1-\sin\varphi}{1+\sin\varphi}\sigma_3=\frac{2c\cos\varphi}{1+\sin\varphi},\quad \sigma_2\ge\frac{\sigma_1+\sigma_3}{2}+\frac{\sigma_1-\sigma_3}{2}\sin\varphi \quad (1b)$$

where σ_1, σ_2 and σ_3 are major, intermediate and minor principal stresses, respectively (Tension stress is considered positive here). b is called the unified strength theory parameter that reflects the influence of intermediate principal stress and also a parameter of strength criterion, with $0\le b\le 1$.

The specific form of strength criterion for certain material depends on the parameter b. For example, the UST reduces to the M-C criterion with b=0; the Generalized Twin-Shear Stress (GTSS) criterion with b=1. The UST consists of a series of piecewise linear strength criteria on the deviatoric plane with the variation of b (Yu 1998).

In 3D stress state (Yu 1998), $\sigma_2= m(\sigma_1+\sigma_3)/2$, where the parameter m is called the coefficient of intermediate principal stress, with $2v\le m\le 1$, v is Poisson's ratio. Therefore $\sigma_2=m(\sigma_1+\sigma_3)/2<(\sigma_1+\sigma_3)/2+(\sigma_1-\sigma_3)\sin\varphi/2$, Eq. (1a) should be adopted. Then Eq. (1a) can be expressed as (From now on, compressive stress is considered positive):

$$\frac{\sigma_1-\sigma_3}{2}=\frac{\sigma_1+\sigma_3}{2}\sin\varphi_t+c_t\cos\varphi_t \quad (2)$$

$$\sin\varphi_t=\frac{b(1-m)+(2+b+bm)\sin\varphi}{2+b(1+\sin\varphi)},\quad c_{ij}=\frac{2(b+1)c_j\cos\varphi_j}{2+b(1+\sin\varphi_j)}\frac{1}{\cos\varphi_{ij}}$$

Eq. (2) can be versatile in reflecting the effect of intermediate principal stress through the parameters b and m. The parameters m and b indicate the magnitude and extent to failure of intermediate principal stress, respectively.

THE UNIFIED SOLUTION OF SHEAR STRENGTH

Originally, shear strength of a single-valued effective stress was searched for unsaturated soil. By the late 1960s, there was increasing awareness that the use of two independent stress state variables would provide an approach more consistent with the principles of continuum mechanics. It was the combination of (σ-u_a) and (u_a-u_w) that proved to be the easiest to apply in engineering practice. A linear form of shear strength for unsaturated soil in term of two independent stress state variables based on the M-C criterion was proposed by Fredlund e and Rahardjo (1993):

$$\tau_f = c' + (\sigma - u_a)\tan\varphi' + (u_a - u_w)\tan\varphi^b \tag{3}$$

where c' is the effective cohesion for saturated soil; φ' is the effective angle of internal friction associated with (σ-u_a); the angle φ^b is related with (u_a-u_w), which represents the increase in shear strength associated with (u_a-u_w). Generally, φ^b tends to less than φ'.

Due to adopting the M-C criterion, Eq. (3) does not take the effect of intermediate principal stress into account. In order to overcome this problem, and moreover Eq. (2) has the same form as the M-C criterion, we can naturally replace c', φ' and φ^b in Eq. (3) with c_t', φ_t' and φ_t^b (m=1 for that (u_a-u_w) is a hydrostatic stress), respectively. Then the unified solution of shear strength for unsaturated soil in term of two stress state variables is expressed as:

$$\tau_f = c_t' + (\sigma - u_a)\tan\varphi_t' + (u_a - u_w)\tan\varphi_t^b \tag{4}$$

$$\sin\varphi_t' = \frac{b(1-m) + (2+b+bm)\sin\varphi'}{2+b(1+\sin\varphi')},\quad c_t' = \frac{2(1+b)c'\cos\varphi'}{2+b(1+\sin\varphi')}\frac{1}{\cos\varphi_t'},$$

$$\sin\varphi_t^b = \frac{2(1+b)\sin\varphi^b}{2+b(1+\sin\varphi^b)}$$

It is evident that the intermediate principal stress σ_2 has been taken into account in Eq. (4) through b and m. With b=0, Eq. (4) is equivalent to Eq. (3). This is one of the main advantages for employing UST. If b is given other values, many new results can be obtained from Eq. (4), which could compare with existing traditional solutions.

THE UNIFIED SOLUTION OF ACTIVE EARTH PRESSURE

The retaining wall is vertical, and its backing is smooth, which extends to infinity. Rankine's active state of failure is illustrated in Figure 1. The cause for active failure is due to the stress generated from soil self-weight, rather than an external load (Lu and

Likos 2004). The vertical net normal stress (σ_v-u_a) is the maximum principal stress and the horizontal net normal stress (σ_h-u_a) is the minimum principal stress. At the limiting equilibrium condition, the stress relations can be obtained as:

$$\sin\varphi_t' = \frac{\left[(\sigma_v - u_a) - (\sigma_h - u_a)\right]/2}{\frac{(\sigma_v - u_a) + (\sigma_h - u_a)}{2} + \left[c_t' + (u_a - u_w)\tan\varphi_t^b\right]\cot\varphi_t'} \tag{5}$$

and rearranging leads to:

$$(\sigma_h - u_a) = (\sigma_v - u_a)k_a - 2c_t'\sqrt{k_a} - 2(u_a - u_w)\tan\varphi_t^b\sqrt{k_a} \tag{6}$$
$$k_a = \tan^2\left(45^\circ - \varphi_t'/2\right)$$

where k_a is the coefficient of active earth pressure for unsaturated soil.

Assuming (σ_v-u_a) is equal to γh, the depth of tension-cracking zone h_o is:

$$h_o = 2\left[c_t' + (u_a - u_w)\tan\varphi_t^b\right]/\left(\gamma\sqrt{k_a}\right) \tag{7}$$

where γ is the unit weight for unsaturated soil.

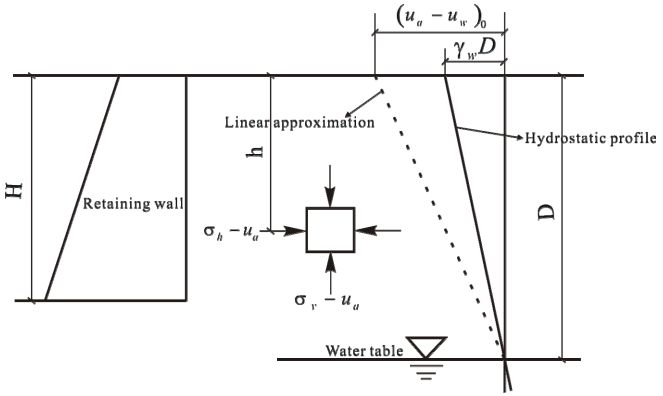

Figure 1. Conceptual profiles of retaining wall backfill and linear matric suction

Case 1: Constant Matric Suction

If the matric suction is assumed constant, i.e. the same at all depths from the ground surface to the water table, the active earth pressure E_a on a retaining wall of height H is obtained by integrating Eq. (6) from h=h_o to h=H. This gives:

$$E_a = \int_{h_0}^{H} (\sigma_h - u_a) dh = \frac{1}{2}\gamma k_a \left(H^2 - h_o^2\right) - 2\left[c_t' + (u_a - u_w)\tan\varphi_t^b\right] \times \sqrt{k_a}\,(H - h_o) \quad (8)$$

Case 2: Linear Matric Suction

When the matric suction decreases linearly with depths from the ground surface to the water table (see Figure 1), the distribution equation of matric suction is:

$$(u_a - u_w)_h = (u_a - u_w)_o (1 - h/D) \quad (9)$$

where D is the depth from the water table to the ground surface. $(u_a\text{-}u_w)_o$ is matric suction at the ground surface. In this case, h_o and E_a can be expressed as:

$$h_0 = \frac{2\left[c_t' + (u_a - u_w)_o \tan\varphi_t^b\right]}{\gamma\sqrt{k_a} + 2(u_a - u_w)_o \tan\varphi_t^b / D} \quad (10)$$

$$E_a = \frac{1}{2}\gamma k_a \left(H^2 - h_o^2\right) - 2c_t' \sqrt{k_a}\,(H - h_o) - 2(u_a - u_w)_o \sqrt{k_a}\tan\varphi_t^b \left[H - \frac{H^2}{2D} - h_o + \frac{h_o^2}{2D}\right] \quad (11)$$

Eqs. (8) and (11) are the unified solutions of active earth pressure for unsaturated soil with constant and linear distribution of matric suction with depths, respectively. Rankine's active earth pressure for saturated soil is a special case with b=0 and $(u_a\text{-}u_w)$=0. The active earth pressure for unsaturated soil based on the M-C criterion is achieved with only b=0. There are many new results with $b \neq 0$. So the unified solution of active earth pressure has a wide application.

DISCUSSIONS

Due to a retaining wall is considered to be in the plane strain state, $\sigma_2=(\sigma_1+\sigma_3)/2$, therefore m=1. Assuming the matric suction is not greater, φ^b is a constant below φ'. The clay unsaturated soil deposit with an 8m vertical cut is at the active limit state (see Figure 1). The soil has the following properties: effective internal friction angle φ'=22°, effective cohesion c'=5kPa, unit weight γ=18kN/m^3 and the water table D=9m. These values are constant throughout the entire depth of the retaining wall.

Figures 2-3 show the active earth pressure E_a with different b for constant and linear distribution of matric suction with depths, respectively. For each case, three different values of b (0, 0.5 and 1) are considered.

In observing Figure 2, it can be seen that E_a are reduced with the increase in the value of b or matric suction $(u_a\text{-}u_w)$. The case (b=0, $(u_a\text{-}u_w)$=0), which corresponds to saturated soil based on the M-C criterion, gives the maximum value. When $(u_a\text{-}u_w)$=50kPa, E_a with b=1 is reduced by 65.3% relative to that with b=0. When b=0.5,

E_a is reduced from 181.5kN/m to 15kN/m with (u_a-u_w) increasing from 0kPa to 100kPa. The latent potentialities of unsaturated soil are brought due to considering the effects of intermediate principal stress and matric suction. With continuously increasing (u_a-u_w), E_a gradually decreases to 0. Therefore, it is entirely possible that no compressive earth pressure acts along the entire depth of a retaining wall adjacent to unsaturated soil with greater matric suction. So the engineering design for unsaturated soil should be adopted with a good shear strength formula, which should incorporate both the influences of intermediate principal stress and matric suction rationally.

Comparison of Figs.2 and 3, the variations of E_a with b and (u_a-u_w) for matric suction linearly decreasing with depths are similar to that of constant matric suction, however the decreasing rate is more slow for the linear matric suction.

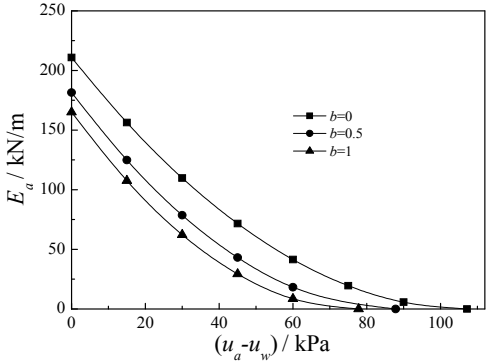

Figure 2. E_a when (u_a-u_w) is constant

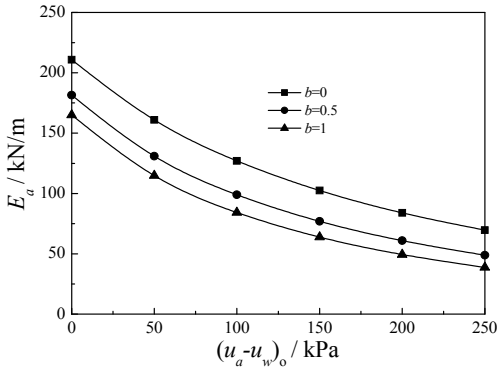

Figure 3. E_a when (u_a-u_w) decreases linearly in depths

CONCLUSIONS

Based on Unified Strength Theory (UST), the unified solution of shear strength for unsaturated soil in terms of two independent state stress variables has been presented. The influence of intermediate principal stress is considered in the new unified solution rationally. With two different distributions of matric suction, the unified solution of active earth pressure for unsaturated soil is obtained, which can naturally avoid the shortages of Rankine's active earth pressure. The active earth pressure is obviously influenced by intermediate principal stress and matric suction. With unified strength theory parameter or matric suction increasing, the active earth pressure decreases drastically. The active earth pressure does not change more rapidly when matric suction decreases linearly with depths.

The latent potentialities of unsaturated soil are achieved due to considering the effect of intermediate principal stress. So a good shear strength formula should consider the effect of intermediate principal stress rationally. Although only the active earth pressure for unsaturated soil is discussed in this paper, the laws of intermediate principal stress and matric suction could be apply to many other geotechnical problems, such as passive earth pressure, limit bearing capacity of strip foundation and slope stability.

REFERENCES

Fredlund, D.G. and Rahardjo, H. (1993). Soil mechanics for unsaturated soils. New York: John Wiley and Sons, lnc.

Houston, S.L., Perez-Garcia, N. and Houston, W.N. (2008). Shear strength and shear-induced volume change behavior of unsaturated soils from a triaxial test program. Journal of Geotechnical and Geoenvironmental Engineering, ASCE, 134 (11), 1619-1632.

Lu, N. and Likos, W.J. (2004). "Unsaturated soil mechanics." New York: John Wiley and Sons, lnc.

Matsuoka, H., Sun, D.A., Kogane, A., Fukuzawa, N. and Ichihara, W. (2002). Stress-strain behavior of unsaturated soil in true triaxial tests. Canadian Geotechnical Journal, 39 (3), 608-619.

Yu, M.H. (1998). Two-shear theory and its application. Beijing: Science Press (in Chinese).

AUTHOR INDEX

Page number refers to the first page of paper.

SUBJECT INDEX

Page number refers to the first page of paper.